

A3G-2015-185420

**INTEGRATING RESIDUAL
STRESS ANALYSIS OF CRITICAL
FASTENER HOLES INTO USAF
DEPOT MAINTENANCE**

**THOMAS B. MILLS, KYLE T. HONEYCUTT, SCOTT
A. PROST-DOMASKY, and
CRAIG L. BROOKS**

**APES, INC.
6669 FYLER AVENUE
ST. LOUIS, MISSOURI 63139**

CONTRACT FA9453-12C-0218

2 November 2014

Final Report for 4 August 2012 – 2 November 2014

DISTRIBUTION STATEMENT A – Approved for public release; distribution is unlimited.
(Ref. #75ABW-2015-0026)

STINFO FINAL REPORT

**AIR FORCE LIFE CYCLE MANAGEMENT CENTER
AFLCMC/WWAEJ
HILL AIR FORCE BASE, UT 84056**



REPORT DOCUMENTATION PAGE				<i>Form Approved</i> OMB No. 0704-0188				
The public reporting burden for this collection of information is estimated to average 1 hour per response, including the time for reviewing instructions, searching existing data sources, gathering and maintaining the data needed, and completing and reviewing the collection of information. Send comments regarding this burden estimate or any other aspect of this collection of information, including suggestions for reducing this burden, to Department of Defense, Washington Headquarters Services, Directorate for Information Operations and Reports (0704-0188), 1215 Jefferson Davis Highway, Suite 1204, Arlington, VA 22202-4302. Respondents should be aware that notwithstanding any other provision of law, no person shall be subject to any penalty for failing to comply with a collection of information if it does not display a currently valid OMB control number. PLEASE DO NOT RETURN YOUR FORM TO THE ABOVE ADDRESS.								
1. REPORT DATE (DD-MM-YY) 02-11-14		2. REPORT TYPE Final		3. DATES COVERED (From - To) August 4, 2012 – November 2, 2014				
4. TITLE AND SUBTITLE Integrating residual stress analysis of critical fastener holes into USAF depot maintenance				5a. CONTRACT NUMBER FA9453-12C-0218				
				5b. GRANT NUMBER N/A				
				5c. PROGRAM ELEMENT NUMBER N/A				
6. AUTHOR(S) Thomas B. Mills, Kyle T. Honeycutt, Scott A. Prost-Domasky, Craig L. Brooks (APES, Inc.); David S. Forsyth, Carl Magnuson (TRI-Austin), Ricardo Actis (ESRD)				5d. PROJECT NUMBER N/A				
				5e. TASK NUMBER N/A				
				5f. WORK UNIT NUMBER N/A				
7. PERFORMING ORGANIZATION NAME(S) AND ADDRESS(ES) APES, Inc. 6669 Fyler Ave. St. Louis, MO 63139				8. PERFORMING ORGANIZATION REPORT NUMBER RIF_CW_R/S_Final				
9. SPONSORING/MONITORING AGENCY NAME(S) AND ADDRESS(ES) Air Force Materiel Command 6057 Box Elder Lane, Bldg 1285 Hill AFB, UT 84056 Attn: Bob Pilarczyk				10. SPONSORING/MONITORING AGENCY ACRONYM(S) AFLCMC/WWAEJ				
				11. SPONSORING/MONITORING AGENCY REPORT NUMBER(S) A3G-2015-185420				
12. DISTRIBUTION/AVAILABILITY STATEMENT Distribution A: Approved for public release; distribution is unlimited. (Ref. #75ABW-2015-0026)								
13. SUPPLEMENTARY NOTES This document contains color.								
14. ABSTRACT The objective of this Rapid Innovation Fund (RIF) program is to integrate finite element simulations of residual stress fields, physically based life prediction methods, and inspections for cold worked (CX) fastener holes into depot maintenance practices. For decades, the aircraft industry has used cold working of fastener holes to enhance the service life (fatigue performance) of critical, highly stressed structure. Although the structure directly benefits and is much less prone to failure, current requirements for structural inspections are very stringent. This is because the current analysis methods used to set inspection intervals do not take into account the beneficial residual stress fields that result from the cold work process. The efforts under this program have shown that the United States Air Force (USAF) can increase inspection intervals by as much as five times if the physically based residual stress fields are incorporated into analysis procedures. This program has successfully integrated a series of tools to accomplish the objective for A-10 application and capture the Return-On-Investment afforded by the implementation.								
15. SUBJECT TERMS structural health, service life prediction, non-destructive inspection, residual stress, cold working								
16. SECURITY CLASSIFICATION OF: <table border="1" style="width: 100%; border-collapse: collapse;"> <tr> <td style="width: 33%; padding: 2px;">a. REPORT UNCLAS</td> <td style="width: 33%; padding: 2px;">b. ABSTRACT UNCLAS</td> <td style="width: 33%; padding: 2px;">c. THIS PAGE UNCLAS</td> </tr> </table>			a. REPORT UNCLAS	b. ABSTRACT UNCLAS	c. THIS PAGE UNCLAS	17. LIMITATION OF ABSTRACT: SAR	18. NUMBER OF PAGES 259	19a. NAME OF RESPONSIBLE PERSON (Monitor) Robert T. Pilarczyk 19b. TELEPHONE NUMBER (Include Area Code) (801) 586-3155
a. REPORT UNCLAS	b. ABSTRACT UNCLAS	c. THIS PAGE UNCLAS						

Standard Form 298 (Rev. 8-98)
Prescribed by ANSI Std. Z39-18

NOTICE AND SIGNATURE PAGE

Using Government drawings, specifications, or other data included in this document for any purpose other than Government procurement does not in any way obligate the U.S. Government. The fact that the Government formulated or supplied the drawings, specifications, or other data does not license the holder or any other person or corporation; or convey any rights or permission to manufacture, use, or sell any patented invention that may relate to them.

Data Rights Legend

Contract Number: FA9453-12C-0218

Contractor Name: APES, Inc.

Contractor Address: 6669 Fyler Ave., St. Louis, MO 63139

Location of Data Rights Information; Page iii

All data generated under the tasks have been developed for the A-10 and shall be nonproprietary (unlimited rights). All existing vendor proprietary data used in the execution of these tasks, such as trade studies, shall be marked as Third Party Proprietary Data and provided to the Government for Government Internal Use Only (not to be disseminated outside the Government). The Government shall have unlimited rights to all intellectual property, material solutions or concepts, including all items, systems, processes, software and technical data developed by the Contractor and/or its subcontractors under this contract. The Government may use any of such items, data, or other property for reprourement or any other purpose as stated in the Defense Federal Acquisition Regulation Supplement (DFARS) definition of “unlimited rights.” The Contractor shall identify and receive written approval from the Procuring Contracting Officer (PCO) prior to committing to the use of any privately developed items, components, processes, computer software and technical data which the Contractor intends to deliver with limited rights, Government purpose rights, or restricted rights. In the case of commercial computer software and documentation, the Government shall have only the rights specified in the license under which the commercial software was obtained (DFARS 227.7202-3). In particular, the data rights for the commercial computer software “StressCheck” and “AFGROW”, presently being used by the A-10 program, shall continue as they presently exist between the USAF and government with the subcontractors, ESRD and LexTech, respectively.

Qualified requestors may obtain copies of this report from the Defense Technical Information Center (DTIC) (<http://www.dtic.mil>).

A3G-2015-185420 HAS BEEN REVIEWED AND IS APPROVED FOR PUBLICATION IN ACCORDANCE WITH ASSIGNED DISTRIBUTION STATEMENT.

Robert Pilarczyk
Lead, A-10 ASIP & Analysis Group
6057 Box Elder Lane, HAFB, UT 84056
AFLCMC/WWAEJ

This report is published in the interest of scientific and technical information exchange, and its publication does not constitute the Government’s approval or disapproval of its ideas or findings.

Table of Contents

List of Figures	viii
List of Tables	xvi
Executive Summary	xxiii
1 Introduction.....	1
1.1 Previous Work	1
1.2 Three Pillars	1
1.2.1 Quality Assurance of Successful Cold Work.....	1
1.2.2 Non-Destructive Inspection of Cracks at Cold Worked Holes	2
1.2.3 Analytical Modeling of Crack Growth through Residual Stress Fields	2
1.3 Benefit to the Warfighter	3
1.3.1 Estimate for Return on Investment	3
1.3.2 Other Benefits	3
1.4 Major Tasks of this Rapid Innovation Program.....	3
2 Basic Material Behavior Tests	4
2.1 Tensile Tests	4
2.2 ASTM E466 Tests for Short Crack Behavior	6
2.2.1 Experimental Procedure.....	7
2.2.2 Test Results	8
2.2.3 Data Reduction Methods.....	9
2.3 Long Crack Behavior.....	20
2.3.1 Test Procedure and Results	21
3 Baseline Cold Worked Hole Behavior Tests	23
3.1 Test Matrix.....	23
3.1.1 Specimen Preparation and CX Procedure.....	26
3.1.2 Test Procedure	29
3.1.3 Experimental Results	29
3.1.4 Discussion of Results	36
4 Residual Stress Measurements & Database.....	37
4.1 Summary of A-10 MODIII Residual Stress Measurements	37
4.2 Coupons from the RIF Program.....	38

4.3	Basics of the Contour Method	41
4.4	Instructions for Data Gathering	41
4.5	Typical Results.....	42
4.6	Residual Stress Database	43
4.6.1	Rules for Processing Files for Inclusion in Residual Stress Database.....	44
4.6.2	Sample Database Images	45
5	Computing Stress Intensity and Crack Front Shape for Cracks in Residual Stress Fields.....	49
5.1	Computation of stress intensity factors.....	49
5.2	Crack Front Shape Progression.....	51
5.2.1	Background	51
5.2.2	Workings of CPT	53
5.3	Summary	61
6	FastenerCam™ Development.....	62
6.1	FastenerCam™ System Details	63
6.2	Laboratory Specimens	69
6.3	Results.....	71
6.4	Conclusions.....	74
7	In-Service NDT Considerations at CX Holes	76
7.1	Introduction.....	76
7.2	Relevant Prior Art	76
7.3	Inspection Techniques	76
7.3.1	Bolt Hole Eddy Current Technique	76
7.3.2	Surface Scan Eddy Current Technique	78
7.3.3	Shear Wave Ultrasonic Technique.....	79
7.4	Specimens	81
7.5	Results.....	85
7.5.1	Preliminary Trials	85
7.5.2	Final Trial - Bolt Hole Eddy Current Results	91
7.5.3	Final Trial - Surface Scan Eddy Current Results.....	101
7.5.4	Final Trial - Ultrasonic Shear Wave Inspection Results.....	106
7.6	Conclusions.....	112
8	Experimental Validation: Crack Growth Modeling in Residual Stress Fields	114

8.1	Edge Margin Testing using CP7 Spectrum.....	114
8.1.1	Specimen Design	114
8.1.2	Test Matrix.....	115
8.1.3	Experimental Results	116
8.1.4	Fatigue Crack Growth Modeling	119
8.2	Coupon Tests for CP-44 Fuselage	123
8.2.1	Specimen Design	123
8.2.2	Spectrum Considerations	125
8.2.3	Test Matrix.....	125
8.2.4	Experimental Results	126
8.2.5	Modeling Results	127
8.2.6	Effects of Retardation	130
8.2.7	Crack Shape Comparison: Analytical vs. Experimental.....	134
8.3	Coupon Tests for T-38 WS63-44% Spar.....	135
8.3.1	Specimen Design	135
8.3.2	Spectrum Considerations	135
8.4	Test Matrix.....	137
8.4.1	Experimental Results	137
8.4.2	Modeling Results	138
9	Conclusions and Recommendations	152
9.1	Conclusions.....	152
9.2	Recommendations.....	154
9.2.1	Technical Challenge: OVERLOADS & UNDERLOADS in SPECTRA .	154
9.2.2	Technical Challenge: LOAD TRANSFER.....	155
9.2.3	Technical Challenge: MULTIPLE ACTIVE CRACKS	155
9.2.4	Technical Challenge: CRACK RETARDATION	155
9.2.5	Technical Challenge: MATERIAL MODEL SENSITIVITY	155
9.2.6	Technical Challenge: STRESS RATIO SHIFT.....	156
9.2.7	Technical Challenge: EFFECT OF CRACKS ON RS REDISTRIBUTION	156
10	References.....	157
11	APPENDIX A: Constant Amplitude CX Fatigue Test Data Tables.....	159
12	APPENDIX B: Fatigue Test Data Tables from Demo Tests	205

13	APPENDIX C: ASTM E 647 Long Crack Data for 2024-T351 and 7075-T651 Aluminum	206
----	---	-----

List of Figures

Figure 1. Tensile test coupon geometry.....	4
Figure 2. Sample force vs. strain plot for tensile coupon 3A1-01-A (2024-T3 aluminum).	6
Figure 3. SENT specimen geometry.....	7
Figure 4. Variable amplitude marker sequence.	8
Figure 5. Typical appearance of marker bands under optical microscopy.	8
Figure 6. Optical fractograph of crack origin and adjacent marker bands in a typical SENT coupon.....	10
Figure 7. Crack growth curves for two SENT coupons tested under identical conditions.	11
Figure 8. da/dN vs. 'a' data for the two coupons.....	11
Figure 9. Overall marker map of a SENT coupon. Axes are in inches.....	12
Figure 10. Marker map zoom from previous figure of bands closest to the crack origin. Axes are in inches.	12
Figure 11. Example of da/dN vs ΔK data as reduced from marker bands. Data are compared to "literature" curve fits.....	13
Figure 12. APES-developed marker band data and MACS-tuned crack growth curve (R = 0.1) compared with various literature "long crack" models and the bounds of the NASA AGARD short crack data for 7075-T6 (Newman and Edwards, 1989).....	15
Figure 13. Historic IDS & MACS compared with EIFS values for RIF SENT coupons (7075-T6/T651).....	16
Figure 14. Historic IDS & MACS compared with EIFS values for RIF SENT coupons (2024-T3/T351).....	16
Figure 15. Crack growth relationships for tuned for short crack behavior (7075- T6/T651).	17
Figure 16. Crack growth relationships for tuned for short crack behavior (2024- T3/T351).	19
Figure 17. Specimen design E2, ASTM E647 middle tension coupon.	21
Figure 18. Long crack growth data for 7075-T651 compared to Harter T and APES material models.....	22
Figure 19. Long crack growth data for 7075-T651 compared to Harter T and APES material models.....	22
Figure 20. AFGROW representation of Marker Block 24.	25
Figure 21. Schematic of the larger dog bone coupon used for CX fatigue tests.....	26
Figure 22. Cold work % associated with different "bins" for nominal 0.25 inch hole.	27

Figure 23. Cold work % associated with different "bins" for nominal 0.375 inch hole..	27
Figure 24. Cold work % associated with different "bins" for nominal 0.5 inch hole.....	28
Figure 25. S-N data for cold work fatigue tests in 2024-T3/T351 aluminum.	33
Figure 26. S-N data for cold work fatigue tests in 2024-T3/T351 aluminum.	33
Figure 27. Cycles to failure as a function of edge margin for the 2024-T3 specimens tested at 22 ksi. Colors indicated degree of cold work (red = 4.3%, blue = 2.8%, green = 3.55%).	34
Figure 28. Cycles to failure as a function of edge margin for the 2024-T3 specimens tested at 25 ksi. Colors indicated degree of cold work (red = 4.3%, blue = 2.8%, green = 3.55%).	34
Figure 29. Log cycles to failure as a function of edge margin for the 7075-T6 specimens tested at 24 ksi. Colors indicated degree of cold work (red = 4.3%, blue = 2.8%, green = 3.55%).	35
Figure 30. Log cycles to failure as a function of edge margin for the 7075-T6 specimens tested at 26.5 ksi. Colors indicated degree of cold work (red = 4.3%, blue = 2.8%, green = 3.55%).	35
Figure 31. Residual stress in two 7075-T651 coupons of different thickness. Coupon on the left is 0.19" thick; the one on the right is 0.436 inch thick. Note that both reach their maximum residual stress on the bore (x axis) at approximately 0.12 inch away from the mandrel entrance face (right side of each image).	36
Figure 32. Contour Method (a) provides good correlation to Neutron Diffraction (b) at lower cost (after DeWald et al., 2009).	41
Figure 33. Typical four-pane view of RS distribution from MatLab visualizer tool used during this program.	42
Figure 34. Typical database view including menu of conditions at left.	46
Figure 35. Four independent data sets that define the interpolation space for the distribution in Figure 36.	47
Figure 36. Interpolated surface from the four database entries in Figure 35.	48
Figure 37. Interpolation parameters associated with Figure 36, above.	48
Figure 38: The modified J-integral	49
Figure 39: principle of superposition to compute SIF due to residual stresses	50
Figure 40: The Contour Integral Method for loaded cracks	50
Figure 41: Residual stress by simulation of cold work process.	51
Figure 42: Stress intensity factors due to residual stresses for a 0.025" corner crack	51
Figure 43. Typical crack shape in a cold-worked hole.	52
Figure 44: CPT Input - Dimensions	54
Figure 45: CPT Input - Material properties	55

Figure 46: CPT Input - Residual stresses.....	56
Figure 47: CPT Input - Loading.....	57
Figure 48: CPT Input - Solver Options.....	58
Figure 49: CPT Output - Crack fronts and Length vs Cycles.....	59
Figure 50: CPT Prediction for a non-cold worked specimen	59
Figure 51: CPT prediction for a cold worked specimen	60
Figure 52: Comparison of a crack front map with prediction.....	60
Figure 53. Deformation around cold worked straight shank fastener holes with different amounts of cold expansion. The left image is out of specification; the right image is in specification. Location of split sleeve “pip” can clearly be seen at the top of each image.....	63
Figure 54: FastenerCam™ Carriage	63
Figure 55: FastenerCam™ Connector Cables	64
Figure 56: FastenerCam™ Power and Communications Box	64
Figure 57: FastenerCam™ Control Interface	65
Figure 58: Window showing that the FastenerCam™ is in Scanning mode and receiving data.....	66
Figure 59: Links to both the Profile Plot and Data for the area just scanned	66
Figure 60: Image of a scanned fastener hole generated by the web interface	67
Figure 61: FastenerCam™ configuration menu.....	67
Figure 62: Proper triggering configuration	68
Figure 63: Proper encoder configuration	69
Figure 64. Hole Pattern 1 for the test plates.....	70
Figure 65. Hole Pattern 2.....	71
Figure 66: Scaling factor (F) used when determining the amount of cold expansion for the holes in the sample plates.	72
Figure 67: The difference between the measured and expected percent of cold expansion per hole diameter for every hole in each of the four difference plate thicknesses....	73
Figure 68. The amount of cold expansion of each hole as measured by FastenerCam™. There is a clear separation between the red 'out-of-spec' points and the green 'in-spec' points.	74
Figure 69. Equipment for the ET – Bolt Hole inspection of cold worked holes specimens.	77
Figure 70. Results of the inspection of the 0.030" by 0.030" inter face notch on the Air force standard block.....	77

Figure 71. Equipment for the ET - SS inspection of cold worked hole specimens.	78
Figure 72. Results of the inspection of the 0.020" and 0.010" deep notches on the Air Force standard block	78
Figure 73. Illustration of the outlining of crack indications.	79
Figure 74. Equipment for the UT – Shear Wave inspection of cold worked hole specimens.....	80
Figure 75. Results of the inspection of a 0.050" corner EDM notch on a TRI coupon...	81
Figure 76. Photograph of one of the target specimens, and a diagram indicating how The possible crack locations are labeled.....	81
Figure 77. A histogram of the crack sizes in the specimen set.	82
Figure 78. A photograph of the facilities for the preliminary trials.....	86
Figure 79. Change in ET-BH signal due to applied load is minimal.....	87
Figure 80. Change in UT signal due to applied load.	88
Figure 81. ET-BH signal for different crack sizes and applied stresses.	89
Figure 82. UT results for different crack sizes and applied stresses.....	90
Figure 83. UT results for different crack sizes and applied stresses.....	90
Figure 84. UT results for different crack sizes and applied stresses.....	91
Figure 85. Eddy Current signal from a 0.018" by 0.026" corner crack, gain increased from setup to show signal better.	92
Figure 86. A log-log model of the 200 kHz ET-BH data.	94
Figure 87. POD fit to all ET – BH 200 kHz data.....	94
Figure 88. ET signal as a Function of Crack Length for 0.278" Diameter Holes and 200 kHz Excitation Frequency.....	95
Figure 89. ET signal as a Function of Crack Length for 0.278" Diameter Holes and 500 kHz Excitation Frequency.....	96
Figure 90. ET signal as a Function of Crack Length for 0.418" Diameter Holes and 200 kHz Excitation Frequency.....	97
Figure 91. ET signal as a Function of Crack Length for 0.418" Diameter Holes and 500 kHz Excitation Frequency.....	98
Figure 92. ET signal as a Function of Crack Length for 0.538" Diameter Holes and 200 kHz Excitation Frequency.....	99
Figure 93. ET signal as a Function of Crack Length for 0.538" Diameter Holes and 500 kHz Excitation Frequency.....	100
Figure 94. Eddy Currents Decay Faster at Higher Frequencies.....	101
Figure 95. Specimen with large crack that measures 0.8" on mandrel entrance face (location with tape measure) broken open to illustrate how crack has yet to pop	

through to mandrel exit face (inspectable side using ET-SS). Plastic zone from the barely-subsurface crack was visible on the surface, but this crack was not detectable using ET-SS.	102
Figure 96. The Complete Set of Results of ET-SS Inspections of the Coupons.	103
Figure 97. The Complete Set of Results of ET-SS Inspections of the Coupons With the 0.100" Thick Coupon Data Plotted in Red	103
Figure 98. Marker band map showing crack shape from CX hole in 0.1" thick material.	104
Figure 99. POD Estimate for ET-SS Inspection of 0.100" Thick Specimens	105
Figure 100. Comparison of the Crack Lengths on the Hole Bore and the Surface.....	106
Figure 101. UT Response as a Function of Crack Length.....	107
Figure 102. POD Estimate for the UT Detection of Cracks as a Function of Crack Length on the Specimen Mandrel Entrance Surface	108
Figure 103. POD Estimate for the UT Detection of Cracks as a Function of Crack Length on the Specimen Mandrel Entrance Surface, for 0.100" Thick Coupons.....	109
Figure 104. POD Estimate for the UT Detection of Cracks as a Function of Crack Length on the Specimen Mandrel Entrance Surface, for Both 0.313" and 0.500" Thick Coupons	110
Figure 105. Residual stress profile at 0.375" hole in 0.1" sheet. Lines for a90 and a90/95 shows that residual stresses range from neutral to slightly tensile at these crack sizes.	111
Figure 106. Residual stress profile at 0.375" hole in 0.5" plate. Lines for a90 and a90/95 shows that residual stresses range from neutral to slightly tensile at these crack sizes.	112
Figure 107. Schematic of cold-work fatigue coupon. Each coupon had one 0.25 inch hole (final ream diameter) at various locations based on target edge margin.	115
Figure 108. AFGROW representation of CP7 spectrum showing the marker band at the end.....	116
Figure 109. Crack growth curves for CP7 spectrum tests, $e/D = 1.39$	117
Figure 110. Crack growth curves for CP7 spectrum tests, $e/D = 1.8$	117
Figure 111. Crack growth curves for CP7 spectrum tests, $e/D = 2.4$	118
Figure 112. Life improvement factors for various edge margins referenced to "no CX" in each category.	119
Figure 113. Mandrel entrance face crack growth vs. flight hours. Experimental data are compared with legacy ASIP approach and with CPT prediction, $e/D = 1.4$. Predicted curve is from BAMF.....	120

Figure 114. Mandrel entrance face crack growth vs. flight hours. Experimental data are compared with legacy ASIP approach and with CPT prediction, $e/D = 1.8$. Predicted curve is from BAMF.....	121
Figure 115. Mandrel entrance face crack growth vs. flight hours. Experimental data are compared with legacy ASIP approach and with CPT prediction, $e/D = 2.4$. Predicted curve is from BAMF.....	121
Figure 116. Marker band map from fracture face of $e/D = 1.8$ coupon. Dashed line represents a crack linking line with an active secondary crack.	122
Figure 117. Predicted crack shape from $e/D = 1.8$ coupon.....	122
Figure 118. Cross-section of the location as represented in the DTA AFGROW model.	124
Figure 119. Cross-section of actual coupon in the region of interest (non-CX condition).	124
Figure 120. Specimen planform. Hole diameter varies based on condition. Dimensions are in inches.	125
Figure 121. Crack length vs. flight hours for all CP44 tests (28 ksi) along with baseline DADTA prediction (24.3 ksi) and baseline DADTA prediction at the revised, higher stress (28 ksi).	126
Figure 122. Crack length vs. flight hours for non-CX tests vs. AFGROW simulation of same condition. AFGROW model used Generalized Willenborg model parameters ($SOLR = 1.6$) from the DADTA. Results are reasonable.....	127
Figure 123. Experimental results compared with non-CX DADTA prediction, Legacy CX assessment (using initial crack size of 0.005 inch and no RS), and a BAMF analysis. BAMF is conservative but does not use retardation.	128
Figure 124. Experimental results compared with non-CX DADTA prediction, Legacy CX assessment (using initial crack size of 0.005 inch and no RS), and a BAMF analysis. BAMF is conservative but does not use retardation.	129
Figure 125. Experimental results compared with non-CX DADTA prediction, Legacy CX assessment (using initial crack size of 0.005 inch and no RS), and a BAMF analysis. BAMF is conservative but does not use retardation.	130
Figure 126. Experimental result for CX coupon compared with analytical results that show the influence of retardation parameters. Retardation parameter for the CX analysis is the same as that used in the in the non-CX DADTA analysis (not retuned). Predicted / Actual Life Ratio is now 75%.	131
Figure 127. Experimental result for CX coupon compared with analytical results that show the influence of retardation parameters. Retardation parameter for the CX analysis is the same as that used in the in the non-CX DADTA analysis (not retuned). Predicted / Actual Life Ratio is now 90% for this case.....	132
Figure 128. Experimental result for CX coupon compared with analytical results that show the influence of retardation parameters. Retardation parameter for the CX	

analysis is the same as that used in the in the non-CX DADTA analysis (not returned). Predicted / Actual Life Ratio is now 98% for this case.....	133
Figure 129. Key take-away points for CX analysis with retardation included.....	134
Figure 130. Comparison of crack shapes between BAMF (left) and experiment (right). Despite multiple site cracking that occurs in reality, crack shapes match well.....	134
Figure 131. Specimen planform. Thickness is 0.25 inch. Final hole diameter is 0.25”	136
Figure 132. Truncated fatigue spectrum as visualized in AFGROW.	136
Figure 133. Experimental data from WS63-44% spar tests. Three groups segregate nicely based on interference level, the only variable.....	137
Figure 134. Crack growth behavior for two different material models at $R = -0.3$	138
Figure 135. Crack growth behavior for two different material models at $R = -0.8$	139
Figure 136. Experimental and analytical crack length vs. spectrum flight hours for MAX CX condition. A Legacy ASIP assessment is also included for reference. The predicted data convention in the legend uses fatigue coupon first (to define initial crack size and shape) and residual stress distribution second.....	140
Figure 137. Experimental and analytical crack length vs. spectrum flight hours for MAX CX condition. A Legacy ASIP assessment is also included for reference. The predicted data convention in the legend uses fatigue coupon first (to define initial crack size and shape) and residual stress distribution second.....	141
Figure 138. Experimental and analytical crack length vs. spectrum flight hours for MAX CX condition. A Legacy ASIP assessment is also included for reference. The predicted data convention in the legend uses fatigue coupon first (to define initial crack size and shape) and residual stress distribution second.....	142
Figure 139. Experimental and analytical crack length vs. spectrum flight hours for MAX CX condition. A Legacy ASIP assessment is also included for reference. The predicted data convention in the legend uses fatigue coupon first (to define initial crack size and shape) and residual stress distribution second.....	143
Figure 140. Experimental and analytical crack length vs. spectrum flight hours for MID CX condition. A Legacy ASIP assessment is also included for reference. The predicted data convention in the legend uses fatigue coupon first (to define initial crack size and shape) and residual stress distribution second.....	144
Figure 141. Experimental and analytical crack length vs. spectrum flight hours for MID CX condition. A Legacy ASIP assessment is also included for reference. The predicted data convention in the legend uses fatigue coupon first (to define initial crack size and shape) and residual stress distribution second.....	145
Figure 142. Experimental and analytical crack length vs. spectrum flight hours for MID CX condition. A Legacy ASIP assessment is also included for reference. The predicted data convention in the legend uses fatigue coupon first (to define initial crack size and shape) and residual stress distribution second.....	146

- Figure 143. Experimental and analytical crack length vs. spectrum flight hours for MID CX condition. A Legacy ASIP assessment is also included for reference. The predicted data convention in the legend uses fatigue coupon first (to define initial crack size and shape) and residual stress distribution second..... 147
- Figure 144. Experimental and analytical crack length vs. spectrum flight hours for MIN CX condition. A Legacy ASIP assessment is also included for reference. The predicted data convention in the legend uses fatigue coupon first (to define initial crack size and shape) and residual stress distribution second..... 148
- Figure 145. Experimental and analytical crack length vs. spectrum flight hours for MIN CX condition. A Legacy ASIP assessment is also included for reference. The predicted data convention in the legend uses fatigue coupon first (to define initial crack size and shape) and residual stress distribution second..... 149
- Figure 146. Experimental and analytical crack length vs. spectrum flight hours for MIN CX condition. A Legacy ASIP assessment is also included for reference. The predicted data convention in the legend uses fatigue coupon first (to define initial crack size and shape) and residual stress distribution second..... 150
- Figure 147. Experimental and analytical crack length vs. spectrum flight hours for MIN CX condition. A Legacy ASIP assessment is also included for reference. The predicted data convention in the legend uses fatigue coupon first (to define initial crack size and shape) and residual stress distribution second..... 151

List of Tables

Table 1. Minimum ROI Calculation for A-10 Fleet.	3
Table 2. ASTM E8-08 test results.....	5
Table 3. Fatigue life results from E466 SENT tests.	9
Table 4. Crack growth curve fits for 7075-T651	18
Table 5. Crack growth curve fits for 2024-T351	20
Table 6. Test matrix for 7075-T6 & T651 coupons. “CA Stress” refers to the constant amplitude cycles between marker bands, whereas “Max Stress” refers to the stress at the 15% overload.	24
Table 7. Test matrix for 2024-T3 & T351 coupons.....	24
Table 8. Factor levels for experimental design, which is repeated for each major alloy type and stress level. *The center point runs had 5 replicates for the high and low stress in 2024-T351 (see Table 5).....	25
Table 9. Degree of CX expected for each of the bins and for each hole diameter.	26
Table 10. Summary of fatigue results from basic cold worked hole experiments, 2024.	30
Table 11. Summary of fatigue results from basic cold worked hole experiments, 7075.	31
Table 12. Summary of earlier residual stress data gathered by USAF and Hill Engineering (other contracts).....	38
Table 13. Details of first specimen group for residual stress measurement.	39
Table 14. Details of second specimen group for residual stress measurement.....	40
Table 15. Metrology of the initial reamer, initial hole diameters, and resulting CX for the class/type hole combinations for Pattern 1.	70
Table 16. Metrology of the initial reamer, initial hole diameters, and resulting CX for the class/type hole combinations for Pattern 2.	71
Table 17. Crack key for NDT coupons. Many coupons deliberately contain no cracks. .	82
Table 18. GLM Fit to the ET-BH Results.....	92
Table 19. GLM fit to the ET-BH results with frequency removed.....	93
Table 20. GLM Fit to the UT Results	108
Table 21. Comparison of experimental and predicted lives. Predicted lives underestimate experimental, but no retardation was used in predictions.	120
Table 22. Predicted SFH to failure using BAMF and CPT compared with experimental results. Note three different analysts produced similar results with two different codes.	128
Table 23. Modeling results compared with experiment for the WS63-44% spar.....	140
Table 24. Test Data, coupon 3D1-16-A.....	159

Table 25. Test Data, coupon 3D1-17-A.....	159
Table 26. Test Data, coupon 3D1-18-A.....	160
Table 27. Test Data, coupon 3D1-13-A.....	160
Table 28. Test Data, coupon 3D1-14-A.....	160
Table 29. Test Data, coupon 3D1-15-A.....	161
Table 30. Test Data, coupon 3D1-02-A.....	161
Table 31. Test Data, coupon 3D1-03-A.....	161
Table 32. Test Data, coupon 3D1-07-A.....	162
Table 33. Test Data, coupon 3D1-08-A.....	162
Table 34. Test Data, coupon 3D1-09-A.....	162
Table 35. Test Data, coupon 3D1-01-A.....	163
Table 36. Test Data, coupon 3D1-19-A.....	164
Table 37. Test Data, coupon 3D1-04-A.....	165
Table 38. Test Data, coupon 3D1-05-A.....	165
Table 39. Test Data, coupon 3D1-06-A.....	166
Table 40. Test Data, coupon 3D1-10-A.....	166
Table 41. Test Data, coupon 3D1-11-A.....	166
Table 42. Test Data, coupon 3D1-12-A.....	167
Table 43. Test Data, coupon 3D3-19-A.....	167
Table 44. Test Data, coupon 3D3-20-A.....	167
Table 45. Test Data, coupon 3D3-21-A.....	168
Table 46. Test Data, coupon 3D3-11-A.....	168
Table 47. Test Data, coupon 3D3-12-A.....	168
Table 48. Test Data, coupon 3D3-13-A.....	169
Table 49. Test Data, coupon 3D3-14-A.....	169
Table 50. Test Data, coupon 3D3-15-A.....	169
Table 51. Test Data, coupon 3D1-06-B.....	170
Table 52. Test Data, coupon 3D1-12-B.....	170
Table 53. Test Data, coupon 3D1-01-B.....	171
Table 54. Test Data, coupon 3D1-02-B.....	171
Table 55. Test Data, coupon 3D1-03-B.....	172
Table 56. Test Data, coupon 3D1-04-B.....	172

Table 57. Test Data, coupon 3D1-05-B.	173
Table 58. Test Data, coupon 3D1-07-B.	173
Table 59. Test Data, coupon 3D1-08-B.	173
Table 60. Test Data, coupon 3D1-09-B.	174
Table 61. Test Data, coupon 3D1-10-B.	174
Table 62. Test Data, coupon 3D1-11-B.	174
Table 63. Test Data, coupon 3D1-35-B.	175
Table 64. Test Data, coupon 3D1-36-B.	175
Table 65. Test Data, coupon 3D1-37-B.	175
Table 66. Test Data, coupon 3D1-38-B.	176
Table 67. Test Data, coupon 3D1-39-B.	176
Table 68. Test Data, coupon 3D1-40-B.	176
Table 69. Test Data, coupon 3D1-44-B.	177
Table 70. Test Data, coupon 3D1-45-B.	177
Table 71. Test Data, coupon 3D1-46-B.	177
Table 72. Test Data, coupon 3D1-50-B.	178
Table 73. Test Data, coupon 3D1-51-B.	178
Table 74. Test Data, coupon 3D1-52-B.	178
Table 75. Test Data, coupon 3D1-59-B.	178
Table 76. Test Data, coupon 3D1-60-B.	179
Table 77. Test Data, coupon 3D1-41-B.	179
Table 78. Test Data, coupon 3D1-42-B.	179
Table 79. Test Data, coupon 3D1-43-B.	180
Table 80. Test Data, coupon 3D1-47-B.	180
Table 81. Test Data, coupon 3D1-48-B.	180
Table 82. Test Data, coupon 3D1-49-B.	181
Table 83. Test Data, coupon 3D1-17-B.	181
Table 84. Test Data, coupon 3D1-18-B.	181
Table 85. Test Data, coupon 3D1-30-B.	182
Table 86. Test Data, coupon 3D1-16-B.	182
Table 87. Test Data, coupon 3D1-28-B.	182
Table 88. Test Data, coupon 3D1-29-B.	183

Table 89. Test Data, coupon 3D1-15-B.....	183
Table 90. Test Data, coupon 3D1-16-C.....	183
Table 91. Test Data, coupon 3D1-17-C.....	184
Table 92. Test Data, coupon 3D1-18-C.....	184
Table 93. Test Data, coupon 3D1-13-C.....	184
Table 94. Test Data, coupon 3D1-14-C.....	185
Table 95. Test Data, coupon 3D1-15-C.....	185
Table 96. Test Data, coupon 3D1-01-C.....	185
Table 97. Test Data, coupon 3D1-02-C.....	186
Table 98. Test Data, coupon 3D1-03-C.....	186
Table 99. Test Data, coupon 3D1-07-C.....	186
Table 100. Test Data, coupon 3D1-08-C.....	187
Table 101. Test Data, coupon 3D1-09-C.....	187
Table 102. Test Data, coupon 3D1-04-C.....	187
Table 103. Test Data, coupon 3D1-26-C.....	188
Table 104. Test Data, coupon 3D1-05-C.....	188
Table 105. Test Data, coupon 3D1-06-C.....	189
Table 106. Test Data, coupon 3D1-10-C.....	189
Table 107. Test Data, coupon 3D1-11-C.....	190
Table 108. Test Data, coupon 3D1-12-C.....	190
Table 109. Test Data, coupon 3D3-10-C.....	190
Table 110. Test Data, coupon 3D3-11-C.....	191
Table 111. Test Data, coupon 3D3-12-C.....	191
Table 112. Test Data, coupon 3D3-13-C.....	192
Table 113. Test Data, coupon 3D3-14-C.....	192
Table 114. Test Data, coupon 3D3-15-C.....	192
Table 115. Test Data, coupon 3D1-05-D.....	193
Table 116. Test Data, coupon 3D1-06-D.....	193
Table 117. Test Data, coupon 3D1-07-D.....	193
Table 118. Test Data, coupon 3D1-01-D.....	194
Table 119. Test Data, coupon 3D1-02-D.....	194
Table 120. Test Data, coupon 3D1-03-D.....	194

Table 121. Test Data, coupon 3D1-11-D.....	194
Table 122. Test Data, coupon 3D1-12-D.....	195
Table 123. Test Data, coupon 3D1-13-D.....	195
Table 124. Test Data, coupon 3D1-14-D.....	195
Table 125. Test Data, coupon 3D1-15-D.....	196
Table 126. Test Data, coupon 3D1-16-D.....	196
Table 127. Test Data, coupon 3D1-20-D.....	196
Table 128. Test Data, coupon 3D1-21-D.....	197
Table 129. Test Data, coupon 3D1-22-D.....	197
Table 130. Test Data, coupon 3D1-26-D.....	197
Table 131. Test Data, coupon 3D1-27-D.....	198
Table 132. Test Data, coupon 3D1-28-D.....	198
Table 133. Test Data, coupon 3D1-29-D.....	198
Table 134. Test Data, coupon 3D1-30-D.....	199
Table 135. Test Data, coupon 3D1-17-D.....	199
Table 136. Test Data, coupon 3D1-18-D.....	199
Table 137. Test Data, coupon 3D1-19-D.....	199
Table 138. Test Data, coupon 3D1-23-D.....	200
Table 139. Test Data, coupon 3D1-24-D.....	200
Table 140. Test Data, coupon 3D1-25-D.....	200
Table 141. Test Data, coupon 3D3-14-D.....	201
Table 142. Test Data, coupon 3D3-16-D.....	202
Table 143. Test Data, coupon 3D3-28-D.....	202
Table 144. Test Data, coupon 3D3-13-D.....	203
Table 145. Test Data, coupon 3D3-30-D.....	203
Table 146. Test Data, coupon 3D3-17-D.....	203
Table 147. Test Data, coupon 3D3-18-D.....	204
Table 148. Test Data, coupon 3D3-29-D.....	204
Table 149. Test Data, coupon 3D2-01-B.....	205
Table 150. Test Data, coupon 3D2-02-B.....	205
Table 151. Test Data, coupon 3D2-03-B.....	205
Table 152. Test Data, coupon 3D2-04-B.....	205

Table 153. Test Data, coupon 3D2-05-B.	205
Table 154. Test Data, coupon 3D2-06-B.	205
Table 155. Test Data, coupon 3D2-07-B.	205
Table 156. Test Data, coupon 3D2-08-B.	205
Table 157. Test Data, coupon 3D2-09-B.	205
Table 158. Test Data, coupon 3D2-10-B.	205
Table 159. Test Data, coupon 3D2-11-B.	205
Table 160. Test Data, coupon 3D2-12-B.	205
Table 161. Test Data, coupon 3D2-14-B.	205
Table 162. Test Data, coupon 3D2-17-B.	205
Table 163. Test Data, coupon 3D2-15-B.	205
Table 164. Test Data, coupon 3D2-16-B.	205
Table 165. Test Data, coupon 3D2-20-B.	205
Table 166. Test Data, coupon 3D2-21-B.	205
Table 167. Test Data, coupon 3D2-22-B.	205
Table 168. Test Data, coupon 3D2-23-B.	205
Table 169. Test Data, coupon 3D2-24-B.	205
Table 170. Test Data, coupon 3D2-25-B.	205
Table 171. Test Data, coupon 3D2-26-B.	205
Table 172. Test Data, coupon 3D2-27-B.	205
Table 173. Test Data, coupon 3-CP44-01.	205
Table 174. Test Data, coupon 3-CP44-03.	205
Table 175. Test Data, coupon 3-CP44-05.	205
Table 176. Test Data, coupon 3-CP44-06.	205
Table 177. Test Data, coupon 3-CP44-09.	205
Table 178. Test Data, coupon 3-CP44-10.	205
Table 179. Test Data, coupon 3-CP44-13.	205
Table 180. Test Data, coupon 3-CP44-14.	205
Table 181. Test Data, coupon T38-WS63-01.	205
Table 182. Test Data, coupon T38-WS63-02.	205
Table 183. Test Data, coupon T38-WS63-05.	205
Table 184. Test Data, coupon T38-WS63-06.	205

Table 185. Test Data, coupon T38-WS63-09.	205
Table 186. Test Data, coupon T38-WS63-10.	205
Table 187. Crack growth data from M(T) panels, 2024-T351.	206
Table 188. Continuation of Table 187. Crack growth data from M(T) panels, 2024-T351.	207
Table 189. Crack growth data from M(T) panels, 7075-T651.	208
Table 190. Continuation of Table 189. Crack growth data from M(T) panels, 7075-T651	209
Table 191. Continuation of Table 190. Crack growth data from M(T) panels, 7075-T651	210

Executive Summary

The objective of this Rapid Innovation Fund (RIF) program is to integrate finite element simulations of residual stress fields, physically based life prediction methods, and inspections for cold worked (CX) fastener holes into depot maintenance practices. For decades, the aircraft industry has used cold working of fastener holes to enhance the service life (fatigue performance) of critical, highly stressed structure. Although the structure directly benefits and is much less prone to failure, current requirements for structural inspections are very stringent. This is because the current analysis methods used to set inspection intervals do not take into account the beneficial residual stress fields that result from the cold work process.

The efforts under this program have shown that the United States Air Force (USAF) can increase inspection intervals by as much as five times if physically based residual stress fields are incorporated into analysis procedures. More importantly, however, the new methodology developed here provides a physical aspect to life assessment (the actual residual stress field) and provides enough margin that CX analyses can use the same 0.05” crack size assumption at a bolt hole that are used at a non-CX hole. Current Aircraft Structural Integrity Program (ASIP) methods for CX holes use a smaller initial crack size that is not physically based, is beyond the capability of current non-destructive inspection capabilities, and can either be overly conservative (under predicting) in some scenarios, and unconservative (over predicting) in others.

The construct of this technology evolution requires three pillars to not only provide assessment capabilities and rules, but to provide risk mitigation as well. After all, the goal here is to push inspection intervals out, to reduce maintenance costs, to increase asset availability, and to not incur unacceptable risk. These three pillars are:

1. Quality Assurance
2. Non-destructive inspection
3. Analysis Tools and Methods for Crack Growth in Residual Stress Fields

The target solution set for this effort addressed straight shank, open holes in 2024-T351 aluminum and 7075-T651 aluminum.

Quality Assurance for Cold Worked Holes

In the past, these residual stress fields have not been included because of a perceived risk to safety (e.g., the risk that the mechanic did not properly cold work a critical location). Although the manufacturers of the hardware used for cold working have tools used to check the presence of cold work, APES proposed to further this quality control capability through rapid scan, semi-automated, laser inspection of the cold worked holes at a key step in the cold work process. These procedures produce a digital documentation of the hole, based on critical metrology, which can be linked with maintenance records. Chapter 6 provides a summary of the product and data developed in support of this technology area.

The FastnerCam™ prototype developed for this effort currently can measure the amount of cold expansion around fastener holes to within 0.5% for diameters over 0.246 inch and in plate thicknesses 0.19 inch or greater. For this project, the prototype was demonstrated using aluminum alloys 2024-T351 and 7075-T651.

The scaling factor used to determine the amount of cold expansion based on the amount of deformed material around the fastener hole was determined experimentally using only three different plate thicknesses. In order to better understand how the scaling factor depends on the plate thickness, more samples of varying plate thicknesses need to be examined.

Finally, if FastnerCam™ is to be used to measure the amount of cold-work around small (with diameters less than 0.246”) fastener holes, its resolution will need to be improved.

In its current form, this tool provides an effective method for establishing pass / fail for a cold worked hole and for recording the data for further use. Utility of the system would be greatly enhanced by increasing resolution and by modifying the function of the system to be non-contact. Both of these possibilities are being examined by the subcontractor, TRI-Austin, for future development.

Non-Destructive Inspection of Cracks at Cold Worked Holes

Another important aspect of the program is inspection for cracks emanating from cold worked fastener holes. Cracks in these residual stress fields take on unique shapes and behaviors as compared to cracks at unworked holes. The objective of this effort was to look at three common non-destructive inspection (NDI) methods used around fastener holes and determine what limitations might exist that would require changes in how these methods are used in locations that are cold worked. The three methods were:

1. Bolt-hole eddy current (ET -- BH)
2. Surface scan eddy Current (ET – SS)
3. Ultrasound (UT)

The results of this study are presented in detail in Chapter 7. Important conclusions from this effort are summarized here:

- ET methods were insensitive to applied loads on a fatigue crack.
- UT methods were very sensitive to applied external loads on a fatigue crack.
- As described in detail in other sections of the final report, cracks generally form at the mandrel entry surface and grow to a significant length before breaking through to the mandrel exit surface. The mandrel exit surface is the one typically accessible for NDI.
- Existing fatigue cracks become easier to detect after CX process.
- ET – BH techniques are not significantly affected by the CX process. The capability guidelines for ET - BH listed in the Structures Bulletin EN-SB-012 can still be applied for aluminum structure.

- ET – SS techniques are affected, due to the change in crack shape. ET – SS inspections will normally be conducted from the mandrel exit face of a CX hole. Fatigue cracks growing in a CX hole in thick structure can become very large without breaking through the mandrel exit face.
 - For aluminum structures of 0.100” or thinner, a reliable detectable crack size of 0.250” in length is reasonable.
 - For aluminum structures of greater than 0.100” thickness, ET – SS applied to the mandrel exit face is not reliable at reasonable crack sizes.
- UT techniques are affected by the CX process. There is a difference between the 0.100” thick specimens and the 0.313” and 0.500” thick specimens evaluated in this work.
 - For aluminum structures of 0.100” or thinner, a detectable crack size of 0.250” length is reasonable.
 - For aluminum structures of greater than 0.100” thickness, a detectable crack size of 0.300” length is reasonable.

Analytical Modeling of Crack Growth through Residual Stress Fields

The technical approach includes enhancements to the StressCheck finite element code for determining stress intensity factors in residual stress fields and the integration of that software package with the commercially-available crack growth code, AFGROW. Provisions were also made to incorporate highly irregular crack shapes associated with cold-worked holes into StressCheck via two separate plug-ins: (1) the Crack Propagation Tool (CPT) developed by team-member Engineering Software Research & Development, Inc. (ESRD) and (2) the Broad Application for Modeling Failure (BAMF), a code developed by the A-10 and T-38 ASIP support groups.

In addition to software enhancements, a residual stress database has been developed and populated during this program. The database supports some common aluminum alloys used in aircraft and addresses variations in material thickness, hole diameter, edge margin, and cold work interference level. The database is easily expandable by the customer. The determination of residual stress uses an advanced measurement technique called the “Contour Method”, a method proven to deliver high-density, two-dimensional representations of residual stress states resulting from the cold work process.

These residual stress inputs have been combined with the analysis suite described above to predict the performance of simulated aircraft components under fatigue load environments, including load spectra specific to wing and fuselage structure on several USAF aircraft.

In most every case, the new methods using BAMF and CPT outperform the legacy ASIP method. However, without crack retardation, the predictions using residual stress tend to fall short of the experimental data by a factor of three.

Important analysis infrastructure has been built and delivered under this program including:

- A residual stress database of common hole diameters, edge margins, and plate thicknesses for 2024-T351 and 7075-T651 aluminum (primarily).
- Two different methods for calculating stress intensity factors for cracks in residual stress fields. Both methods have been incorporated into the fracture mechanics module that is commercially available with StressCheck v10.1
- Two separate crack growth engines for doing the multipoint crack progression necessary for allowing cracks form realistic shapes in simulation.

The typically excellent crack shape agreement we see between experiment and analysis have provided a strong validation of the shape of the residual stress being produced by the Contour Method. There still appears to be a fair amount of variability in the RS magnitude even amongst replicates. At this point we do not know how much of variability results from uncertainty in measurement and how much of it originates in the cold work process itself.

1 Introduction

The objective of this Rapid Innovation Fund (RIF) program is to integrate finite element simulations of residual stress fields, physically based life prediction methods, and inspections for cold worked (CX) fastener holes into depot maintenance practices. For decades, the aircraft industry has used cold working of fastener holes to enhance the service life (fatigue performance) of critical, highly stressed structure. Although the structure directly benefits and is much less prone to failure, current requirements for structural inspections are very stringent. This is because the current analysis methods used to set inspection intervals do not take into account the beneficial residual stress fields that result from the cold work process.

1.1 Previous Work

Analytical Processes/Engineered Solutions, Inc. (APES) conducted several research projects related to engineered residual stress during the last five years including a Small Business Innovation Research (SBIR) Phase I related to laser peening (contract FA8117-09-C006) and a SBIR Phase I, SBIR Phase II, and SBIR Phase-II add-on contract (#s FA8650-08-M-3842, FA8650-09-C-3941, and FA8650-04-D-3446/0042, respectively) related to cold worked holes. These efforts have shown that the United States Air Force (USAF) can increase inspection intervals by as much as five times if physically based residual stress fields are incorporated into analysis procedures.

1.2 Three Pillars

The construct of this technology evolution requires three pillars to not only provide assessment capabilities and rules, but to provide risk mitigation as well. After all, the goal here is to push inspection intervals out, to reduce maintenance costs, to increase asset availability, and to not incur unacceptable risk. These three pillars are:

1. Quality Assurance
2. Non-destructive inspection
3. Analysis Tools and Methods for Crack Growth in Residual Stress Fields

The target solution set for this effort addressed straight shank, open holes in 2024-T351 aluminum and 7075-T651 aluminum.

1.2.1 Quality Assurance of Successful Cold Work

In the past, these residual stress fields have not been included because of a perceived risk to safety (e.g., the risk that the mechanic did not properly cold work a critical location). Although the manufacturers of the hardware used for cold working have tools used to check the presence of cold work, APES proposed to further this quality control capability through rapid scan, semi-automated, laser inspection of the cold worked holes at a key step in the cold work process. These procedures produce a digital documentation of the hole, based on critical metrology, which can be linked with maintenance records. Chapter 6 provides a summary of the product and data developed in support of this technology area.

1.2.2 Non-Destructive Inspection of Cracks at Cold Worked Holes

Another important aspect of the program is inspection for cracks emanating from cold worked fasteners holes. Cracks in these residual stress fields take on unique shapes and behaviors as compared to cracks at unworked holes. The objective of this effort was to look at three common non-destructive inspection methods used around fastener holes and determine what limitations might exist that would require changes in how these methods are used in locations that are cold worked. The three methods were:

1. Bolt-hole eddy current
2. Surface scan eddy Current
3. Ultrasound

The results of this study are presented in detail in Chapter 7.

1.2.3 Analytical Modeling of Crack Growth through Residual Stress Fields

The USAF has expressed considerable interest for the development of analytical methods that allow for effective modeling of crack growth through residual stress fields. Our team's technical approach gathered the support of the USAF A-10, T-38, & F-16 Aircraft Structural Integrity Program (ASIP) managers and engineers as well as the Air Force Life Cycle Management Center (AFLCMC) Technical Engineering Services Directorate. Collectively, these three ASIP offices are responsible for nearly 2000 USAF aircraft.

The technical approach includes enhancements to the StressCheck finite element code for determining stress intensity factors in residual stress fields and the integration of that software package with the commercially-available crack growth code, AFGROW. Provisions were also made to incorporate highly irregular crack shapes associated with cold-worked holes into StressCheck via two separate plug-ins: (1) the Crack Propagation Tool developed by team-member Engineering Software Research & Development, Inc. (ESRD) and (2) the Broad Application for Modeling Failure (BAMF), a code endemic to A-10 and T-38 ASIP.

In addition to software enhancements, a residual stress database has been developed and populated during this program. The database supports some common aluminum alloys used in aircraft and addresses variations in material thickness, hole diameter, edge margin, and cold work interference level. The database is easily expandable by the customer. The determination of residual stress uses an advanced measurement technique called the "Contour Method", a method proven to deliver high-density, two-dimensional representations of residual stress states resulting from the cold work process.

These residual stress inputs are being combined with the analysis suite described above to predict the performance of simulated aircraft components under fatigue load environments, including load spectra specific to wing and fuselage structure on several USAF aircraft.

Chapters 4, 5, and 8 provide details on the analytical capabilities we have developed and the associated validation activities.

1.3 Benefit to the Warfighter

The benefit of this technology is that it will have a direct and immediate effect on inspection programs, where inspections of critical airframe structure with cold worked holes would be required less frequently without risk to safety. This reduction in inspections would greatly reduce depot flow days and labor costs and would increase aircraft availability.

1.4 Major Tasks of this Rapid Innovation Program

This project was subdivided into eight major task groups:

- Baseline material tests, to ensure the materials used for model development perform as expected.
- Data development of basic CX hole fatigue behavior, to understand important parameters and failure processes for modeling.
- Determination of residual stress for a wide variety of hole parameters data using the Contour Method.
- Development of a Residual Stress Database to allow for rapid review and for application of Contour Method data in finite element programs.
- Modification of existing computer codes (mostly StressCheck p-version finite element software) to allow for computations of stress intensity for cracks embedded in residual stress fields.
- Establishing communication between new versions of StressCheck, the USAF multi-point crack growth code known as BAMF (Broad Application for Modeling Failure), and the commercially available crack growth engine, AFGROW, and using the resulting software suite to model crack growth in the residual stress fields.
- Development and delivery of a prototype laser scanning device to provide quality assurance of successful cold work of a fastener hole and to provide a digital record in the form of a deformation map.. The tool has been named FastenerCamTM by the developer, Texas Research Institute—Austin.
- Examination of various in-service non-destructive testing (NDT) methods to gauge their performance at cold work holes. Methods examined were bolt hole eddy current, surface scan eddy current, and ultrasound.

The next several chapters of this report deal with these subjects separately and in detail. Conclusions and a recommended path forward can be found in the summary sections of this report.

2 Basic Material Behavior Tests

A series of basic material tests were performed under this program to ensure that the response of the supplied materials was appropriate under monotonic and fatigue conditions. These tests included ASTM E8 tensile, ASTM E466-type fatigue, and ASTM E647 fatigue crack growth tests. The details for and results of each test program are included in the remaining sections of Chapter 2.

2.1 Tensile Tests

A total of eighteen specimens (six nominal geometries/materials, and three replicates of each) were tested to determine yield strength, elongation, and ultimate tensile strength using the ASTM E8-08 test protocol. Nine of the coupons were made from 2024-T3 / T351, with three each in 0.1 inch, 0.313 inch, and 0.5 inch thicknesses. The same matrix was repeated for 7075-T6 / T651 aluminum. Specimen geometry is shown in Figure 1.

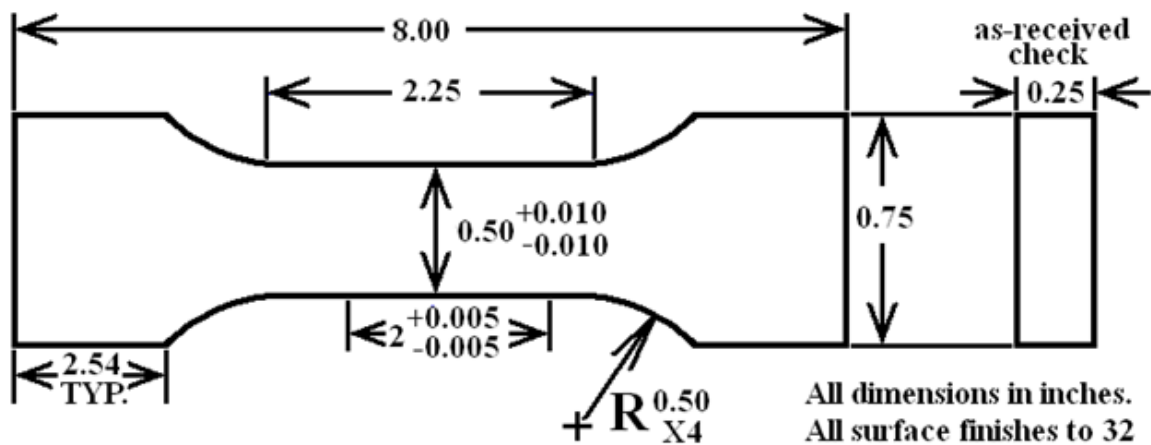


Figure 1. Tensile test coupon geometry.

Each specimen's gage section width and thickness were measured at three locations along the gage length, the cross-sectional area computed at each location, and the minimum area was recorded in the table below.

Elongation at failure was measured by scribing two lines on each specimen and measuring the distance change between them before the test, and then again after fracture. These lines were in the gage section of the specimens, nominally two inches apart prior to test, and the average distance at three locations along each line was used to account for any skew.

A force vs. strain curve was generated for each specimen and the graphical 0.2% offset method was used to determine the yield force, and along with the minimum area, the yield stress F_{ty} . A summary of results is in Table 2. A sample force-strain curve is shown in Figure 2. The slope of the leftmost diagonal line was used to compute the

elastic Young's Modulus E . The peak-valley hold meters inside the MTS software were used to capture the maximum force applied during each test, this force was then used with the cross-sectional area to compute the ultimate stress, F_m .

Table 1. ASTM E8-08 test results.

Specimen ID	Material (Alum. alloy)	Nominal Width (inch)	Nominal Thickness (inch)	Min. Area (in ²)	Elongation strain @ failure	Yield Stress F_{ty} (ksi)	Ult. Stress F_{tu} (ksi)	Young's Modulus E (psi)
3A1-01A	2024-T3	0.5	0.1	0.0501	18.7%	52.5	70.5	1.17E+07
3A1-02A	2024-T3	0.5	0.1	0.0501	24.8%	52.1	70.3	1.07E+07
3A1-03A	2024-T3	0.5	0.1	0.0501	20.6%	51.5	70.2	1.04E+07
3A1-01B	2024-T351	0.5	0.3125	0.1560	20.2%	56.8	70.2	1.13E+07
3A1-02B	2024-T351	0.5	0.3125	0.1561	20.3%	56.8	70.0	1.20E+07
3A1-03B	2024-T351	0.5	0.3125	0.1562	23.2%	56.8	70.4	1.14E+07
3A1-06B	2024-T351	0.5	0.5	0.2536	24.5%	54.3	67.8	1.13E+07
3A1-07B	2024-T351	0.5	0.5	0.2537	23.7%	54.3	67.8	1.07E+07
3A1-08B	2024-T351	0.5	0.5	0.2539	22.9%	54.2	67.7	1.10E+07
3A1-01C	7075-T6	0.5	0.1	0.0492	15.2%	74.8	82.6	9.89E+06
3A1-02C	7075-T6	0.5	0.1	0.0492	15.7%	74.7	82.4	1.04E+07
3A1-03C	7075-T6	0.5	0.1	0.0493	15.0%	74.5	82.2	1.17E+07
3A1-01D	7075-T651	0.5	0.3125	0.1593	13.9%	77.4	82.6	1.08E+07
3A1-02D	7075-T651	0.5	0.3125	0.1593	14.2%	77.8	83.5	1.44E+07
3A1-03D	7075-T651	0.5	0.3125	0.1594	14.0%	77.8	83.1	1.19E+07
3A1-06D	7075-T651	0.5	0.5	0.2485	17.7%	74.9	81.2	1.08E+07
3A1-07D	7075-T651	0.5	0.5	0.2484	18.4%	75.1	81.0	1.13E+07
3A1-08D	7075-T651	0.5	0.5	0.2585	18.1%	75.3	81.5	1.18E+07

All tests were conducted under fixed displacement rates of the MTS actuator. In order to speed up test time, for all 2024-T3 and 2024-T351 specimens, the fixed displacement rate was increased once at a strain value of 0.010 inches/inch. For all 7075-T6 and 7075-T651 specimens, the fixed displacement rate was increased once at a strain value of 0.012 inches/inch. In order to prevent damage to the extensometer at specimen fracture, the extensometer was removed at a strain value of 0.09 inches/inch and 0.04 inches/inch for the 2024 and 7075 alloys, respectively.

Some slipping of the extensometer's knife edges was noted on specimens 3A1-07B, 3A1-02D, and 3A1-06D. Corrections were made in the force-strain curves for these three

specimens, these corrections had only a minimal impact on the computations of F_{ty} and E .

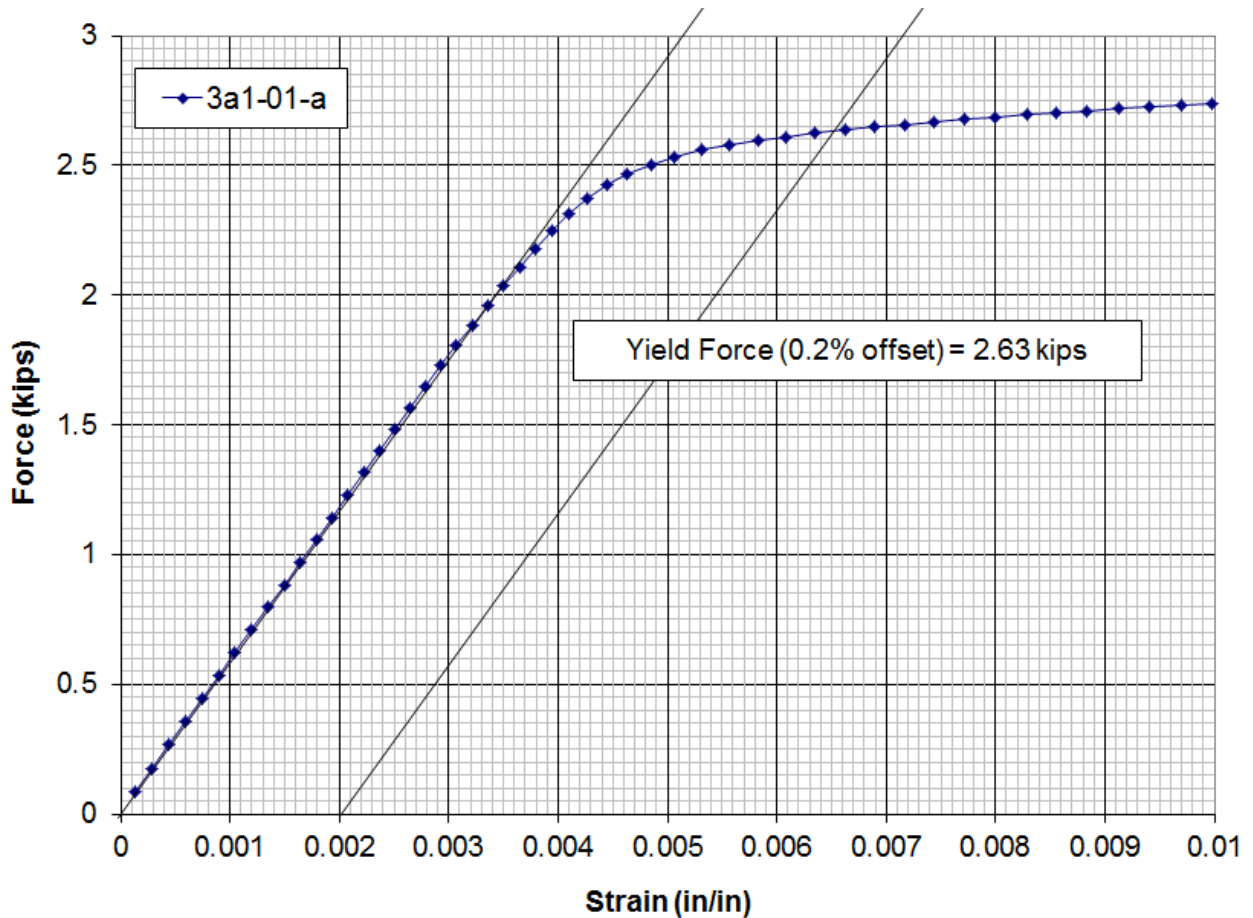


Figure 2. Sample force vs. strain plot for tensile coupon 3A1-01-A (2024-T3 aluminum).

2.2 ASTM E466 Tests for Short Crack Behavior

A series of 18 experiments was conducted using ASTM E466 type coupons, modified with a single edge notch tension (SENT) geometry. The specimen (see Figure 3) was designed to accommodate the Newman-Raju K solutions (Newman & Raju, 1986) for corner and surface cracks in the SENT geometry, which are the same solutions found in AFGROW.

Nine of the coupons were made from 2024-T3 / T351, with three each in 0.1 inch, 0.313 inch, and 0.5 inch thicknesses. The same matrix was repeated for 7075-T6 / T651 aluminum.

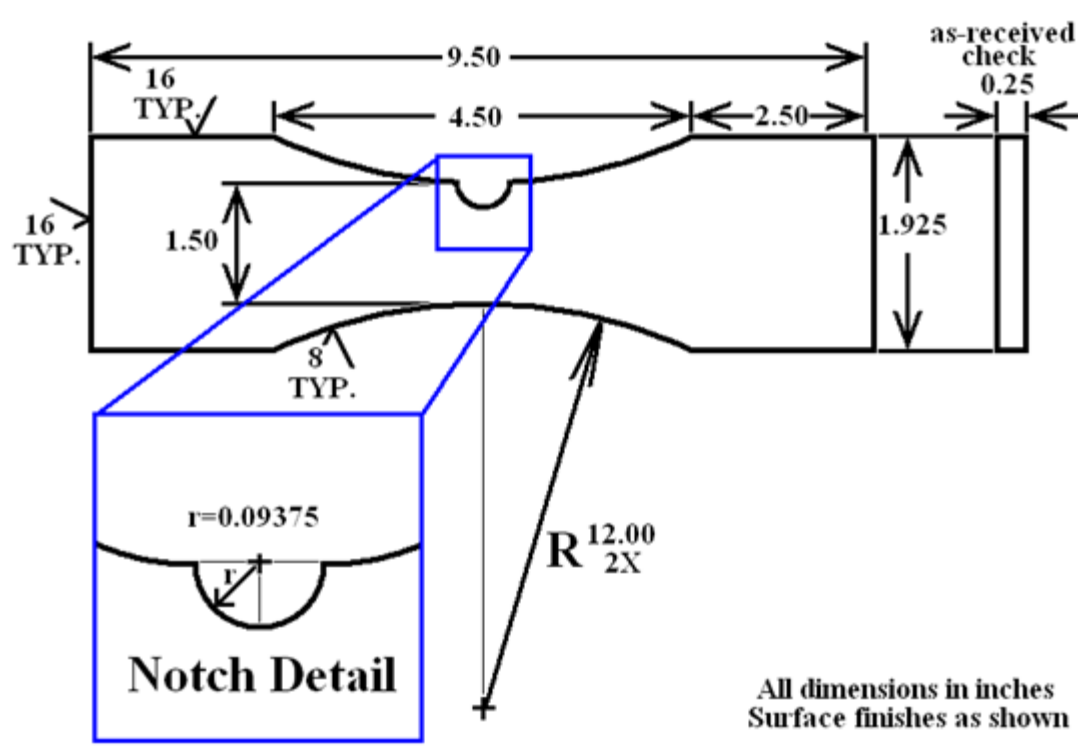


Figure 3. SENT specimen geometry.

2.2.1 Experimental Procedure

The specimens were designed to conform to ASTM Standard E466 and were tested under fatigue loading to fracture using customized marker sequences (Figure 4). The spectrum consisted of a large block of constant stress ratio cycles, followed by blocks of variable amplitude cycles that produce identifiable patterns on the fracture face. The typical appearance of the bands using optical microscopy is shown in Figure 5.

All tests were conducted to fracture under load control at a constant frequency of 10Hz and in dry laboratory air conditions.

No artificial crack starters were used, and no inspections were conducted during cycling.

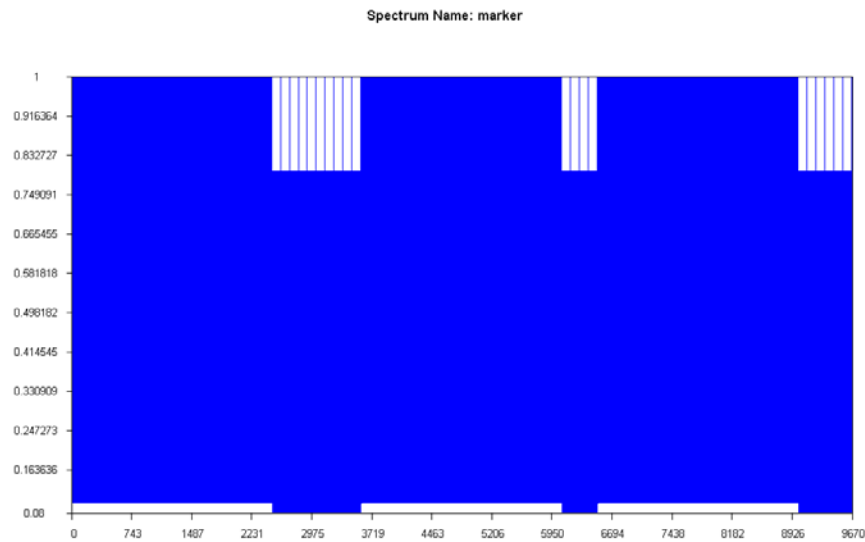


Figure 4. Variable amplitude marker sequence.

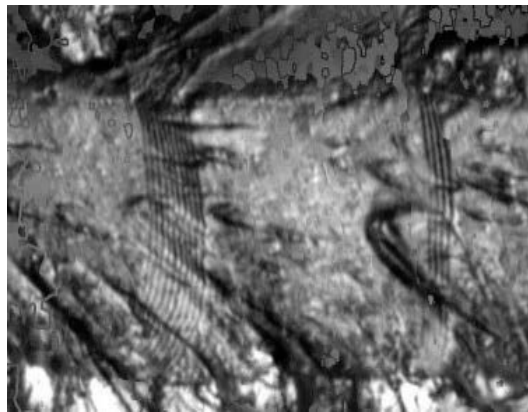


Figure 5. Typical appearance of marker bands under optical microscopy.

Marker bands are beneficial in that they effectively mark crack fronts at different points in specimen life, which makes it possible to construct both crack growth rate (da/dN) and crack size and shape (related to ΔK) directly from the fracture face at any time after test completion. The record is permanent as long as the fracture faces are protected. The use of marker bands greatly reduces labor during testing, reduces specimen time in the load frame, and allows data reduction to occur while other tests are on-going.

2.2.2 Test Results

Cycles to failure were recorded for each coupon (Table 3). These cycles-to-failure were used along with coupon geometry, previously-developed short crack material files (da/dN vs. ΔK in the form of *.lkp files for AFGROW), and AFGROW COM capability to develop an equivalent initial flaw size (EIFS) for each coupon. These EIFS values were compared to historically developed initial discontinuity states (IDS) and Matched

Analytical Crack Sized (MACS) for the two alloys. Since the EIFS values fit within the IDS distribution for the two alloys, it was determined that further data reduction and adjustment of the APES short crack material models was *not* required. The basic procedures for the historical data development are presented in Section 2.3. The results (Section 2.4) show how these most recent data compare with historical data.

Table 2. Fatigue life results from E466 SENT tests.

Coupon ID	Stock Info		Specimen Gauge Section		Test & Spectrum Info			
Coupon	Material	Thickness (inch)	Width (inch)	Thickness (inch)	Test Stress (ksi)	Max Load (kips)	Test Cycles	Spectrum Passes
3C1-01-A	2024-T3	0.100	1.505	0.100	20.0	3.0	59,010	6.1
3C1-02-A	2024-T3	0.100	1.504	0.099	20.1	3.0	83,911	8.7
3C1-03-A	2024-T3	0.100	1.502	0.100	19.5	2.9	125,710	13.0
3C1-01-B	2024-T351	0.313	1.500	0.313	17.0	8.0	181,360	18.8
3C1-02-B	2024-T351	0.313	1.500	0.313	17.0	8.0	160,000	16.5
3C1-03-B	2024-T351	0.313	1.499	0.313	17.0	8.0	182,760	18.9
3C1-06-B	2024-T351	0.500	1.502	0.510	17.0	13.0	161,796	16.7
3C1-07-B	2024-T351	0.500	1.500	0.510	17.0	13.0	166,696	17.2
3C1-08-B	2024-T351	0.500	1.501	0.510	17.0	13.0	205,282	21.2
3C1-01-C	7075-T6	0.100	1.501	0.099	16.0	2.4	113,553	11.7
3C1-03-C	7075-T6	0.100	1.501	0.098	17.3	2.6	118,116	12.2
3C1-05-C	7075-T6	0.100	1.501	0.098	17.4	2.6	203,496	21.0
3C1-02-D	7075-T651	0.313	1.501	0.319	17.0	8.1	90,173	9.3
3C1-03-D	7075-T651	0.313	1.500	0.319	17.0	8.1	121,165	12.5
3C1-04-D	7075-T651	0.313	1.502	0.319	17.0	8.1	93,212	9.6
3C1-08-D	7075-T651	0.500	1.500	0.501	17.0	12.8	220,153	22.8
3C1-09-D	7075-T651	0.500	1.500	0.500	17.0	12.8	74,364	7.7
3C1-10-D	7075-T651	0.500	1.501	0.500	17.0	12.8	220,949	22.8

2.2.3 Data Reduction Methods

This section describes how we develop da/dN vs. ΔK data from the SENT coupons and then how we incorporate IDS distributions to tune the engineering crack growth model for 2024-T351 and 7075-T651 aluminum. These models were derived from data provided by Single Edge Notch Tension (SENT) coupons under previous programs.

2.2.3.1 Constructing basic da/dN vs. ΔK data

Our basic crack growth data reduction protocols require post-mortem optical microscopy of marker bands. Our data development process involves measuring:

- Feature responsible for crack formation (e.g., particles or inclusions)
- Crack growth (a vs. N) based on marker band data
- Crack growth rate data (da/dN vs. a) derived from a vs. N data
- Crack growth rate data (da/dN vs. ΔK) derived from a vs. N data and crack shape at select intervals.
- First detectable crack size (and related ΔK and/or K_{max}).

Figure 6 shows a typical optical fractograph. The particle at the crack nucleation site is shown as are several nearby marker bands. This image was taken at 500x on a Nikon MM-60 measuring microscope.

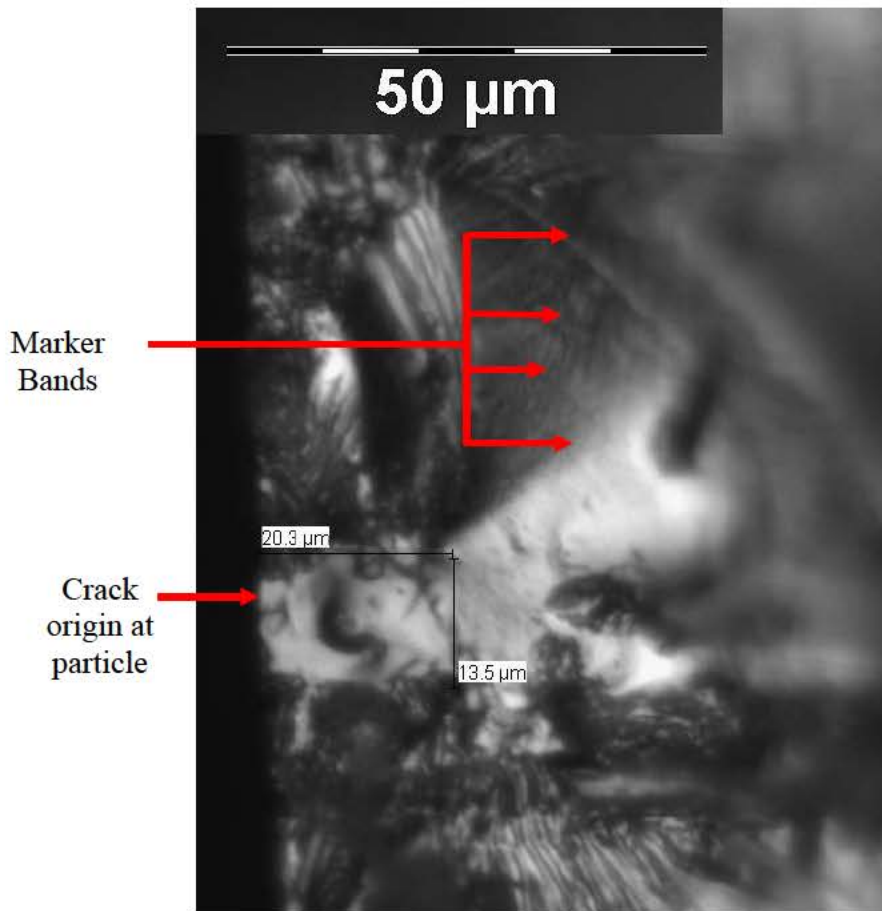


Figure 6. Optical fractograph of crack origin and adjacent marker bands in a typical SENT coupon.

An example of a $\log S$ vs. N data from marker bands are shown in Figure 7. Here two coupons that were tested under identical parameters (remote max stress and R) show very different fatigue lives. Both coupons were tested at 12 ksi remote max stress and $R = -0.33$; however, one coupon (CW2-SENT21) exhibited a fatigue life of 182k cycles, and the other (CW2-SENT22) exhibited a fatigue life of 2.97M cycles.

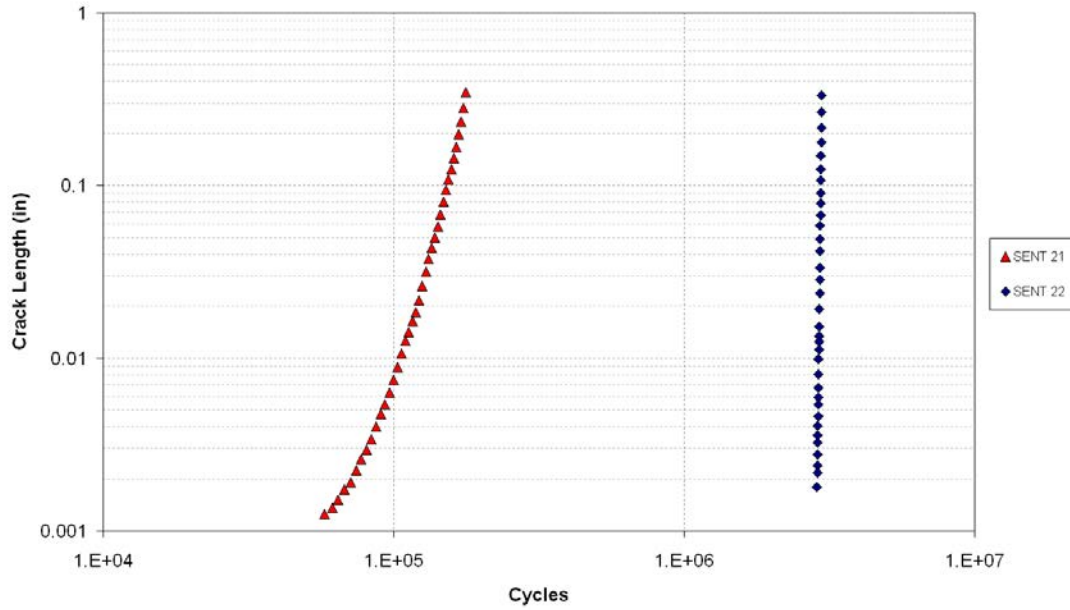


Figure 7. Crack growth curves for two SENT coupons tested under identical conditions.

As dissimilar as the total lives are, crack growth rate behavior (where it could be measured) was essentially equal. Figure 8 plots the data from these to experiments as da/dN vs. a .

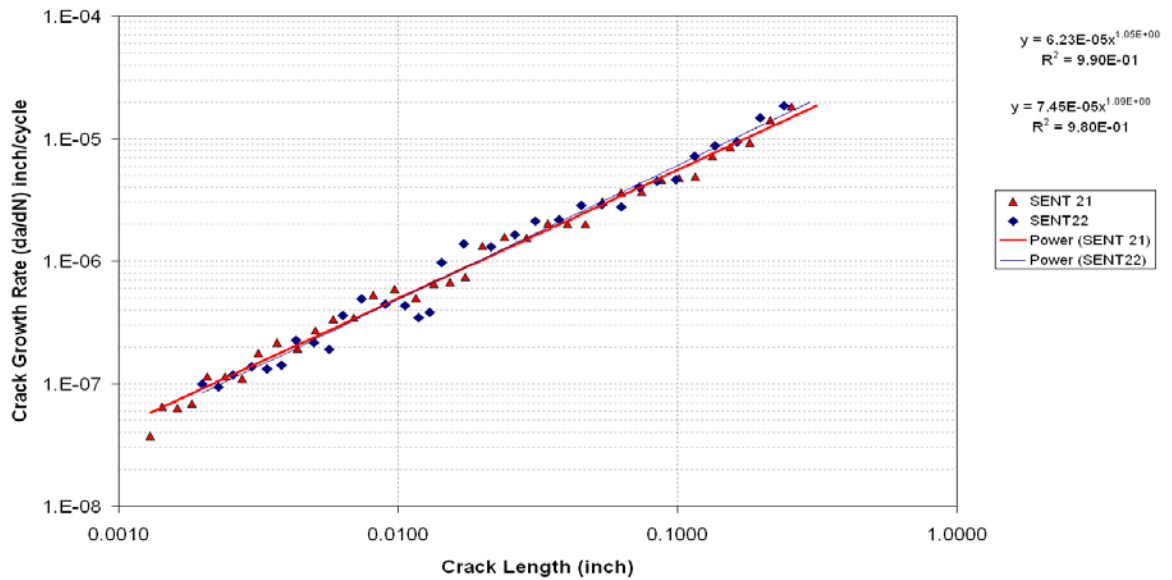


Figure 8. da/dN vs. ' a ' data for the two coupons.

The next chart shows sample marker band maps (Figure 9) for a typical coupon. Bands closest to the origin are shown on a zoomed map (Figure 10).

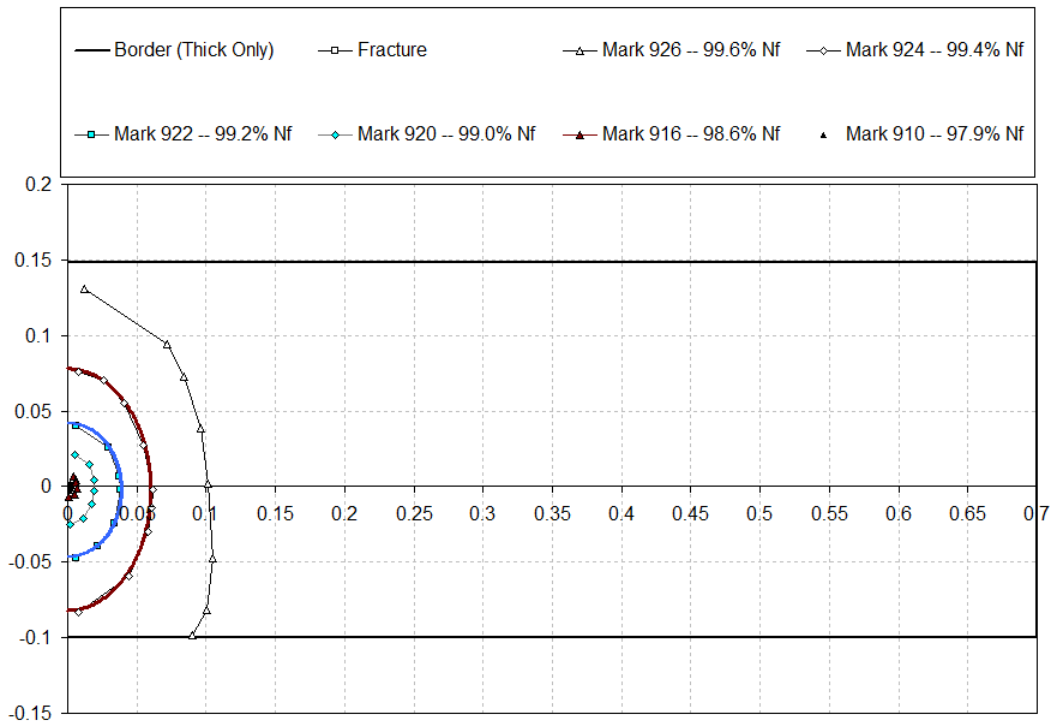


Figure 9. Overall marker map of a SENT coupon. Axes are in inches.

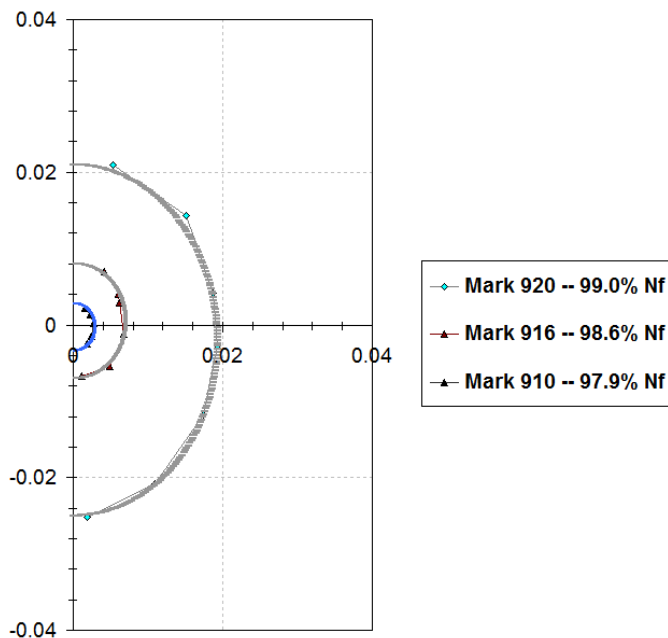


Figure 10. Marker map zoom from previous figure of bands closest to the crack origin. Axes are in inches.

Figure 11 shows the finished product for one coupon, where marker data are ultimately reduced to da/dN vs. ΔK data. The example here (at $R = +0.1$) is plotted along with various literature curve fits for 7075-T651 aluminum, including the NASGRO material database (as contained in AFGROW), the Harter-T curve fit from AFGROW, and the curve fit found in the Damage Tolerance Design Handbook (1983), but for $R = +0.02$.

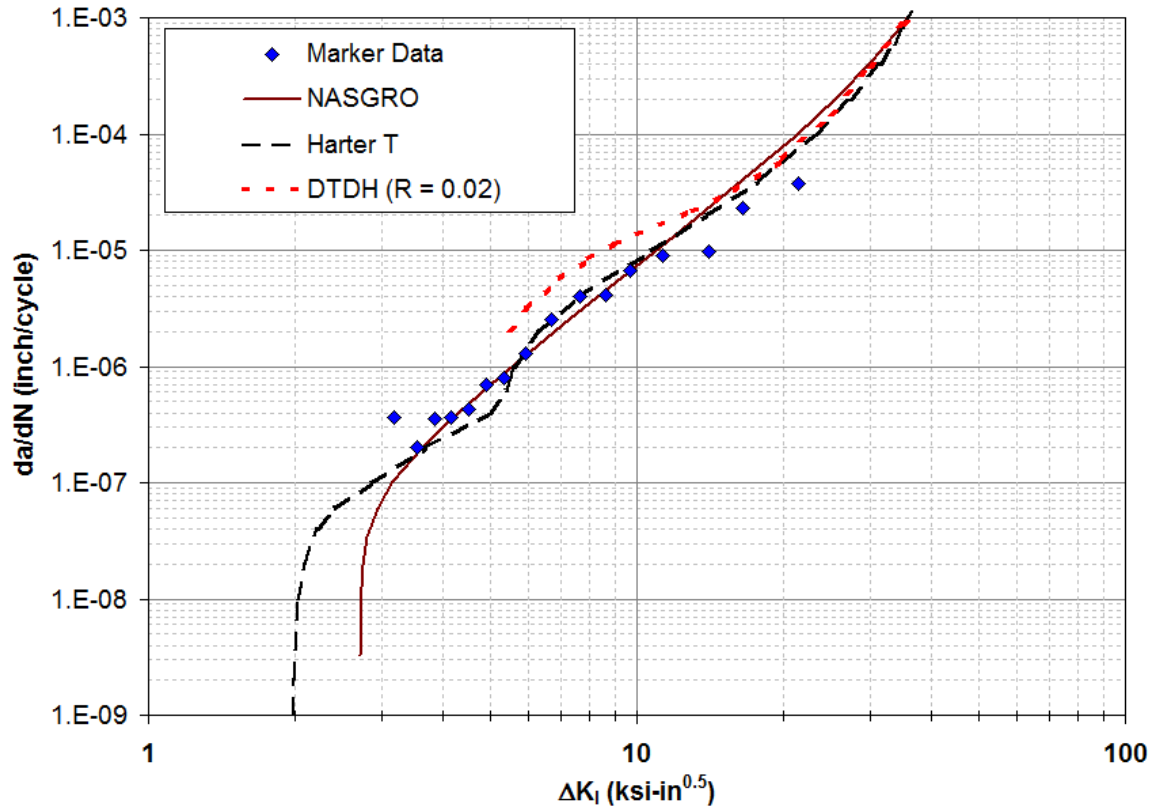


Figure 11. Example of da/dN vs ΔK data as reduced from marker bands. Data are compared to “literature” curve fits.

2.2.3.2 Matched Analytical Crack Size of Initial Discontinuity State

This section details the development of short crack matched curves for lower regions of the da/dN vs. ΔK relationships.

Three different terms are critical to the discussions of this section:

1. IDS, or Initial Discontinuity State. The physical features that causes cracking in a test coupon (in these cases, particles or inclusions).
2. EIFS, or Equivalent Initial Flaw Size. The initial crack size that, via some form of crack growth relationship (da/dN vs. ΔK), produces a predetermined life (cycles) at some final crack size.
3. MACS, or Matched Analytical Crack Size. Iteration of the EIFS distribution for a set of data that results in the EIFS distribution closely matching the IDS

distribution. This typically requires manipulating the crack growth curve in regimes where there is no physical crack growth data (near threshold).

The IDS distribution represents physical starting crack sizes, which are used as inputs into traditional crack growth analysis for the crack growth code, AFGROW. However, for the IDS sizes to be realistic as initial cracks, the material crack growth curve (in the form of da/dN vs. ΔK) must be tuned slightly to generate Matched Analytical Crack Size (MACS) distributions that replicate, as best possible, the IDS distributions (hence the term, “Matched” Analytical Crack Size). Typically, data generated by ASTM standard coupons, such as C(T) or M(T) coupons included in E647, have higher crack growth thresholds, and use of models derived from these types of coupons will result in “no grow” scenarios for cracks typical of IDS sizes.

In constructing the MACS distributions, each specimen tested was modeled using the automation (COM) capabilities in AFGROW, wherein cycles to each detectable marker band and to ultimate failure, specimen geometry, crack geometry, marker load sequence, and stress level were all input, and AFGROW returned a series of starting crack sizes (equivalent initial flaw sizes, or EIFS) for each specimen. The reason there was a series of values and not a point value is that each specimen provides many opportunities to calculate an EIFS (from the origin to various crack sizes and different points in life, as determined by fractographic marker band data). Often times we are computing 20 or more different EIFS values for each coupon, although this is highly variable depending on the number of detectable marker bands in the coupon.

For the data development in 7075-T651 alone, we computed 480 discrete EIFS values for 23 different SENT coupons. These EIFS values were matched to the IDS distribution of the entire data set, 28 coupons. In all of the coupons tested, only one crack formed per coupon, so no multiple site damage is evident. Thus, only one IDS value is identified with each coupon. The value used for each coupon is the average of the X & Y dimensions for the particle that caused a fatigue crack to form.

Generally, the goal of the exercise is to try to drive the EIFS to approximate the IDS at the 10th, 50th, and 90th percentile values on a cumulative distribution function, thereby making a MACS distribution. To accomplish this, long crack data from the literature were blended to accommodate short crack data derived from marker band data (i.e., models were fit to the data where data existed). At lower stress intensity values, where no short crack marker band data existed, and at values lower than long-crack thresholds shown in literature data, the crack growth curves were further adjusted to create the MACS distribution.

Figure 12 shows several literature models for 7075-T651 (or T6511, Harter T) compared to the physical marker band data and the tuned MACS/IDS – derived curve. Also shown are the approximate bounds of the NASA AGARD short crack data from Newman and Edwards (1989).

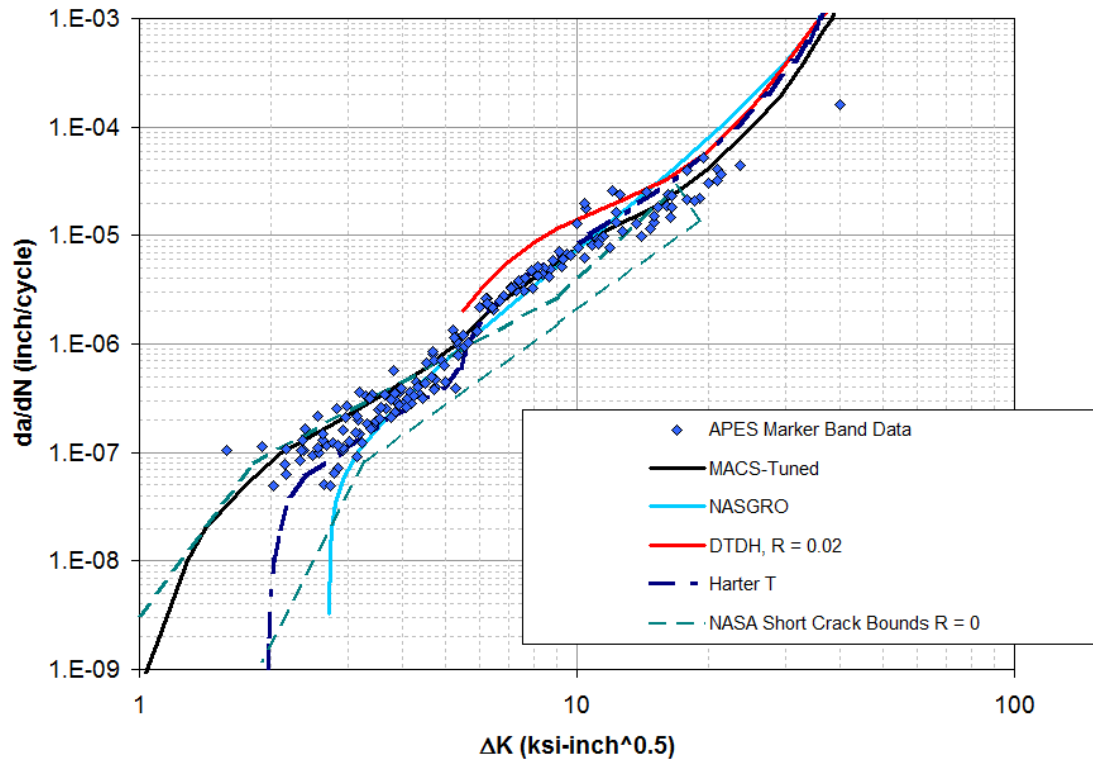


Figure 12. APES-developed marker band data and MACS-tuned crack growth curve ($R = 0.1$) compared with various literature “long crack” models and the bounds of the NASA AGARD short crack data for 7075-T6 (Newman and Edwards, 1989).

Similar approaches have been applied in the past to produce short crack material models for 2024-T351.

Figure 13 and Figure 14 show the MACS distributions and IDS distributions for 7075-T6/T651 and 2024-T3/T351, respectively. Also shown on these figures is the EIFS values computed for the SENT coupons tested for the RIF program. The EIFS values are placed at their corresponding percentile of the IDS distribution for the alloy. This shows that the EIFS values are of the scale we expect for these alloys, so we determined that no further adjustment of the historic short crack material models was necessary.

The families of da/dN vs. ΔK curves we use for 7075-T6/T651 and 2024-T3/T351 are shown in Figure 15 and Figure 16.

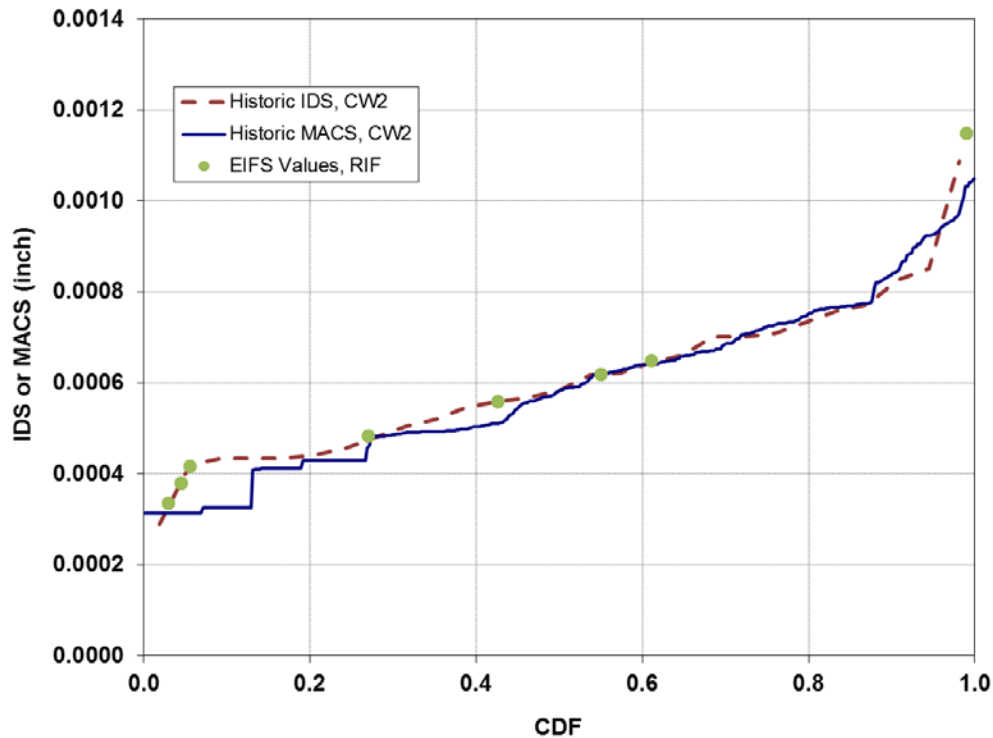


Figure 13. Historic IDS & MACS compared with EIFS values for RIF SENT coupons (7075-T6/T651).

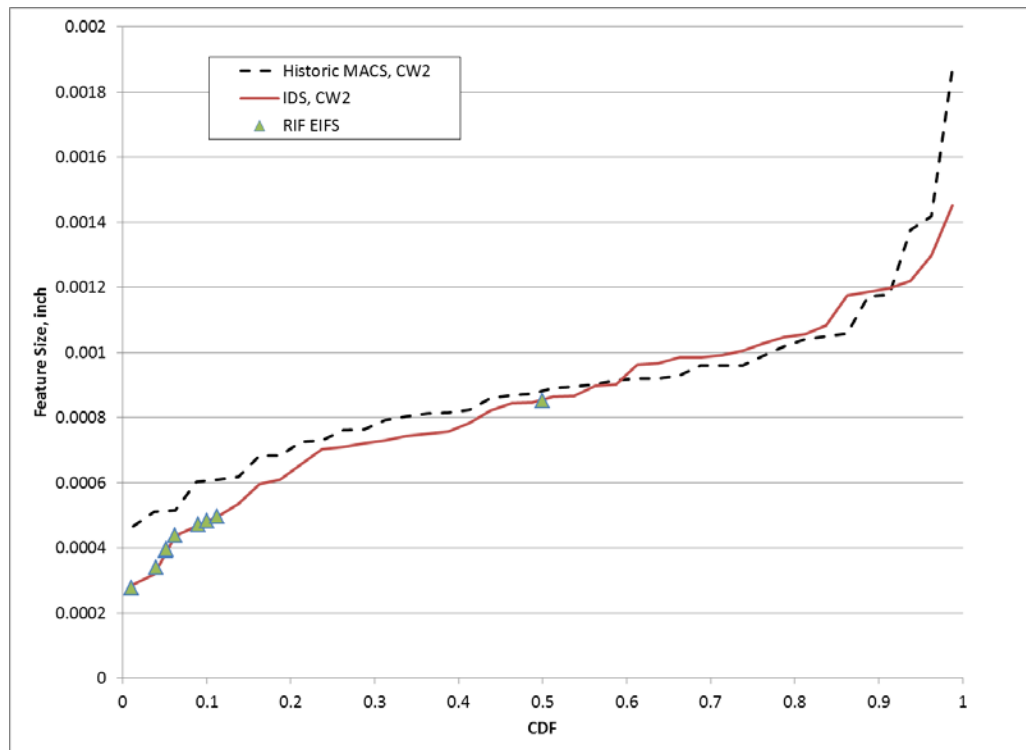


Figure 14. Historic IDS & MACS compared with EIFS values for RIF SENT coupons (2024-T3/T351).

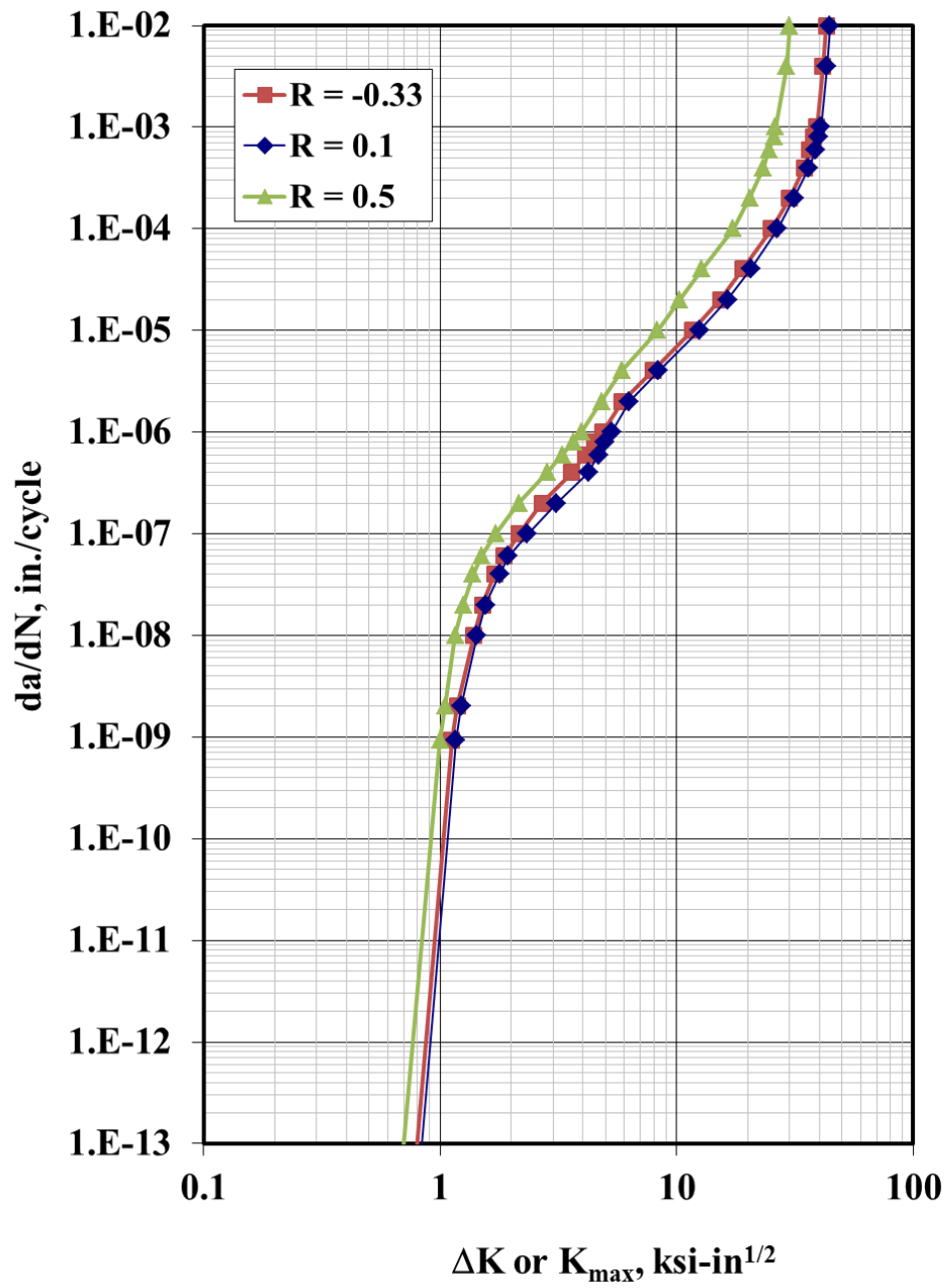


Figure 15. Crack growth relationships for tuned for short crack behavior (7075-T6/T651).

Table 3. Crack growth curve fits for 7075-T651

	Stress Ratio		
	-0.33	0.1	0.5
da/dN (inch/cycle)	ΔK ksi-in ^{0.5}		
1.00E-15	0.673	0.708	0.589
9.33E-10	1.119	1.164	1.000
2.00E-09	1.183	1.225	1.050
1.00E-08	1.387	1.429	1.159
2.00E-08	1.510	1.556	1.250
4.00E-08	1.694	1.779	1.374
6.00E-08	1.862	1.940	1.496
1.00E-07	2.148	2.339	1.718
2.00E-07	2.692	3.097	2.148
4.00E-07	3.606	4.236	2.825
6.00E-07	4.102	4.656	3.281
8.00E-07	4.519	4.943	3.673
1.00E-06	4.853	5.297	3.954
2.00E-06	5.888	6.281	4.797
4.00E-06	7.943	8.375	5.848
1.00E-05	11.641	12.474	8.279
2.00E-05	15.276	16.406	10.304
4.00E-05	19.011	20.512	12.735
1.00E-04	25.119	26.607	17.338
2.00E-04	30.061	31.333	20.324
4.00E-04	34.594	36.224	23.227
6.00E-04	36.560	38.637	24.547
8.00E-04	37.844	39.811	25.704
1.00E-03	39.084	40.644	26.182
4.00E-03	41.536	43.053	29.107
1.00E-02	43.000	44.361	29.992

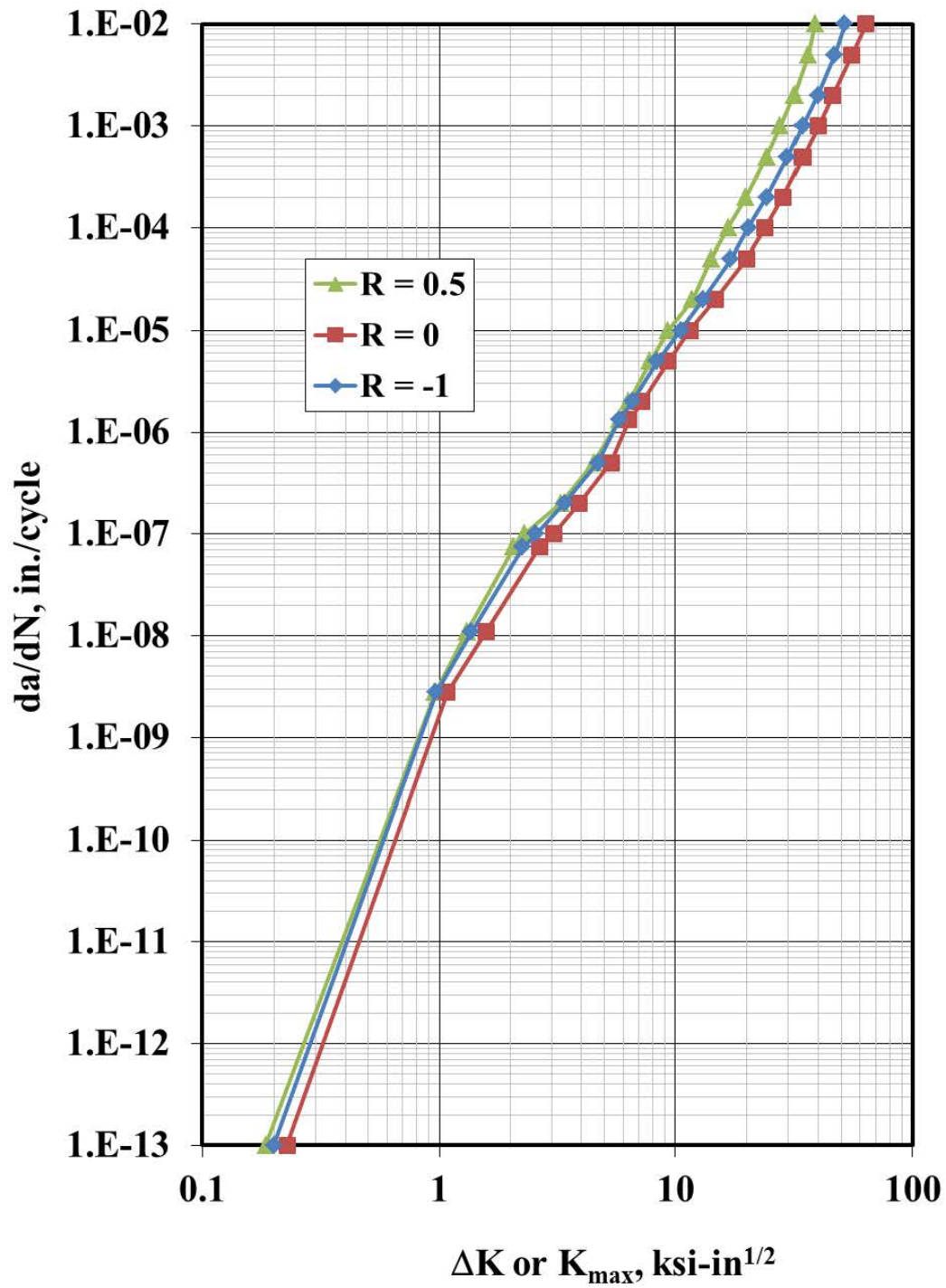


Figure 16. Crack growth relationships for tuned for short crack behavior (2024-T3/T351).

Table 4. Crack growth curve fits for 2024-T351

	Stress Ratio		
	-1.000	0.000	0.500
da/dN (inch/cycle)	ΔK ksi-in^{0.5}		
1.00E-13	0.200	0.227	0.184
2.75E-09	0.967	1.076	0.959
1.10E-08	1.363	1.574	1.309
7.41E-08	2.253	2.655	2.065
1.00E-07	2.571	3.041	2.296
2.00E-07	3.405	3.917	3.289
5.00E-07	4.704	5.346	4.529
1.32E-06	5.790	6.353	5.768
2.00E-06	6.564	7.200	6.353
5.00E-06	8.370	9.300	7.798
1.00E-05	10.518	11.500	9.333
2.00E-05	13.064	14.700	11.830
5.00E-05	17.159	20.000	14.180
1.00E-04	20.439	24.000	16.710
2.00E-04	24.351	28.500	19.902
5.00E-04	29.775	34.500	24.371
1.00E-03	34.381	40.000	27.787
2.00E-03	39.805	46.000	31.832
5.00E-03	46.868	55.500	36.212
1.00E-02	51.740	63.500	38.635
2.00E-02	56.683	73.000	40.452
5.00E-02	62.714	83.000	41.646
1.00E-01	65.722	87.000	43.123

2.3 Long Crack Behavior

In addition to the SENT tests, ASTM Standard E647 crack growth tests were conducted to ensure that long crack behavior of the material we purchased for this program matched that of literature and APES material models. We tested two thicknesses (0.313 and 0.5 inch nominal plates) in two aluminum alloys: 2024-T351 and 7075-T651. We were only spot checking material behavior, not conducting a full material characterization process, so only stress ratio was checked ($R = 0.1$). A schematic of the coupon design is shown in Figure 17.

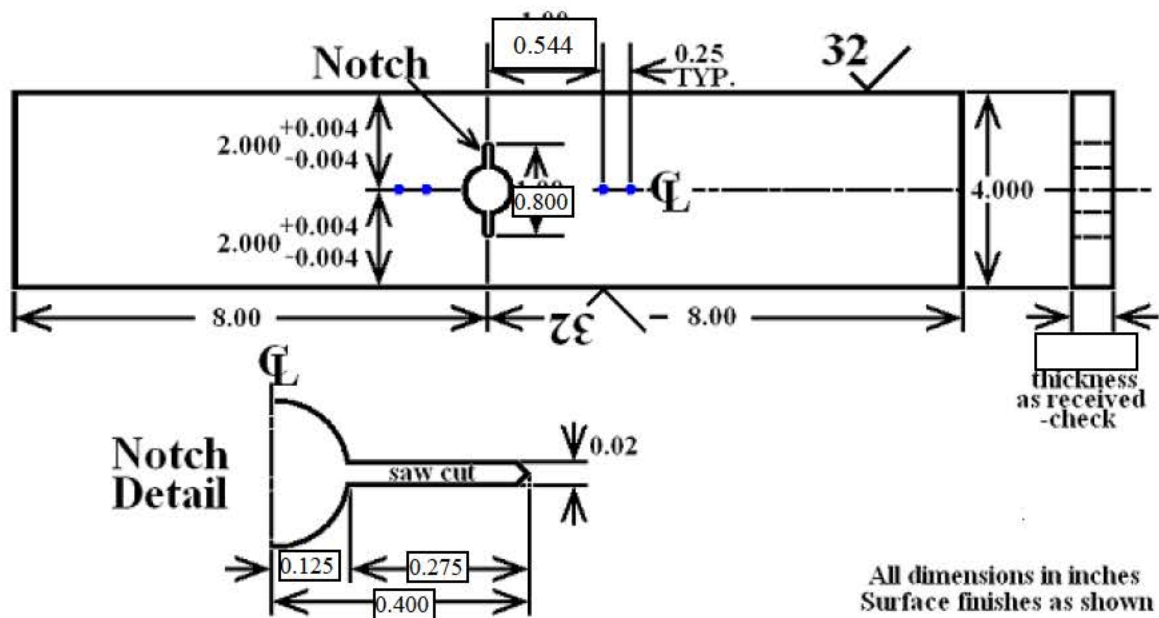


Figure 17. Specimen design E2, ASTM E647 middle tension coupon.

2.3.1 Test Procedure and Results

All test procedures and data reduction procedures followed those outlined in ASTM E-647, including those for load-shedding pre-crack procedures and for crack growth data intervals for optical inspection.

Data were collected using optical traveling microscopes and crack opening displacement (clip gauges). Tests were K -increasing only, and as such started at ΔK values of 5.5 to 6 ksi $\sqrt{\text{in}}$. Test data are shown in Figure 18 (7075-T651) and Figure 19 (2024-T351). Each figure also shows long-crack models for Harter T and the APES material models (discussed in the previous section).

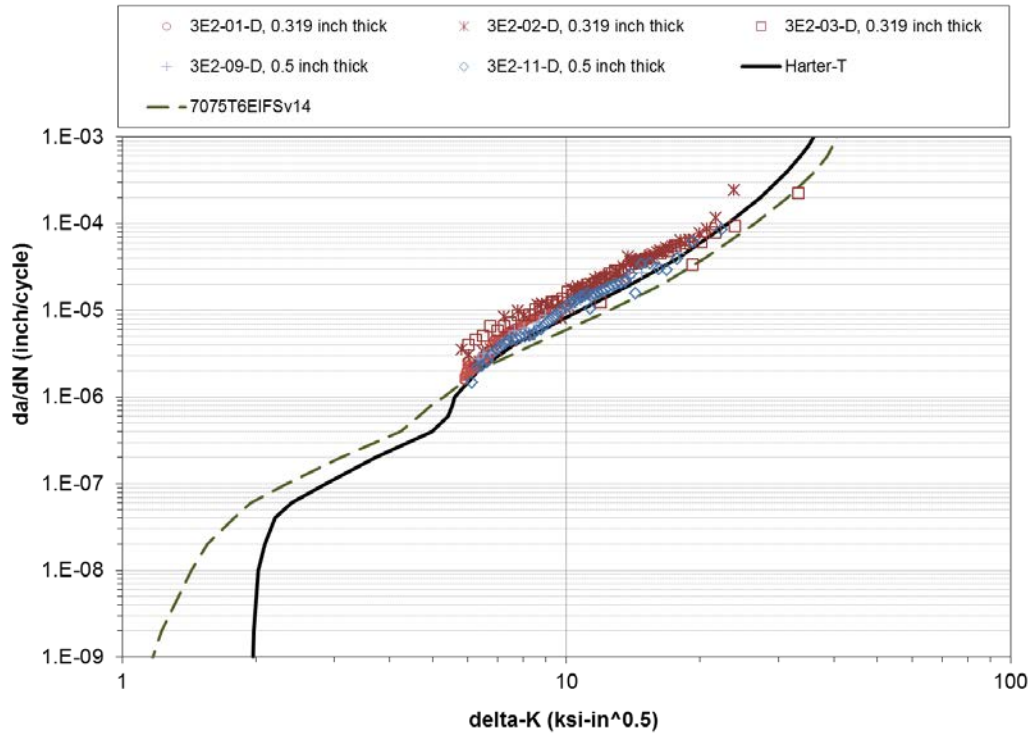


Figure 18. Long crack growth data for 7075-T651 compared to Harter T and APES material models.

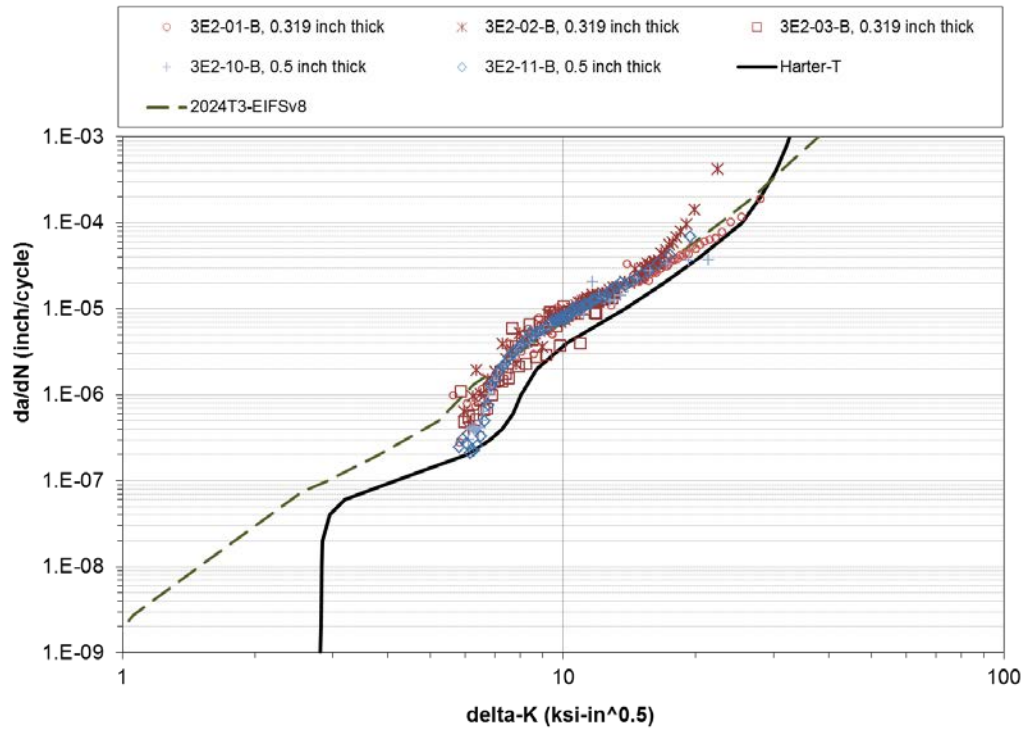


Figure 19. Long crack growth data for 7075-T651 compared to Harter T and APES material models.

3 Baseline Cold Worked Hole Behavior Tests

This section provides details of the cold-worked hole fatigue tests completed under Task 2 of this program. The purpose of these tests were to provide development data for modeling correlation using the analytical tools (StressCheck, BAMF, AFGROW) that were enhanced and integrated under this program.

These tests also helped illustrate the important aspects of cold-worked holes that govern fatigue response: namely edge margin and interference (CX) level. The other variables in the experimental design, hole diameter and plate thickness, did not have a strong effect on fatigue life.

The materials and product forms examined in this phase of the work included:

- 2024-T3 aluminum sheet, 0.1 inch thick
- 2024-T351 aluminum plate, 0.313 inch thick
- 2024-T351 aluminum plate, 0.5 inch thick.
- 7075-T6 aluminum sheet, 0.1 inch thick
- 7075-T651 aluminum plate, 0.313 inch thick
- 7075-T651 aluminum plate, 0.5 inch thick

The above materials were tested using:

- Two (2) stress levels (slightly different for 7075 vs 2024)
- Three (3) hole diameters
- Three (3) edge margins
- Three (3) cold-work interference levels

The basic test matrix for 7075 is shown in Table 6; 2024 is shown in Table 7.

3.1 Test Matrix

The test matrices for 7075 and 2024 included three different thicknesses (0.1" sheet, and 0.313" and 0.5" plate), three hole diameters (0.25", 0.375", and 0.5"), three different edge margins (1.39, 1.8, and 2.4) and three different cold working levels (identified in the tables as High, Middle, and Low—details follow). Furthermore, each alloy was tested using two stresses (slightly different between alloys).

The thicknesses, hole diameters, and edge margins are the same as found in a residual stress measurement matrix conducted for 7075-T651 (see Chapter 4).

The experimental design is fractional factorial focusing on the “boundaries” of the design space (combination of high and low settings for each of the variables) with the fourth factor (CX Level) being determined by product of the other three factor levels (see Table 8). The design also features a large number of replicates that represent the “center” combination of variables ($e/D = 1.8$, $t = 0.313$, $D = 0.375$, $CX = \text{Middle}$).

Table 5. Test matrix for 7075-T6 & T651 coupons. “CA Stress” refers to the constant amplitude cycles between marker bands, whereas “Max Stress” refers to the stress at the 15% overload.

CX Hole Coupons (7075)								
Material	Thickness	Gauge Width	Hole D	Edge Margin	CX Level	Max Stress	CA Stress	# Tests
7075-T6	0.100	1.50	0.500	1.39	High	30.477	26.500	3
7075-T651	0.313	1.50	0.375	1.80	Middle	30.477	26.500	3
7075-T651	0.500	1.50	0.500	1.39	Low	30.477	26.500	3
7075-T651	0.500	2.40	0.500	2.40	High	30.477	26.500	3
7075-T6	0.100	2.40	0.500	2.40	Low	30.477	26.500	3
7075-T6	0.100	1.50	0.250	2.40	High	30.477	26.500	3
7075-T651	0.500	1.50	0.250	1.39	High	30.477	26.500	3
7075-T651	0.500	1.50	0.250	2.40	Low	30.477	26.500	3
7075-T6	0.100	1.50	0.250	1.39	Low	30.477	26.500	3
7075-T6	0.100	1.50	0.500	1.39	High	27.602	24.000	3
7075-T651	0.313	1.50	0.375	1.80	Middle	27.602	24.000	3
7075-T651	0.500	1.50	0.500	1.39	Low	27.602	24.000	3
7075-T651	0.500	2.40	0.500	2.40	High	27.602	24.000	3
7075-T6	0.100	2.40	0.500	2.40	Low	27.602	24.000	3
7075-T6	0.100	1.50	0.250	2.40	High	27.602	24.000	3
7075-T651	0.500	1.50	0.250	1.39	High	27.602	24.000	3
7075-T651	0.500	1.50	0.250	2.40	Low	27.602	24.000	3
7075-T6	0.100	1.50	0.250	1.39	Low	27.602	24.000	3

Table 6. Test matrix for 2024-T3 & T351 coupons.

CX Hole Coupons (2024)								
Material	Thickness	Gauge Width	Hole D	Edge Margin	CX Level	Max Stress	CA Stress	# Tests
2024-T3	0.100	1.50	0.500	1.39	High	28.752	25.000	3
2024-T351	0.313	1.50	0.375	1.80	Middle	28.752	25.000	5
2024-T351	0.500	1.50	0.500	1.39	Low	28.752	25.000	3
2024-T351	0.500	2.40	0.500	2.40	High	28.752	25.000	3
2024-T3	0.100	2.40	0.500	2.40	Low	28.752	25.000	3
2024-T3	0.100	1.50	0.250	2.40	High	28.752	25.000	3
2024-T351	0.500	1.50	0.250	1.39	High	28.752	25.000	3
2024-T351	0.500	1.50	0.250	2.40	Low	28.752	25.000	3
2024-T3	0.100	1.50	0.250	1.39	Low	28.752	25.000	3
2024-T3	0.100	1.50	0.500	1.39	High	25.302	22.000	3
2024-T351	0.313	1.50	0.375	1.90	Middle	25.302	22.000	5
2024-T351	0.500	1.50	0.500	1.39	Low	25.302	22.000	3
2024-T351	0.500	2.40	0.500	2.40	High	25.302	22.000	3
2024-T3	0.100	2.40	0.500	2.40	Low	25.302	22.000	3
2024-T3	0.100	1.50	0.250	2.40	High	25.302	22.000	3
2024-T351	0.500	1.50	0.250	1.39	High	25.302	22.000	3
2024-T351	0.500	1.50	0.250	2.40	Low	25.302	22.000	3
2024-T3	0.100	1.50	0.250	1.39	Low	25.302	22.000	3

Table 7. Factor levels for experimental design, which is repeated for each major alloy type and stress level. *The center point runs had 5 replicates for the high and low stress in 2024-T351 (see Table 5).

A	B	C	A*B*C	Replicates
Thickness	Hole D	Edge Margin	CX Level	
-1	1	-1	1	3
0	0	0	0	3 or 5*
1	1	-1	-1	3
1	1	1	1	3
-1	1	1	-1	3
-1	-1	1	1	3
1	-1	-1	1	3
1	-1	1	-1	3
-1	-1	-1	-1	3

The spectra, while mostly “constant amplitude”, do contain marker bands with a 15% overload. These overload cycles are also followed by a block of compressive cycles that hit 27% of the peak stress in the spectrum (**note:** it is possible that this compressive cycle block altered the original residual stress state. This will be studied under future efforts). The purpose of the compression block is to help mitigate any retardation effects caused by the 15% overload. Tests conducted under this program in ASTM E647 coupons (M(T) geometry without residual stress) did not show any load interaction (retardation) effects due to this marker sequence. This marker sequence (called MB24, Figure 20) has proven to be effective at marking fracture faces of cold-worked coupons.

Figure 21 shows the basic planform of the fatigue coupon design. Specimens with two different gauge widths are used with the small version (1.5” gauge width) being directly scaled down from the smaller version (2.4” gauge width--shown).

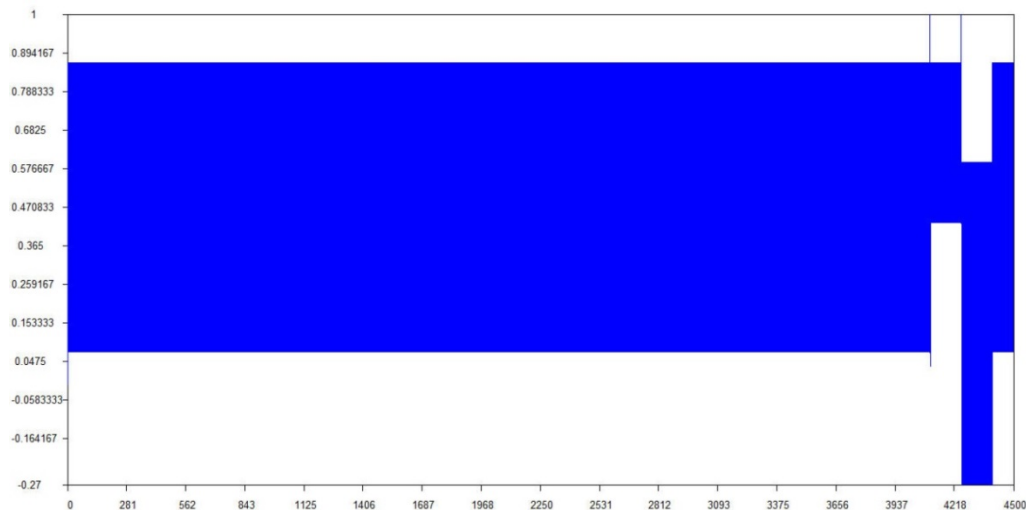


Figure 20. AFGROW representation of Marker Block 24.

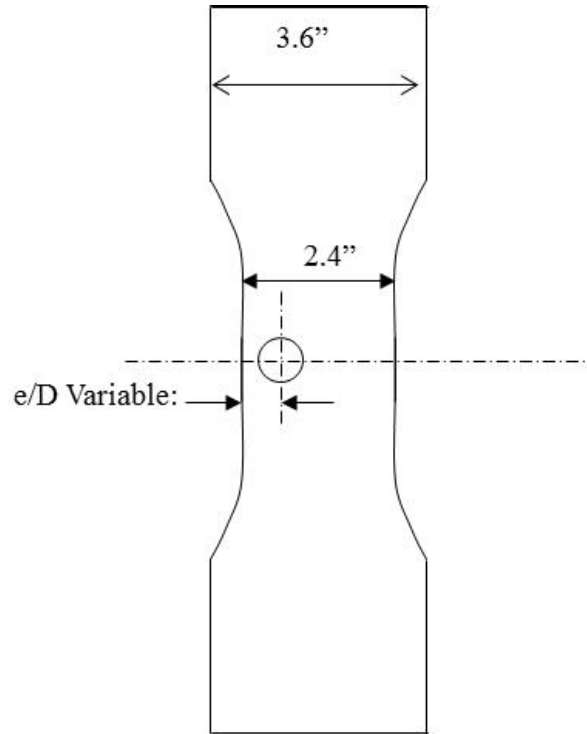


Figure 21. Schematic of the larger dog bone coupon used for CX fatigue tests.

3.1.1 Specimen Preparation and CX Procedure

APES has machined custom reamers to enable us to produce highly controlled bins of cold-work interference levels in the various coupons. The actual degree of cold work typical of a bin varies with hole diameter, but Table 9 shows a general guide. Figure 22 – Figure 24 show more detailed metrology results.

Table 8. Degree of CX expected for each of the bins and for each hole diameter.

Diameter (inch)	MAX CX%		MID CX%		MIN CX%	
	Mean	Stdev	Mean	Stdev	Mean	Stdev
0.250	4.27	0.11	N/A	N/A	2.69	0.23
0.375	3.99	0.05	3.44	0.06	2.93	0.21
0.500	3.95	0.05	N/A	N/A	2.91	0.12

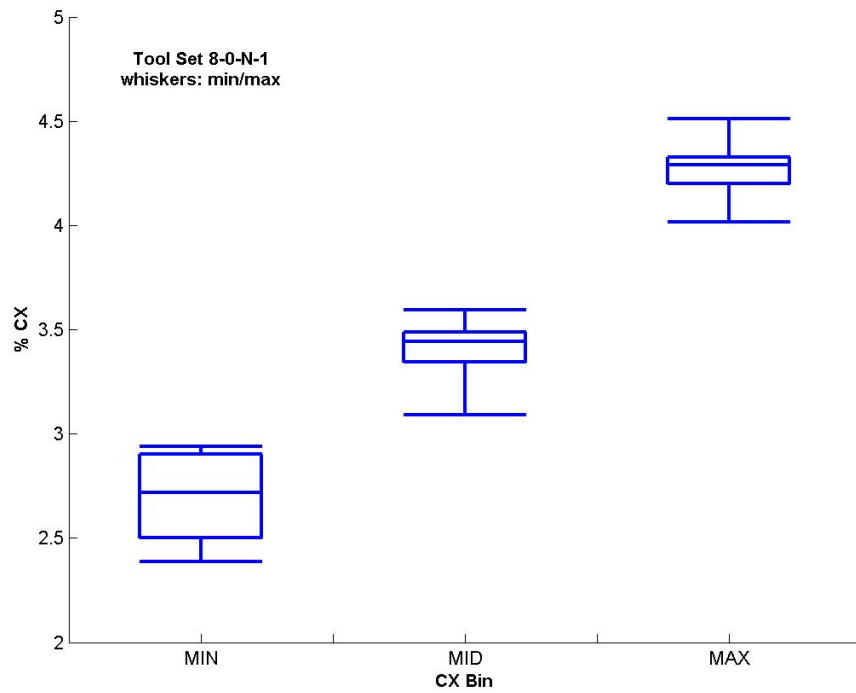


Figure 22. Cold work % associated with different "bins" for nominal 0.25 inch hole.

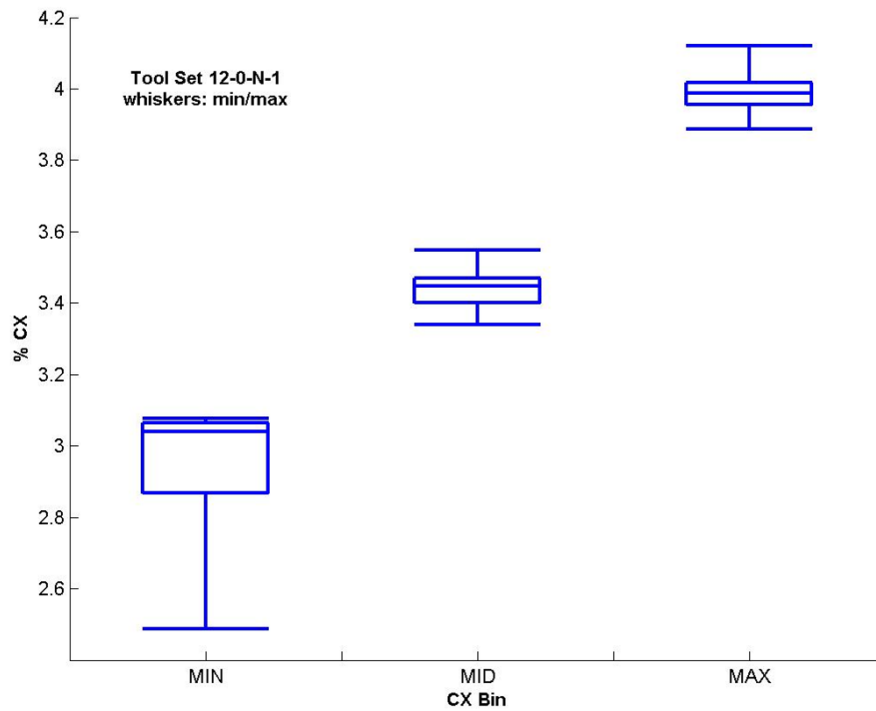


Figure 23. Cold work % associated with different "bins" for nominal 0.375 inch hole.

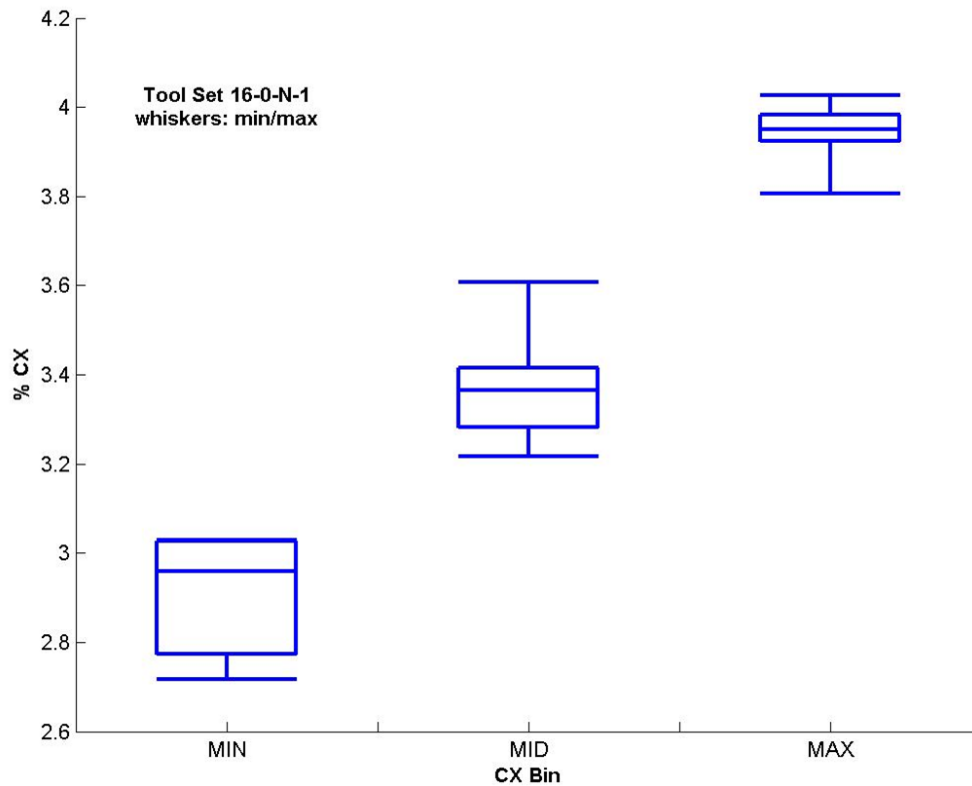


Figure 24. Cold work % associated with different "bins" for nominal 0.5 inch hole.

The basic specimen preparation procedure follows:

- Specimen blank machined by professional machine shop
- Initial ream hole placed in coupon using FTI stock reamers (MAX CX%) or custom reamers (MID CX% and MIN CX%) by professional machine shop using precision mill.
- Hole carefully deburred by hand using Scotch-Brite pads¹.
- Diameter of initial reamed hole measured using Nikon MM-60 measuring microscope to determine actual CX% for individual coupon. To

¹ Holes were hand deburred to protect corner integrity and provide a 90-degree rather than a chamfered corner. This was done to assist in locating the "corner", which was a zero reference origin for Contour Method measurements.

determine interference level, we use our actual (measured) mandrel diameter in conjunction with nominal sleeve thickness reported by FTI.

- Hole bore is dusted / cleaned as necessary.
- Hole is cold worked using standard FTI split sleeve procedures
- Hole final-reamed using stock FTI reamers at APES
- Surface of specimen around hole polished to aid in crack detection.

3.1.2 Test Procedure

All testing completed at APES was either completed in a 22 kip MTS frame or 55 kip MTS frame depending on specimen size and load requirements. Both frames are controlled by an MTS FlexTest 40 controller using Multipurpose TestWare to enable variable amplitude testing (necessary because of the marker blocks).

All specimens were tested with a relative humidity < 40% (air conditioned) and a temperature of approximately 75°F. Frequency for the spectrum was 8 Hz, which was governed by high-load coupons being tested on the 55 kip frame.

During the testing, specimens were monitored for cracking using a traveling microscope. The goal was to attempt to catch development along the mandrel entrance face at sizes around 0.02 inch and again at 0.05 inch. From there the tests progressed to failure with inspections of opportunity being conducted using the optical traveling microscope. We also used 45-degree inspection mirrors to monitor hole bores for cracking; however, useful crack length measurements was not typically possible, as multiple site damage tends to dominate the bore. Furthermore, many of these cracks are actually arrested “secondary” cracks with the primary cracking in the bore direction actually progressing subsurface.

3.1.3 Experimental Results

Cycles to failure are reported for the two alloys in Table 10 (2024) and Table 11 (7075). Tabular data in bold are coupons that were added beyond the original experimental design. Tabular data in bold italics are for coupons that underwent crack arrest during testing.

Data for the two alloys is presented in typical stress life (S-N) in Figure 25 and Figure 26. Analysis of the results sought to establish strong correlations between the test variables and fatigue life. Variables such as hole diameter and plate thickness did not correlate to life, whereas interference level (degree of CX) and edge margin did.

Figure 27 and Figure 28 show the fatigue life in 2024-T3 plotted against edge margin and color coded for interference level (red = 4.3%, blue = 2.8%, green = 3.55%). Note that at the low edge margin ($e/D = 1.39$), the max and min cold work data overlap, showing that the low edge margin influences are overpowering the effectiveness of the cold work (FTI recommends a minimum edge margin of 1.8 for various reasons). At the higher edge margin of 2.4, the data clearly segregate as a function of interference level. The center points (edge margin 1.8 and intermediate interference level) fall in the center of the life

distributions. This same basic behavior is shown in the 7075-T6 material (see Figure 29 and Figure 30).

Table 9. Summary of fatigue results from basic cold worked hole experiments, 2024.

Specimen ID	Max Stress	"CA" Stress	Cycles to Failure	Material	Thickness (inch)	Edge Margin	Hole Diameter	CX %	CX LEVEL
3D1-16-A	25.3	22.0	100,107	2024-T3	0.1	1.39	0.25	2.78	MIN
3D1-17-A	25.3	22.0	122,409	2024-T3	0.1	1.39	0.25	2.67	MIN
3D1-18-A	25.3	22.0	94,016	2024-T3	0.1	1.39	0.25	2.55	MIN
3D1-13-A	28.75	25.0	81,212	2024-T3	0.1	1.39	0.25	2.77	MIN
3D1-14-A	28.75	25.0	50,990	2024-T3	0.1	1.39	0.25	2.46	MIN
3D1-15-A	28.75	25.0	75,348	2024-T3	0.1	1.39	0.25	2.72	MIN
3D1-02-A	25.3	22.0	96,785	2024-T3	0.1	1.39	0.5	3.96	MAX
3D1-03-A	25.3	22.0	86,880	2024-T3	0.1	1.39	0.5	3.93	MAX
3D1-07-A	25.3	22.0	61,187	2024-T3	0.1	1.39	0.5	3.91	MAX
3D1-08-A	28.75	25.0	36,563	2024-T3	0.1	1.39	0.5	3.93	MAX
3D1-09-A	28.75	25.0	30,426	2024-T3	0.1	1.39	0.5	3.91	MAX
3D1-01-A	30.0	25.0	47,296	2024-T3	0.1	1.39	0.5	3.95	MAX
3D1-19-A	25.3	22.0	793,872	2024-T3	0.1	2.4	0.25	4.28	MAX
3D1-04-A	25.3	22.0	764,182	2024-T3	0.1	2.4	0.25	4.21	MAX
3D1-05-A	25.3	22.0	262,605	2024-T3	0.1	2.4	0.25	4.18	MAX
3D1-06-A	25.3	22.0	640,126	2024-T3	0.1	2.4	0.25	4.15	MAX
3D1-10-A	28.75	25.0	139,877	2024-T3	0.1	2.4	0.25	4.3	MAX
3D1-11-A	28.75	25.0	175,844	2024-T3	0.1	2.4	0.25	4.33	MAX
3D1-12-A	28.75	25.0	169,598	2024-T3	0.1	2.4	0.25	4.2	MAX
3D3-19-A	25.3	22.0	85,260	2024-T3	0.1	2.4	0.5	2.82	MIN
3D3-20-A	25.3	22.0	75,385	2024-T3	0.1	2.4	0.5	2.88	MIN
3D3-21-A	25.3	22.0	78,183	2024-T3	0.1	2.4	0.5	2.60	MIN
3D3-11-A	25.3	22.0	94,109	2024-T3	0.1	2.4	0.5	2.84	MIN
3D3-12-A	25.3	22.0	89,611	2024-T3	0.1	2.4	0.5	2.84	MIN
3D3-13-A	28.75	25.0	54,903	2024-T3	0.1	2.4	0.5	2.85	MIN
3D3-14-A	28.75	25.0	47,529	2024-T3	0.1	2.4	0.5	2.83	MIN
3D3-15-A	28.75	25.0	41,761	2024-T3	0.1	2.4	0.5	2.67	MIN
3D1-06-B	24.15	21.0	672,840	2024-T351	0.314	1.8	0.375	3.42	MID
3D1-12-B	24.15	21.0	272,797	2024-T351	0.314	1.8	0.375	3.37	MID
3D1-01-B	25.3	22.0	231,036	2024-T351	0.314	1.8	0.375	3.36	MID
3D1-02-B	25.3	22.0	408,988	2024-T351	0.314	1.8	0.375	3.4	MID
3D1-03-B	25.3	22.0	266,994	2024-T351	0.314	1.8	0.375	3.36	MID
3D1-04-B	25.3	22.0	223,229	2024-T351	0.314	1.8	0.375	3.4	MID
3D1-05-B	25.3	22.0	348,660	2024-T351	0.314	1.8	0.375	3.4	MID
3D1-07-B	28.75	25.0	129,663	2024-T351	0.314	1.8	0.375	3.44	MID
3D1-08-B	28.75	25.0	96,891	2024-T351	0.314	1.8	0.375	3.41	MID
3D1-09-B	28.75	25.0	105,194	2024-T351	0.314	1.8	0.375	3.42	MID
3D1-10-B	28.75	25.0	97,752	2024-T351	0.314	1.8	0.375	3.42	MID
3D1-11-B	28.75	25.0	92,889	2024-T351	0.314	1.8	0.375	3.42	MID
3D1-35-B	25.3	22.0	84,778	2024-T351	0.5	1.39	0.25	4.33	MAX
3D1-36-B	25.3	22.0	109,346	2024-T351	0.5	1.39	0.25	4.28	MAX
3D1-37-B	25.3	22.0	104,392	2024-T351	0.5	1.39	0.25	4.22	MAX
3D1-38-B	28.75	25.0	54,670	2024-T351	0.5	1.39	0.25	4.2	MAX
3D1-39-B	28.75	25.0	56,784	2024-T351	0.5	1.39	0.25	4.38	MAX
3D1-40-B	28.75	25.0	49,678	2024-T351	0.5	1.39	0.25	4.21	MAX
3D1-44-B	25.3	22.0	120,479	2024-T351	0.5	1.39	0.5	2.93	MIN
3D1-45-B	25.3	22.0	89,021	2024-T351	0.5	1.39	0.5	2.99	MIN
3D1-46-B	25.3	22.0	115,194	2024-T351	0.5	1.39	0.5	2.97	MIN
3D1-50-B	28.75	25.0	35,251	2024-T351	0.5	1.39	0.5	3.02	MIN
3D1-51-B	28.75	25.0	49,106	2024-T351	0.5	1.39	0.5	2.96	MIN
3D1-52-B	28.75	25.0	43,309	2024-T351	0.5	1.39	0.5	2.95	MIN
3D1-59-B	24.15	21.0	335,835	2024-T351	0.5	2.4	0.25	2.72	MIN
3D1-60-B	24.15	21.0	274,997	2024-T351	0.5	2.4	0.25	2.70	MIN
3D1-41-B	25.3	22.0	428,956	2024-T351	0.5	2.4	0.25	2.74	MIN
3D1-42-B	25.3	22.0	250,432	2024-T351	0.5	2.4	0.25	2.66	MIN
3D1-43-B	25.3	22.0	343,509	2024-T351	0.5	2.4	0.25	2.78	MIN
3D1-47-B	28.75	25.0	113,007	2024-T351	0.5	2.4	0.25	2.8	MIN
3D1-48-B	28.75	25.0	99,183	2024-T351	0.5	2.4	0.25	2.58	MIN
3D1-49-B	28.75	25.0	128,659	2024-T351	0.5	2.4	0.25	2.73	MIN
3D3-17-B	25.3	22.0	755,006	2024-T351	0.5	2.4	0.5	4	MAX
3D3-18-B	25.3	22.0	664,477	2024-T351	0.5	2.4	0.5	3.94	MAX
3D3-30-B	25.3	22.0	743,830	2024-T351	0.5	2.4	0.5	3.94	MAX
3D3-16-B	27	23.5	271,111	2024-T351	0.5	2.4	0.5	4.05	MAX
3D3-28-B	28.75	25.0	156,057	2024-T351	0.5	2.4	0.5	3.97	MAX
3D3-29-B	28.75	25.0	189,594	2024-T351	0.5	2.4	0.5	3.95	MAX
3D3-15-B	30.0	25.0	218,279	2024-T351	0.5	2.4	0.5	3.98	MAX

Table 10. Summary of fatigue results from basic cold worked hole experiments, 7075.

Specimen ID	Max Stress	"CA" Stress"	Cycles to Failure	Material	Thickness (inch)	Edge Margin	Hole Diameter	CX %	CX LEVEL
3D1-16-C	27.6	24.0	61,085	7075-T6	0.1	1.39	0.25	2.76	MIN
3D1-17-C	27.6	24.0	46,456	7075-T6	0.1	1.39	0.25	2.83	MIN
3D1-18-C	27.6	24.0	39,843	7075-T6	0.1	1.39	0.25	2.57	MIN
3D1-13-C	30.48	26.5	18,318	7075-T6	0.1	1.39	0.25	2.69	MIN
3D1-14-C	30.48	26.5	42,967	7075-T6	0.1	1.39	0.25	2.75	MIN
3D1-15-C	30.48	26.5	37,222	7075-T6	0.1	1.39	0.25	2.79	MIN
3D1-01-C	27.03	23.5	86,110	7075-T6	0.1	1.39	0.5	3.92	MAX
3D1-02-C	27.03	23.5	48,749	7075-T6	0.1	1.39	0.5	3.92	MAX
3D1-03-C	27.03	23.5	50,206	7075-T6	0.1	1.39	0.5	3.86	MAX
3D1-07-C	30.48	26.5	25,580	7075-T6	0.1	1.39	0.5	3.86	MAX
3D1-08-C	30.48	26.5	33,501	7075-T6	0.1	1.39	0.5	3.88	MAX
3D1-09-C	30.48	26.5	23,572	7075-T6	0.1	1.39	0.5	3.93	MAX
3D1-04-C	27.6	24.0	315,715	7075-T6	0.1	2.4	0.25	4.27	MAX
3D1-26-C	27.6	24.0	291,083	7075-T6	0.1	2.4	0.25	4.23	MAX
3D1-05-C	27.6	24.0	369,443	7075-T6	0.1	2.4	0.25	4.28	MAX
3D1-06-C	27.6	24.0	1,452,484	7075-T6	0.1	2.4	0.25	4.22	MAX
3D1-10-C	30.48	26.5	109,039	7075-T6	0.1	2.4	0.25	4.32	MAX
3D1-11-C	30.48	26.5	87,962	7075-T6	0.1	2.4	0.25	4.39	MAX
3D1-12-C	30.48	26.5	132,279	7075-T6	0.1	2.4	0.25	4.28	MAX
3D3-10-C	27.6	24.0	42,742	7075-T6	0.1	2.4	0.5	2.89	MIN
3D3-11-C	27.6	24.0	35,000	7075-T6	0.1	2.4	0.5	2.89	MIN
3D3-12-C	27.6	24.0	84,025	7075-T6	0.1	2.4	0.5	2.90	MIN
3D3-13-C	30.48	26.5	23,744	7075-T6	0.1	2.4	0.5	2.81	MIN
3D3-14-C	30.48	26.5	19,771	7075-T6	0.1	2.4	0.5	2.87	MIN
3D3-15-C	30.48	26.5	18,321	7075-T6	0.1	2.4	0.5	2.80	MIN
3D1-05-D	27.6	24.0	136,907	7075-T651	0.318	1.8	0.375	3.46	MID
3D1-06-D	27.6	24.0	160,794	7075-T651	0.318	1.8	0.375	3.51	MID
3D1-07-D	27.6	24.0	223,856	7075-T651	0.318	1.8	0.375	3.34	MID
3D1-01-D	30.48	26.5	42,052	7075-T651	0.318	1.8	0.375	3.43	MID
3D1-02-D	30.48	26.5	42,239	7075-T651	0.318	1.8	0.375	3.41	MID
3D1-03-D	30.48	26.5	51,485	7075-T651	0.318	1.8	0.375	3.35	MID
3D1-11-D	27.6	24.0	61,503	7075-T651	0.5	1.39	0.25	4.43	MAX
3D1-12-D	27.6	24.0	81,629	7075-T651	0.5	1.39	0.25	4.30	MAX
3D1-13-D	27.6	24.0	79,703	7075-T651	0.5	1.39	0.25	4.30	MAX
3D1-14-D	30.48	26.5	41,313	7075-T651	0.5	1.39	0.25	4.53	MAX
3D1-15-D	30.48	26.5	44,605	7075-T651	0.5	1.39	0.25	4.22	MAX
3D1-16-D	30.48	26.5	55,555	7075-T651	0.5	1.39	0.25	4.25	MAX
3D1-20-D	27.6	24.0	52,260	7075-T651	0.5	1.39	0.5	3.01	MIN
3D1-21-D	27.6	24.0	74,315	7075-T651	0.5	1.39	0.5	2.97	MIN
3D1-22-D	27.6	24.0	50,115	7075-T651	0.5	1.39	0.5	2.94	MIN
3D1-26-D	30.48	26.5	29,375	7075-T651	0.5	1.39	0.5	2.89	MIN
3D1-27-D	30.48	26.5	36,204	7075-T651	0.5	1.39	0.5	2.95	MIN
3D1-28-D	30.48	26.5	26,603	7075-T651	0.5	1.39	0.5	3.00	MIN
3D1-29-D	27.6	24.0	106,780	7075-T651	0.5	2.4	0.25	2.21	MIN
3D1-30-D	27.6	24.0	113,282	7075-T651	0.5	2.4	0.25	2.67	MIN
3D1-17-D	27.6	24.0	110,281	7075-T651	0.5	2.4	0.25	2.78	MIN
3D1-18-D	27.6	24.0	366,538	7075-T651	0.5	2.4	0.25	2.77	MIN
3D1-19-D	27.6	24.0	63,401	7075-T651	0.5	2.4	0.25	2.75	MIN
3D1-23-D	30.48	26.5	39,344	7075-T651	0.5	2.4	0.25	2.58	MIN
3D1-24-D	30.48	26.5	36,592	7075-T651	0.5	2.4	0.25	2.77	MIN
3D1-25-D	30.48	26.5	50,449	7075-T651	0.5	2.4	0.25	2.75	MIN
3D3-14-D	27.03	23.5	999,000	7075-T651	0.5	2.4	0.5	3.88	MAX
3D3-16-D	27.60	24.0	4,782,801	7075-T651	0.5	2.4	0.5	3.97	MAX
3D3-28-D	27.60	24.0	6,000,000	7075-T651	0.5	2.4	0.5	3.97	MAX
3D3-13-D	28.75	25.0	415,645	7075-T651	0.5	2.4	0.5	3.94	MAX
3D3-30-D	28.75	25.0	407,535	7075-T651	0.5	2.4	0.5	3.96	MAX
3D3-17-D	30.48	26.5	214,020	7075-T651	0.5	2.4	0.5	4.06	MAX
3D3-18-D	30.48	26.5	214,339	7075-T651	0.5	2.4	0.5	3.97	MAX
3D3-29-D	30.48	26.5	264,969	7075-T651	0.5	2.4	0.5	4.03	MAX

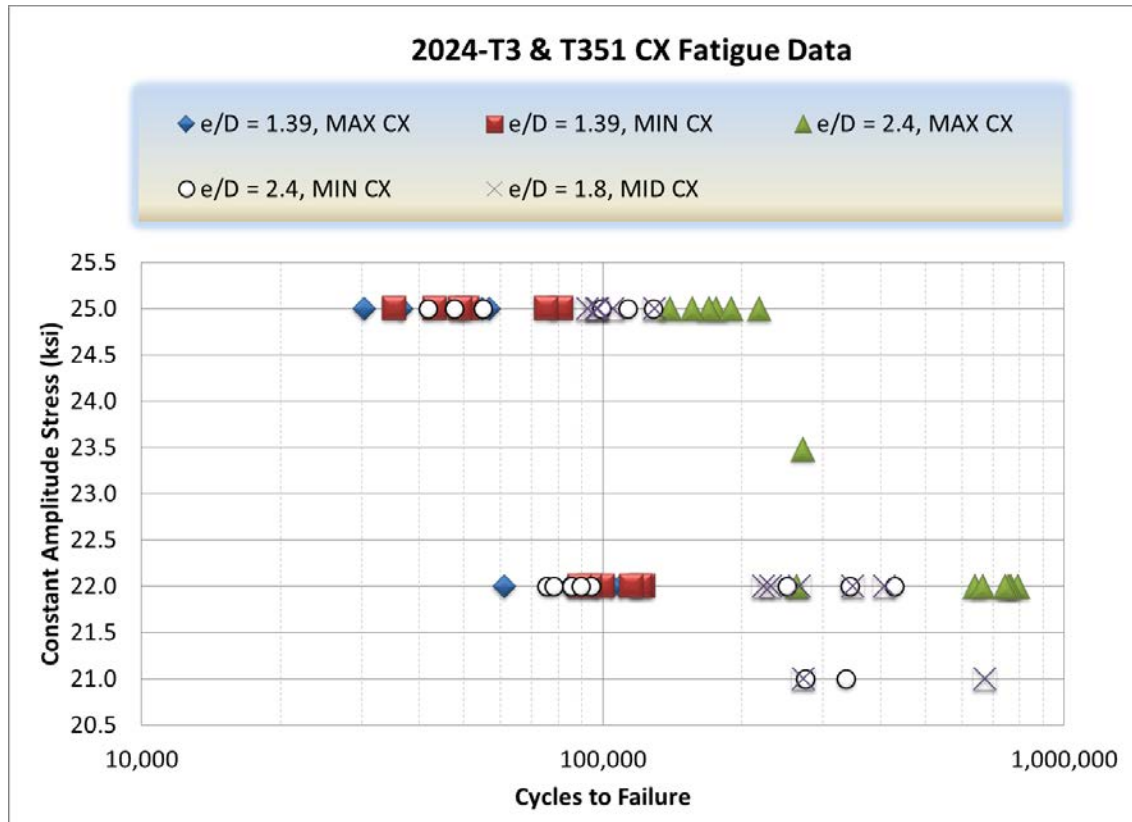


Figure 25. *S-N data for cold work fatigue tests in 2024-T3/T351 aluminum.*

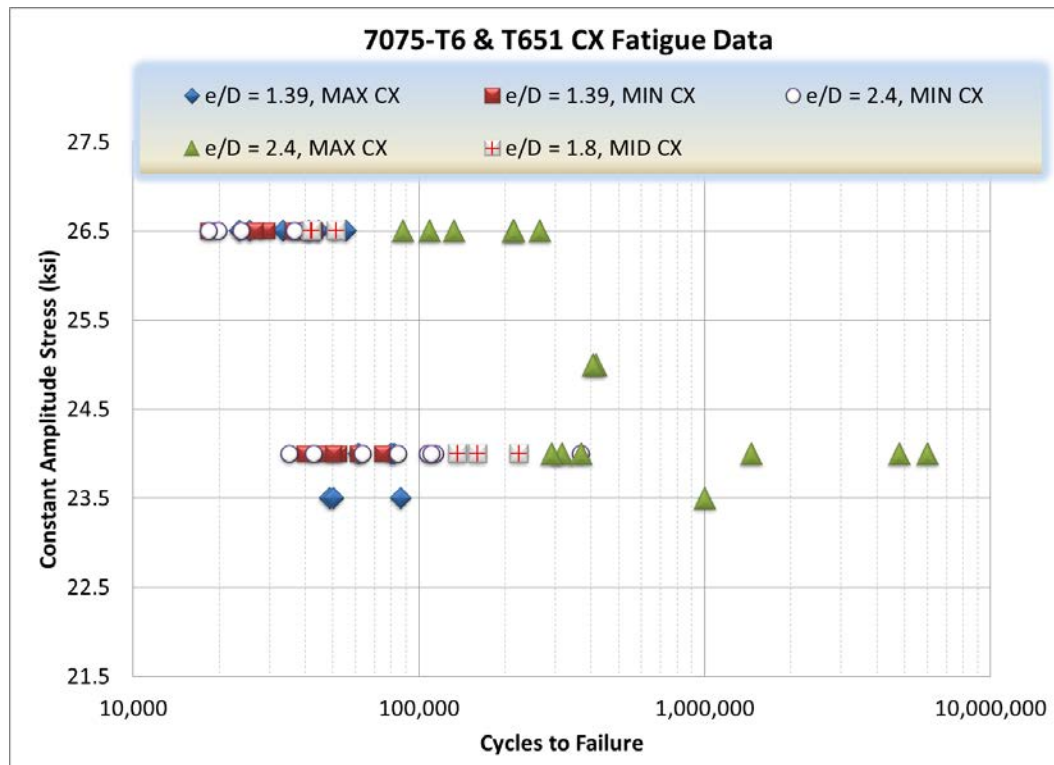


Figure 26. *S-N data for cold work fatigue tests in 2024-T3/T351 aluminum.*

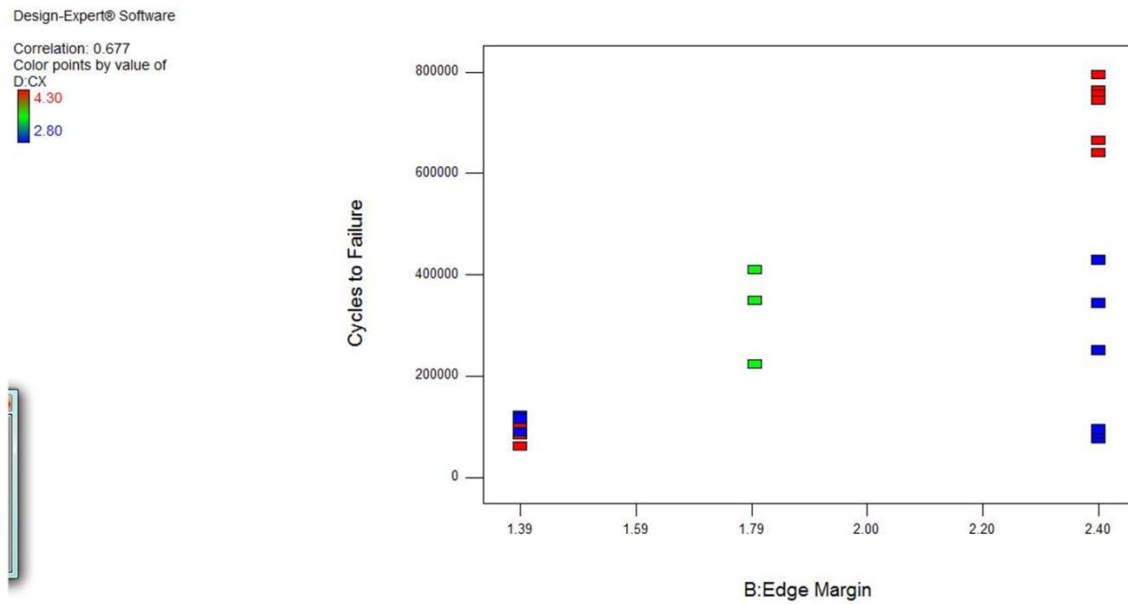


Figure 27. Cycles to failure as a function of edge margin for the 2024-T3 specimens tested at 22 ksi. Colors indicated degree of cold work (red = 4.3%, blue = 2.8%, green = 3.55%).

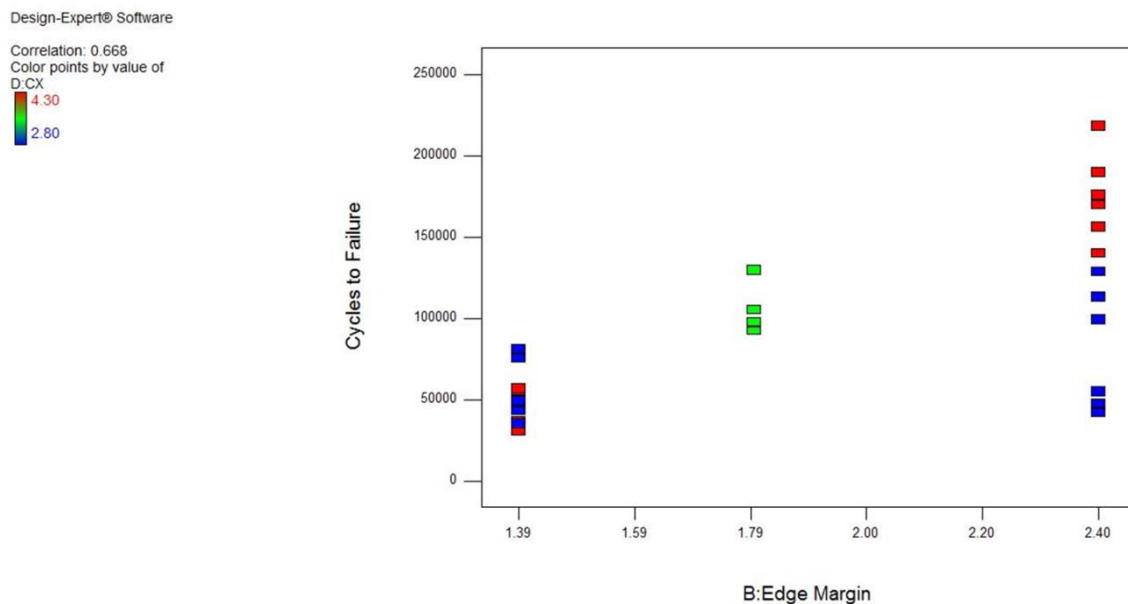


Figure 28. Cycles to failure as a function of edge margin for the 2024-T3 specimens tested at 25 ksi. Colors indicated degree of cold work (red = 4.3%, blue = 2.8%, green = 3.55%).

Design-Expert® Software

Correlation: 0.550

Color points by value of

D: CX

4.30

2.80

D: CX: 4.30

X: 2.40

Y: 5.4993

Std: 7

Run: 24

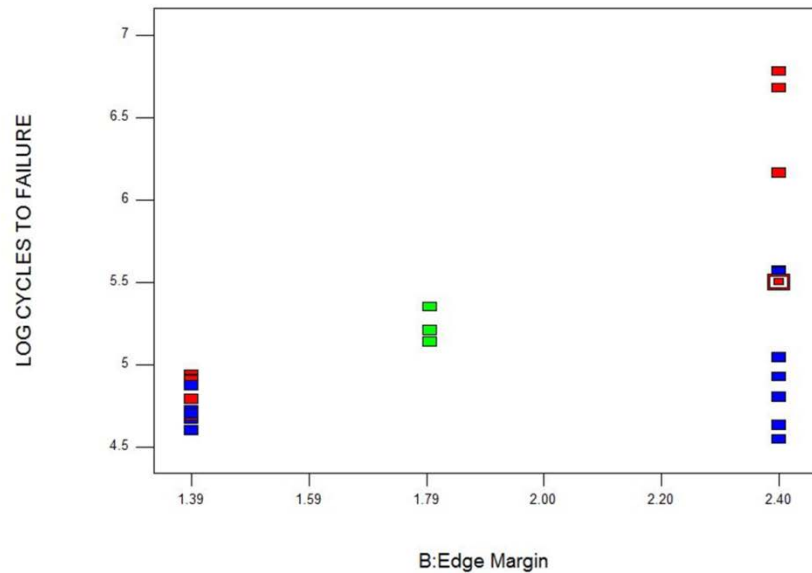


Figure 29. Log cycles to failure as a function of edge margin for the 7075-T6 specimens tested at 24 ksi. Colors indicated degree of cold work (red = 4.3%, blue = 2.8%, green = 3.55%).

Design-Expert® Software

Correlation: 0.462

Color points by value of

D: CX

4.30

2.80

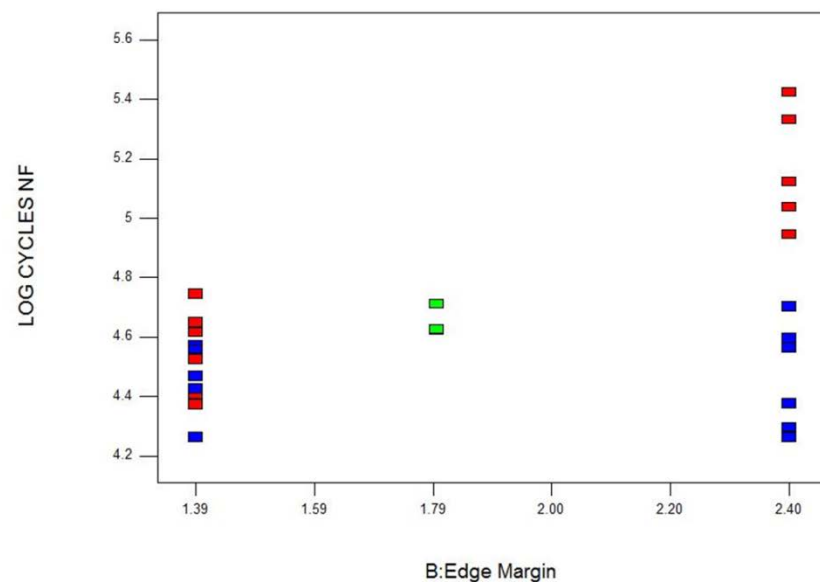


Figure 30. Log cycles to failure as a function of edge margin for the 7075-T6 specimens tested at 26.5 ksi. Colors indicated degree of cold work (red = 4.3%, blue = 2.8%, green = 3.55%).

3.1.4 Discussion of Results

Analysis of residual stress data from the contour method and a thorough understanding of fatigue failure processes at cold work holes help us explain why the parameters in the experimental design have various effects.

3.1.4.1 Hole Diameter

Hole diameter was not a major driver in fatigue response. As DeWald et al (2013) showed recently, the residual stress distributions scale with hole diameter, so that the data “collapse” when tangential hoop stresses are plotted as a function of distance from the hole normalized by radius (x/r). While it would seem that this effect would make cracks at larger holes grow slower for longer distances than cracks at small holes, this is offset by geometric effects of the larger holes and by the fact that larger diameter holes tend to have lesser degrees of interference for maximum (for example) amount of cold work in the specification.

3.1.4.2 Plate Thickness

Plate thickness (in the ranges evaluated) does not appear to have a major effect primarily because the nature of the residual stress distribution up the bore tends to be somewhat insensitive to this dimension (Figure 31). Examination of the data in the residual stress database (see Section 4) shows that, as a rule, the stresses at the mandrel entrance face are the least compressive. They then “increase” to some maximum compressive value approximately 0.1 inch up the bore, and then stay consistent until dropping again near the mandrel exit face. This basic trend exists whether the plate is 0.19 inch thick or 0.5 inch thick. The catch is that 99% of the life at a typical cold worked hole is consumed at crack sizes that are 0.15 inch or smaller. Thus, by the time cracks get large enough to start “taking advantage” of the extra material in the thickness direction, the residual stress effects are gone and failure is imminent.

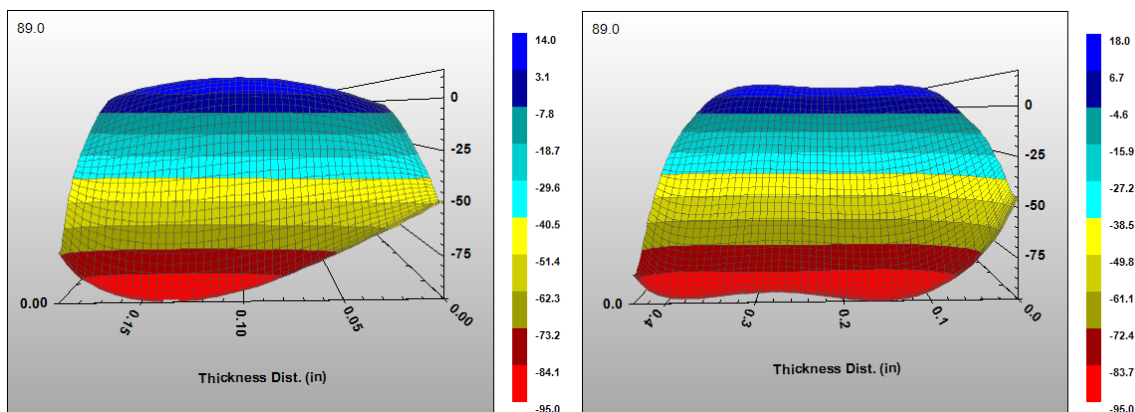


Figure 31. Residual stress in two 7075-T651 coupons of different thickness. Coupon on the left is 0.19” thick; the one on the right is 0.436 inch thick. Note that both reach their maximum residual stress on the bore (x axis) at approximately 0.12 inch away from the mandrel entrance face (right side of each image).

4 Residual Stress Measurements & Database

This chapter describes the residual stress measurement process and data matrices for this project. These data were ultimately included in a residual stress database that was delivered under this program. For presentation purposes, the data are divided into three groups:

1. Mod-III groups (see Table 12).
2. Thirty-seven (37) coupons manufactured from 7075-T6 sheet and 7075-T651 aluminum plate of various thicknesses (Table 13).
3. Twenty-eight (28) cold-worked coupons (+ four spares) were manufactured from various aluminum alloys of various thicknesses. A few of the coupons were also made of 4340 steel (180 ksi ultimate heat treat). See Table 14 for details.

The data from the third group were developed under a previous, separate program (see Section 4.1). These data were gathered using other protocols, but for purposes of the database development, it was possible to make the data compatible.

4.1 Summary of A-10 MODIII Residual Stress Measurements

Residual stress was measured by the contour method measurement process in 38 coupons of varying dimensions, materials, hole diameters, number of holes and cold work levels. Contour method measurements by Hill Engineering, Inc. To quantify repeatability, replicate measurements were made for each coupon group. This project was funded by A-10 TLPS, Modernization III PWS 3.5.8 program.

All coupons started with same dimensions except for four coupons (C1 and C2)—flat plate, 4 in. wide, 5 in. high, and 0.25 in. thick. Hole diameters varied from 0.25 in. to 0.75 in. Most coupons had one centered hole, other coupons had two or three holes. All coupons were symmetric: holes of single hole coupons were drilled in the center of the plate; each hole in the two (2) hole coupons were each drilled the same distance from the nearest free edge; two holes in the three-hole coupons were drilled the same distance from the free edges, and the 3rd hole centered in the plate. The measurement matrix is found in Table 12. The following effects were measured:

1. cold working level (all within process tolerances), coupon groups A2/E1-X/E2,
2. hole size, coupon groups A1/A2/A3 (2024) and D1/D2/D3 (7075),
3. edge margins, coupon groups B1/B2/B3,
4. hole interactions, coupon groups C1-X/C2-X, and
5. material effects, coupon groups A1/A2/A3 (2024-T351) and D1/D2/D3 (7075-T651).

Table 11. Summary of earlier residual stress data gathered by USAF and Hill Engineering (other contracts).

Coupon Group	Holes	Width, W in.	Height H in.	Thickness t, in.	Diameter D in.	e/D	Material	Replicates
A1	1	4	5	0.25	0.25	8	2024-T351	3
A2	1	4	5	0.25	0.5	4	2024-T351	5
A3	1	4	5	0.25	0.75	2.67	2024-T351	3
B1	2	4	5	0.25	0.5	1.2	2024-T351	2
B2	2	4	5	0.25	0.5	1.5	2024-T351	2
B3	2	4	5	0.25	0.5	2	2024-T351	2
C1-X	3	1.8	5	0.25	0.25	1.2	2024-T351	2
C2-X	3	3.6	5	0.25	0.5	1.2	2024-T351	2
D1	1	4	5	0.25	0.25	8	7075-T651	3
D2	1	4	5	0.25	0.5	4	7075-T651	3
D3	1	4	5	0.25	0.75	2.67	7075-T651	3
E1-X	1	4	5	0.25	0.5	4	2024-T351	5
E2	1	4	5	0.25	0.5	4	2024-T351	3

4.2 Coupons from the RIF Program

The design for all of the coupons under this program was a simple 5-inch long by 4-inch wide rectangle. Thicknesses varied by stock (see Table 13 and Table 14). These same tables also show the hole diameters and edge margins for each coupon. Residual stresses were measured along the 4-inch width dimension.

Specimens were prepared up through the initial ream process by a professional machine shop. Then, APES cold worked each coupon using the appropriate FTI or custom tooling. The holes were then final reamed to their target diameters. Each hole was deburred lightly without breaking the corners.

Table 12. Details of first specimen group for residual stress measurement.

Residual Stress Plates (Coupon K)						
Material	Thickness	Hole D (final ream)	Edge Margin	Hole Center (distance from edge)	Specimen IDs	# Plates
7075-T6	0.19	0.25	1.8	0.450	3K1-04-C 3K1-05-C	2
7075-T651	0.436	0.25	1.8	0.450	3K1-19-D 3K1-20-D	2
7075-T6	0.19	0.5	1.8	0.900	3K1-06-C 3K1-07-C	2
7075-T651	0.436	0.5	1.8	0.900	3K1-21-D 3K1-22-D	2
7075-T6	0.19	0.25	3.0	0.750	3K1-08-C 3K1-09-C	2
7075-T651	0.436	0.25	3.0	0.750	3K1-23-D 3K1-24-D	2
7075-T6	0.19	0.5	3.0	1.500	3K1-10-C 3K1-11-C	2
7075-T651	0.436	0.5	3.0	1.500	3K1-25-D 3K1-26-D	2
7075-T6	0.1	0.375	2.4	0.900	3K1-01-C 3K1-02-C	2
7075-T651	0.5	0.375	2.4	0.900	3K1-30-D 3K1-31-D	2
7075-T651	0.313	0.17	2.4	0.408	3K1-01-D 3K1-02-D	2
7075-T651	0.313	0.58	2.4	1.392	3K1-03-D 3K1-04-D	2
7075-T651	0.313	0.375	1.39	0.521	3K1-05-D 3K1-06-D	2
7075-T651	0.313	0.375	3.41	1.279	3K1-07-D 3K1-08-D	2
7075-T651	0.313	0.375	2.4	0.900	3K1-09-D 3K1-10-D 3K1-11-D 3K1-12-D 3K1-13-D 3K1-14-D	6
7075-T651	0.436	0.375	1.8	0.675	3K1-27-D	1
7075-T651	0.313	0.25	2.4	0.600	3K1-15-D	1
7075-T6	0.19	0.375	3.0	1.125	3K1-12-C	1

Table 13. Details of second specimen group for residual stress measurement.

Material	Thickness	CX Level	Final Ream Dia. (inch)	Edge Margin	Specimen
2024-T3	0.19	MAX	0.3750	1.5	3K1-04-A
2024-T3	0.19	MAX	0.3750	1.5	3K1-05-A
2024-T3	0.19	MIN	0.3750	1.5	3K1-06-A
2024-T3	0.19	MIN	0.3750	1.5	3K1-07-A
2024-T3	0.19	MAX	0.4375	1.3	3K1-08-A
2024-T3	0.19	MAX	0.4375	1.3	3K1-09-A
2024-T351	0.313	MAX	0.3750	1.8	3K1-01-B
2024-T351	0.313	MID	0.3750	1.8	3K1-02-B
2024-T351	0.313	MIN	0.3750	1.8	3K1-03-B
2024-T351	0.5	MAX	0.5000	2.4	3K1-04-B
2024-T351	0.5	MID	0.5000	2.4	3K1-05-B
2024-T351	0.5	MID	0.5000	2.4	3K1-06-B
2024-T351	0.5	MIN	0.5000	2.4	3K1-07-B
2024-T351	0.5	MIN	0.5000	2.4	3K1-08-B
7050-T7451	0.5	MAX	0.3750	1.4	3K1-01-E
7050-T7451	0.5	MAX	0.3750	1.4	3K1-02-E
7050-T7451	0.5	MAX	0.3750	1.4	3K1-03-E
7050-T7451	0.5	MAX	0.3750	2.4	3K1-04-E
7050-T7451	0.5	MAX	0.3750	2.4	3K1-05-E
7050-T7451	0.5	MAX	0.3750	2.4	3K1-06-E
4340 Steel	0.25	MAX	0.2500	1.4	3K1-01-F
4340 Steel	0.25	MAX	0.2500	1.4	3K1-02-F
4340 Steel	0.25	MAX	0.2500	1.4	3K1-03-F
4340 Steel	0.25	MAX	0.2500	2.4	3K1-04-F
4340 Steel	0.25	MAX	0.2500	2.4	3K1-05-F
4340 Steel	0.25	MAX	0.2500	2.4	3K1-06-F
7075-T7351	0.25	MAX	0.2500	3.8	3K1-01-G
7075-T7351	0.25	MAX	0.2500	3.8	3K1-02-G
7075-T7351	0.25	MID	0.2500	3.8	3K1-03-G
7075-T7351	0.25	MID	0.2500	3.8	3K1-04-G
7075-T7351	0.25	MIN	0.2500	3.8	3K1-05-G
7075-T7351	0.25	MIN	0.2500	3.8	3K1-06-G
Orange Italics:	SPARES. Not used.				

4.3 Basics of the Contour Method

Residual stress measurements will be made with the Contour Method; these measurements are made on each coupon first by cutting a coupon with wire electric discharge machining (EDM) at a measurement plane, then using a scanning laser profilometer to measure displacement of the plane. The fundamental idea of the Contour Method is that, after cutting the coupon, the measurement plane will deform slightly as it relaxes due the residual stress on that plane. A finite element simulation uses the negative of the deformed surface as the imposed displacement boundary condition on the measurement plane, and with information about the material's constitutive behavior, the stresses that result from the application of the imposed displacement (which will deform the surface back to its original, flat shape) are assumed to be the residual stresses in the coupon before dissection. The advantage of this method is that stresses normal to the surface can be determined for a 2D plane, in contrast to most other residual stress measurement techniques, which can measure stress only in a 1D direction. More information about the method can be found in Prime (2009). A schematic representation of the basis of the method and resulting residual stress contours for a welded work piece are shown in Figure 32 from DeWald et. al (2009).

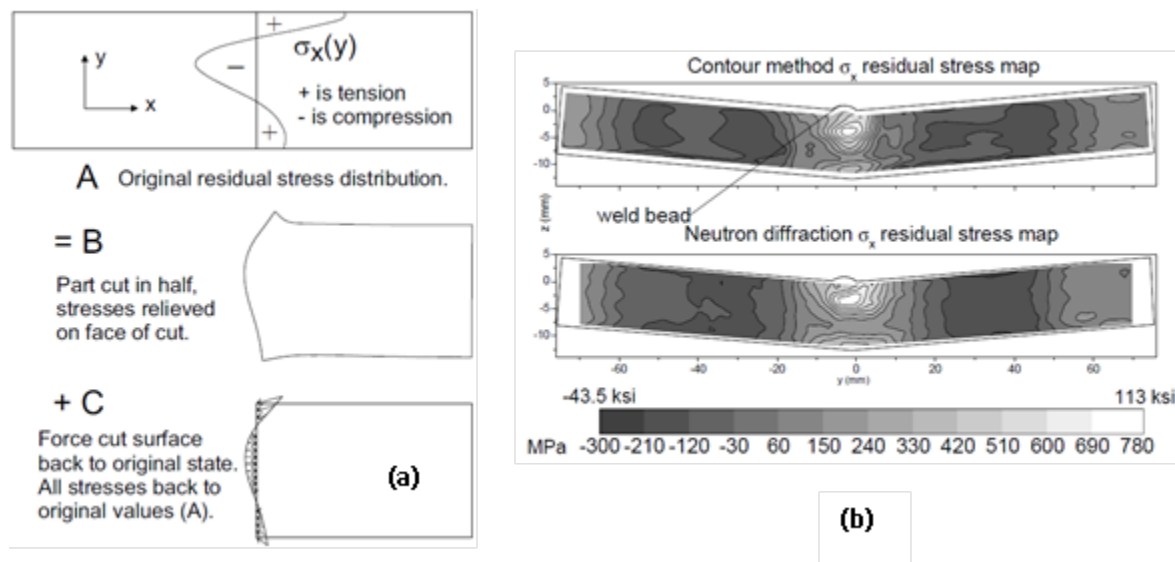


Figure 32. Contour Method (a) provides good correlation to Neutron Diffraction (b) at lower cost (after DeWald et al., 2009).

4.4 Instructions for Data Gathering

Hill Engineering was the subcontractor that provided the contour method measurements under this program. Hill Engineering has a lot of experience in this method and has a long working relationship with the USAF customer. Hill Engineering has their own

protocols for gathering and reducing data. We simply provided some basic requirements for method, data density, and specimen orientation for processing:

- Use the contour method to quantify the residual stress over the plane passing through the center of the hole.
- Use a consistent convention for each coupon where *the face opposite the ID label marks* is the $Y = 0$ plane (mandrel entrance face). The reference location ($X = 0$) for the X-axis shall be the side of the coupon on the short edge of the fastener hole.
- Supply the data for each coupon as tabulated values with an X-Y coordinate and a magnitude (the residual stress). Data density was to be sufficient to allow APES to construct a detailed surface. Review of other contour method data showed that a grid spacing of approximately 0.005 inch was common.

4.5 Typical Results

The Contour Method provides a 2D map of the residual stresses on the cut surface. APES constructed a visualizer in MatLab to quickly examine the data. A typical residual stress plot as shown in the visualizer is presented in

Figure 33. Four views are present, which we have labeled as a) isometric, b) top, c) front, and d) side.

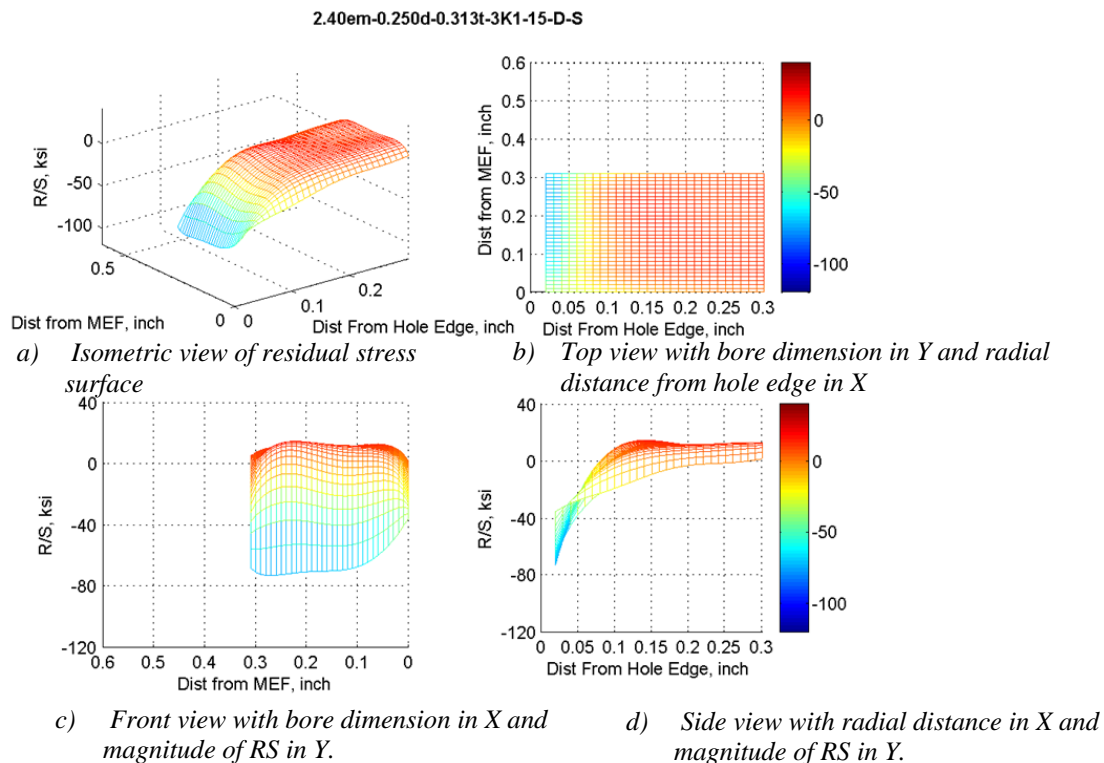


Figure 33. Typical four-pane view of RS distribution from MatLab visualizer tool used during this program.

4.6 Residual Stress Database

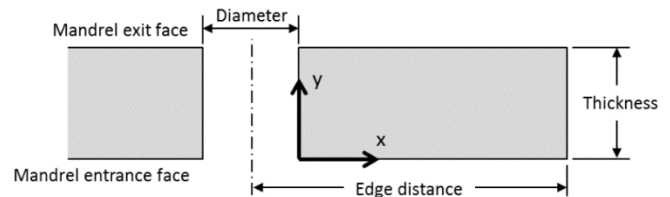
One of the inputs required for the prediction of crack growth behavior at a cold worked fastener hole is the matrix of residual stresses along the anticipated plane of crack growth. These residual stresses are produced by the cold working process and drastically change the crack growth behavior, when compared to a crack growing at a non-cold worked hole. Under this program, residual stress matrices were produced using variations in alloy, material thickness, hole diameter, hole edge distance, and interference level.

For this program, APES, Inc. and ESRD, Inc. have produced a database to facilitate rapid interrogation, visualization, and interpolation of residual stress data based on the test matrices described in Section 4. The database is a deliverable under this contract, and it comes with a 13-page document (RS Database Documentation.pdf) that explains its workings.

Basically, the residual stress database rs_database.dll is a .Net assembly that can be COM (component object model)-registered along with its type library rs_database.tlb. The DLL is accessible from any COM-enabled application, and it provides a standalone residual stress profile visualizer for visualization and interpolation.

The database searches for a subfolder 'db' which contains *.rs files. Additional *.rs files may be added by the user. Each *.rs file represents one data entry with a set of parameters and a residual stress point cloud. The database entry .rs file format is an ASCII format with the following structure: Any number of (x,y,Sz) points may be specified. Any number of digits after the decimal place is acceptable. Dimensional units must be inches and stress units must be ksi. Comments can be placed on any line after a '%' character. The (x,y) points must define a rectangular grid but can be in any order with arbitrary spacing.

```
materialName (string)
comments (string)
th (double)
dia (double)
ed (double)
pctCX (double)
x1 (double), y1 (double), Sz1 (double)
x2 (double), y2 (double), Sz2 (double)
x3 (double), y3 (double), Sz3 (double)
x4 (double), y4 (double), Sz4 (double)
x5 (double), y5 (double), Sz5 (double)
```



For example:

```
7075-T6 % material
3K1-01-C % comments
0.100000 % thickness
0.375000 % diameter
0.900000 % edge distance
4.000000 % coldwork percentage
0.000000, 0.000000, -32.100000
0.000000, 0.002000, -35.500000
0.000000, 0.004000, -38.700000
0.000000, 0.006000, -40.900000
```

0.000000, 0.008000, -42.600000
0.000000, 0.011000, -43.900000
0.000000, 0.013000, -44.800000

The database interpolator uses a 4D Delaunay simplex finder. A simplex is found which encloses the given query/interpolation point described by input parameters. The vertices of the simplex are database entries, and the query point is interpolated between the vertices. For additional details refer to the user's guide supplied with the database, **RS Database Documentation.pdf**.

Note that for purposes of interpolation, it is only possible to have one representative curve for each unique set of parameters. In all cases thus far, however, there are replicates. Thus, it was necessary to average the residual stresses in these situations. The rules for data evaluation and preparation are shown in the following section. *Even though the RS database contains averaged values for a given set of conditions, all individual RS files have been delivered to the USAF, so it is possible to evaluate sensitivity of fatigue life to variability in RS data if desired.*

4.6.1 Rules for Processing Files for Inclusion in Residual Stress Database

To provide database integrity, it was necessary to construct a set of rules for processing the data as received from Hill Engineering. These rules and procedures are:

1. **One data set per parameter set.** Only one data set is allowed for each combination of material, CX level, Diameter, thickness, and edge distance (but the data set is based on replicate measurements).
2. **Adjust thickness to nominal values.** Visualizer has some trouble plotting data properly if the maximum “y” (thickness direction) coordinate is smaller than the nominal values—extrapolated values are plotted as constants from last known point(s).
3. **Origin.** Set all first points (origins) to (0,0).
4. **Different CX%.** For files that use other than nominal CX values—we have a good idea of actual CX % because toolset dimensions were carefully controlled—use MIN CX%=3, MID CX%=3.5, and MAX CX%=4.0 regardless of actual value.
5. **Averaging Single Hole Coupons.** For symmetric, one hole coupons, there is one left side and one right side. If coordinate points are the same on each side, average the left and right side and create one file for the database. If coordinate points are not the same on each side, use cubic splines to interpolate data the same combinations of (x,y) coordinates. Average left and right, create one file for the database.
6. **Averaging Multiple Hole Coupons.** For symmetric, two or three hole coupons, there are 2 ‘short’ sides—there are two ligaments from the holes nearest the free edges to the free edge. There is therefore one left side and one right side. If coordinate points are the same on each side, average the left and right side and create one file for the database. If coordinate points are not the same on each side,

- use cubic splines to interpolate data the same combinations of (x,y) coordinates. Average left and right, create one file for the database.
7. **Handling Offset Hole Coupons.** Create a file of the short side and put in the database.
 8. **Averaging Replicates.** If there are replicates, average across all replicates and across both the left and right sides. If coordinate points are the same on each side, average the left and right side and create one file for the database. If coordinate points are not the same on each side, use cubic splines to interpolate data the same combinations of (x,y) coordinates. Average left and right, then create one file for the database
 9. **Flipped Coordinates.** Using our best judgment, swap y coordinates for files which residual stress data has been flipped. Typically, the y=0 data is the “mandrel entrance face” and usually easily identified by the magnitude of the R/S, which is generally lower on the mandrel entrance face compared to the mandrel exit face. If the opposite is true, it may be appropriate to flip the y-coordinate of the data.

Special note: The binning of % CX as MIN, MID, and MAX was necessary to improve interpolation capabilities. For instance, many of the coupons were processed using “MAX CX%, but the actual percentage of cold work for a MAX interference conditions varies substantially based on the toolset used (from 4.75% with toolset 4-3-N and 3.63% for toolset 18-1-N). Thus, we have reassigned all MAX interference conditions to a CX value of 4% regardless of diameter and actual CX%. A similar pattern was followed for the MID and MIN interference levels as shown in item 4 above.

4.6.2 Sample Database Images

Screen shots from the database visualizer are shown in the figures contained in this section. Figure 34 shows a typical visualizer view. The condition selected is highlighted in the contents menu on the left.

Figure 35 shows a series of four independent database entries that are interpolated to produce the distribution in Figure 36. Figure 37 is also included to show the parameters that define the interpolated condition, which is roughly in the center of the available interpolation space.

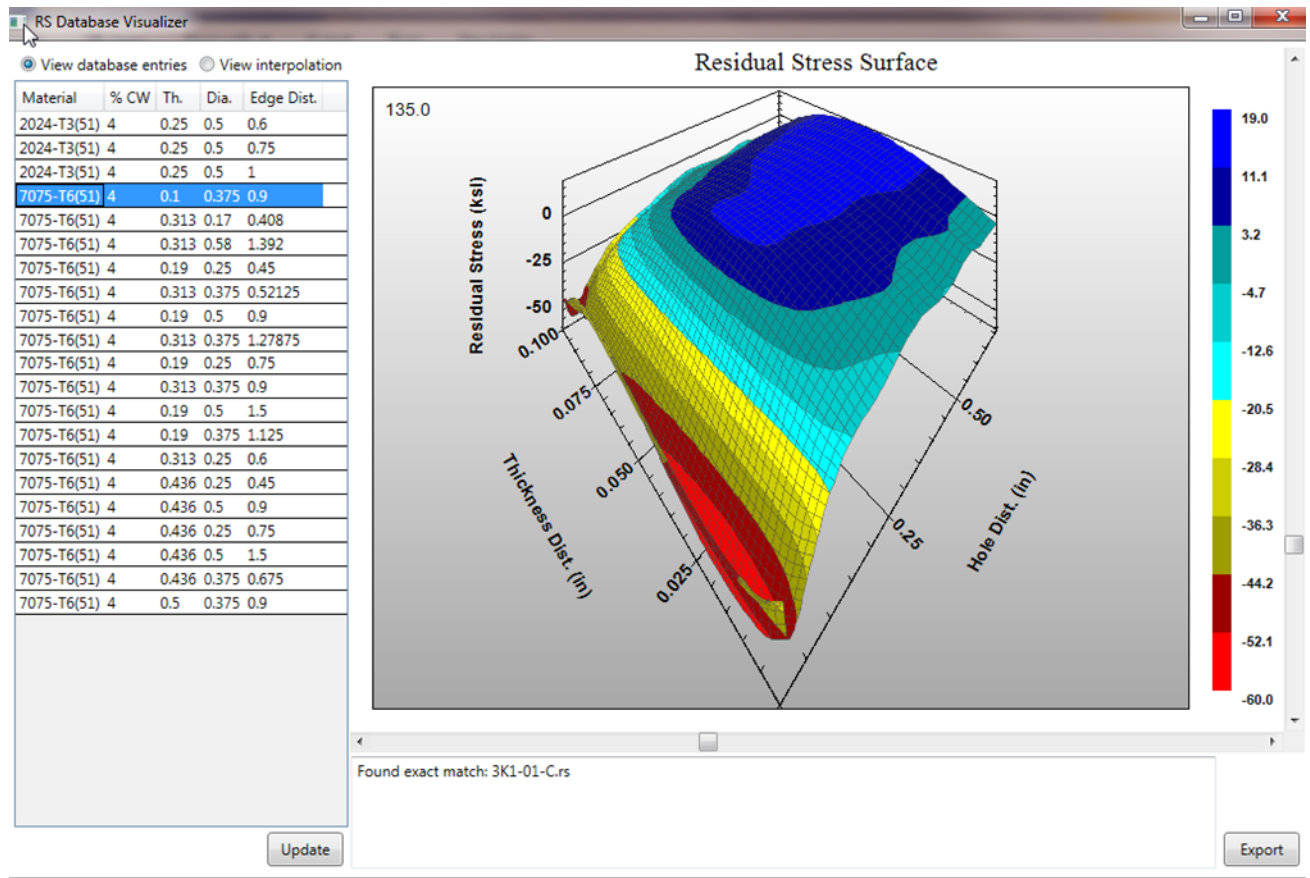


Figure 34. Typical database view including menu of conditions at left.

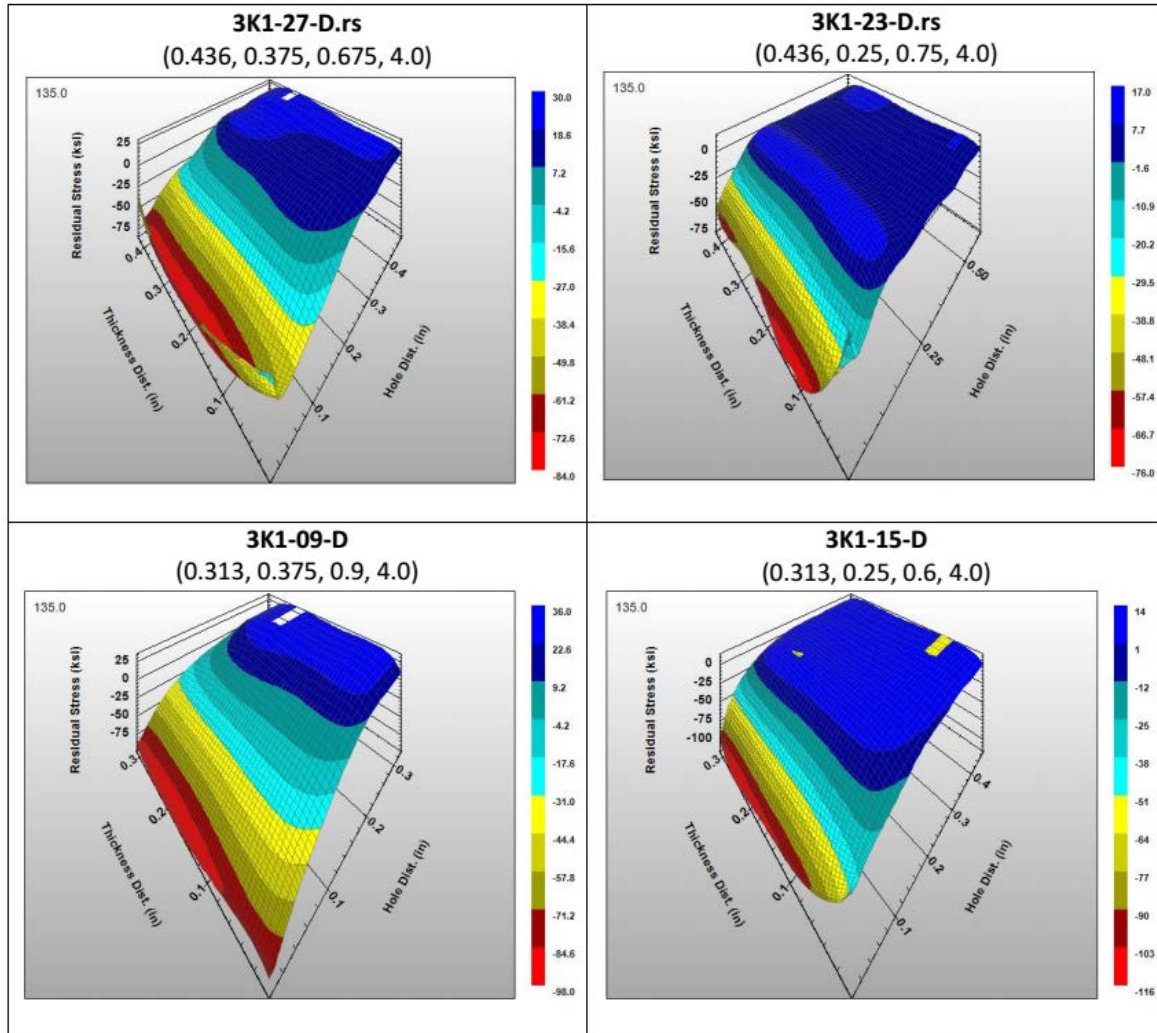


Figure 35. Four independent data sets that define the interpolation space for the distribution in Figure 36.

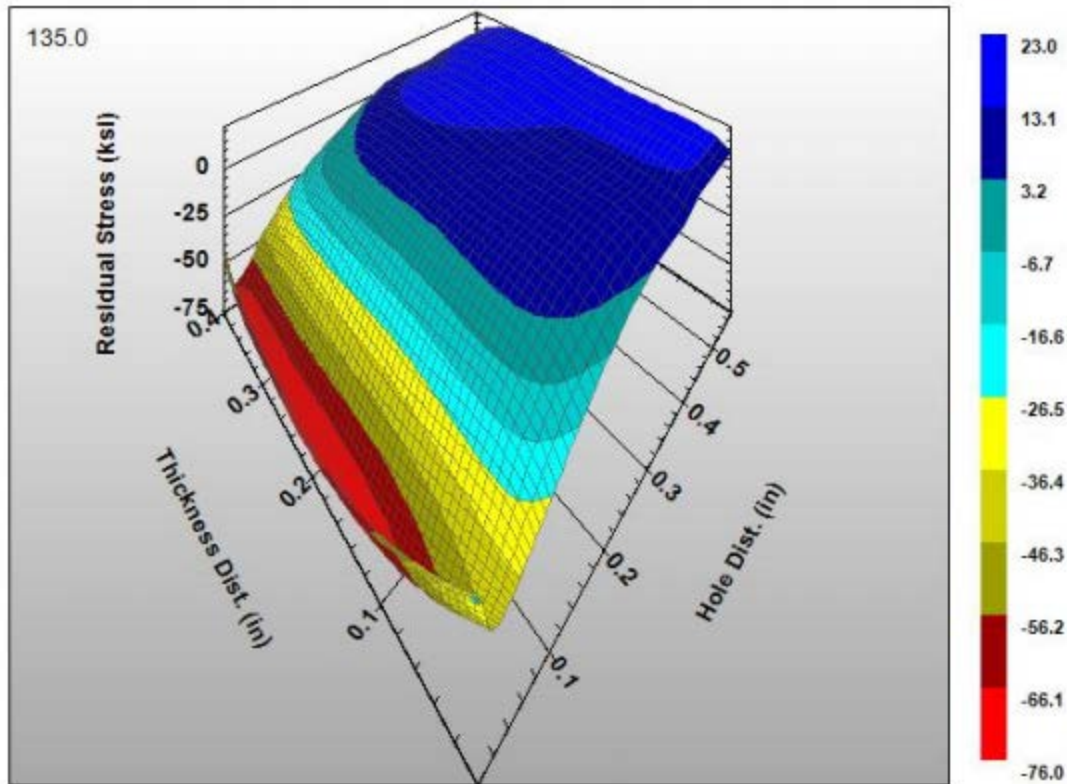


Figure 36. Interpolated surface from the four database entries in Figure 35.

Material:	7075-T651	
Percent coldwork:	4	%
Thickness:	0.4	in
Diameter:	0.35	in
Edge distance:	0.75	in

Figure 37. Interpolation parameters associated with Figure 36, above.

5 Computing Stress Intensity and Crack Front Shape for Cracks in Residual Stress Fields

This chapter summarizes the work performed by Engineering Software Research and Development (ESRD), Inc. to incorporate functionality to the finite element analysis software product StressCheck in support of the this program.

The work was actually divided into three parts:

1. Computation of stress intensity factors
2. Development of a residual stress database
3. Crack front shape progression

This chapter only deals with items (1) and (3). The details of the residual stress database are provided in Chapter 4.

5.1 Computation of stress intensity factors

Functionality was added to StressCheck to compute Stress Intensity Factors (SIFs) in the presence of residual stresses due to cold-expanded holes. This functionality was implemented in StressCheck 10.1 released on June 2014.

To account for residual stresses in the computation of SIFs, two approaches were implemented to analyze cracks emanating from cold-worked holes: The modified J-integral and the modified Contour Integral Method (CIM).

- A modification of the Rice J-integral for cracks in a residual stress field was implemented in which the residual stresses are treated as initial strains (Lei et al., 2000). The J-integral works extremely well provided the complete residual stress field is available (from measurements or simulation) to perform the analysis. The modified J-integral is summarized in Figure 38.

$$J = \int_{\Gamma} \left(W \delta_{ij} - \sigma_{ij} \frac{\partial u_j}{\partial x_1} \right) n_i dS + \underbrace{\int_A \sigma_{ij} \frac{\partial \varepsilon_{ij}^0}{\partial x_1} dA}_{\text{Correction term for residual stresses (from [1])}}$$

$$W = \int_0^{\varepsilon_{ij}^m} \sigma_{ij} d\varepsilon_{ij}^m \quad \left. \vphantom{\int_0^{\varepsilon_{ij}^m}} \right\} \text{Mechanical strain energy density}$$

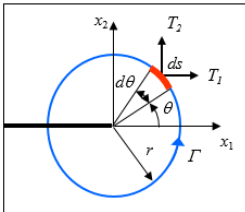
$$\varepsilon_{ij} = \varepsilon_{ij}^m + \varepsilon_{ij}^0 \quad \left. \vphantom{\varepsilon_{ij}} \right\} \text{Total strain = mechanical strain + initial/residual strain}$$


Figure 38: The modified J-integral

The J-integral components J_I , J_{II} and J_{III} are converted to the corresponding SIFs K_I , K_{II} , K_{III} by the following relations:

$$K_I = \sqrt{\tilde{E} J_I} \quad K_{II} = \sqrt{\tilde{E} J_{II}} \quad K_{III} = \sqrt{2G J_{III}}$$

$$\text{Plane-stress: } \tilde{E} = E \quad \text{Plane-strain: } \tilde{E} = \frac{E}{1 - \nu^2} \quad G = \frac{E}{2(1 + \nu)}$$

- An alternative approach for computing SIFs was implemented by applying the principle of superposition as indicated in Figure 39.

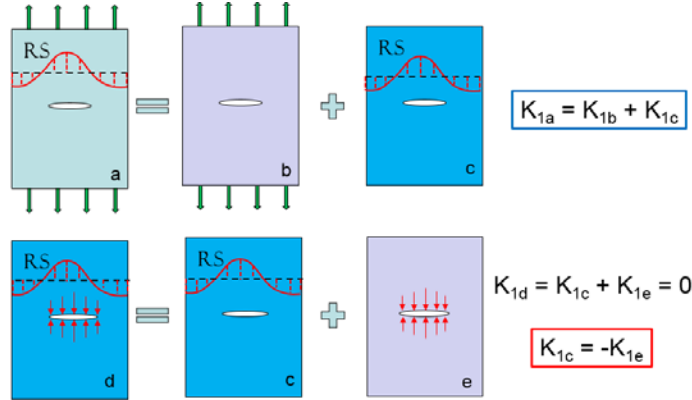


Figure 39: principle of superposition to compute SIF due to residual stresses

The effect of residual stresses are accounted for by loading the faces of the crack with the traction distribution required to restore the traction-free boundary condition when the crack is introduced in the residual stress field. The use of the modified Contour Integral Method (CIM) to account for loaded crack faces (Pereira and Duarte, 2006) was implemented and the results compared with those obtained from the J-integral (Figure 40). The CIM with loaded crack implementation is faster than the J-integral and is ideally suited when only one component of the residual stress tensor is available, for example, from experimentally measured residual stresses using the contour method (Prime, 2001).

CIM as implemented in StressCheck 9.2

$$K_I = \int_{\Gamma_2} \left(T_x^{(u)} v_x + T_y^{(u)} v_y - T_x^{(v)} u_x - T_y^{(v)} u_y \right) ds + \int_{\Gamma_3} \left(T_x^{(3)} v_x + T_y^{(3)} v_y \right) ds + \int_{\Gamma_4} \left(T_x^{(4)} v_x + T_y^{(4)} v_y \right) ds.$$

Modification for loaded crack faces implemented in SC10.1

Figure 40: The Contour Integral Method for loaded cracks

Loading the crack with a traction distribution normal to the crack face and computing the SIF using CIM-LC was compared with the J-integral when the specimen was loaded with the full {RS} tensor from a simulated CW operation. The approach is illustrated in Figure 41.

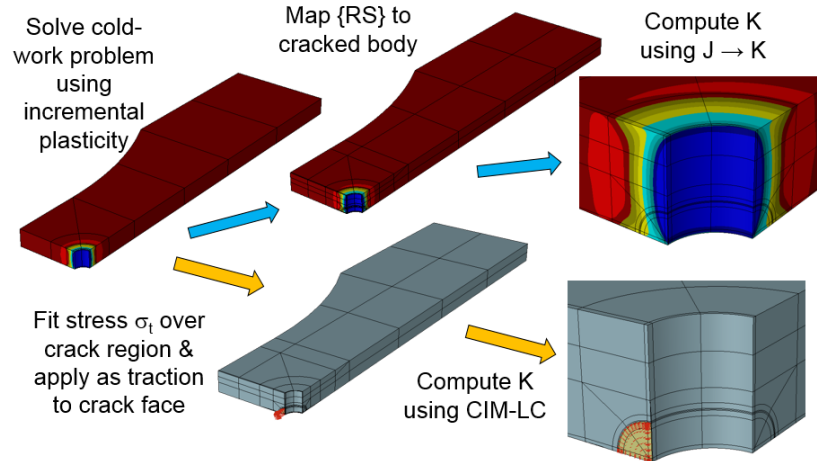


Figure 41: Residual stress by simulation of cold work process

The comparison between the two approaches for computing the value of K_I due to residual stresses only along the crack front of a 0.025" corner crack is illustrated in Figure 42.

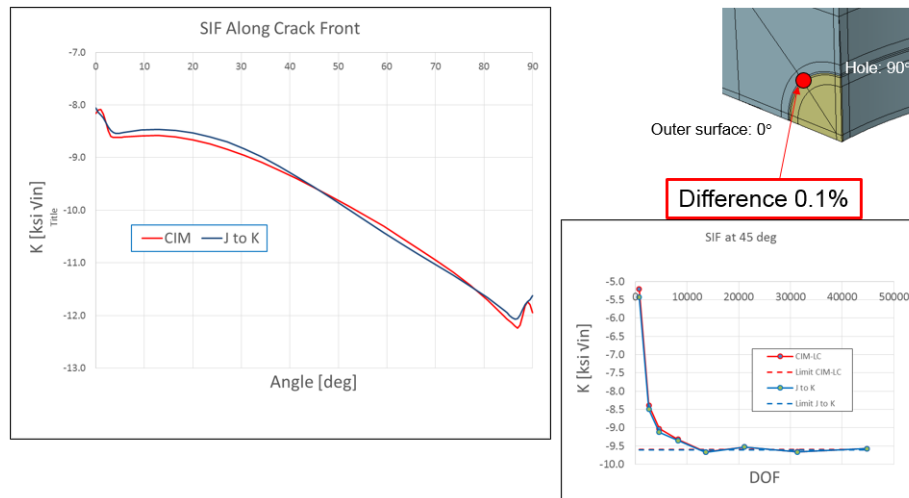


Figure 42: Stress intensity factors due to residual stresses for a 0.025" corner crack

5.2 Crack Front Shape Progression

This section discusses the development of a crack propagation tool for the prediction of fatigue life in specimens with a cold-expanded hole with an initial pre-crack subjected to constant or variable amplitude loading.

5.2.1 Background

The crack shapes associated with cold worked holes are unusual (see Figure 43). In this figure, the X axis is the mandrel entrance face, and the Y axis is the hole bore. Individual data series represent shape of the crack front at different points in the life (e.g., the series Pri-9.3% indicates the position and shape of the primary crack front at 9.3% of total life).

Note the bulbous shape developed by the crack as it grows larger and the intense pinning of the crack front approximately 0.1 inch up the bore.

These unusual behaviors are not captured by traditional two-point elliptical crack fronts (such as those used for part-through cracks in traditional crack growth codes), and the use of a two-point elliptical crack front will cause erroneous results in life prediction. In many cases, a purely two-point crack with computation points at the surface will not grow in a residual stress field. In the analysis, the crack must be able to seek out the path of least resistance in the residual stress field, which the multi-point approach allows it to do.

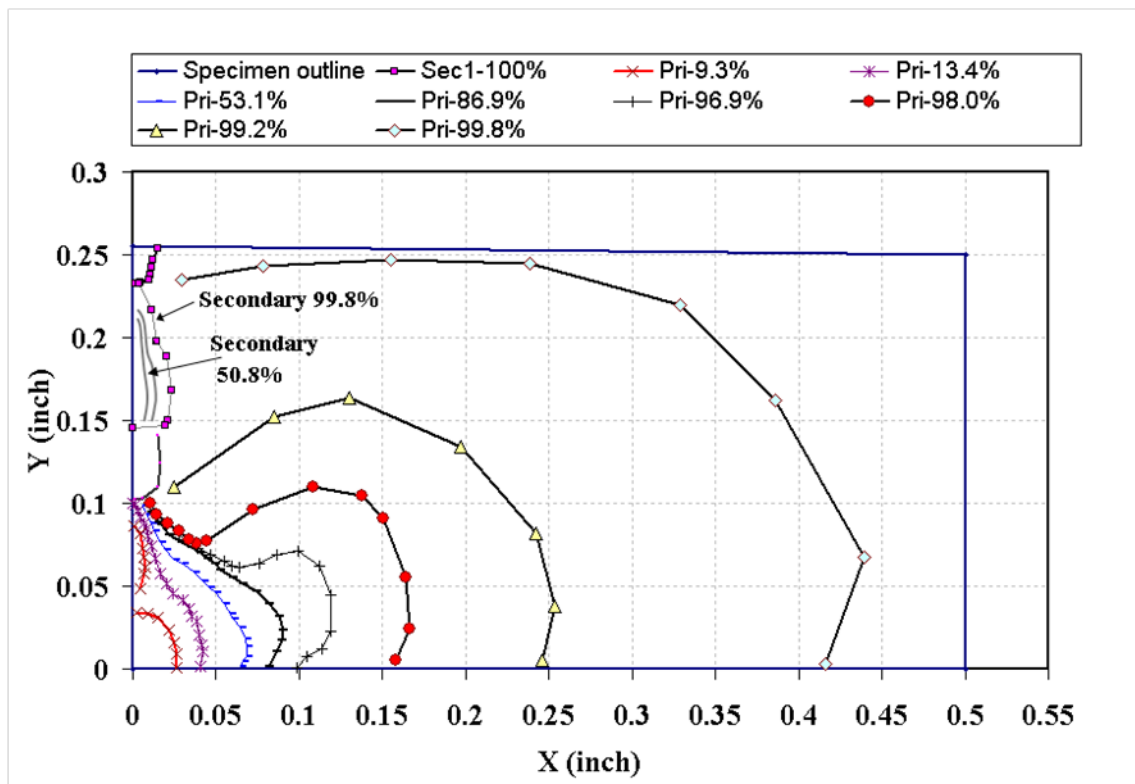


Figure 43. Typical crack shape in a cold-worked hole.

This multi-point crack propagation capability was previously developed by Hodges (2012)—Broad Application for Modeling Failure (BAMF). BAMF uses the plug-in capabilities of AFGROW with StressCheck to achieve this capability.

During the course of this program, the inclusion of new residual stress capabilities in StressCheck required a new release of that code. There were many compatibility problems between BAMF and StressCheck that arose during this transition, so a crack propagation tool (CPT) was developed within StressCheck to provide a rapid assessment tool for crack growth in residual stress fields for this program. Functionally, it works similarly to BAMF, but it is limited to only a couple of geometries (based on fatigue

coupon geometries from our testing program) and does not use AFGROW as a crack growth engine (CPT will be modified to use AFGROW in future versions).

The issues with BAMF and StressCheck were eventually resolved, so we now have two software packages that can be used to evaluate crack growth at cold-worked holes. These codes were used to cross validate extensively during this program, and they both performed well and provided similar results (see Section 8).

5.2.2 Workings of CPT

The crack propagation model is based on the following considerations:

- The driver of fatigue crack propagation is the stress intensity factor amplitude ΔK_I (LEFM).
- The principle of superposition is applicable and the residual stresses due to cold working only affect the stress ratio, R , of the load cycle.
- For each crack increment, the crack grows in the direction normal to the crack front.
- The crack growth takes place in the plane of the initial flaw.
- The relation between the rate of crack growth per load cycle (da/dN) and ΔK_I is obtained from experimentally-derived $da/dN - \Delta K$ curves at fixed stress ratios, and curves derived for thru-cracks are applicable for corner cracks.
- Interpolation is used for finding da/dN for R -ratios not covered by the experimental data.
- No assumptions are made regarding the shape of the crack.

The Crack Propagation Tool (CPT) was developed as a standalone application which communicates with StressCheck 10.1 via COM for the computation of the SIFs. The input to the CPT include the basic dimensions of the test specimen (dogbone or rectangular) as shown in Figure 44. All dimensions are in inch units.

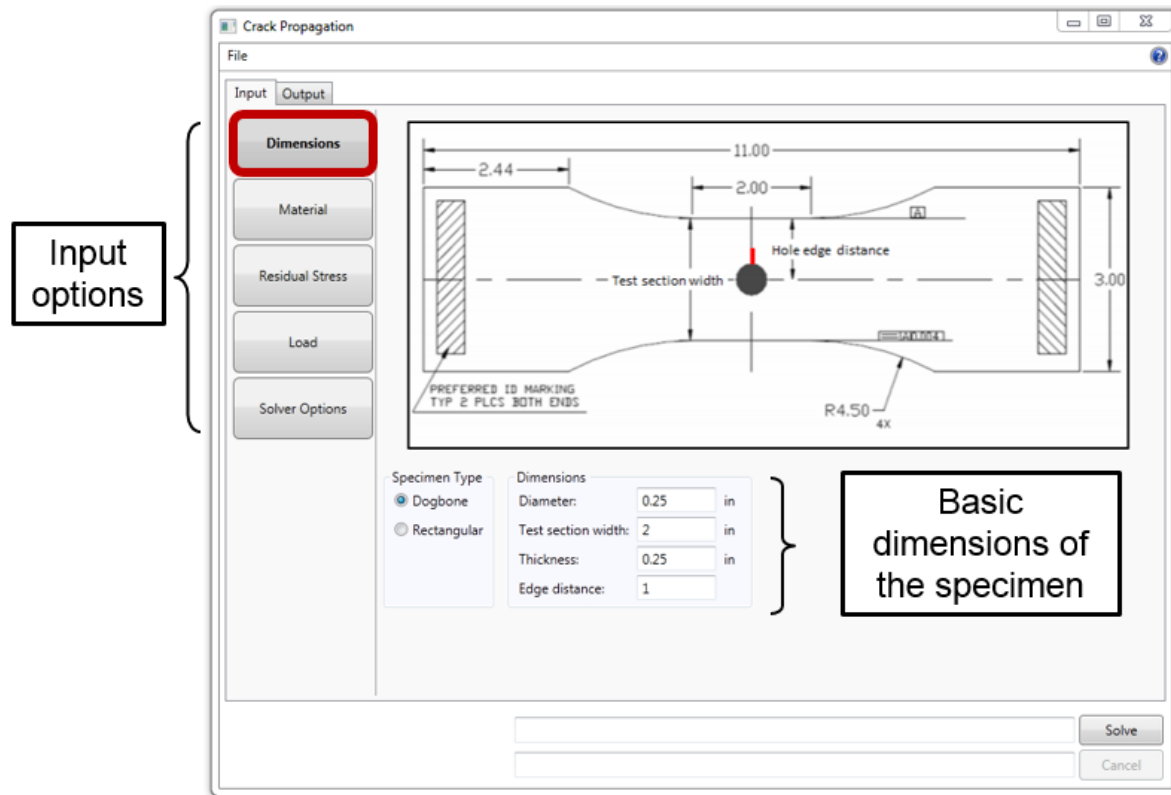


Figure 44: CPT Input - Dimensions

Next, the material properties of the specimen must be provided as shown in Figure 45. The data can be imported from AFGROW by reading a *.lkp file. A graph of the imported $da/dN - \Delta K$ curves is displayed for visual feedback. Also the type of interpolation for finding da/dN for R-ratios not covered by the experimental data is selected in this page.

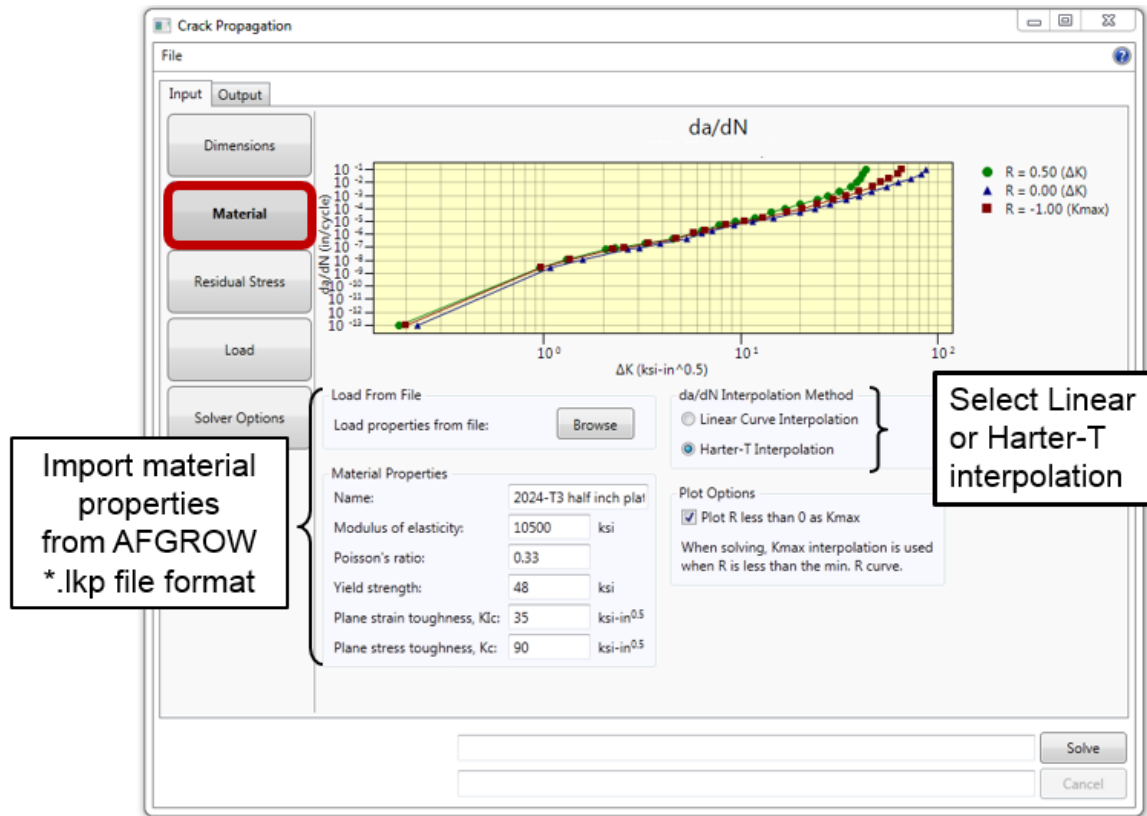


Figure 45: CPT Input - Material properties

Three options are available for residual stresses: (a) No residual stresses; (b) Fitted surface over user-provided RS tabular data; (c) Residual stresses extracted from the RS database described in Section 4. For cases (b) and (c), the tabular input data is displayed in the graphical region of the GUI and the user then performs a polynomial fitting for use in the computation of the SIF by the CIM with loaded crack faces during the solution (Figure 46).



Figure 46: CPT Input - Residual stresses

Two options are available for loading the specimen: (a) constant amplitude loading and (b) spectrum loading. In the case of spectrum loading, the AFGROW *.sp3 / *.sub file format is expected and the imported data is presented in tabular and graphical form to the user as shown in Figure 47.

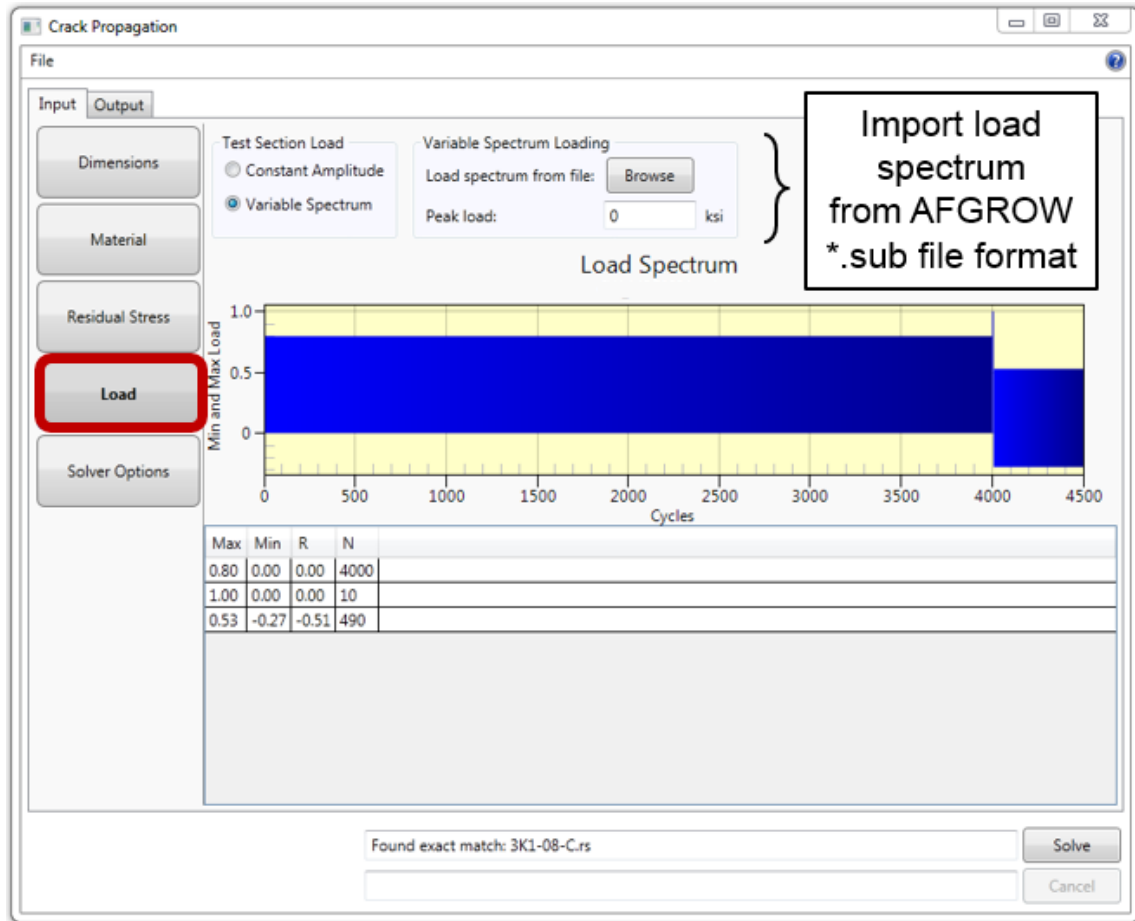


Figure 47: CPT Input - Loading

Finally, the input for the solver option is entered. This consists of the crack parameters for the initial flaw size, the size of the integration step and maximum number of steps and the number of StressCheck runs for each crack increment as shown in Figure 48.

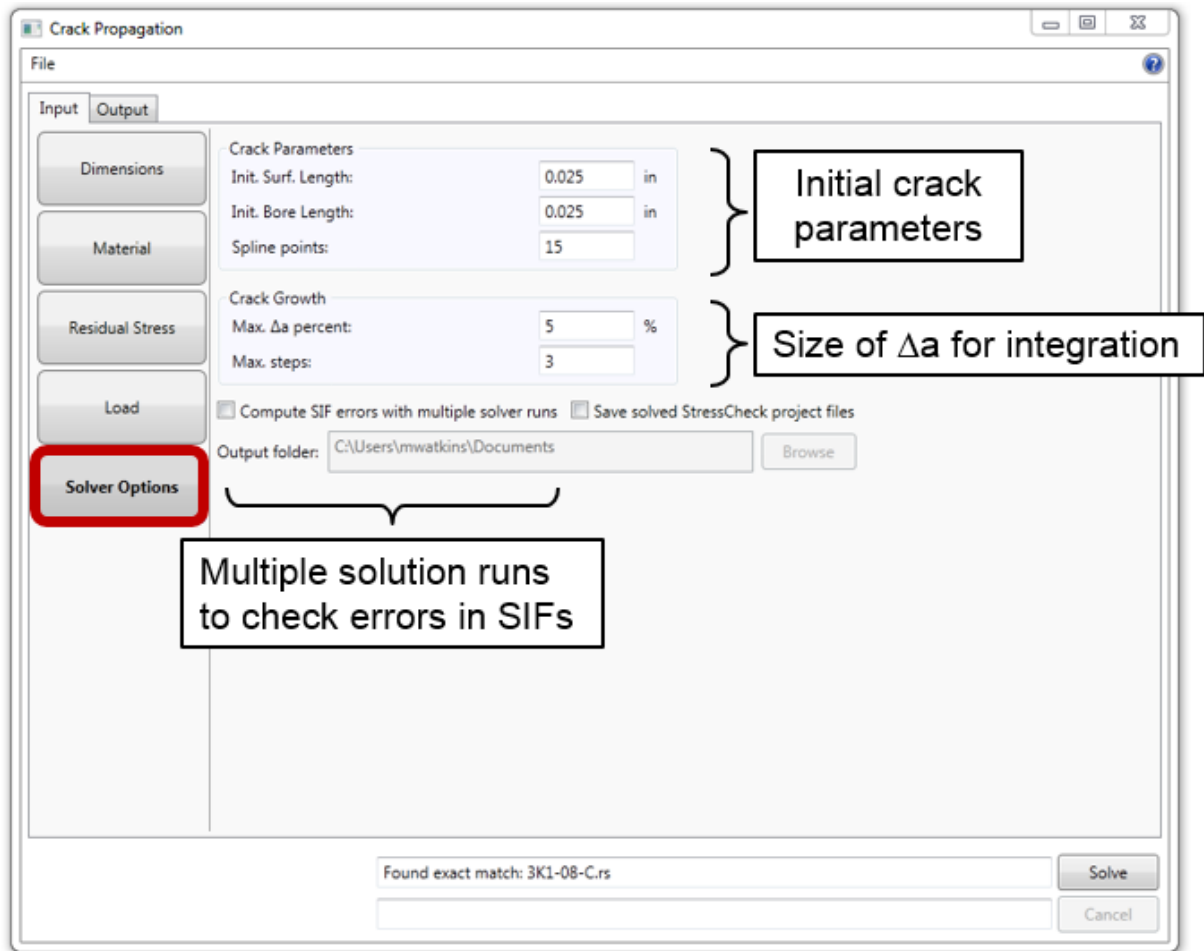


Figure 48: CPT Input - Solver Options

Once all the input data has been entered, the user clicks on the Solve button, and the CPT communicates with StressCheck via COM to determine the SIFs along the crack front for the mechanical load and the residual stresses and based on the model described above determines the position of the crack front for the next iteration. The process continues until the max number of steps is reached.

The results are presented in the Output tab of the CPT in two forms: The crack front associated with each crack step and the crack length along the mandrel entrance surface and the bore of the hole as a function of the number of cycles. Figure 49 shows the two output modalities.

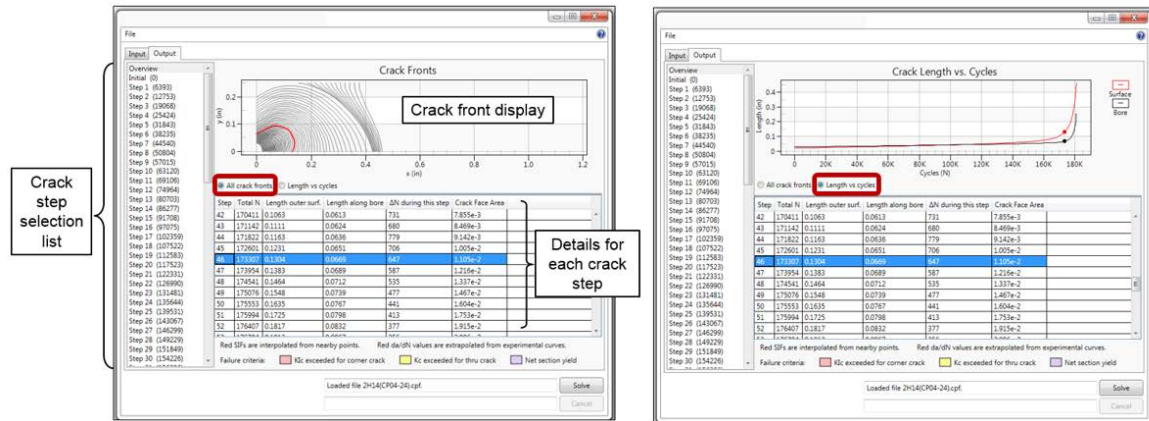


Figure 49: CPT Output - Crack fronts and Length vs Cycles

The predictions of fatigue crack propagation life have been compared with experiments for specimens with and without cold worked holes. Figure 50 shows the prediction for a non-cold worked specimen (solid and dashed lines) and the experimental data obtained from Pilarczyk (2008) for a rectangular coupon of 7075-T651 aluminum alloy with a 1/2" diameter hole. The shape of the crack front is also shown in the figure.

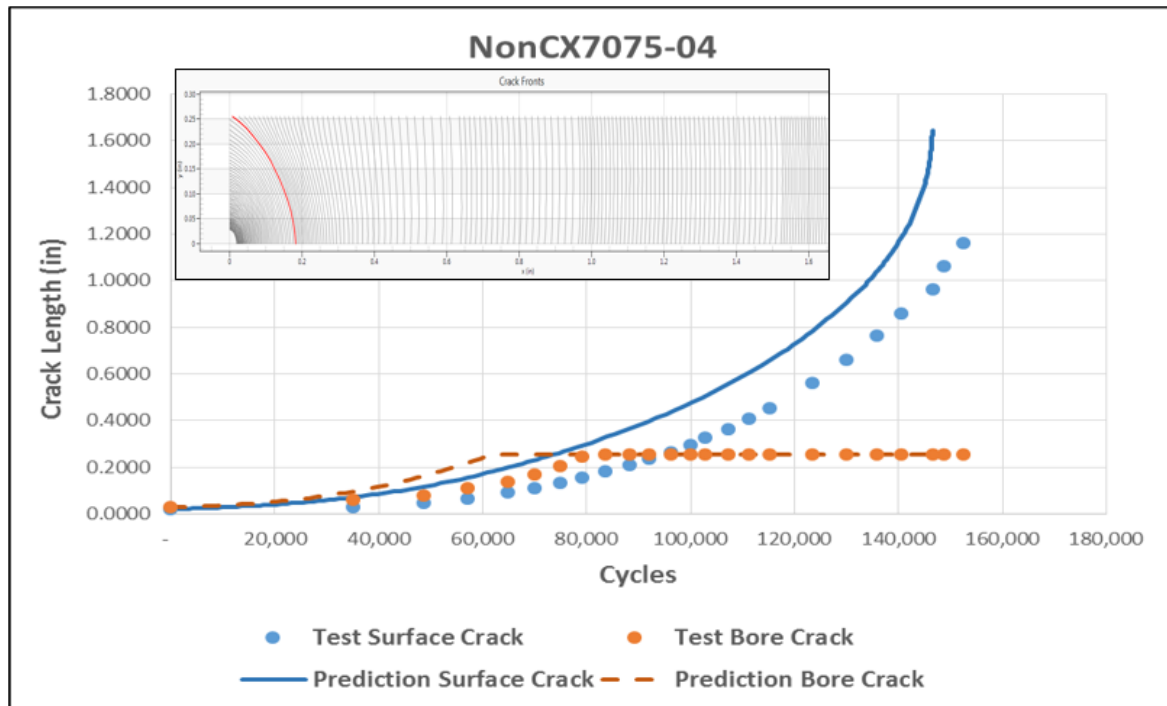


Figure 50: CPT Prediction for a non-cold worked specimen

Figure 51 shows the prediction for a dogbone specimen of 2024-T3 aluminum alloy with a 1/4" cold worked hole under constant amplitude loading. The agreement between experiment and prediction is very good, and the crack shape is very close to those found by fractographic examination of specimens tested with spectrum loading with marker cycles as shown in Figure 52.

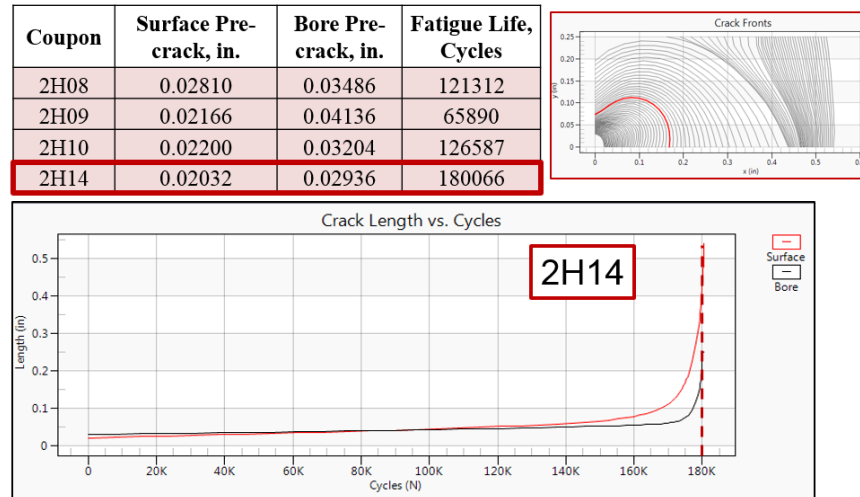


Figure 51: CPT prediction for a cold worked specimen

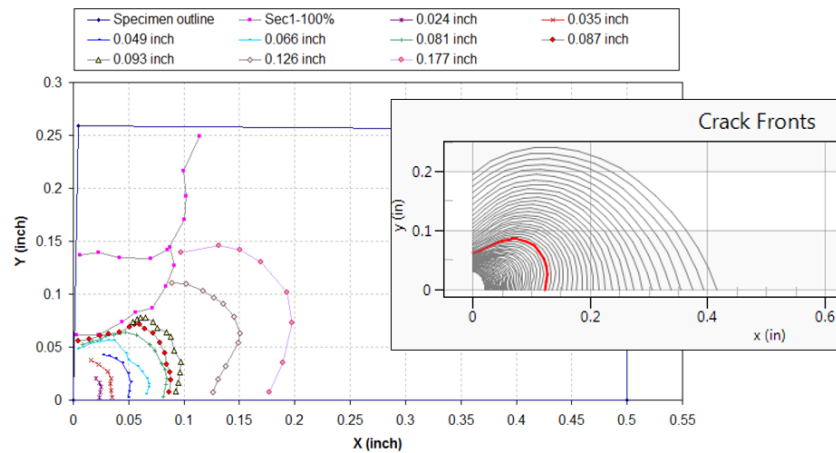


Figure 52: Comparison of a crack front map with prediction

In summary, the underlying mathematical model implemented in the CPT was clearly defined with a clear layout of the inputs and outputs. For in-plane crack propagation only the component of the residual stress tensor normal to the plane is required, and the K_{RES} is computed independently of K_{MECH} at each control point along the crack front using the contour integral method for loaded crack faces implemented in StressCheck 10.1.

The proposed model implemented in the CPT accounts for the beneficial effects of RS in the calculation of fatigue life of cracks in CX holes. It provides good estimates of crack

propagation life and the crack propagation maps are consistent with experimental observations.

5.3 Summary

All the tasks assigned to ESRD have been completed within the performance period according to the following details:

- Computation of SIFs
 - Completed and available in SC 10.1 since 6/15/2014
 - Implementation of the modified J-integral in StressCheck
 - Implementation of an algorithm to convert J to K
 - Implementation of the CIM-Loaded Cracks in StressCheck
- RS input and RS Database
 - Completed and available for CPT and other applications
 - Developed rs_database.dll for inter process communication
- Crack propagation
 - Completed model for crack propagation from cold-expanded holes
 - Implemented in CPT, a standalone tool using SC10.1

6 FastenerCam™ Development

This chapter describes the results of the TRI/Austin subcontract to APES related to development of a quality assurance tool designed to assess and document the results of a cold work process in a depot or field environment.

This task was to:

- Design, manufacture, and demonstrate a functional prototype of a tool (FastenerCam™) for use in quality control of the cold worked hole process. This tool is designed to:
 - Measure the final hole diameter
 - Measure the out of plane deformation around the hole
 - Approximate the original hole diameter and thus the amount the hole has been cold expanded

Nominal cold work often targets four percent cold expansion, but variability in the process can produce actual cold expansion ranges from three to five percent while still being within machining tolerance. Metrology of the hole and of the deformation around the hole (after cold work but before final ream) can determine whether or not the hole is in spec and where in the spec the dimensions fall.

The basic goal here is to produce a post-process tool that can determine a pass / fail status for a cold worked hole. Eventually we would like to see the concept develop to have enough resolution and accuracy to be able to ascertain—in a passing scenario—just how much CX is imparted to the hole (i.e., where in the specification each hole lies). Ultimately, these data should relate to residual stress level, which we know to have a direct, significant influence on computed and physical fatigue response.

We have studied the actual out-of-plane deformation (e.g. Figure 53) typical of alloy types (2024-T3/T351 and 7075-T6/T651 aluminum) and thickness ranges (0.1”, 0.19”, 0.313”, and 0.5”) of interest to the USAF.

To accomplish this task, TRI/Austin has developed the FastenerCam™. FastenerCam™ has a sliding laser profilometer with a 0.002” by 0.008” area resolution and 0.0003” height resolution. Laser profilometry was used instead of using structured light by integrating a Moiré projection grating with a digital camera as mentioned in the proposal in order to obtain the needed height resolution. The out-of-plan deformation around holes that have been cold expanded 4% is less than 0.008” high. Thus, very precise height measurements are required to accurately determine the amount a fastener hole has been cold expanded.

Software to control the FastenerCam™ through a web browser from any WiFi enabled device has been developed. As such, any ruggedized laptop or tablet can be used with FastenerCam™.

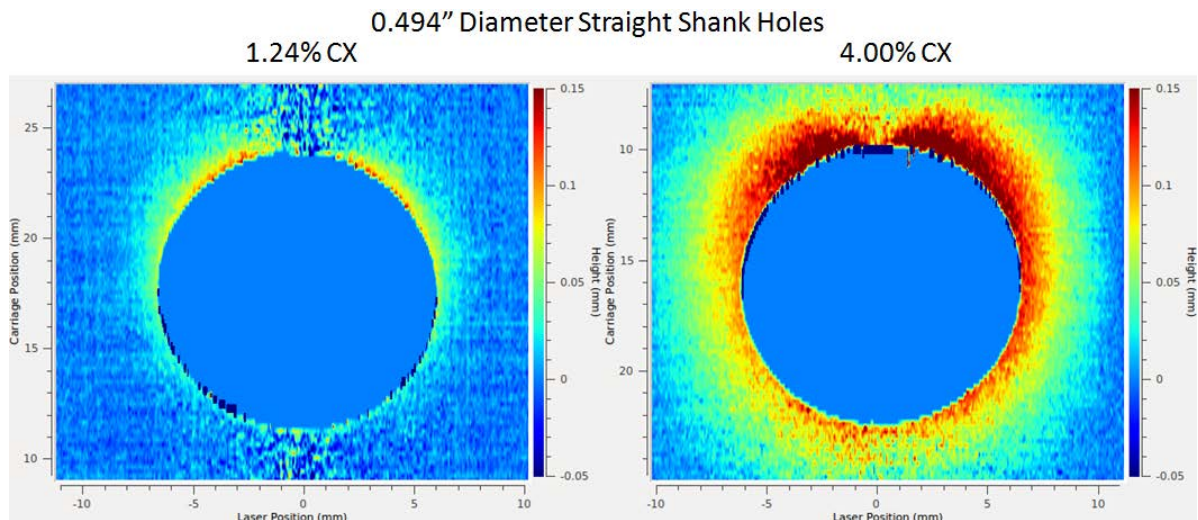


Figure 53. Deformation around cold worked straight shank fastener holes with different amounts of cold expansion. The left image is out of specification; the right image is in specification. Location of split sleeve “pip” can clearly be seen at the top of each image.

6.1 FastenerCam™ System Details

FastenerCam™ is comprised of three main parts: 1) a laser profilometer, 2) a power and communications box, and 3) a computer. The FastenerCam's™ laser profilometer is mounted on a sliding carriage (Figure 54). The sliding carriage stabilizes the profilometer at a constant distance from the fastener hole while the laser is scanned across the cold-worked hole. Rubber feet prevent the carriage from damaging the plate surface and prevent the carriage from sliding during use.



Figure 54: FastenerCam™ Carriage

The three cables coming from the laser profilometer (Figure 55) and connecting it to the power and communications box are for: 1) power to the laser profilometer, 2) communications with the profilometer, and 3) communications with the linear encoder. The power and communications box (Figure 56) contains a rechargeable battery allowing up to 16 hours of FastenerCam™ use as well as an IEEE 108.11 WiFi access point. The WiFi access point allows any WiFi equipped computer to wirelessly control and retrieve the data from the FastenerCam™ via any web browser.



Figure 55: FastenerCam™ Connector Cables

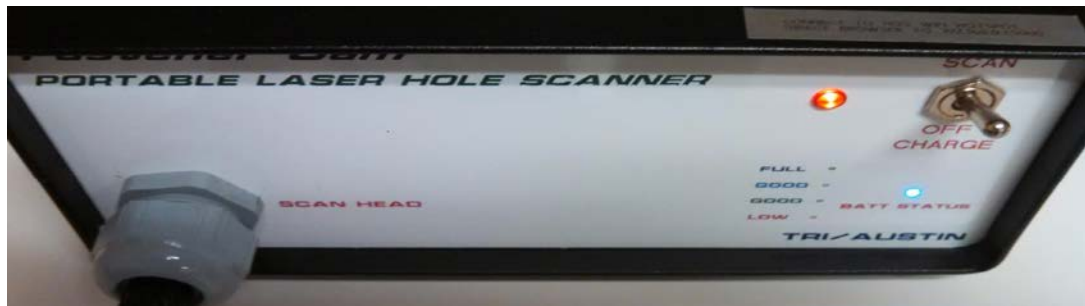


Figure 56: FastenerCam™ Power and Communications Box

To operate the FastenerCam™, first turn on the power and control box. The LED on the front of the box indicates the battery status: Off) battery is fully charged, Blue) the battery is charged and does not need to be recharged, Green) the battery is still charged but should be recharged when convenient, Red) the battery should be recharged as soon as possible. Once the system is on, the computer can join the “FastenerCam” network (password: En7r0piC). The control interface is accessed through any web browser at “192.168.0.1:5000”. The web interface is shown in Figure 57.

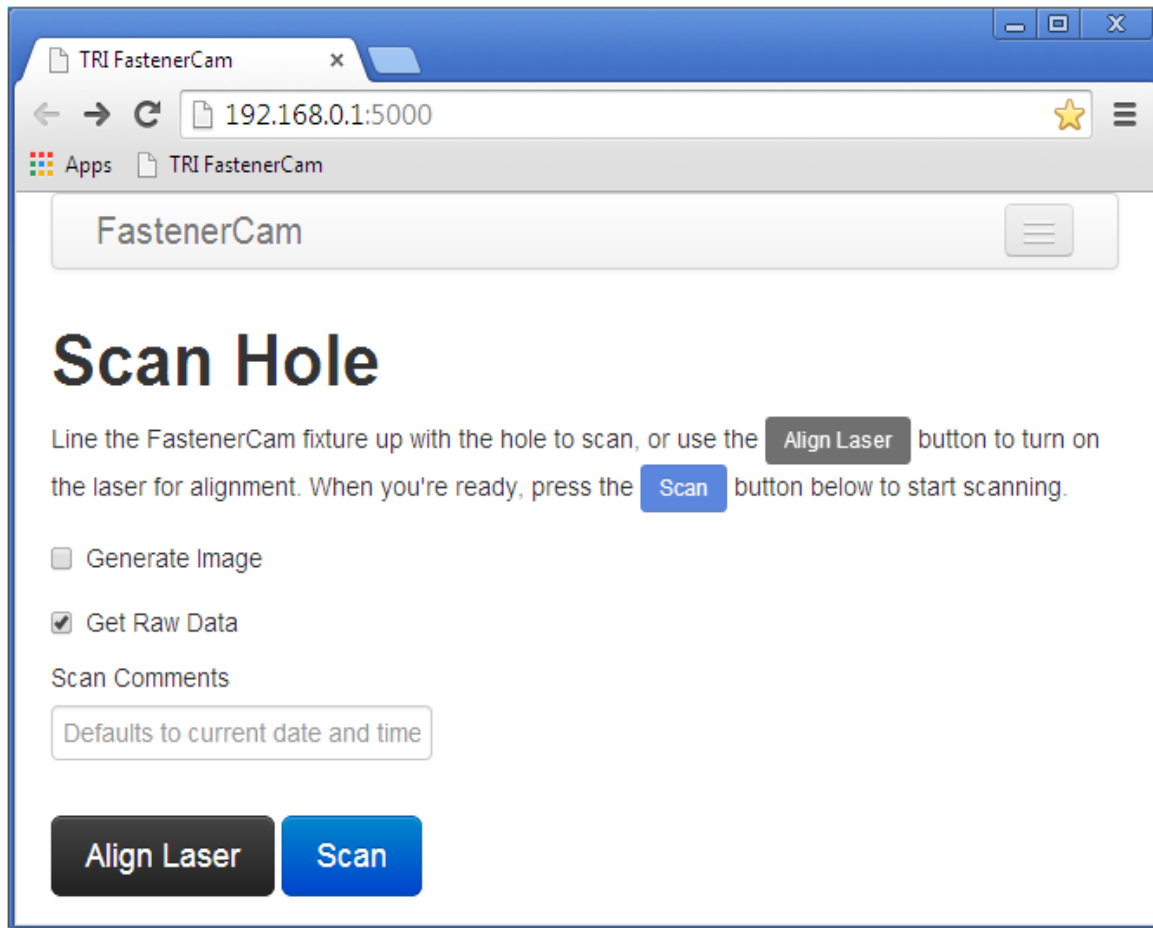


Figure 57: FastenerCam™ Control Interface

The FastenerCam™ carriage should be placed so that the laser is roughly one inch from the hole center and the center of the laser line is aligned with the center of the hole (selecting the “Align Laser” button can help with this by activating the laser so that the user can see its location – it may take a couple of seconds for the laser activate). The legs can be raised and lowered independently to make the scanner parallel to the hole surface roughly an inch away. The user should always select the box next to “Get Raw Data” in order to save the profile data for future analysis. Selecting “Generate Image” will bring up an image of the scanned area after the scan is completed; this is only needed to double check that the area was properly scanned and can take several seconds to generate. Once the carriage is in place to start the scan, selecting “Scan” will bring up the window shown in Figure 58. After a couple of seconds to allow the laser to activate (the laser line will not be visible until after the laser profilometer has started to move), slowly use the handle on the top of the FastenCam™ carriage to slide the laser profilometer across the hole until the laser is roughly on inch from the hole center opposite the starting location. While scanning the hole, the laser will blink on and off as is moves across the hole area;

this is normal behavior. It should take roughly ten seconds to complete the scan. Once the hole area has been completely scanned, wait another five seconds for the data to finish transmitting to the Power and Control box before select the “Stop” button on the scanning window shown in Figure 58.

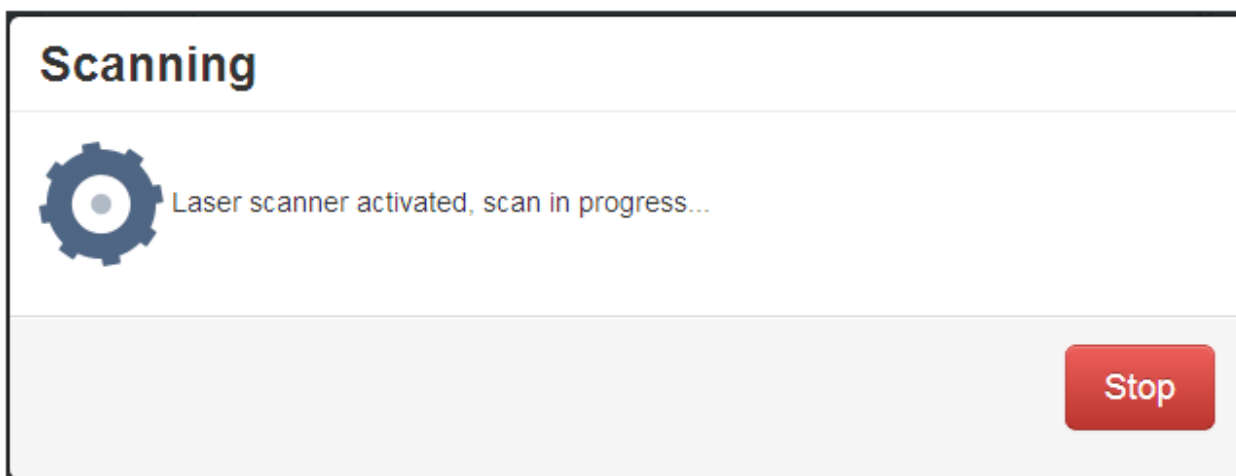


Figure 58: Window showing that the FastenerCam™ is in Scanning mode and receiving data

After the scan has been stopped, “Scan Complete!” will appear at the bottom of the FastenerCam™ Control Interface (Figure 57) as shown in Figure 59. If the “Generate Image” option was selected, the image can be viewed by clicking “Get Profile Plot”; a sample image of a scanned hole is shown in Figure 60. Clicking “Get Profile Data” will download the raw data to the computer with a randomly generated name. When the data file is downloaded to the computer, it should be saved in an appropriate folder and renamed so that the scanned hole’s location is adequately conveyed. This data file can then be opened in the FastenerCam™ software. The software tells the user the hole radius and if it has been properly cold worked.

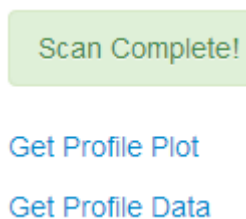


Figure 59: Links to both the Profile Plot and Data for the area just scanned

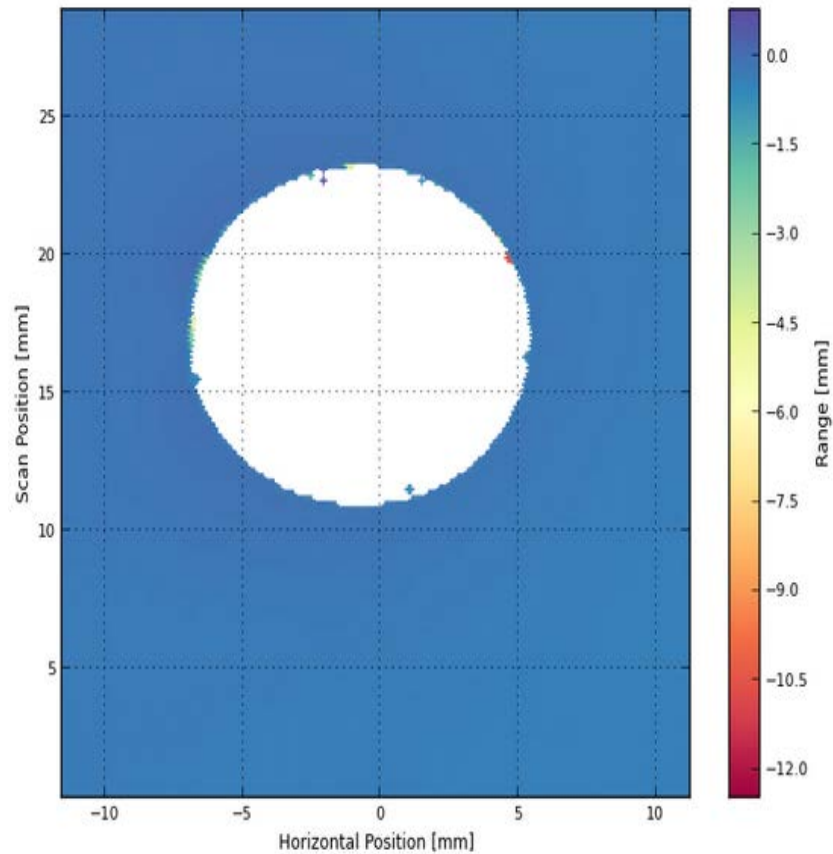


Figure 60: Image of a scanned fastener hole generated by the web interface

The FastenerCam™ hardware should only have to be configured once. Clicking on the square button in the top right corner of the Control Interface will bring up the menu shown in Figure 61. Before any configuration settings can be changed, the user must login by clicking on “Login”. The user name is “admin”, and the password is also “admin”.



Figure 61: FastenerCam™ configuration menu

After logging in, both the trigger and encoder can be configured. The trigger should be configured as shown in Figure 62. For scanning a complete hole area, the trigger type needs to be “Encoder”. “Trigger On Digital Input Only?” should not be selected; this will gray out and deactivate the “Scans Per Second” box. To reliably collect all the profile data, the “Trigger Distance” should be 0.2 mm and the “Trigger Direction” should be bidirectional.

Configure Triggering

Type Of Trigger

Encoder ▼

Trigger on encoder readings

☐ Trigger On Digital Input Only?

Scans Per Second

300

Time triggering only

Trigger Distance (mm)

0.2

Trigger Direction

Bidirectional ▼

Figure 62: Proper triggering configuration

The FastenerCam is equipped with a linear encoder. The encoder model is “RLS LM10IC050” with a resolution of 0.05 mm. The encoder should be configured as shown in Figure 63.

Configure Encoder

Encoder Model

RLS LM10IC050

Resolution (mm)

0.05

Figure 63: Proper encoder configuration

6.2 Laboratory Specimens

The FastenerCam™ prototype system was used to measure the amount of deformation around 800 cold worked fastener holes and determine the amount each hole had been cold expanded. There are five samples of each of four fastener hole **type** in each of two alloys, four plate thicknesses, and five nominal (**classes**) final hole diameters. The variables follow:

- Two alloys: 2024-T3/T351 & 7075-T6/T651
- Four plate thickness in each alloy: 0.1, 0.19, 0.313, 0.5 inch
- Five nominal hole diameters (post cold work):
 - Class A: 0.168 inch
 - Class B: 0.246 inch
 - Class C: 0.374 inch
 - Class D: 0.494 inch
 - Class E: 0.574 inch
- Four types of each hole class, which are defined by varying the initial ream diameter in closely controlled “bins” (see Table 15 and Table 16).

The expected amount of cold expansion was determined by APES, Inc. using a precision optical microscope (Nikon MM-60) with 0.00002 inch resolution to measure the initial ream diameter of the holes. These measurements were then coupled with the measured mandrel major diameter and the nominal sleeve thickness (for the split sleeves) to determine the amount of interference, thus percent cold work. The percent cold work for each hole class/type combination is also provided in Table 15 and Table 16. The averages and standard deviations were determined using a sample size of eight for each hole class/type.

A total of sixteen plates were manufactured, 24” long by 12” wide, that each had 50 holes. Two separate hole patterns, which we simply called Pattern 1 and Pattern 2. Figure 64 and Figure 65 show the hole patterns for each plate.

Note that during the cold work process, the 0.1” sheets tended to bend inward while pulling the mandrel through the split sleeve. This bending distorts the measured displaced material volume around the hole due to the hole expansion and, as can be seen in our analyses, results in erroneous cold expansion calculations.

A tenth of an inch is quite thin for cold working, and often times, we would expect to either be working through stacked structure or using backing blocks. The FTI guidance suggested that backing blocks should be used when dealing with diameters that are more than five times the sheet thickness. However, we experienced problems with out of plane deformation at diameter/thickness ratios that are much less.

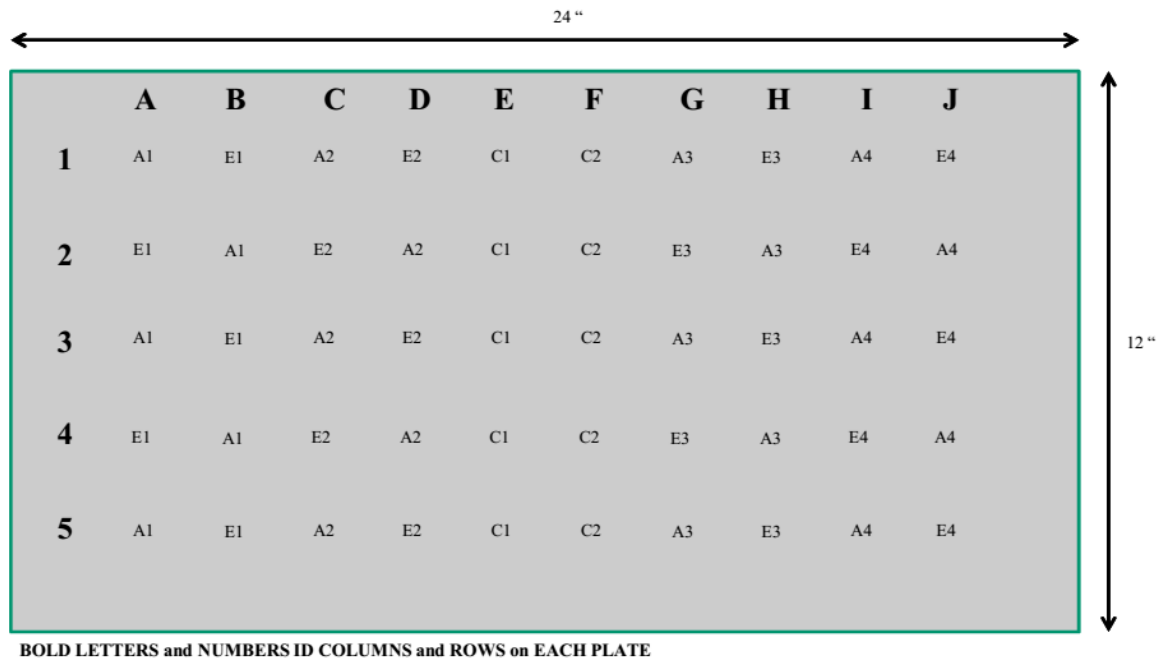


Figure 64. Hole Pattern 1 for the test plates.

Table 14. Metrology of the initial reamer, initial hole diameters, and resulting CX for the class/type hole combinations for Pattern 1.

Tool Set	Hole Type	Initial Reamer (D inch)	Average Initial Hole D (inch)	Stdev D	Average CX	Stdev CX	Average Delta (inch)
4-3-N FTI	A1	0.16010	0.16048	0.00010	4.75%	0.07%	0.00038
4-3-N-MID	A2	0.16140	0.16166	0.00020	3.98%	0.13%	0.00026
4-3-N-MIN	A3	0.16280	0.16352	0.00028	2.80%	0.18%	0.00072
4-OVER	A4	0.16550	0.16577	0.00016	1.40%	0.10%	0.00027
12-0-N FTI	C1	0.35920	0.35974	0.00023	3.99%	0.07%	0.00053
12-0-N-MID	C2	0.36120	0.36171	0.00011	3.42%	0.03%	0.00051
18-1-N FTI	E1	0.55300	0.55342	0.00005	3.63%	0.01%	0.00041
18-1-N-MID	E2	0.55520	0.55572	0.00032	3.20%	0.06%	0.00052
18-1-N-MIN	E3	0.55690	0.55719	0.00015	2.93%	0.03%	0.00029
18-OVER	E4	0.56600	0.56743	0.00045	1.07%	0.08%	0.00143

	A	B	C	D	E	F	G	H	I	J
1	B1	D1	B2	D2	C3	C4	B3	D3	B4	D4
2	D1	B1	D2	B2	C3	C4	D3	B3	D4	B4
3	B1	D1	B2	D2	C3	C4	B3	D3	B4	D4
4	D1	B1	D2	B2	C3	C4	D3	B3	D4	B4
5	B1	D1	B2	D2	C3	C4	B3	D3	B4	D4

Figure 65. Hole Pattern 2.

Table 15. Metrology of the initial reamer, initial hole diameters, and resulting CX for the class/type hole combinations for Pattern 2.

Tool Set	Hole Type	Initial Reamer D (inch)	Average Initial Ream D (inch)	Stdev D	Average CX	Stdev CX	Average Delta (inch)
8-0-N FTI	B1	0.23560	0.23572	0.00020	4.41%	0.09%	0.00012
8-0-N-MID	B2	0.23720	0.23832	0.00020	3.27%	0.09%	0.00112
8-0-N-MIN	B3	0.23880	0.23978	0.00043	2.63%	0.18%	0.00098
8-OVER	B4	0.24250	0.24325	0.00045	1.17%	0.19%	0.00075
12-0-N-MIN	C3	0.36270	0.36320	0.00023	3.00%	0.06%	0.00049
12-OVER	C4	0.36900	0.36966	0.00018	1.20%	0.05%	0.00066
16-0-N FTI	D1	0.47420	0.47462	0.00019	4.00%	0.04%	0.00041
16-0-N-MID	D2	0.47670	0.47720	0.00027	3.44%	0.06%	0.00050
16-0-N-MIN	D3	0.47870	0.47927	0.00028	2.99%	0.06%	0.00057
16-OVER	D4	0.48700	0.48754	0.00020	1.24%	0.04%	0.00054

6.3 Results

The amount of cold expansion around a fastener hole can be determined by measuring the deformation around the hole. As the hole is expanded, some of the material undergoes plastic deformation and is pushed to the surface of the plate. The volume of this material is dependent on the type of material (here two aluminum alloys, 2024-T3 and 7075-T6 aluminum were studied), the plate thickness (h), the hole's starting radius (r), and the holes final cold expanded radius (R). The volume of the extruded material (V) can then be calculated as:

$$V = \pi * (R^2 - r^2) * h * F$$

The scaling factor (F) is the portion of the material which is displaced to the top of the plate. Assuming half of the material is moved to the top of the plate and half to the bottom would make $F = 0.5$. However, as measured, F is dependent on both the plate thickness and the hole's diameter and was analytically fit to both of these. As the plate thickness increases, F also increases and appears to approach 0.5 (Figure 66). A detailed analysis of the scaling factor, F, is currently limited by the small number of sample plate thicknesses in this study; only four plate thicknesses were used (0.1", 0.19", 0.131", and 0.5") and the data from the 0.1" plate had to be discarded due to plate bending during the cold expansion process. The scaling factor used when analyzing the holes in the 0.1" plate was linearly extrapolated from the values of the other three plates ($F = 0.25$).

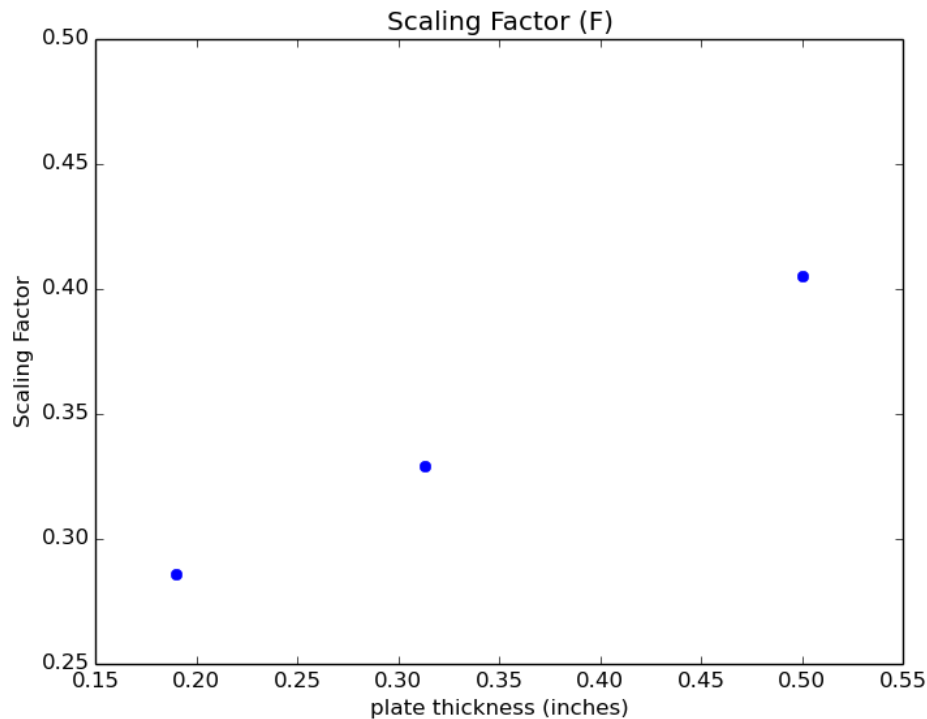


Figure 66: Scaling factor (F) used when determining the amount of cold expansion for the holes in the sample plates.

As seen in Figure 67 the plate bending of the 0.1" thick plate leads to a wide distribution of measured cold expansion with many measurements yielding negative results – due to the plate being bent inwards. For the three thicker plates (0.19", 0.313", and 0.5"), the measured expansion is within 0.5% of the expected expansion except for the smallest holes. Figure 67 shows the difference between the measured and expected cold expansion per each hole diameter. These plots make it easy to see that the FastnerCam™

system underestimates the amount of cold expansion around small holes. FastenerCam™ currently has a 0.002” resolution in the laser scanning direction and 0.008” in the carriage scanning direction. Since almost all of the deformation is within one-half the hole radius from the hole edge, this yields only five data points of deformation in the carriage scanning direction when measuring the smallest holes. In order to measure the cold expansion of holes only 0.168” in diameter, the FastenerCam™'s resolution would need to be twice what it is currently.

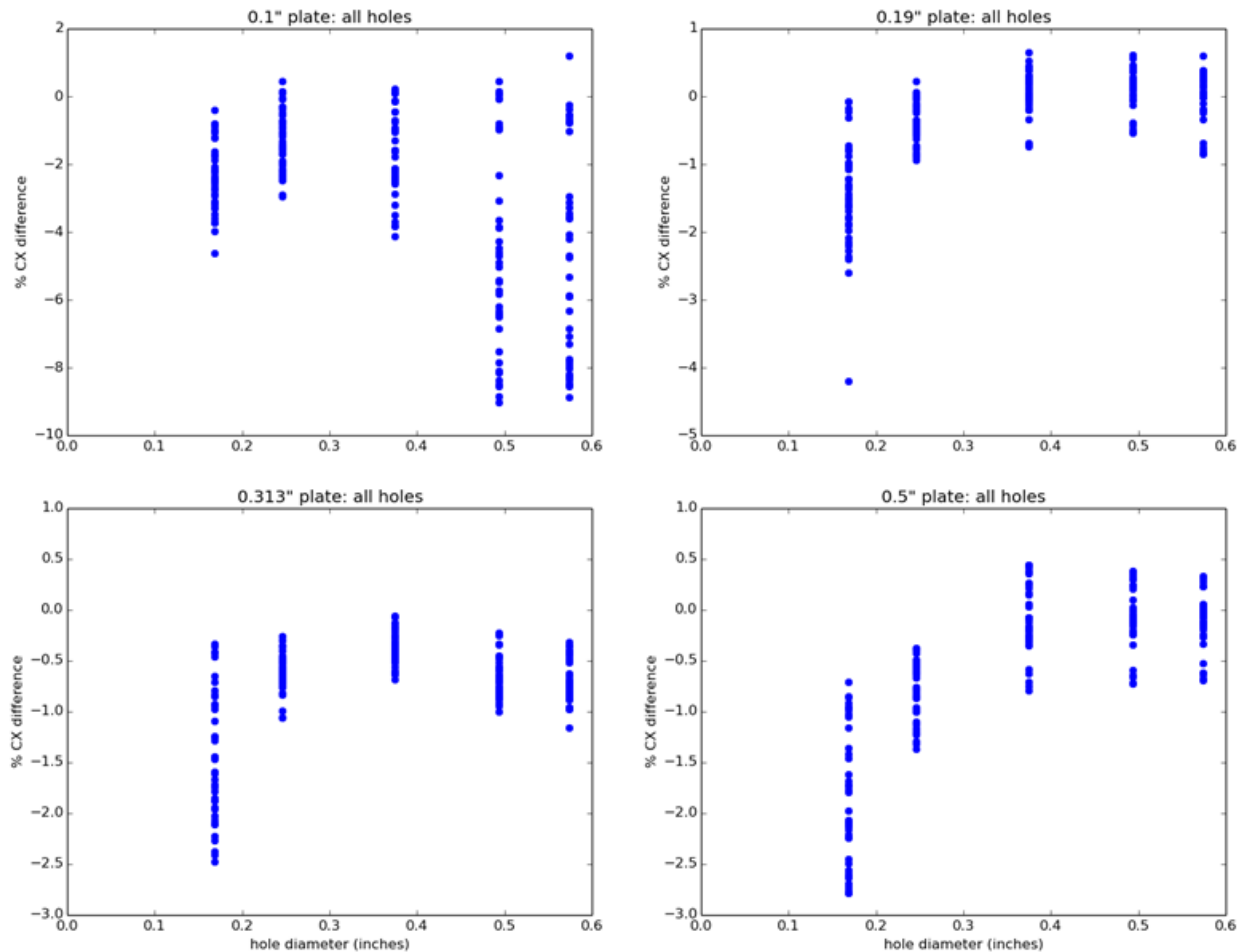


Figure 67: The difference between the measured and expected percent of cold expansion per hole diameter for every hole in each of the four difference plate thicknesses.

FastenerCam™ can distinguish between cold expanded hole which are 'in-spec' (hole types 1 – 3) and the holes which are 'out-of-spec' (hole type 4). Figure 68 shows the clear separation between the measured cold expansion for 'in-spec' and 'out-of-spec' holes for the holes larger than 0.2 inch diameter and in plates thicker than 0.1 inch. Distinguishing between properly and improperly cold expanded holes is an essential quality assurance tool that gives the technician doing the process a “go/no-go” indication immediately after the cold expansion has been completed.

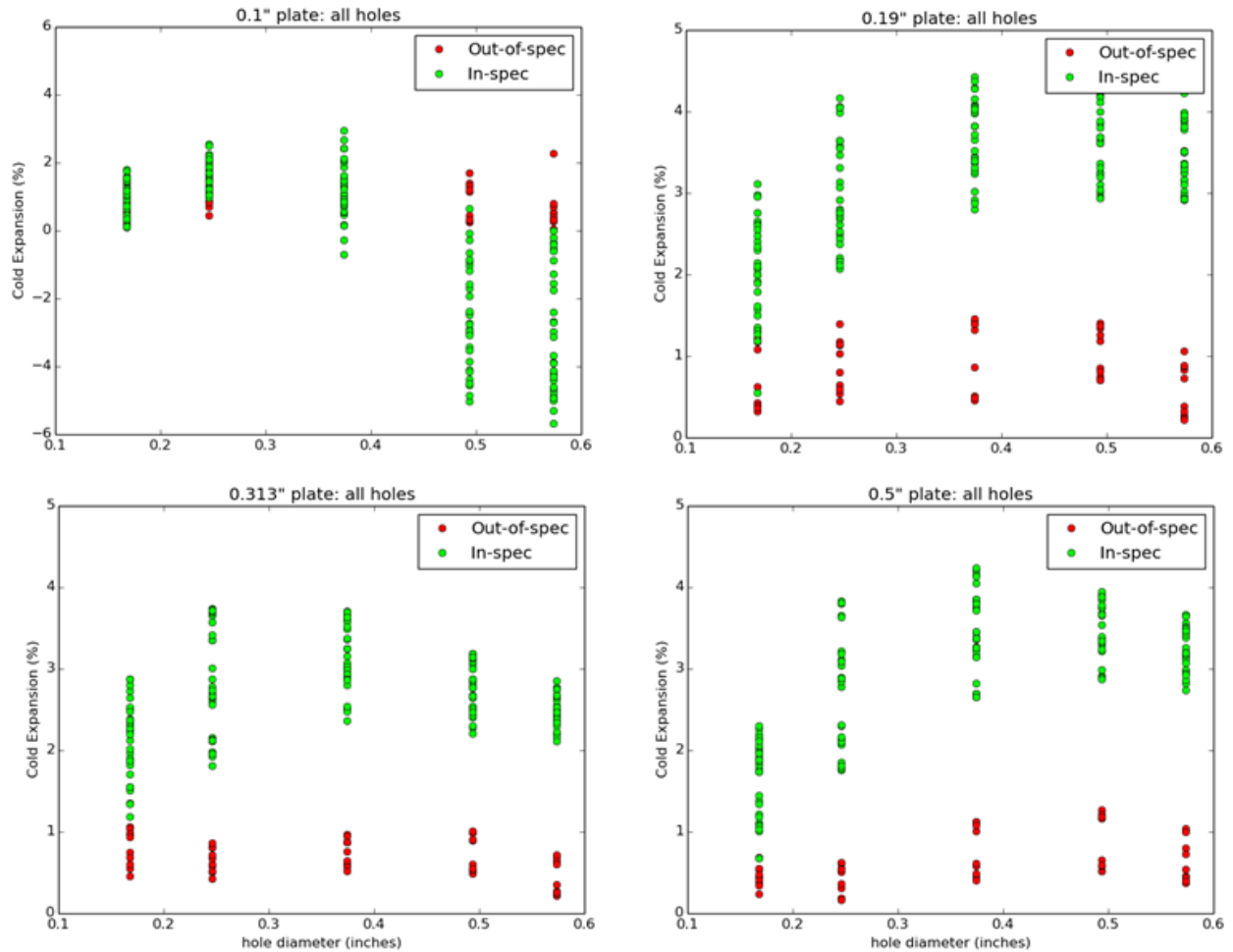


Figure 68. The amount of cold expansion of each hole as measured by FastenerCam™. There is a clear separation between the red 'out-of-spec' points and the green 'in-spec' points.

6.4 Conclusions

This chapter described the results of the task is to design, manufacture, and demonstrate a functional prototype of a tool (FastenerCam™) for use in quality control of the cold worked hole process.

The FastnerCam™ prototype developed for this effort currently can measure the amount of cold expansion around fastener holes to within 0.5% for diameters over 0.246 inch and in plate thicknesses 0.19 inch or greater. For this project, the prototype was demonstrated using aluminum alloys 2024-T351 and 7075-T651. **NOTE:** data for 0.1 inch thick sheet and smaller diameter holes could not be analyzed adequately. For the 0.1 inch sheet, out-of-plane bending confounded the data. For the smallest hole diameter (0.167 inch) resolution of the FastenerCam™ was inadequate (this is being corrected for future versions).

The scaling factor used to determine the amount of cold expansion based on the amount of deformed material around the fastener hole was determined experimentally using only three different plate thicknesses. In order to better understand how the scaling factor depends on the plate thickness, more samples of varying plate thicknesses need to be examined.

Finally, if FastenerCam™ is to be used to measure the amount of cold-work around small (with diameters less than 0.246”) fastener holes, its resolution will need to be improved.

In its current form, this tool provides an effective method for establishing pass / fail for a cold worked hole and for recording the data for further use. Utility of the system would be greatly enhanced by increasing resolution and by modifying the function of the system to be non-contact. Both of these possibilities are being examined by the subcontractor, TRI-Austin, for future development.

7 In-Service NDT Considerations at CX Holes

7.1 Introduction

This report describes the results of task 9 on the TRI/Austin subcontract to APES, prime contract Integrating Residual Stress Analysis of Critical Fastener Holes into USAF Depot Maintenance. The main goal of this task was to conduct nondestructive inspection (NDI) studies of cold-worked (CX) holes to establish detection capability of “faying surface” crack geometries and bore crack geometries.

First, a small preliminary study was conducted with specimens in a load frame at APES facilities, to allow application of loads and crack growth while inspections were performed.

Second, a larger study was performed to generate enough data to estimate reliability and compare with Air Force standard instructions.

7.2 Relevant Prior Art

There are a few documented studies in the literature describing the impact of crack closure on ultrasonic inspection response. The best documented is Harding et al. (2006). In this work, Harding et al. report on a strong relationship between ultrasonic signal reflection at a crack face and the contact stress. As the crack faces are pressed together, the signal decreases dramatically.

Various works have reported on eddy current response as a function of notch width, but we are not aware of any studies like Harding et al. where an external force was varied on the crack faces. In Fahr and Forsyth (1997), we presented results from different types of fatigue cracks and EDM notches in engine disks, and noted that the chemistry of the crack faces made a large difference, rather than crack closure for various fatigue crack types.

7.3 Inspection Techniques

Three different standard Air Force inspection techniques were examined in this work:

- bolt hole eddy current (ET-BH)
- surface scan eddy current (ET-SS)
- shear wave ultrasonic (UT)

These techniques are described in the following sections.

7.3.1 Bolt Hole Eddy Current Technique

The bolt hole eddy current technique used was performed in accordance with standard USAF techniques. All holes were scanned at 200 kHz and 500 kHz using the corresponding Nortec bolt hole probe and a mini-mite rotating scanner. A Nortec 500D instrument was used (see Figure 69).



Figure 69. Equipment for the ET – Bolt Hole inspection of cold worked holes specimens.

Standardization was per normal Air Force rotary scanner ET-BH technique, adjusting the phase and amplitude of the response to the 0.030" x 0.030" interface notch on the Air Force standard ET block, as shown in Figure 70. All crack indications were documented and the screen presentation of the ET-BH signal was saved.

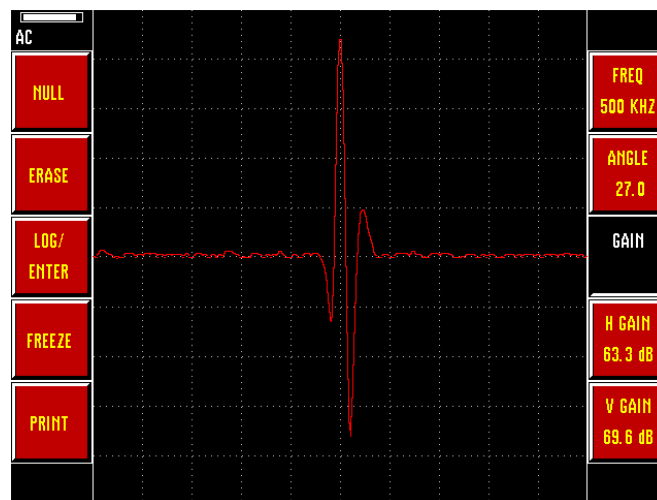


Figure 70. Results of the inspection of the 0.030" by 0.030" inter face notch on the Air force standard block.

7.3.2 Surface Scan Eddy Current Technique

The surface scan eddy current technique used was performed in accordance with standard USAF techniques. All holes were scanned at 200 kHz using a Nortec pencil probe and a circle template. A Nortec 500D instrument was used (see Figure 71).

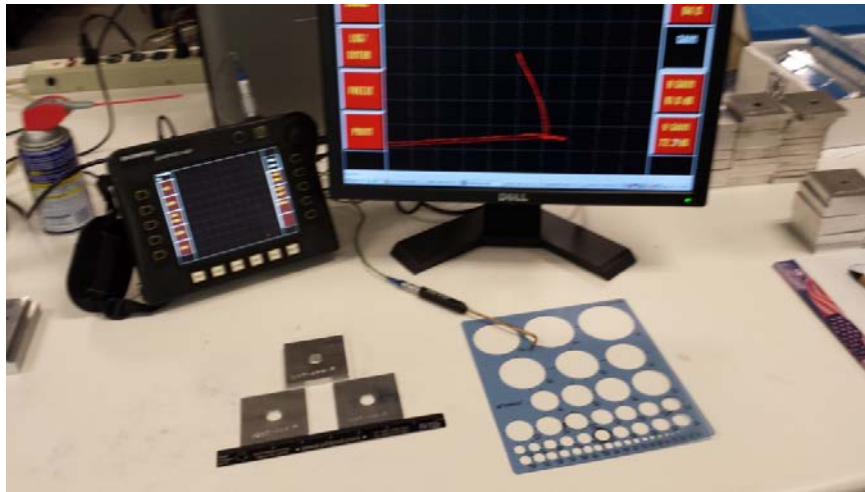


Figure 71. Equipment for the ET - SS inspection of cold worked hole specimens.

Standardization was per normal Air Force surface ET-SS technique, adjusting the phase and amplitude of the response to the 0.020" and 0.010" deep notches on the Air Force standard ET block, as shown in Figure 72. All crack indications were documented and the screen presentation of the ET-SS signal was saved.

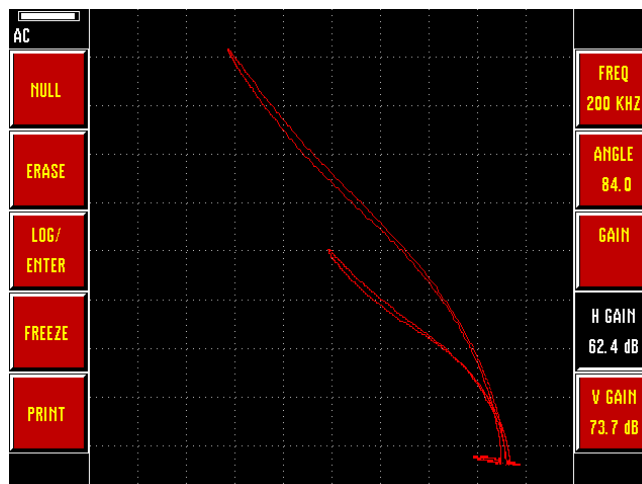


Figure 72. Results of the inspection of the 0.020" and 0.010" deep notches on the Air Force standard block

All specimens that had crack indications were marked with a fine point sharpie at increments of 0.100". Pencil probe scans were performed on each line as shown in Figure 73. Pencil probe scans were also taken between the lines shown which would roughly be at 0.050" increments. Screen shot were taken for each crack indication. The probe was centered over the line or centered between two lines for the measurements.

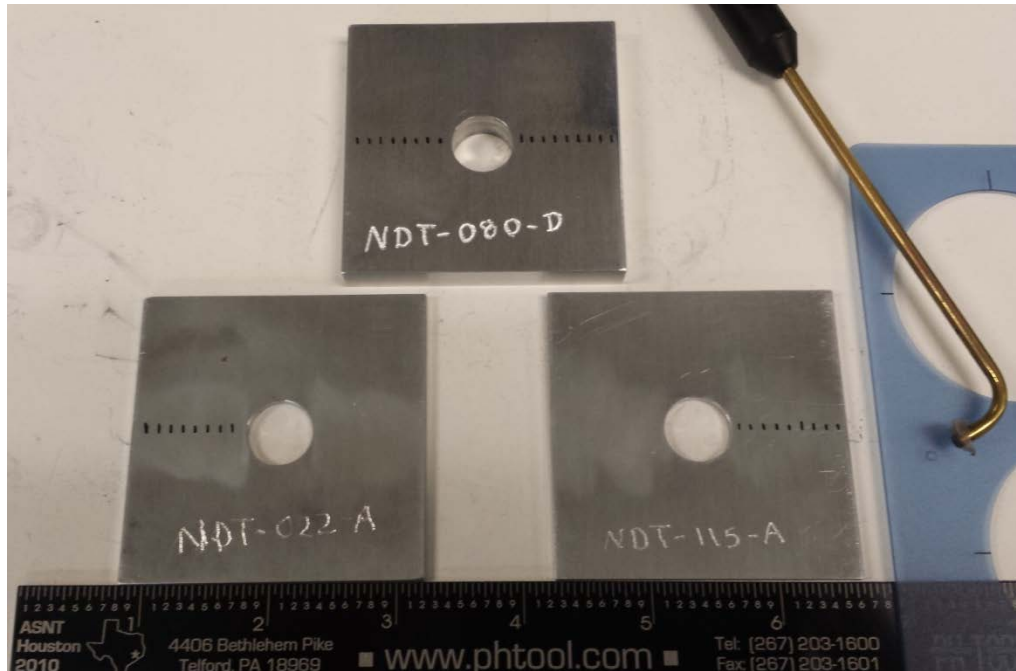


Figure 73. Illustration of the outlining of crack indications.

7.3.3 Shear Wave Ultrasonic Technique

All specimens were scanned at 10 MHz using a UniWest UT-1281 shear wave transducer. A Sonatest Masterscan 330 instrument was used (see Figure 74).

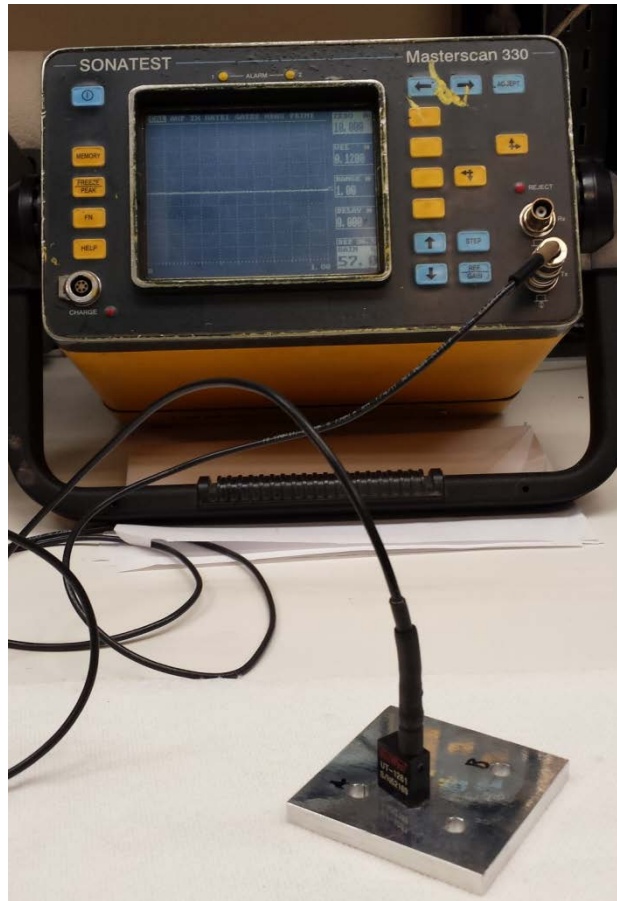


Figure 74. Equipment for the UT – Shear Wave inspection of cold worked hole specimens

Standardization was per an Air Force angle beam Ultrasonic inspection technique, adjusting for the different thicknesses of coupons. Standardization was performed using TRI coupons with EDM notches. All crack indications (see Figure 75) were documented and saved.

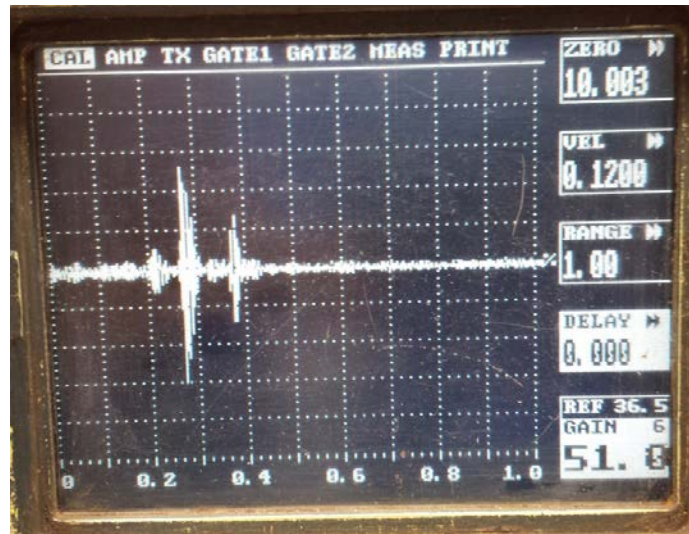


Figure 75. Results of the inspection of a 0.050" corner EDM notch on a TRI coupon

7.4 Specimens

The targets are fatigue cracks starting at cold worked holes in aluminum, of dimensions typical of aircraft structure. The coupons are all squares of 2" side length. Holes were 0.278", 0.418", or 0.538" in diameter. The loads were oriented to produce cracks at the Left and Right locations as noted in Figure 76 below. These specimens were manufactured by APES and provided to TRI. A histogram of the crack sizes in the coupons is shown in Figure 77. A full "crack key" that shows the crack size in each of the 118 coupons made for this phase of the project is shown in Table 17.

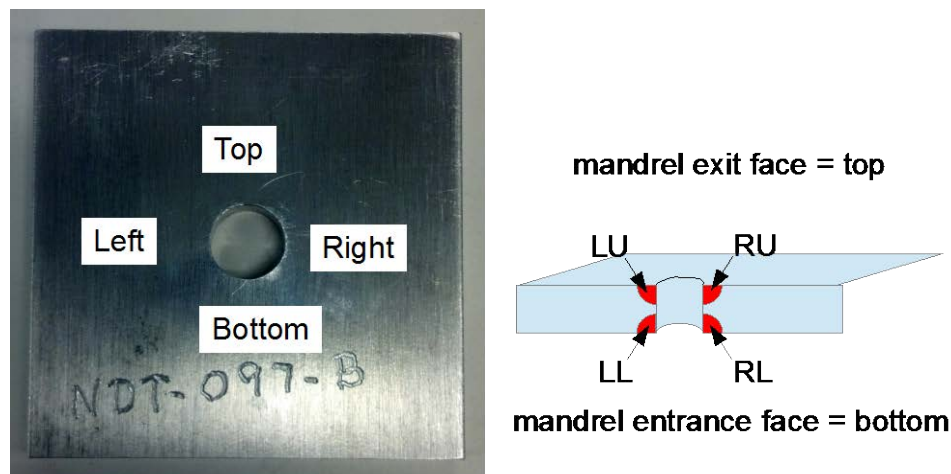


Figure 76. Photograph of one of the target specimens, and a diagram indicating how The possible crack locations are labeled.

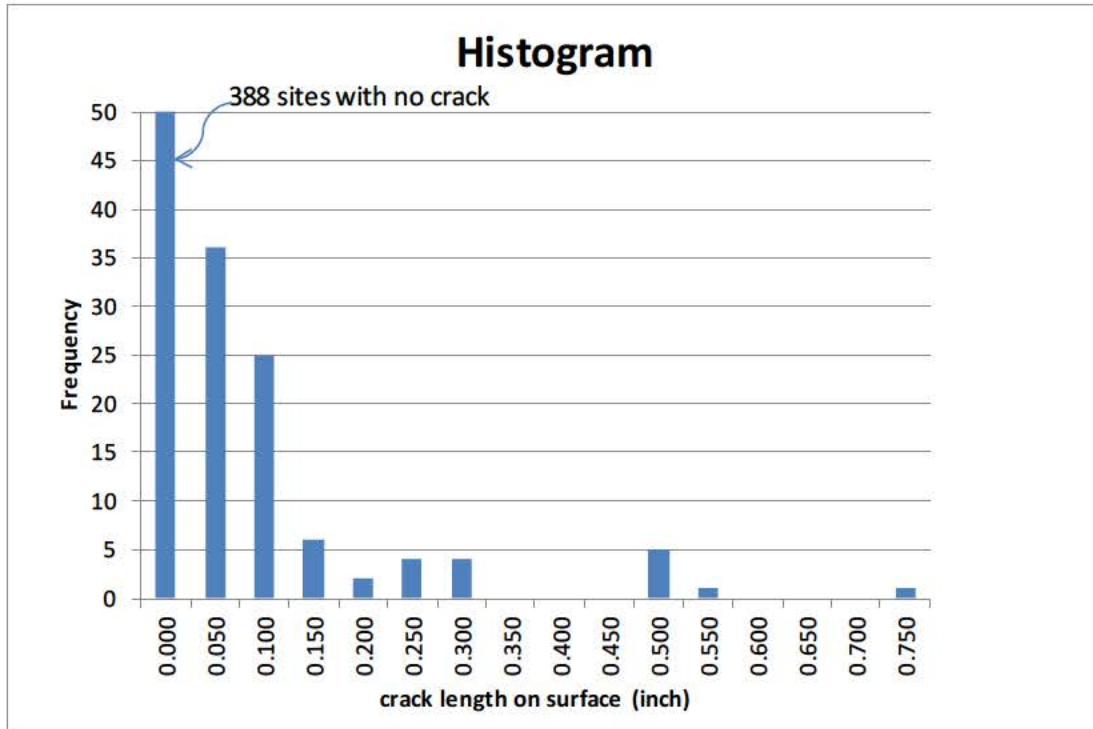


Figure 77. A histogram of the crack sizes in the specimen set.

Table 16. Crack key for NDT coupons. Many coupons deliberately contain no cracks.

Coupon ID	Hole D	Thickness	Primary Face (inch)	Primary Bore (inch)		Secondary Face (inch)	Secondary Bore (inch)
NDT-001-A	0.278	0.100	0.046	0.093			
NDT-002-B	0.418	0.500	0.050	0.078			
NDT-003-C	0.418	0.100	0.030	0.042		0.030	0.047
NDT-004-B	0.418	0.313					
NDT-005-B	0.538	0.500					
NDT-006-A	0.538	0.100	0.114	thru			
NDT-007-C	0.418	0.100	0.500	thru		0.037	0.070
NDT-008-A	0.278	0.100					
NDT-009-C	0.538	0.100	0.044	thru		0.017	0.032
NDT-010-C	0.538	0.100	0.090	thru		0.030	0.035
NDT-011-D	0.418	0.313					
NDT-012-D	0.278	0.313	0.020	0.119			
NDT-013-B	0.418	0.313					
NDT-014-B	0.278	0.500	0.076	0.081			
NDT-015-B	0.278	0.313	0.247	0.177		0.085	0.134
NDT-016-D	0.418	0.313					

NDT-017-D	0.418	0.313					
NDT-018-B	0.418	0.500	0.749	0.275		0.202	0.138
NDT-019-D	0.538	0.500	0.495	0.141		0.077	cannot detect
NDT-020-A	0.278	0.100					
NDT-021-A	0.418	0.100	0.019	0.030			
NDT-022-A	0.538	0.100	0.072	thru		0.090	thru
NDT-023-A	0.278	0.100					
NDT-024-C	0.538	0.100	0.281	thru		0.040	thru
NDT-025-C	0.278	0.100	0.053	thru		0.032	0.070
NDT-026-B	0.418	0.313					
NDT-027-A	0.418	0.100	0.249	thru		0.089	thru
NDT-028-A	0.278	0.100					
NDT-029-C	0.278	0.100	0.249	R		0.034	0.052
NDT-030-D	0.418	0.313					
NDT-031-B	0.418	0.313					
NDT-032-C	0.278	0.100					
NDT-033-D	0.538	0.500					
NDT-034-D	0.538	0.500					
NDT-035-B	0.418	0.313					
NDT-036-B	0.538	0.313	0.034	0.050			
NDT-037-D	0.418	0.500	0.099	0.084			
NDT-038-A	0.278	0.100					
NDT-039-B	0.278	0.313	0.072	0.106			
NDT-040-C	0.278	0.100					
NDT-041-D	0.418	0.313					
NDT-042-B	0.418	0.313					
NDT-043-B	0.278	0.500	0.043	0.055			
NDT-044-D	0.278	0.313	0.040	0.053			
NDT-045-B	0.278	0.313	0.050	0.073			
NDT-046-B	0.418	0.313					
NDT-047-D	0.418	0.313					
NDT-048-C	0.278	0.100					
NDT-049-A	0.278	0.100					
NDT-050-D	0.538	0.500					
NDT-051-B	0.418	0.313	0.500	thru		0.075	0.087
NDT-052-D	0.278	0.500	0.121	0.085			
NDT-053-D	0.538	0.500	0.047	0.789			
NDT-054-B	0.418	0.313					
NDT-055-B	0.278	0.500	0.116	0.085			
NDT-056-D	0.418	0.313					
NDT-057-D	0.418	0.313					

NDT-058-B	0.538	0.500					
NDT-059-C	0.418	0.100	0.045	thru		0.033	0.055
NDT-060-B	0.538	0.313	0.119	0.184		0.045	0.061
NDT-061-D	0.418	0.313	0.052	0.086		0.047	0.069
NDT-062-C	0.538	0.100	0.119	thru		0.033	0.047
NDT-063-D	0.418	0.313	0.080	0.090			
NDT-064-C	0.278	0.100					
NDT-065-B	0.538	0.500					
NDT-066-D	0.418	0.313					
NDT-067-D	0.418	0.313					
NDT-068-A	0.278	0.100					
NDT-069-D	0.538	0.500	0.044	0.053			
NDT-070-A	0.278	0.100					
NDT-071-D	0.538	0.500					
NDT-072-B	0.538	0.500					
NDT-073-C	0.538	0.100	0.072	thru		0.036	thru
NDT-074-D	0.418	0.313	0.048	0.067			
NDT-075-B	0.418	0.500	0.499	0.219		0.037	0.048
NDT-076-B	0.538	0.500					
NDT-077-B	0.538	0.500					
NDT-078-C	0.278	0.100					
NDT-079-B	0.538	0.500					
NDT-080-D	0.538	0.313	0.250	0.176		0.087	0.114
NDT-081-D	0.538	0.500					
NDT-082-D	0.538	0.500					
NDT-083-B	0.538	0.313	0.053	0.053		0.018	0.016
NDT-084-D	0.418	0.500	0.086	0.086			
NDT-085-D	0.538	0.500					
NDT-086-D	0.538	0.500					
NDT-087-C	0.278	0.100	0.018	0.026			
NDT-088-A	0.418	0.100	0.056	thru			
NDT-089-A	0.278	0.100					
NDT-090-A	0.278	0.100	0.078	thru		0.035	0.038
NDT-091-D	0.538	0.500					
NDT-092-B	0.538	0.500	0.029	0.020			
NDT-093-C	0.278	0.100					
NDT-094-D	0.278	0.500	0.052	0.057			
NDT-095-B	0.538	0.500	0.270	cannot read		0.168	cannot detect
NDT-096-A	0.278	0.100					
NDT-097-B	0.418	0.313	0.046	0.072			
NDT-098-C	0.278	0.100					

NDT-099-A	0.278	0.100	0.498	thru		0.094	thru
NDT-100-B	0.538	0.500	0.068	0.086			
NDT-101-C	0.278	0.100					
NDT-102-B	0.538	0.500					
NDT-103-B	0.418	0.313	0.022	0.029			
NDT-104-B	0.538	0.500					
NDT-105-D	0.278	0.313	0.492	0.199			
NDT-106-A	0.538	0.100	0.251	thru		0.169	thru
NDT-107-D	0.538	0.313	0.018	0.037			
NDT-108-C	0.278	0.100					
NDT-109-D	0.538	0.500					
NDT-110-D	0.418	0.500	0.070	0.081			
NDT-111-B	0.418	0.313					
NDT-112-C	0.278	0.100					
NDT-113-D	0.538	0.313	0.123	0.130		0.097	0.083
NDT-114-B	0.538	0.500					
NDT-115-A	0.538	0.100	0.045	0.076			
NDT-116-B	0.418	0.313					
NDT-117-D	0.278	0.500	0.028	0.039			
NDT-118-A	0.538	0.100	0.046	0.064			

7.5 Results

7.5.1 Preliminary Trials

A small set of experiments was conducted at APES facilities in concert with cold working and fatigue crack growth in coupons. A photograph of the load frame and NDT equipment is shown in Figure 78.

There were two separate experiments performed in these trials:

- Case 1. Evaluate the detectability of cracks under different loads, before and after cold working the hole.
 - 0.050” corner crack in 0.250” diameter hole in 0.250” thick Al 7075-T6
 - Specimens 3D2-03-D, 3D2-04-D
- Case 2. Evaluate the detectability of cracks grown in a hole with CX.
 - Same conditions as above, no starter notch.
 - Specimens 3D2-01-D, 3D2-02-D



Figure 78. A photograph of the facilities for the preliminary trials

7.5.1.1 Preliminary Trial – Detection of Cracks Under Different Loads

For this trial, we began with a 0.050” corner crack in 0.250” diameter hole in 0.250” thick Al 7075-T6. Both ET-BH and UT techniques were applied, and the applied load was varied and measurements repeated. Then the hole was cold worked, and the variation in applied load was repeated.

The ET-BH results are shown in Figure 79 below. There are no trends, indicating that the results are all within normal measurement scatter.

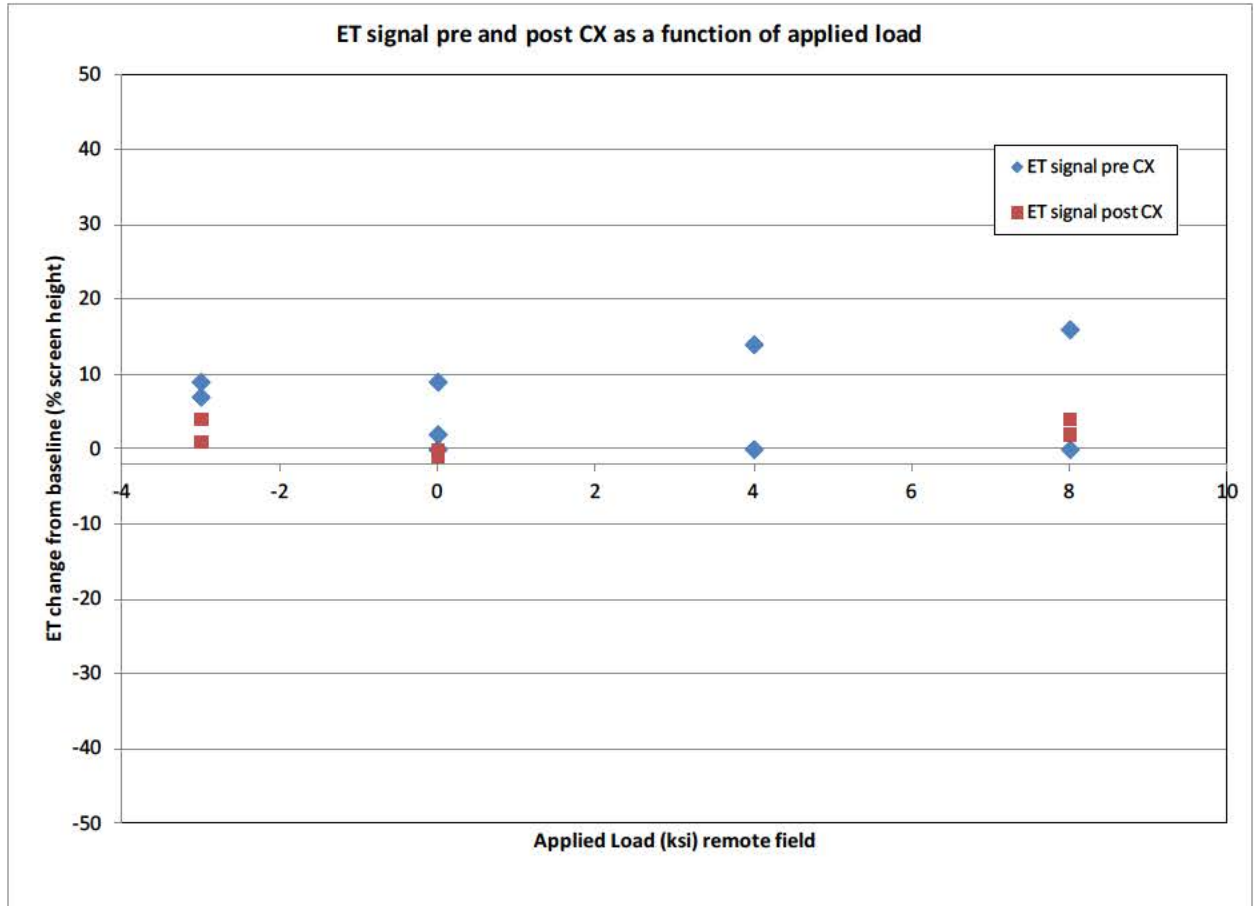


Figure 79. Change in ET-BH signal due to applied load is minimal.

The UT results are shown in Figure 80 below. There is a clear trend of signal increasing with increasing tension opening the crack faces. The post CX values are very similar to the pre CX values.

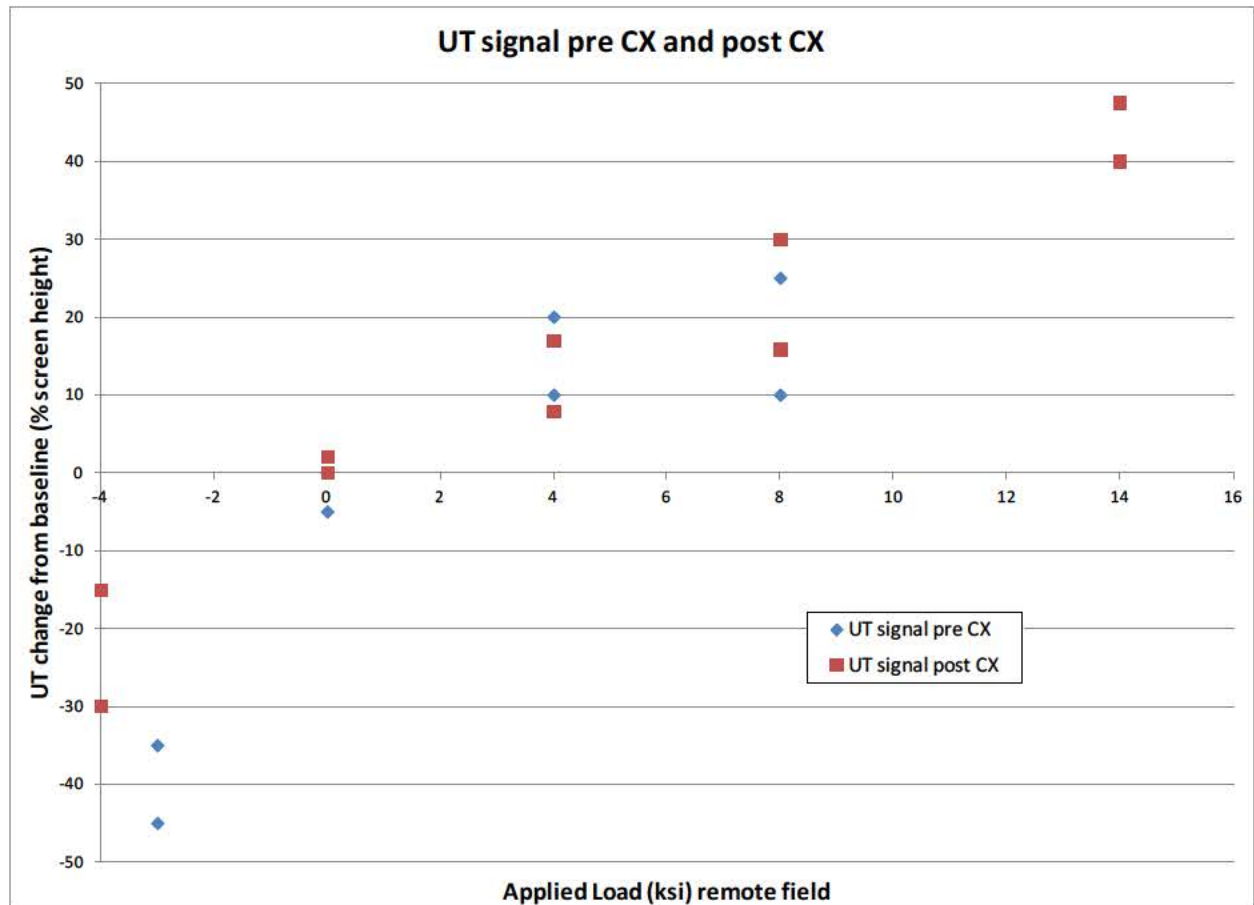


Figure 80. Change in UT signal due to applied load.

7.5.1.2 Preliminary Trial – Detection of Cracks Grown Post Cold Work

For this trial, two specimens were manufactured, holes were cold worked, then the specimens were subject to fatigue and the resulting cracks monitored during growth using a traveling microscope. At intervals, the fatigue was stopped and ET-BH and UT measurements were made at different applied static loads.

The ET-BH results are shown in Figure 81 below. These results are typical of ET-BH response to varying crack sizes. The changing in applied load makes no significant change to the ET-BH response, as was found in the previous section. It can be seen that a 0.050" corner crack gives signals from 30 – 50% screen height, easily detectable.

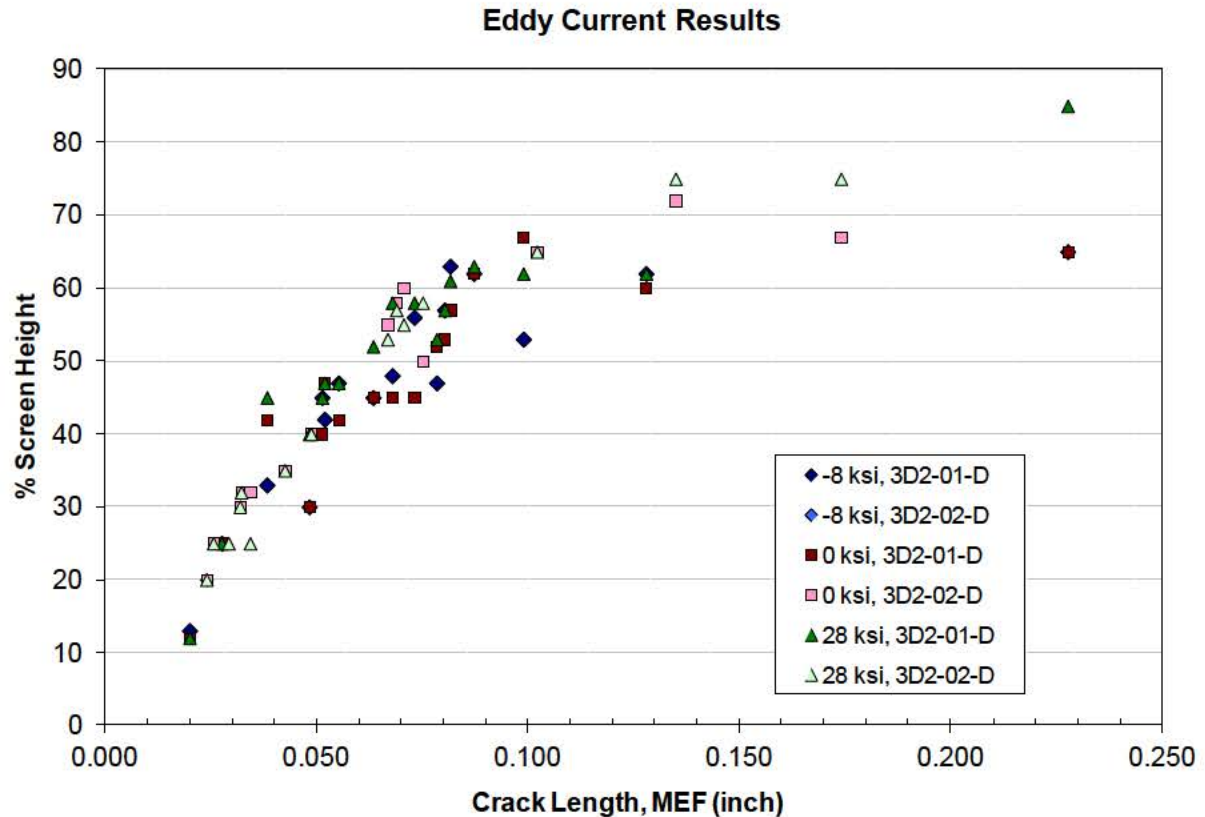


Figure 81. ET-BH signal for different crack sizes and applied stresses.

The UT results are more complicated, as the signal is affected by the applied load. Figure 82 shows the results for 0 ksi and -8 ksi (that is, compressive) stresses applied to the crack. Figure 83 shows the results for 7, 10, and 14 ksi tension stresses. Figure 84 shows the results for 20 and 28 ksi tension stresses.

The UT results show strong differences due to the applied loads, as expected. Even up to 28 ksi, the response is still increasing.

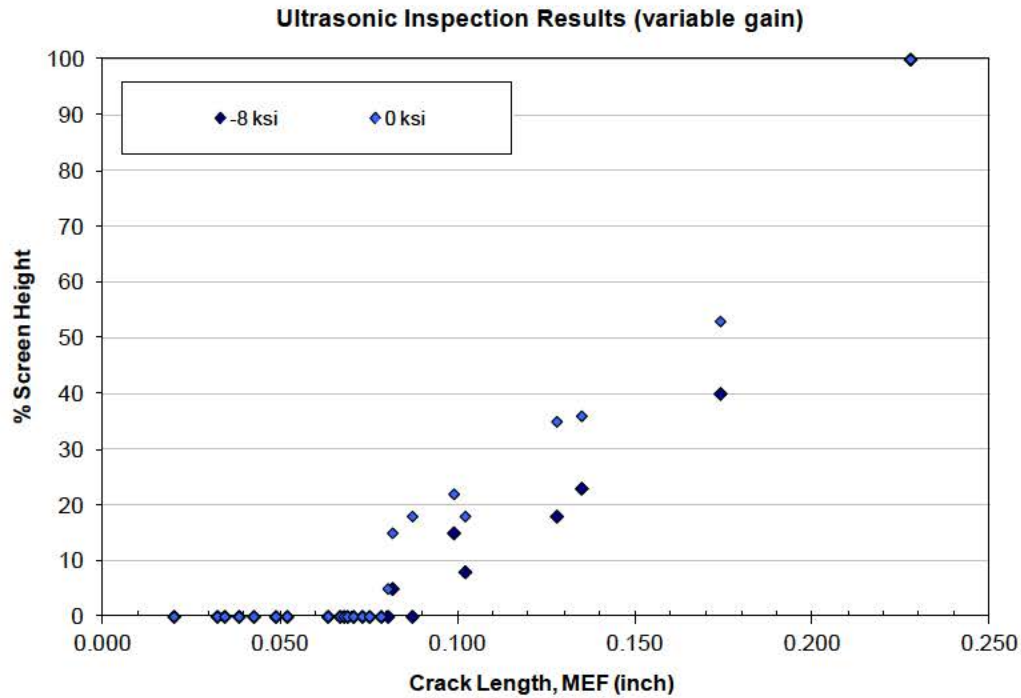


Figure 82. UT results for different crack sizes and applied stresses.

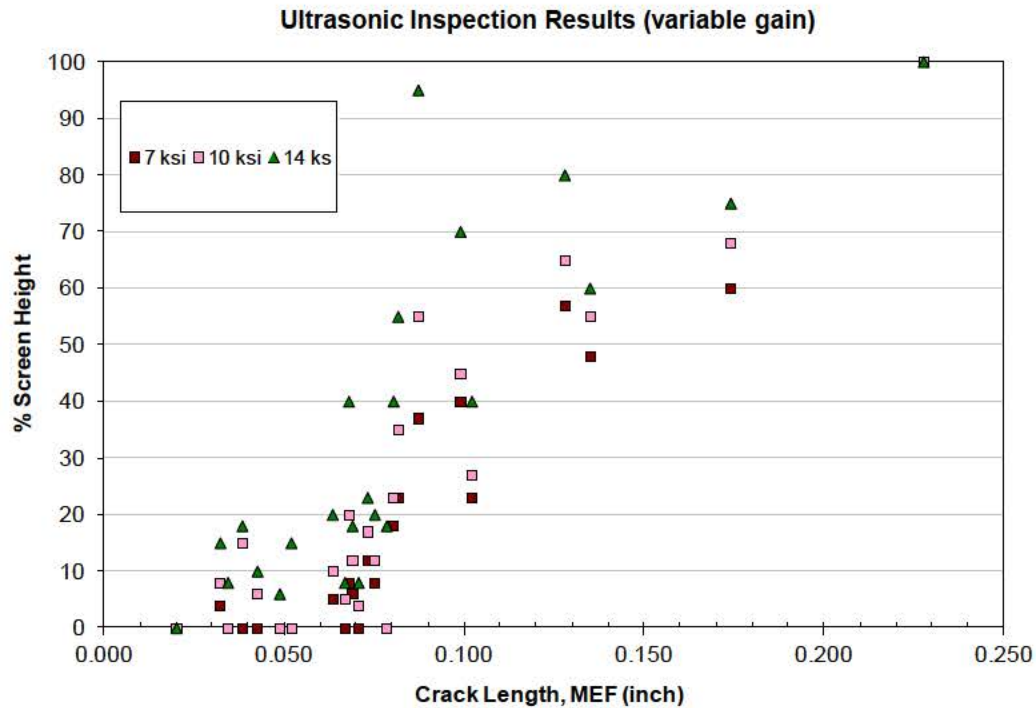


Figure 83. UT results for different crack sizes and applied stresses.

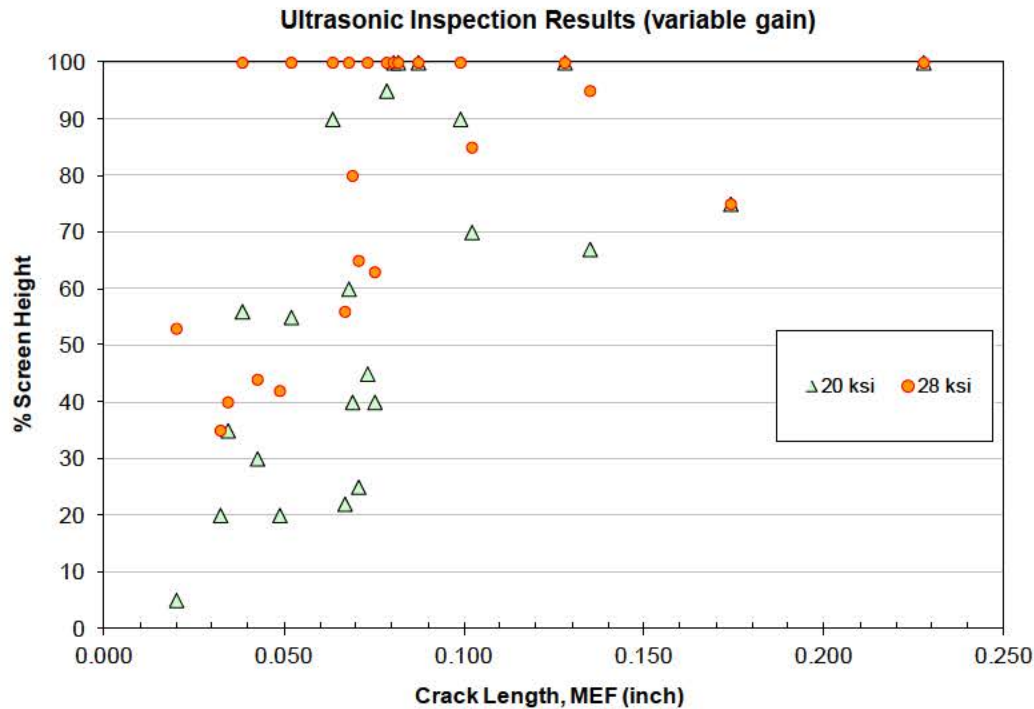


Figure 84. UT results for different crack sizes and applied stresses.

7.5.2 Final Trial - Bolt Hole Eddy Current Results

Each hole diameter was inspected using a different bolt hole probe, as the probe diameters must be closely matched and almost fill the hole for best response. We also looked at two frequencies, 200 kHz and 500 kHz, which are the lower and upper ends of the Air Force suggested range for standard bolt hole ET inspection. The following subsections describe the results for each hole/probe size and frequency.

In all cases, the gain has to be modified from the standard setup on some holes to avoid saturation. We measured the response of the probes to the Air Force standard block at various gain settings, and used this relationship of gain to amplitude to “normalize” all the different gain settings to the gain level required to achieve 80% full screen height on the Air Force standard block for the matching diameter. This does result in equivalent readings greater than 100%.

For each of the data sets, all of the cracks are easily detected. Some are below the Air Force standard of 40% FSH, but are well above the noise level. This is shown in Figure 85 below. The gain has been increased from the standard setup to show the response better.

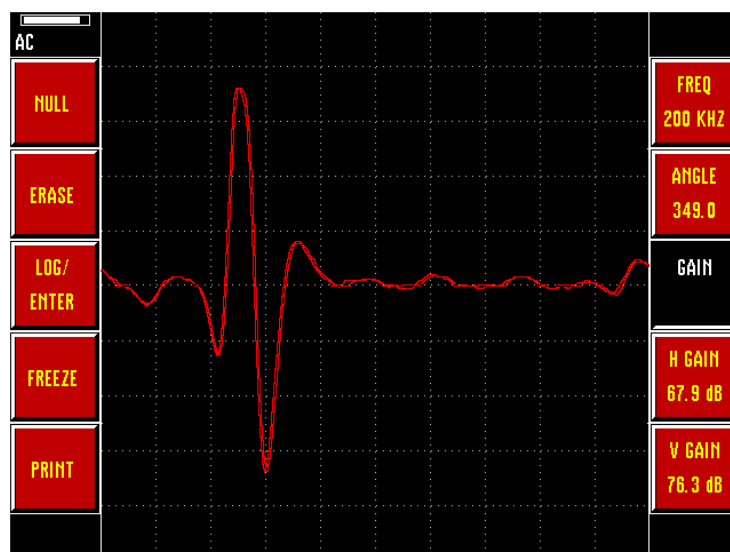


Figure 85. Eddy Current signal from a 0.018" by 0.026" corner crack, gain increased from setup to show signal better.

A standard way to determine the effects of different inputs on a measured value is to use Generalized Linear Modeling (GLM) and ANOVA. We can describe inspection data in terms of a model relating the measured outcome (i.e. % screen height) to a set of parameters that may be relevant to the signal. For this data, the model included diameter, thickness, frequency, and importantly the "size" of the discontinuity under inspection.

This is a well-known procedure. R version 2.14.2 was used to make the calculations, and summaries are shown below. First, we fit a model that uses all inputs as possible explanatory variables. The results are shown below in Table 18.

Table 17. GLM Fit to the ET-BH Results

	Estimate	Std. Error	z value	p value
diameter	0.06912	0.50845	0.136	0.89186
thickness0.313	-0.03436	0.12328	-0.279	0.78047
thickness0.5	-0.06234	0.13643	-0.457	0.64775
face_length	0.98061	0.32546	3.013	0.00259 **
bore_length	0.69552	0.53894	1.291	0.19686
frequency500	0.72612	0.11036	6.58	4.72E-11 ***
alloy7075	-0.07128	0.10534	-0.677	0.49863
Signif. codes: 0 '***' 0.001 '**' 0.01 '.' 0.1 'x' 1				

The GLM results indicate that the only important factors are frequency and length. Removing frequency to see if any of the other factors may be important to a single frequency inspection yields the following (Table 19), and we see that thickness and hole diameter are not important effects. The important crack dimension is face length.

Table 18. GLM fit to the ET-BH results with frequency removed.

	Estimate	Std. Error	z value	p value
diameter	0.03847	0.50892	0.076	0.93974
thickness0.313	-0.03831	0.12326	-0.311	0.75598
thickness0.5	-0.06639	0.13639	-0.487	0.62643
face_length	0.97493	0.32551	2.995	0.00274 **
bore_length	0.69644	0.53894	1.292	0.19627
alloy7075	-0.06731	0.10533	-0.639	0.52282
Signif. codes: 0 '***' 0.001 '**' 0.01 '*' 0.05 '.' 0.1 'x' 1				

All of the data was pooled by frequency and used to estimate POD. The lack of missed cracks makes a “hit/miss” type analysis unworkable, so an “a versus a” analysis was performed, using the mh1823 version 3.1.2 software. The data is not a great fit for this analysis, as shown below in Figure 86. The results are shown in Figure 87. The a_{90} and $a_{90/95}$ values are very small, as has been found in previous studies from laboratory specimens. An in-depth statistical analysis could be performed to try and estimate where the POD falls off, but that occurs below any of the measured data and would require extrapolation.

The problems in analysis are because the data are so good. However, the Air Force standard for a detectable crack size of 0.050” length using bolt hole eddy current is easily achieved by this data set.

The key difference between the performance on these test coupons and performance in the depot or field is the hole quality. Hand machining of holes followed by insertion and removal of fasteners can result in out of round holes or surface damage. These cause noise in the ET signal and degrade POD. Thus the performance shown here should not be expected in the depot/field, and we recommend the use of the performance metrics from the Structures Bulletin EN-SB-012.

An example of the effect on bolt hole ET signals from noisy holes is documented in Forsyth (2009).

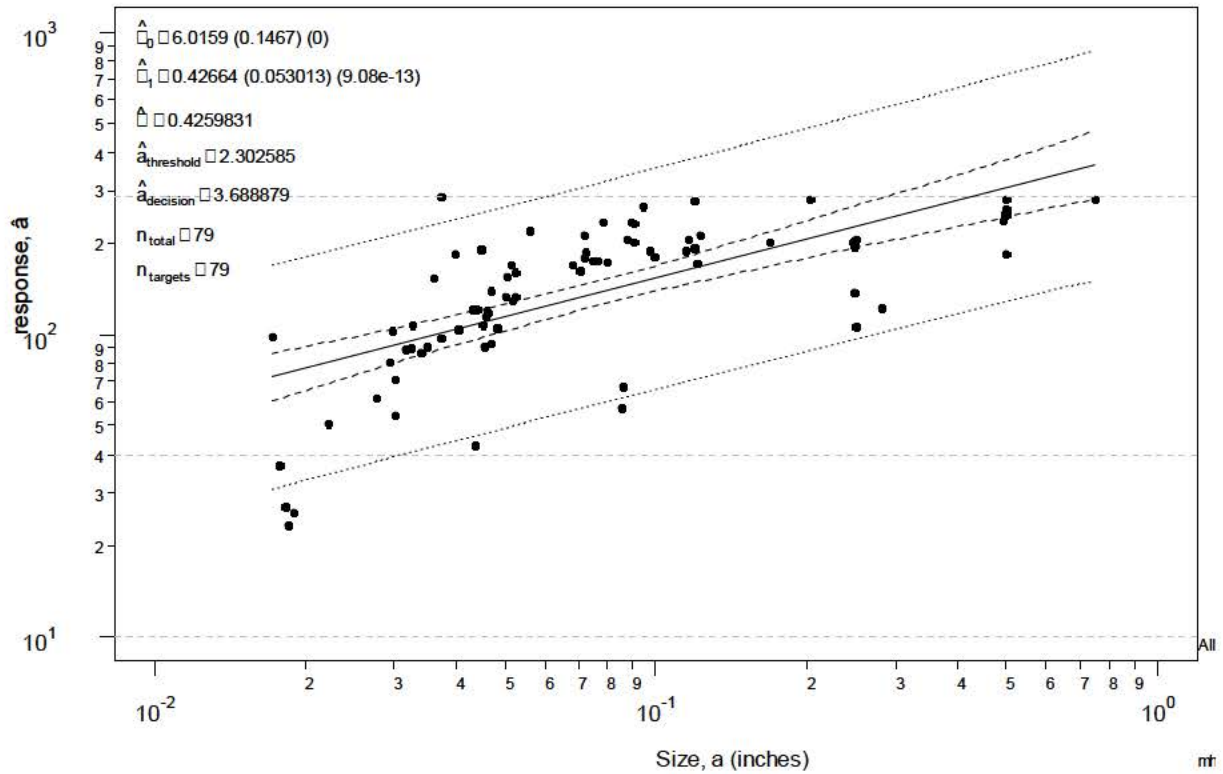


Figure 86. A log-log model of the 200 kHz ET-BH data.

All ET - BH 200kHz

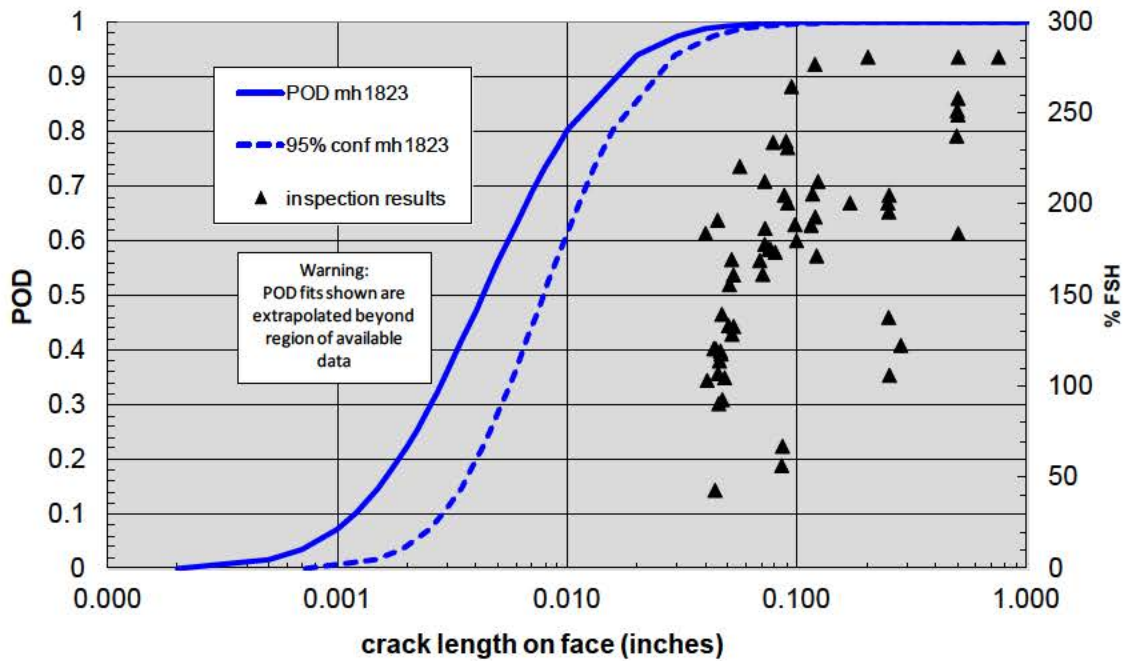


Figure 87. POD fit to all ET - BH 200 kHz data.

7.5.2.1 Diameter 0.278" Frequency 200 kHz

Figure 88 below shows the ET results on the 0.278" diameter hole specimens at a frequency of 200 kHz.

The smallest crack, 0.018" on the face and 0.026" on the bore, is easily detected at 23% FSH.

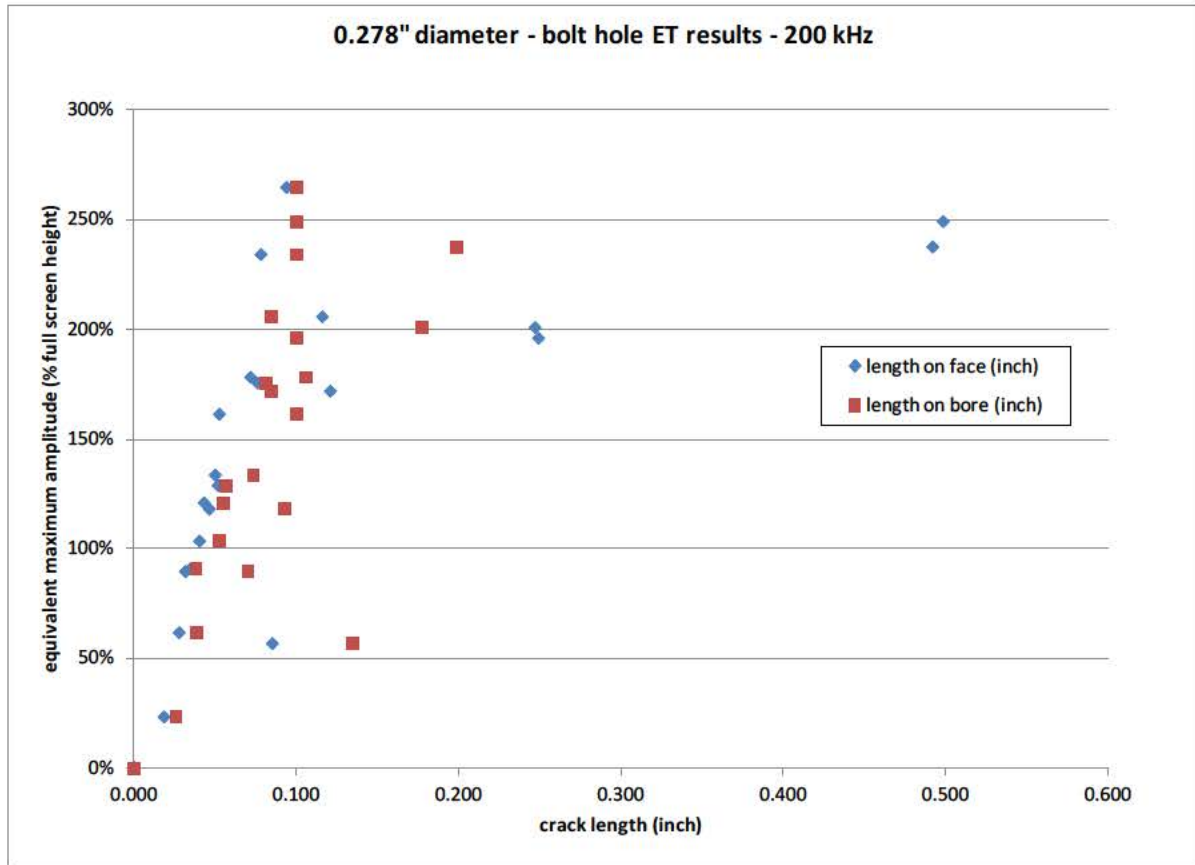


Figure 88. ET signal as a Function of Crack Length for 0.278" Diameter Holes and 200 kHz Excitation Frequency

7.5.2.2 Diameter 0.278" Frequency 500 kHz

Figure 89 below shows the ET results on the 0.278" diameter hole specimens at a frequency of 500 kHz.

There are no missed cracks in this data set at the typical threshold setting of 40% FSH. The smallest crack, 0.018" on the face and 0.026" on the bore, is easily detected at 70% FSH, the smallest response of any of the cracks.

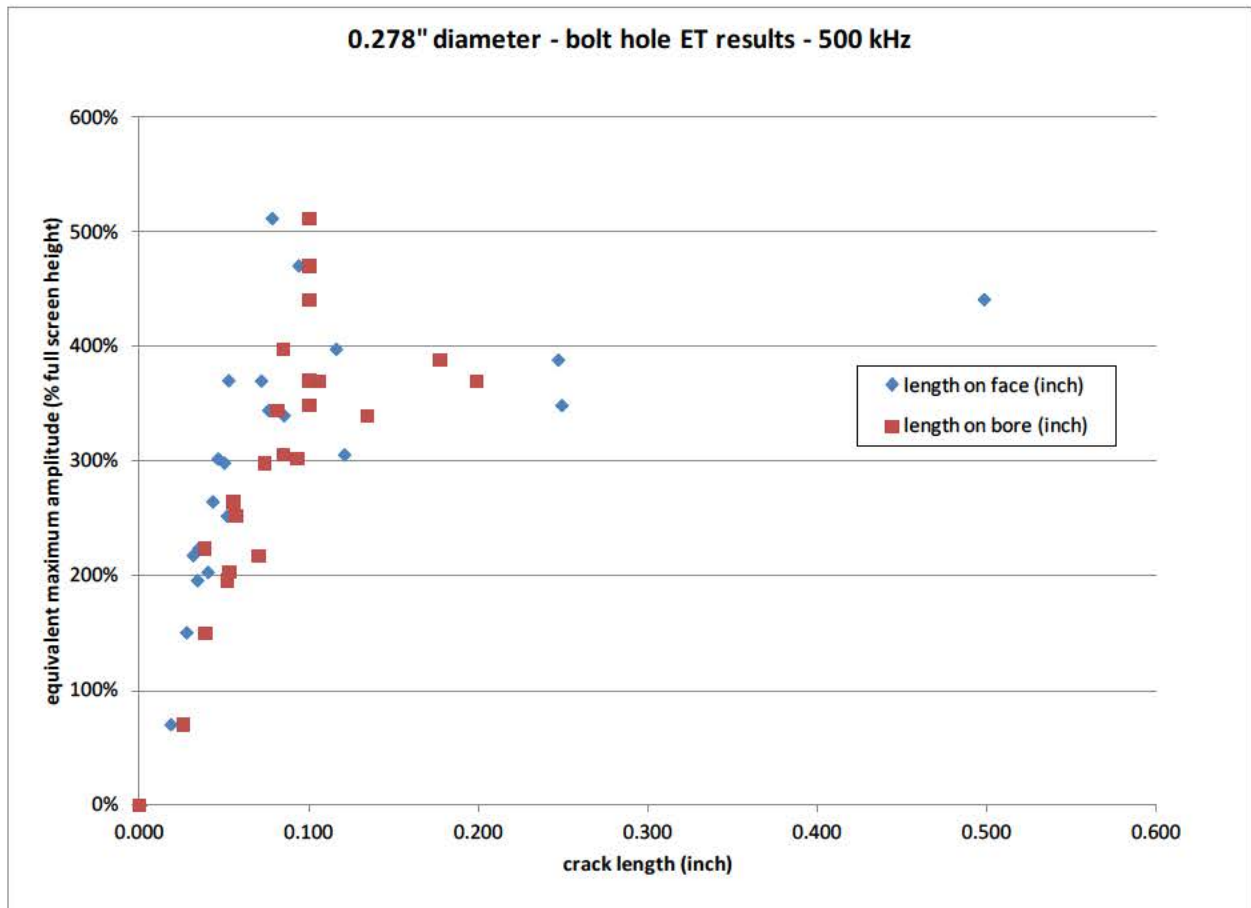


Figure 89. ET signal as a Function of Crack Length for 0.278" Diameter Holes and 500 kHz Excitation Frequency

7.5.2.3 Diameter 0.418" Frequency 200 kHz

Figure 90 below shows the ET results on the 0.418" diameter hole specimens at a frequency of 200 kHz.

The smallest crack, 0.019" on the face and 0.030" on the bore, is easily detected at 26% FSH, the smallest response of any of the cracks.

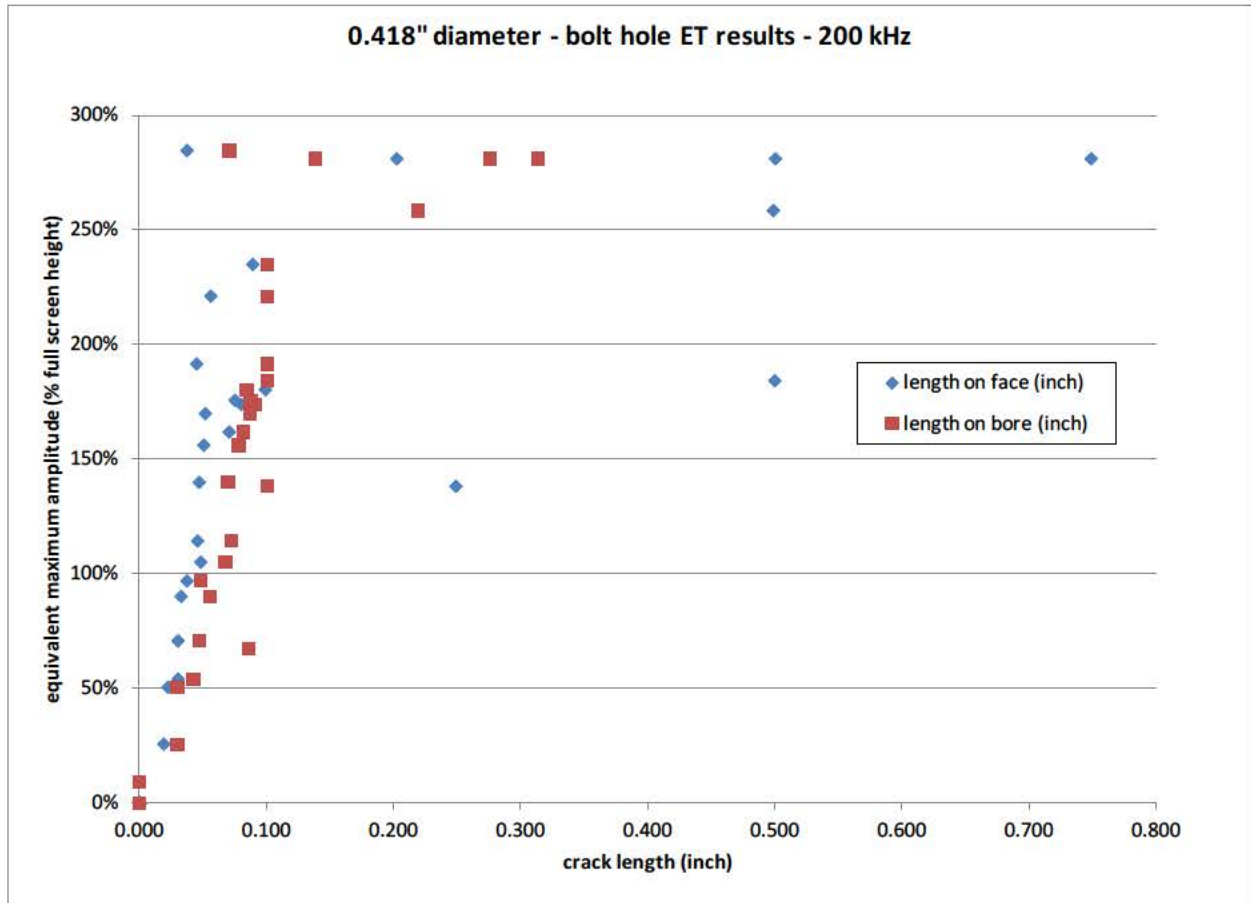


Figure 90. ET signal as a Function of Crack Length for 0.418" Diameter Holes and 200 kHz Excitation Frequency

7.5.2.4 Diameter 0.418" Frequency 500 kHz

Figure 91 below shows the ET results on the 0.418" diameter hole specimens at a frequency of 500 kHz.

There are no missed cracks in this data set at the typical threshold setting of 20% FSH. The smallest crack, 0.019" on the face and 0.030" on the bore, is easily detected at 73% FSH, the smallest response of any of the cracks.

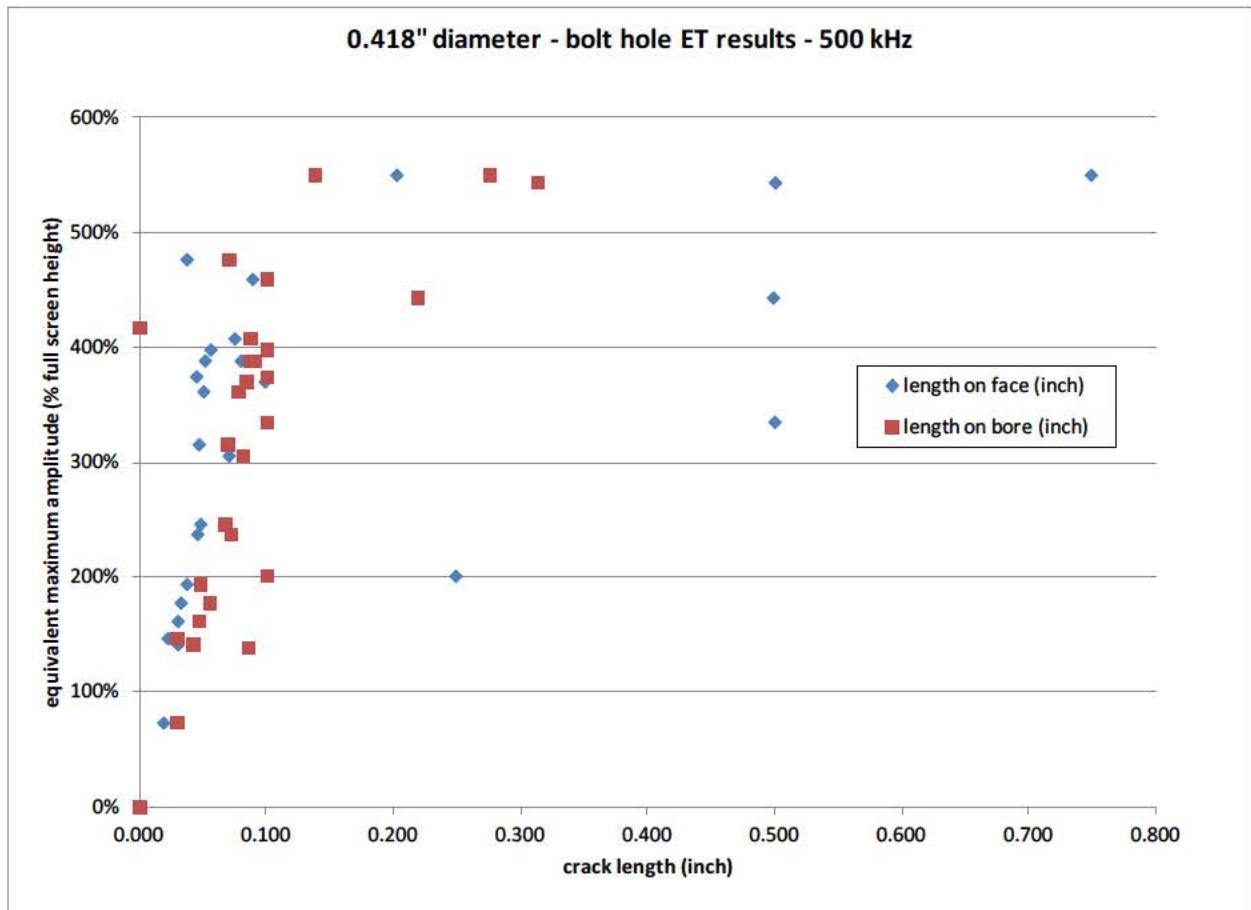


Figure 91. ET signal as a Function of Crack Length for 0.418" Diameter Holes and 500 kHz Excitation Frequency

7.5.2.5 Diameter 0.538" Frequency 200 kHz

Figure 92 below shows the ET results on the 0.538" diameter hole specimens at a frequency of 200 kHz.

The smallest crack, 0.016" on the bore and 0.018 on the face, is easily detected at 37% FSH, and the smallest response of any of the cracks is 27% FSH.

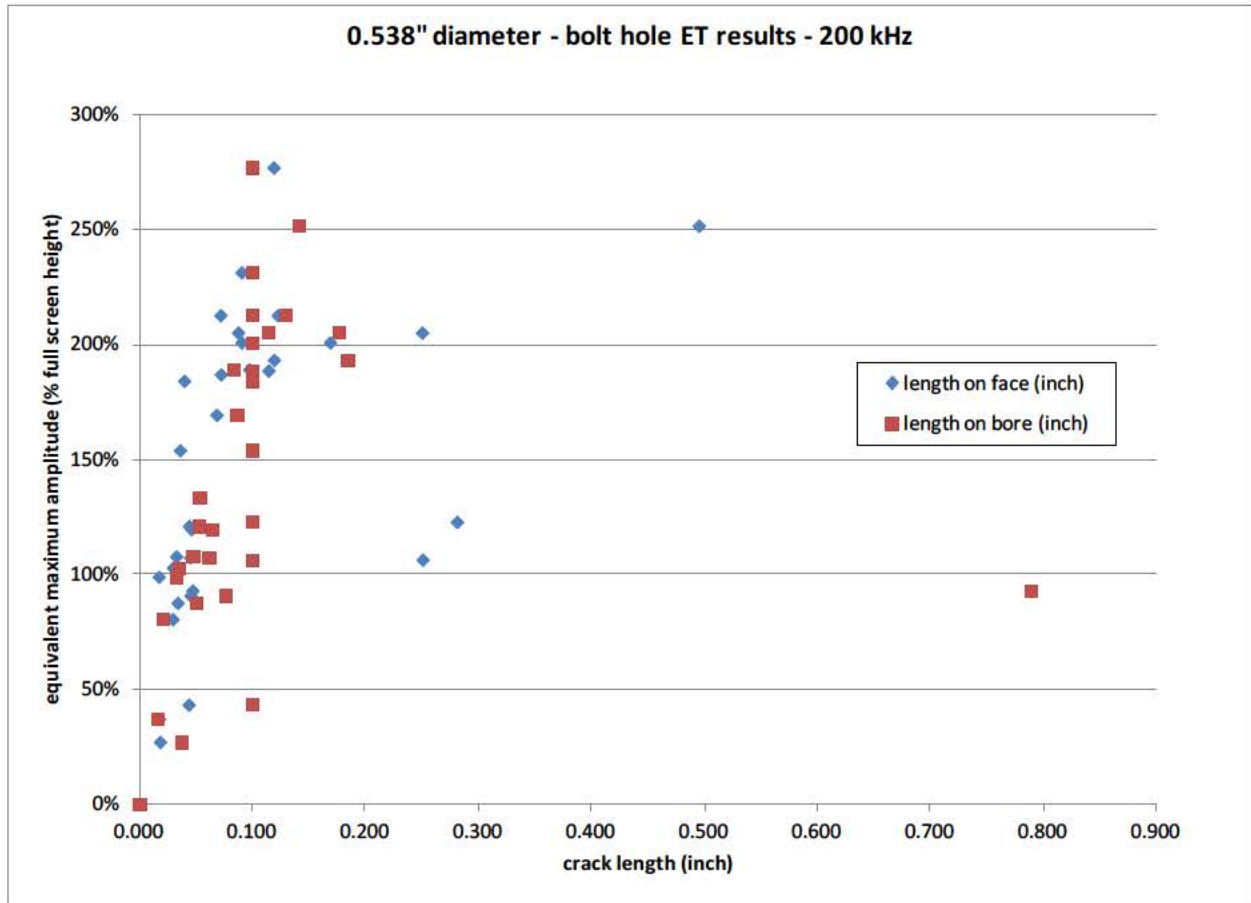


Figure 92. ET signal as a Function of Crack Length for 0.538" Diameter Holes and 200 kHz Excitation Frequency.

7.5.2.6 Diameter 0.538" Frequency 500 kHz

Figure 93 below shows the ET results on the 0.538" diameter hole specimens at a frequency of 500 kHz.

There are no missed cracks in this data set at the typical threshold setting of 20% FSH. The smallest crack, 0.016" on the bore and 0.018" on the face, is easily detected at 91% FSH, and the smallest response of any of the cracks is 78% FSH.

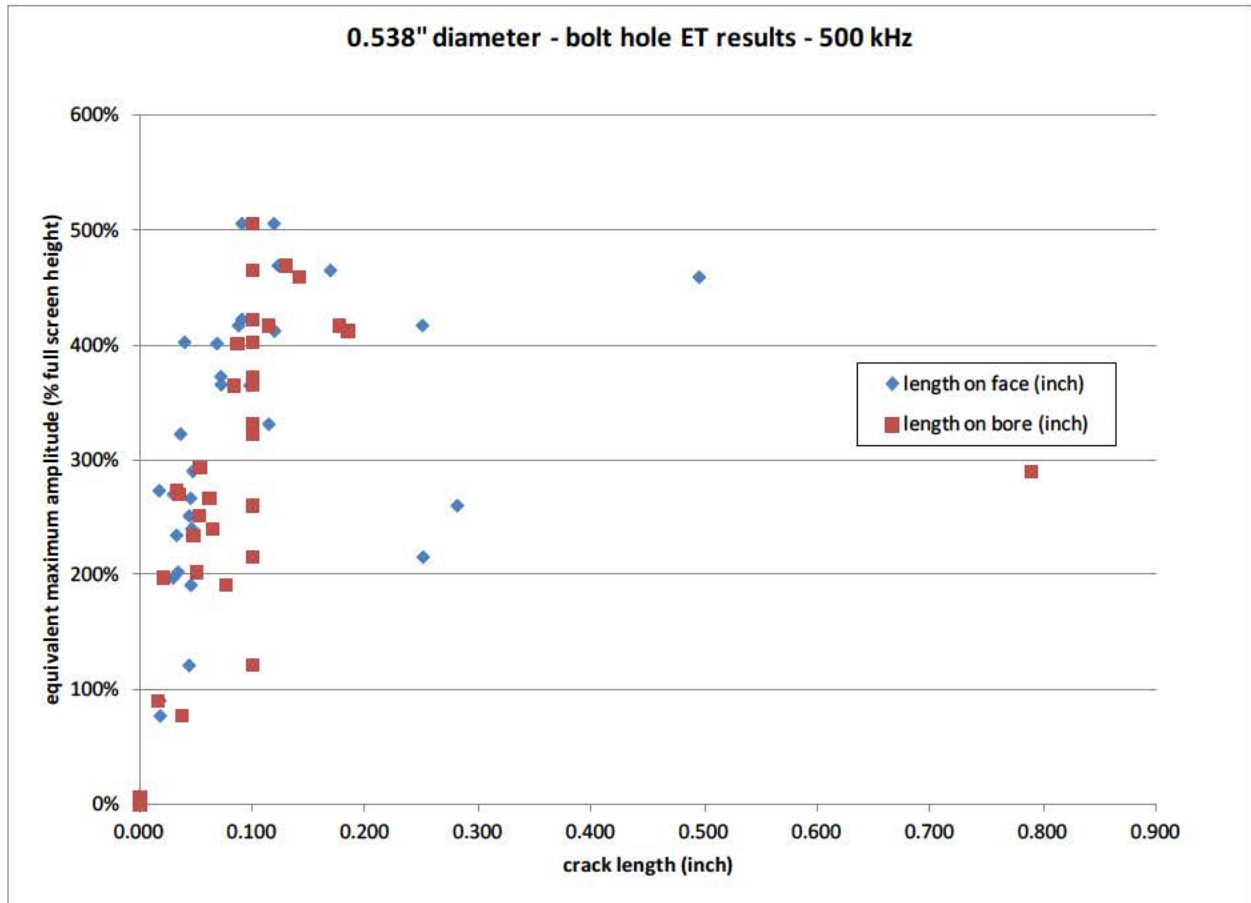


Figure 93. ET signal as a Function of Crack Length for 0.538" Diameter Holes and 500 kHz Excitation Frequency

7.5.3 Final Trial - Surface Scan Eddy Current Results

All ET-SS data reported in this section was taken at a 200 kHz inspection frequency. This is a typical upper limit prescribed by the manufacturers for pencil probes. Higher frequencies become noisier, as they are very sensitive to any probe wobble or surface scratches. Lower frequencies penetrate deeper, but are more diffuse and less sensitive (see Figure 94).

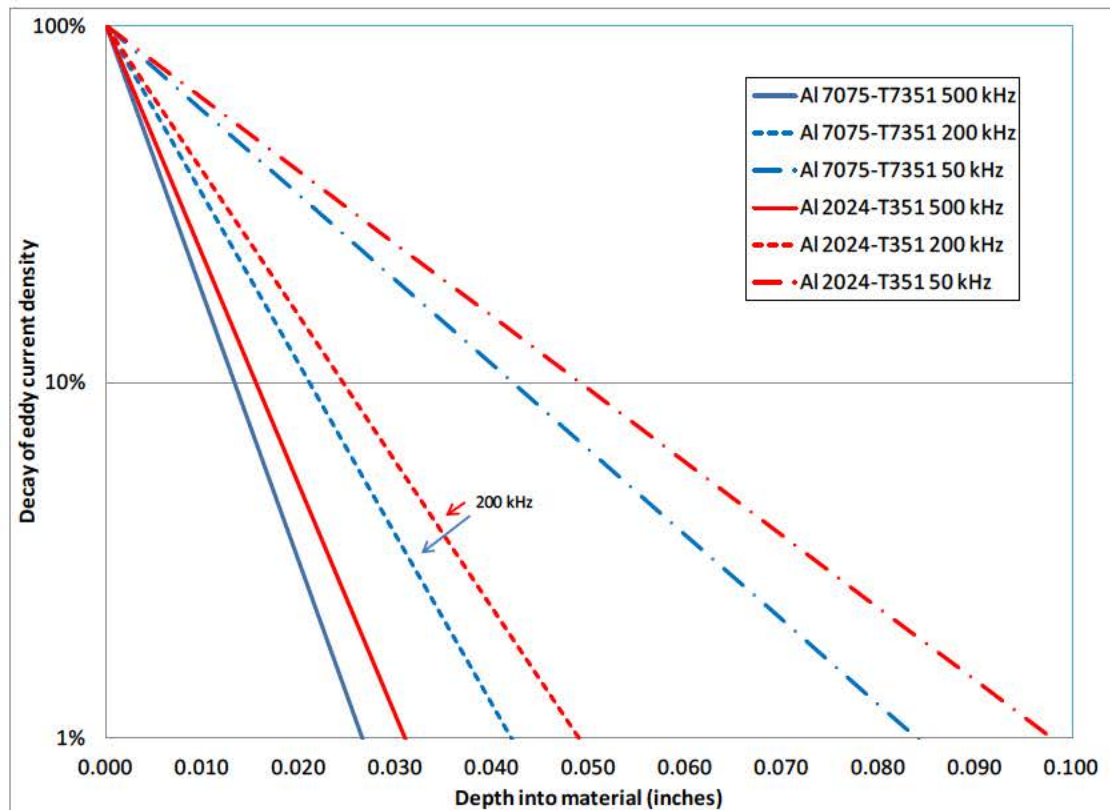


Figure 94. Eddy Currents Decay Faster at Higher Frequencies

The consequence of the physics illustrated in Figure 94 is that even a thin layer of intact material underneath the pencil probe is able to conduct eddy currents with little change in density from a thick layer. Due to the nature of the cracks in the cold worked holes, we have cracks in the sample set with long surface lengths on the mandrel entrance side (0.500" and more in a few cases) that have not broken through the mandrel exit side (see Figure 95), which is the side that is accessible in normal aircraft usage. This is especially the case for the thicker specimens.

All of the ET-SS data, in terms of the maximum signal response as a function of the crack length on the opposite side from the inspection side, is shown in Figure 96 below. There are three different coupon thicknesses, 0.100", 0.313", and 0.500". When we look at this data to see the effect of thickness, we see that almost all of the detected cracks were from the 0.100" thick set (see Figure 97). This can be explained by the fact that crack at CX

holes in 0.100" material have actually overcome the residual stress field and have turned into typical through cracks (see Figure 98).

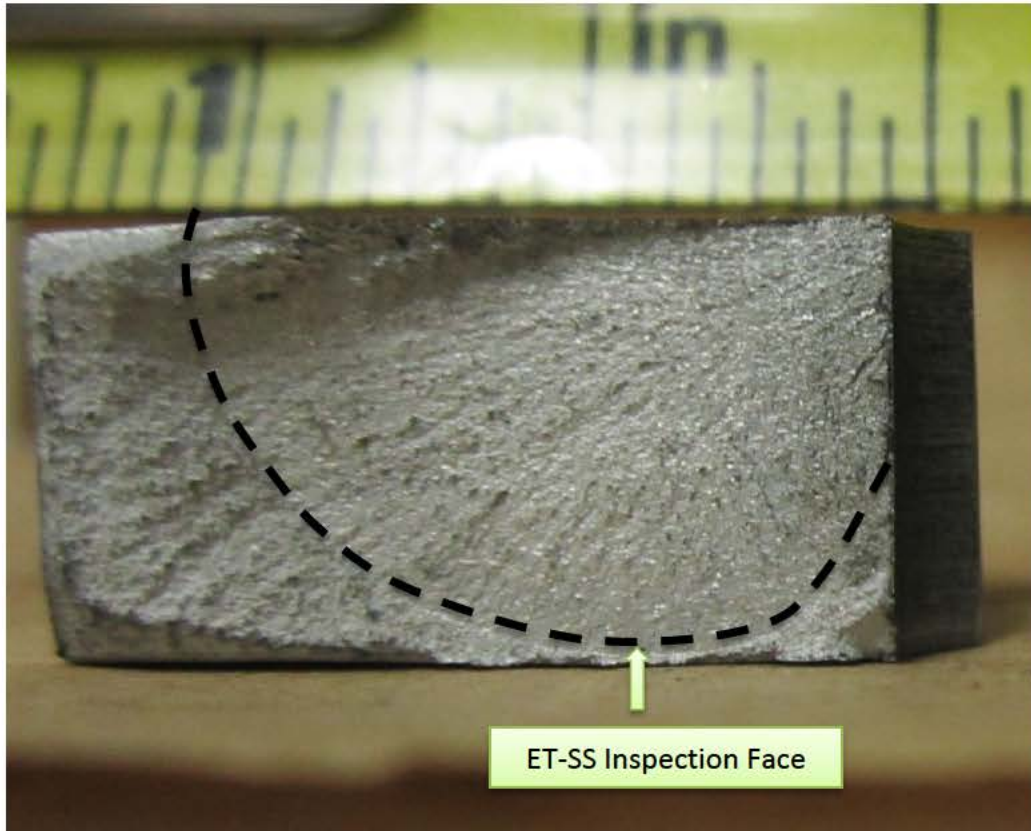


Figure 95. Specimen with large crack that measures 0.8" on mandrel entrance face (location with tape measure) broken open to illustrate how crack has yet to pop through to mandrel exit face (inspectable side using ET-SS). Plastic zone from the barely-subsurface crack was visible on the surface, but this crack was not detectable using ET-SS.

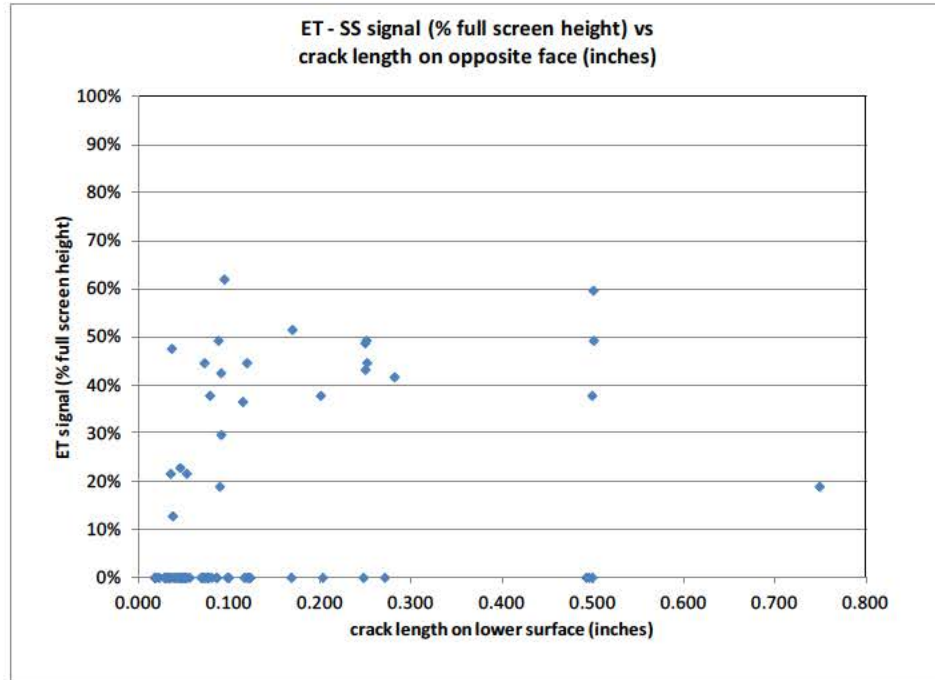


Figure 96. The Complete Set of Results of ET-SS Inspections of the Coupons.

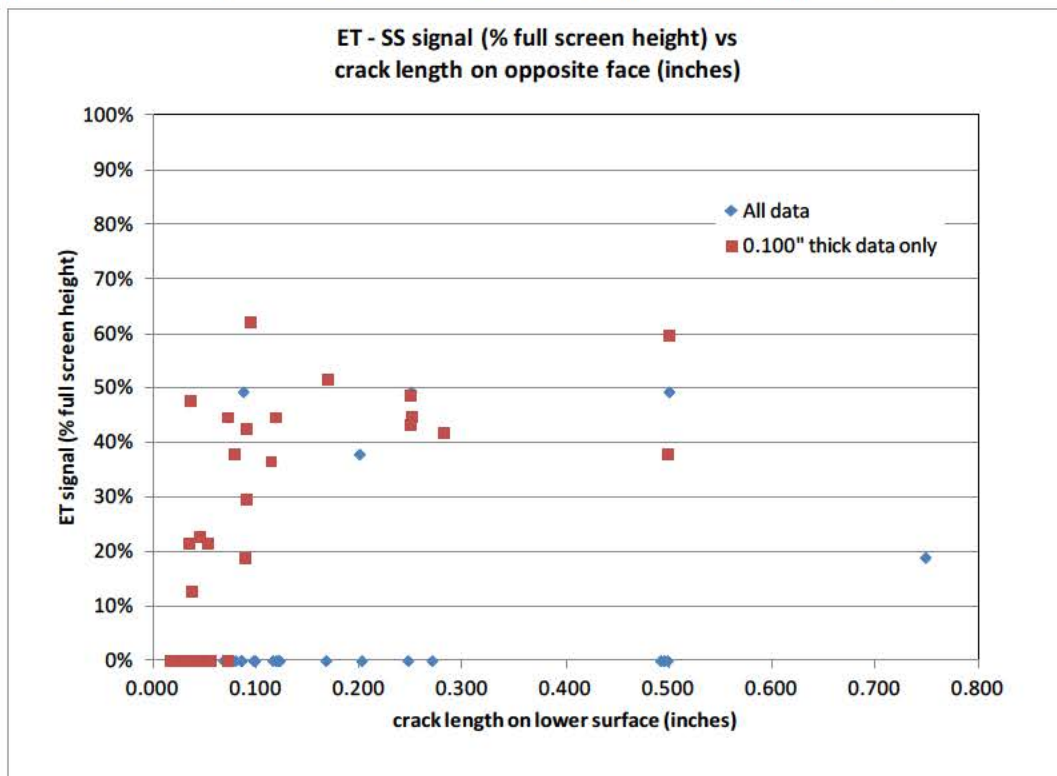


Figure 97. The Complete Set of Results of ET-SS Inspections of the Coupons With the 0.100" Thick Coupon Data Plotted in Red

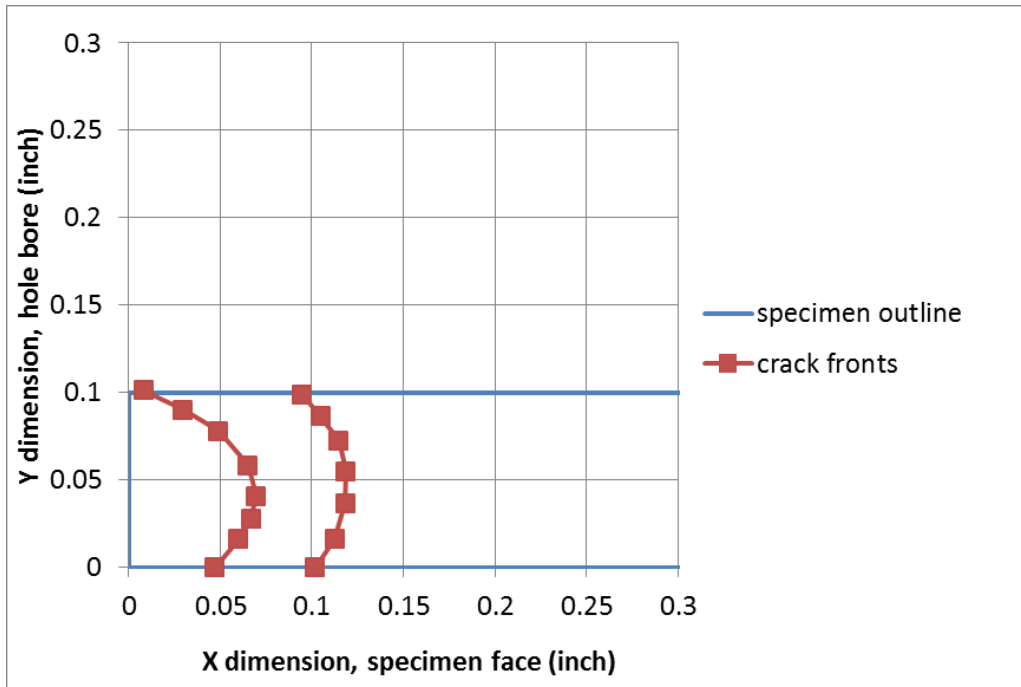


Figure 98. Marker band map showing crack shape from CX hole in 0.1" thick material.

The results of all the ET-SS data cannot be fit with a POD. There are two important reasons:

1. The results are too poor.
2. The data are actually from different families: A 0.250" long crack in the thicker coupons is nowhere near breaking the surface, so it is much harder to detect than in the 0.100" thick coupon where it has likely broken the surface.

Evaluation of the 0.500" thick and 0.313" thick coupon data proved fruitless. There is essentially zero POD for this inspection on these types of cracks. The data from the 0.100" thick coupons is examined in the following subsection.

7.5.3.1 ET – SS Results on 0.100" Thick Coupons

The Air Force guideline for the detection threshold to use for surface scan ET on aluminum is:

“Any 10% or higher vertical deflection that is distinguishable (separated) from the background noise and not caused by lift-off or part geometry shall warrant further examination and rescanning of the area of interest.”

We did not use an “ \hat{a} versus a ” analysis to estimate POD, as the data does not satisfy some of the required assumptions on linearity of transformed response and constant deviance. This data can still be used with a “hit/miss” type POD analysis, and that is

what is reported. The analysis was performed with TRI/Austin in-house software that has been shown to be equivalent to the guidelines in MIL-HDBK-1823.

The POD results are shown in Figure 99 below. There is a large spread between the mean estimate of POD and the 95% confidence bound due to the relatively small sample set (only 32 cracks in 0.100" thick coupons). The crack length at 90% POD (a_{90}) is about 0.150", and the 95% lower confidence bound at this POD ($a_{90/95}$) is about 0.360".

We recommend that the ET-SS inspection not be used to maintain safety on cold worked holes in aluminum. We could recommend using it for 0.100" and thinner plate, if more data was made available. As seen in Figure 99, there is not much data in this set at the a_{90} value and higher, and only 32 cracks total. If new data follows the trends shown here, it may be possible to use performance metrics from the Structures Bulletin EN-SB-012 for structure 0.100" or thinner.

Since the next thickness larger than 0.100" in our set was 0.313", it is possible that there may be intermediate thicknesses where ET-SS is useful. Additional data will be required to make that determination.

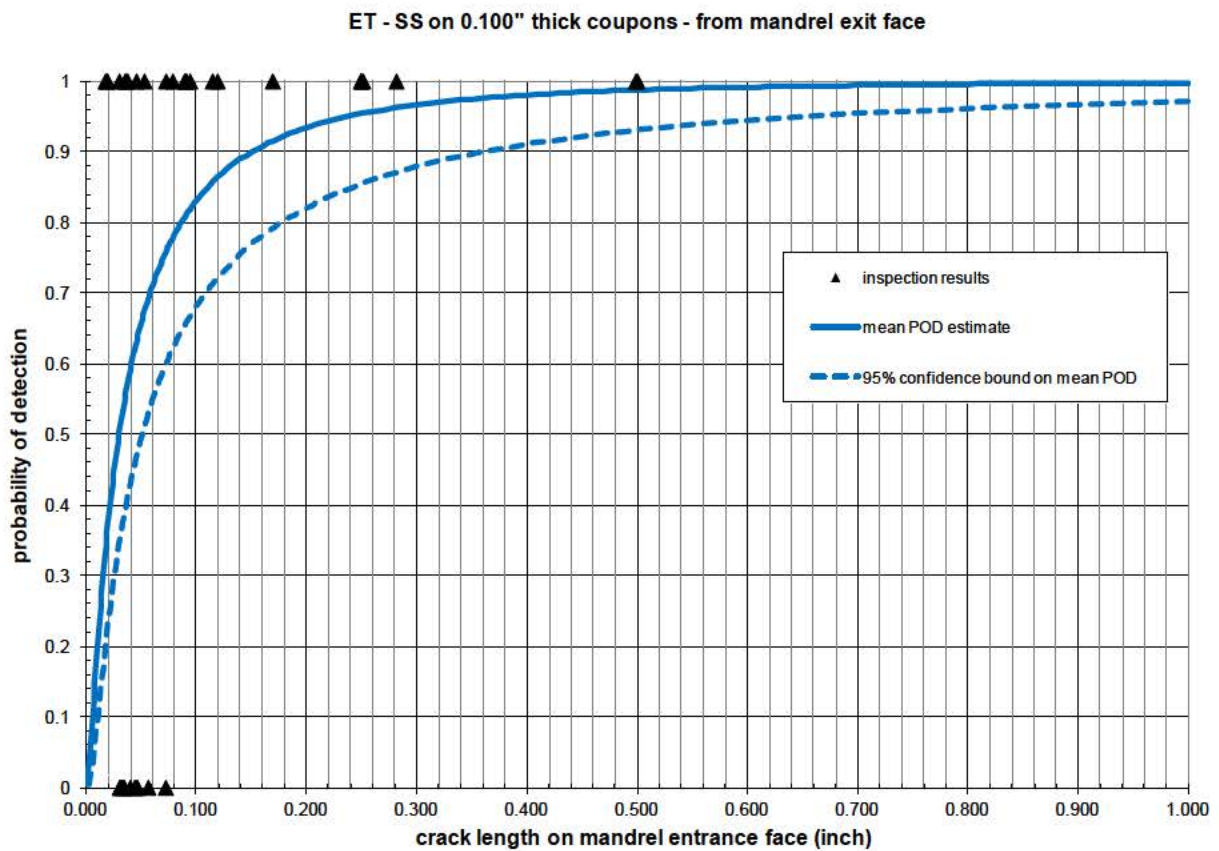


Figure 99. POD Estimate for ET-SS Inspection of 0.100" Thick Specimens

7.5.4 Final Trial - Ultrasonic Shear Wave Inspection Results

The UT shear wave inspection was moderately successful. It was difficult to resolve what side the crack was on, mandrel entrance or mandrel exit, especially in the 0.100" and 0.313" thick specimens. The nature of the crack shapes in these specimens means that crack progression up the bore is in step with on the face for some time. For the 0.100" thick specimens, this stays close until the crack is through. For the thicker specimens, the bore growth stalls out and the face keeps growing, as shown in Figure 100. The large number of values at a bore length of 0.100" are through cracks in the 0.100" specimens. Because of this, our POD estimates are in terms of length on face rather than length on bore, as length on bore can be nearly static as the crack continues to grow. Note that crack length on face means on the mandrel entrance face.

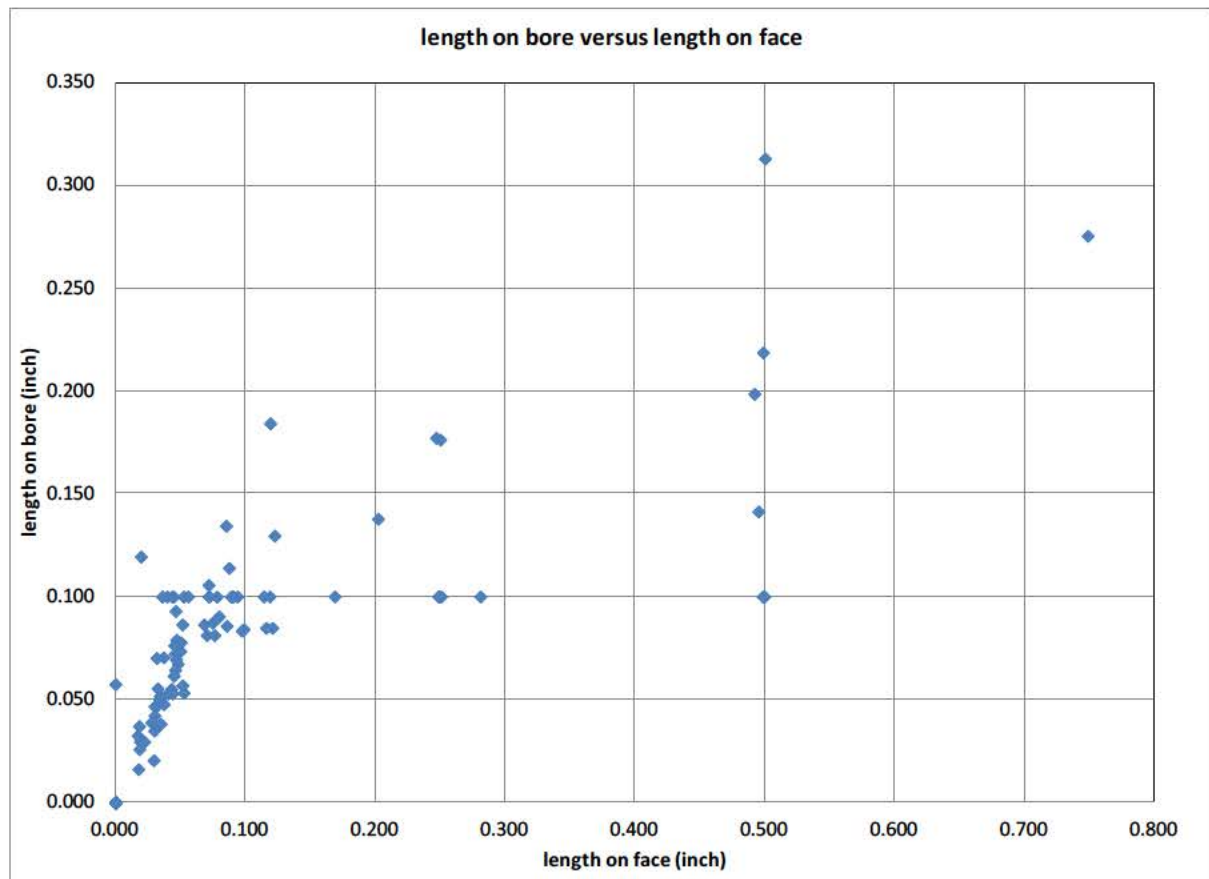
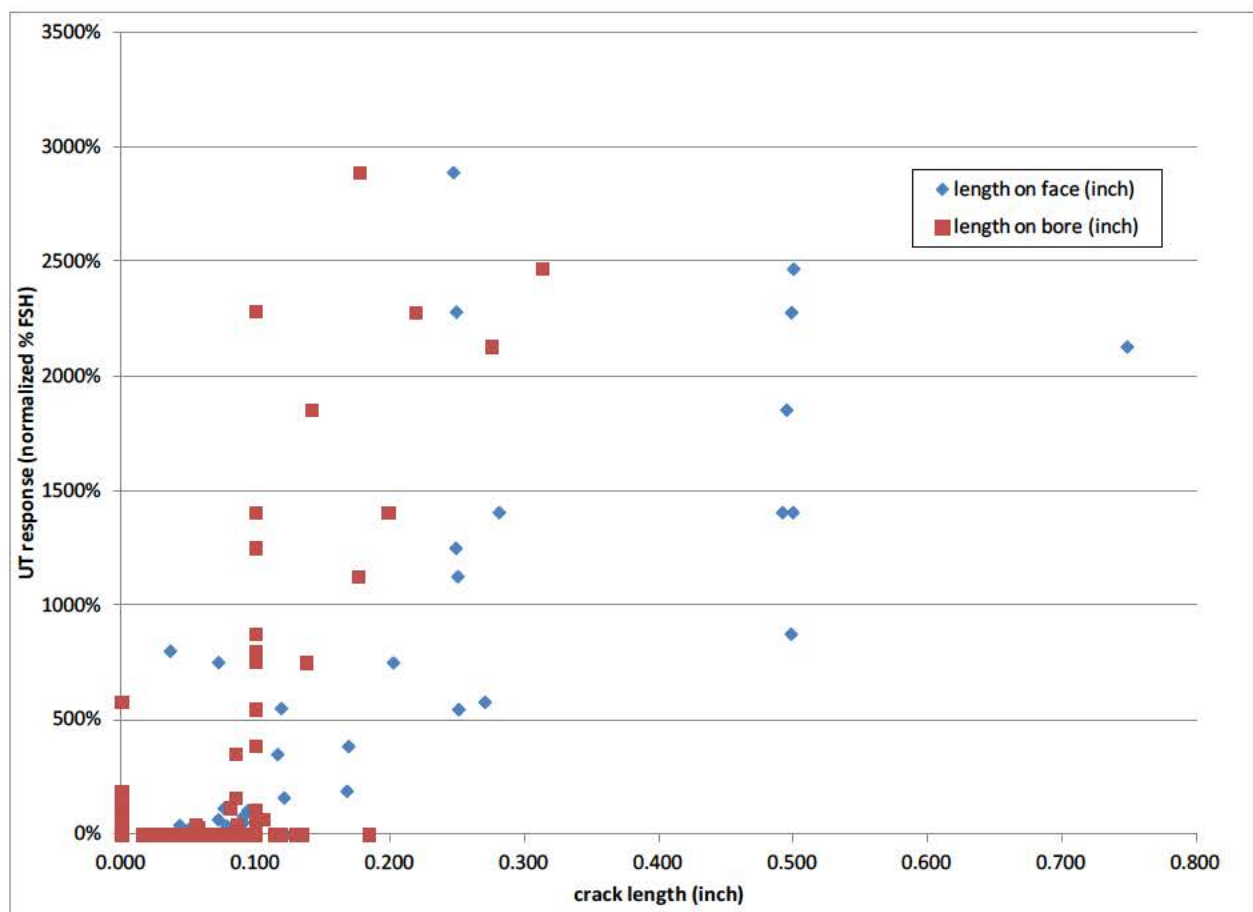


Figure 102 shows the POD results for all the coupons. This is typical for a noisy, manual inspection: there are many overlapping hits and misses, and eventually larger cracks that are detected. The false call rate is 6.5%.

A standard way to determine the effects of different inputs on a measured value is to use Generalized Linear Modeling (GLM) and ANOVA. We can describe inspection data in terms of a model relating the measured outcome (i.e. % screen height) to a set of parameters that may be relevant to the signal. For this data, the model included material, diameter, thickness, and importantly the “size” of the discontinuity under inspection.

This is a well-known procedure. R version 2.14.2 was used to make the calculations, and summaries are shown below. First, we fit a model that uses all inputs as possible explanatory variables. The results are shown below in Table 20.



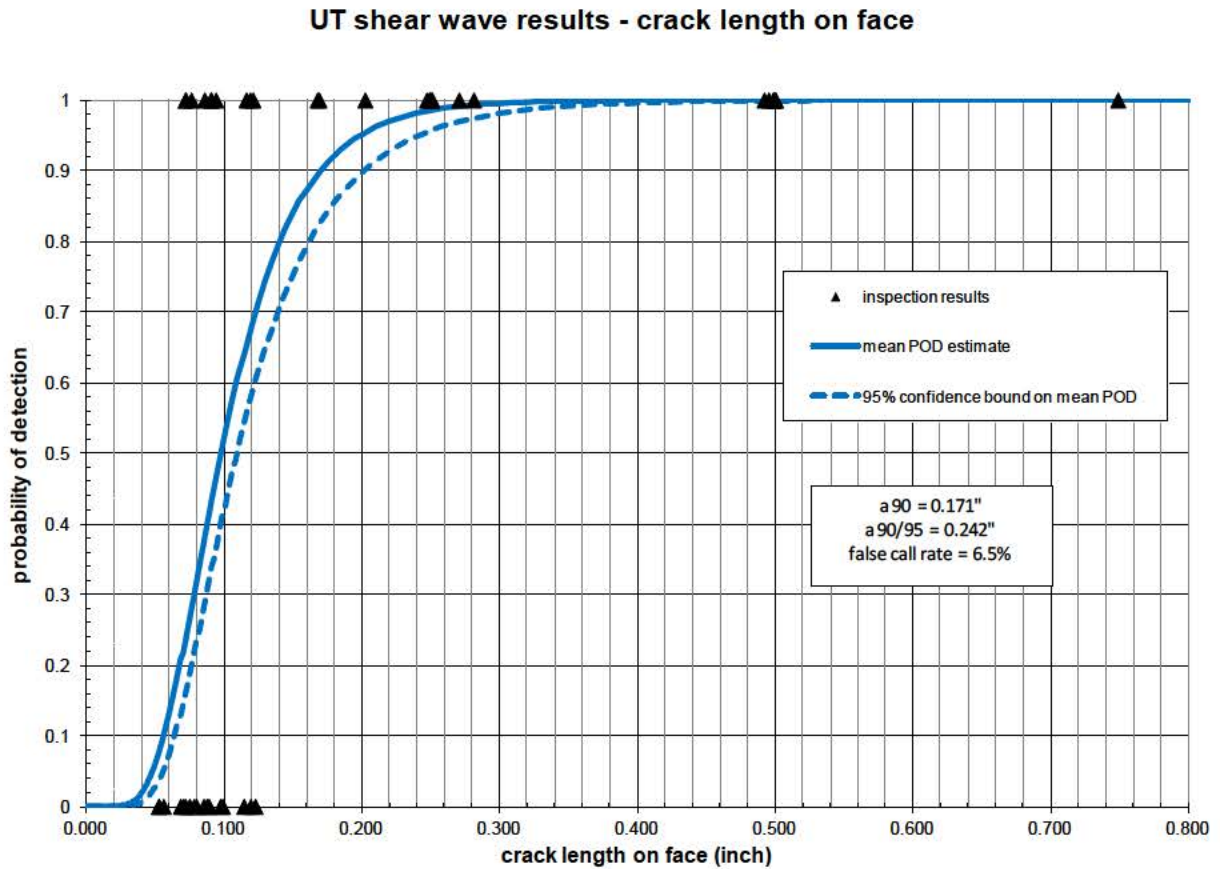


Figure 102. POD Estimate for the UT Detection of Cracks as a Function of Crack Length on the Specimen Mandrel Entrance Surface

Table 19. GLM Fit to the UT Results

	Estimate	Std. Error	z value	p value
diameter	0.7912	0.6932	1.141	0.2537 x
thickness	-3.0498	0.4489	-6.794	1.09e-11 ***
face length	5.1034	0.4239	12.039	< 2e-16 ***
bore length	7.4763	1.0555	7.083	1.41e-12 **
Signif. codes: 0 '***' 0.001 '**' 0.01 '*' 0.05 '.' 0.1 'x' 1				

The GLM results indicate that the diameter is not a significant factor, but thickness and unsurprisingly the crack sizes are key factors in the UT measurement.

The POD fits were then repeated, with the data broken into two groups: data from the 0.100" thick coupons is fit in Figure 103, and data from both the 0.313" and 0.500" thick coupons are fit as a group in Figure 104.

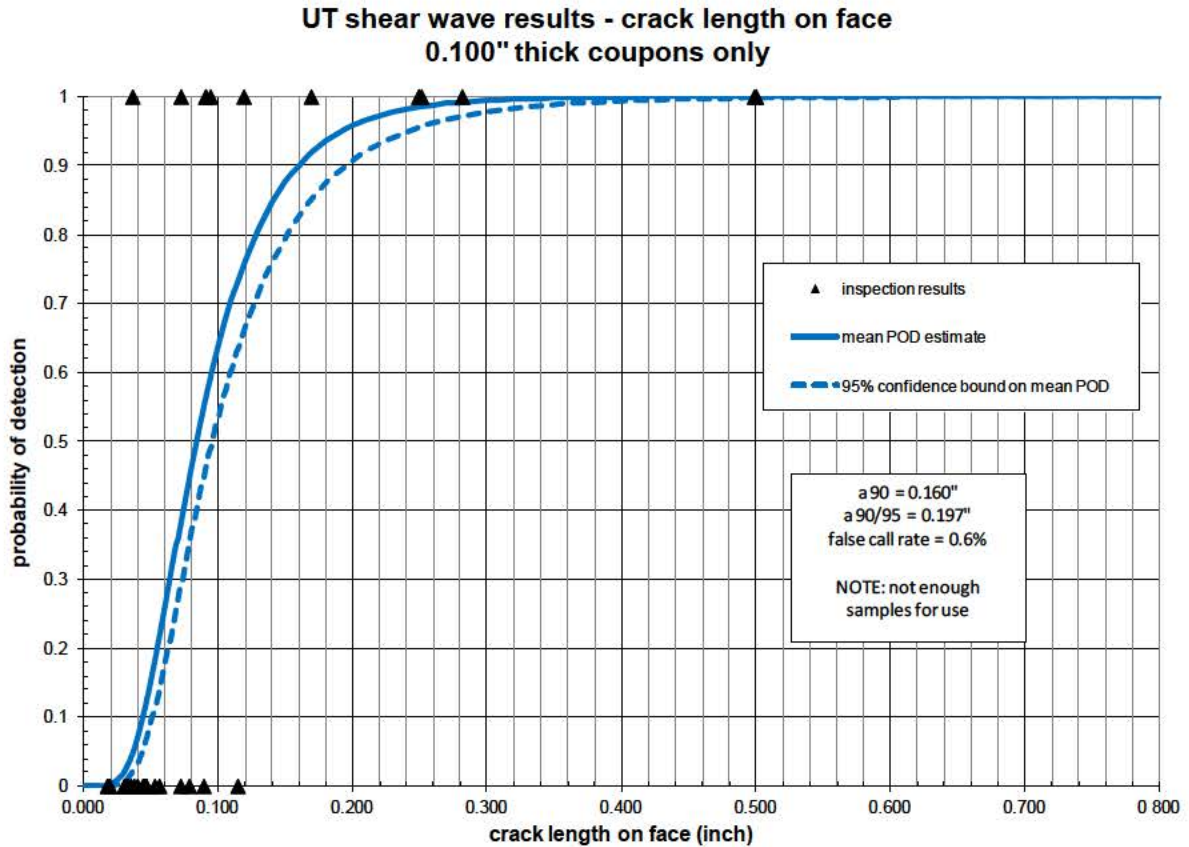


Figure 103. POD Estimate for the UT Detection of Cracks as a Function of Crack Length on the Specimen Mandrel Entrance Surface, for 0.100" Thick Coupons

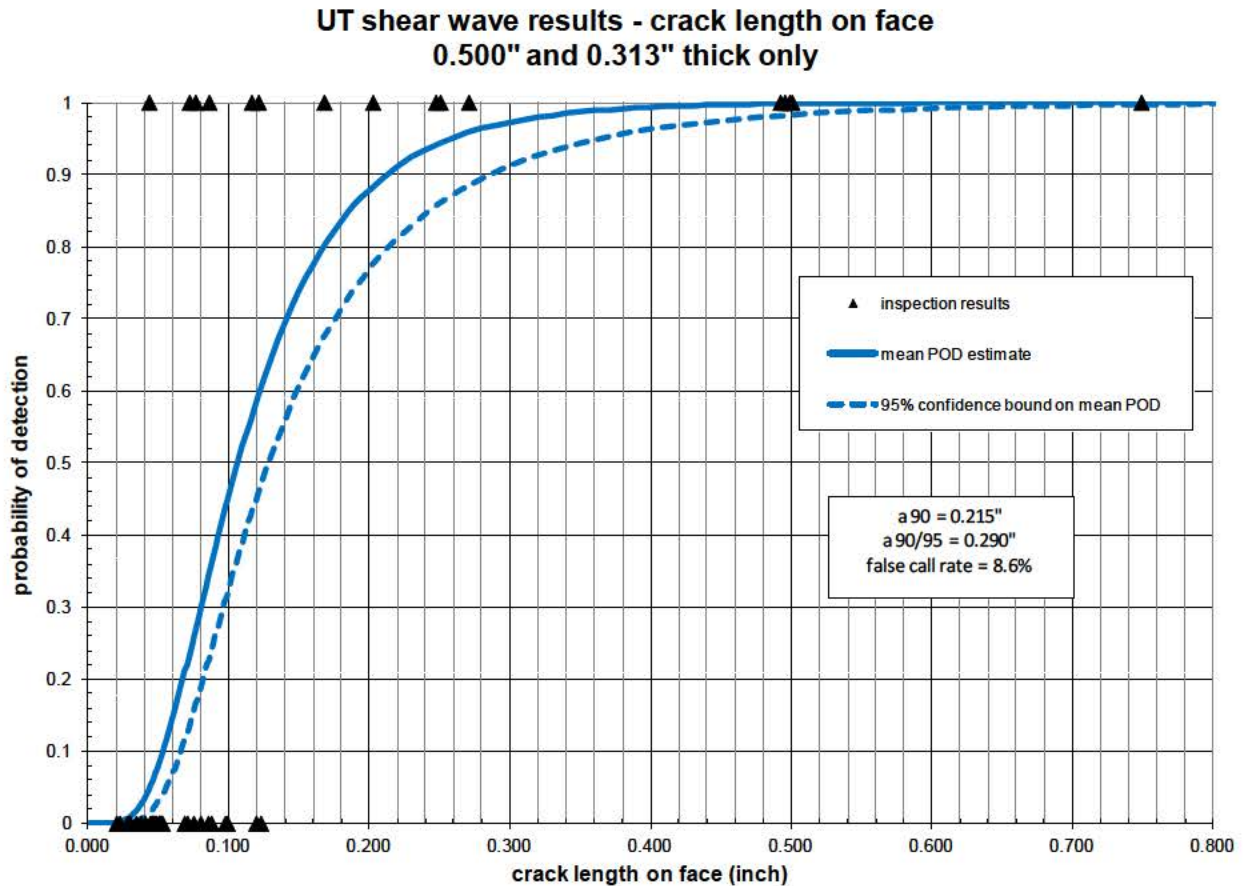


Figure 104. POD Estimate for the UT Detection of Cracks as a Function of Crack Length on the Specimen Mandrel Entrance Surface, for Both 0.313" and 0.500" Thick Coupons

Note that the a_{90} and $a_{90/95}$ crack sizes for all of the thicknesses are well beyond the zone of residual compressive stress and are actually in a region of slight tensile residual stresses. Figure 105 shows an example of residual stress as function of distance from the hole bore along with the a_{90} and $a_{90/95}$ crack sizes in 0.1" sheet. Figure 106 repeats this information for 0.5" plate. Both examples are in 7075-T6 aluminum.

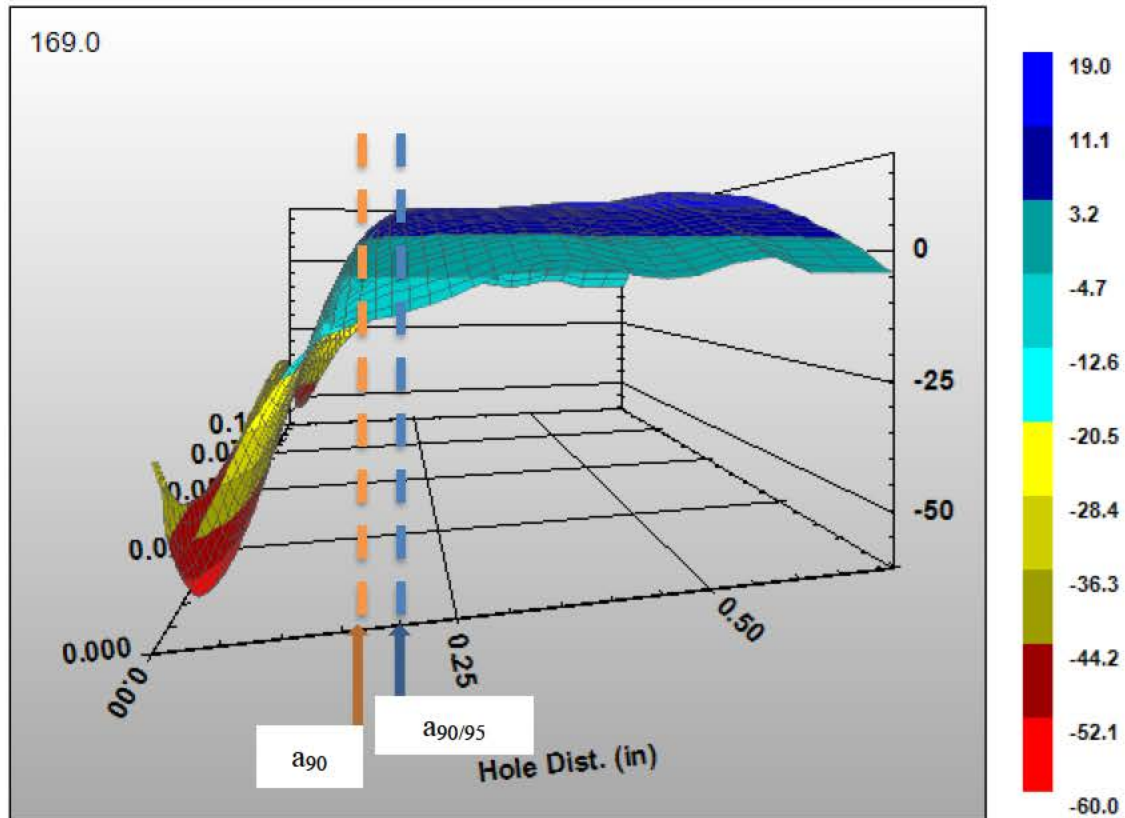


Figure 105. Residual stress profile at 0.375" hole in 0.1" sheet. Lines for a_{90} and $a_{90/95}$ shows that residual stresses range from neutral to slightly tensile at these crack sizes.

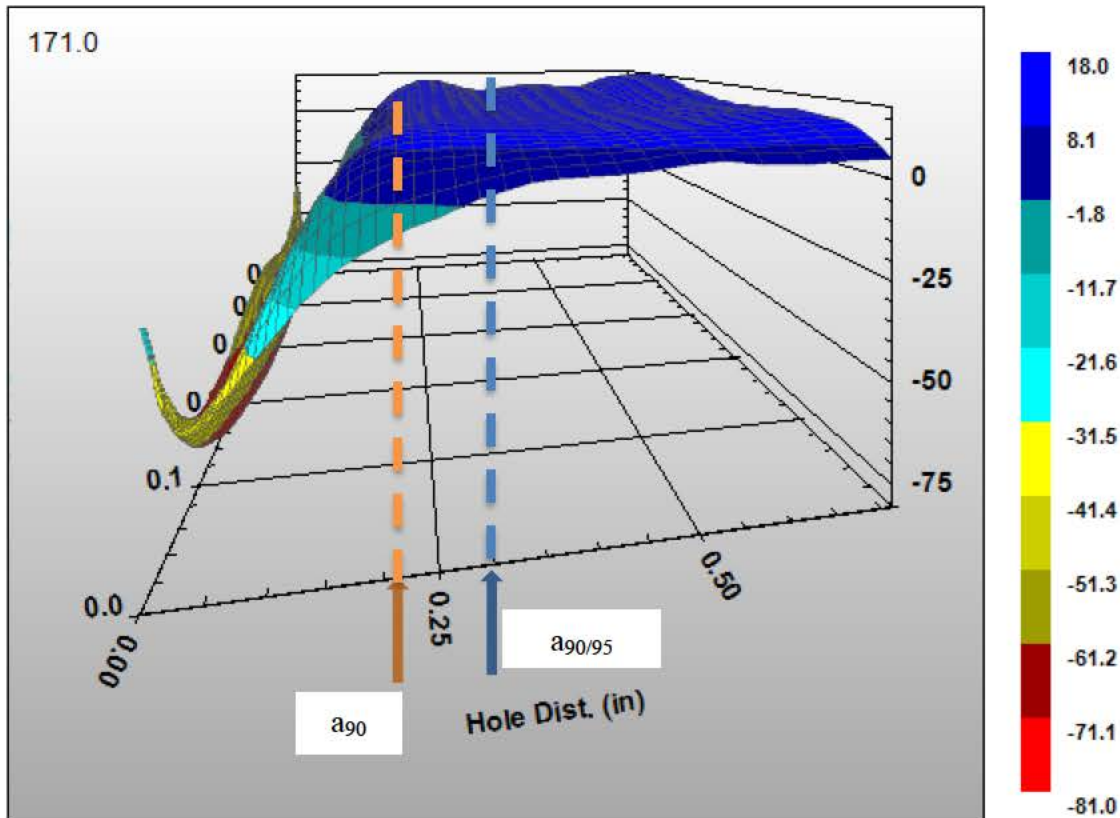


Figure 106. Residual stress profile at 0.375" hole in 0.5" plate. Lines for a_{90} and $a_{90/95}$ shows that residual stresses range from neutral to slightly tensile at these crack sizes.

7.6 Conclusions

This report describes the results of task 9 on the TRI/Austin subcontract to APES, prime contract Integrating Residual Stress Analysis of Critical Fastener Holes into USAF Depot Maintenance. The goal was to conduct nondestructive inspection (NDI) studies of cold-worked (CX) holes to establish detection capability of "faying surface" crack geometries and bore crack geometries.

The three most common NDI methods for fatigue crack detection in airframes in field/depot environments were evaluated:

- bolt hole eddy current (ET-BH)
- surface scan eddy current (ET-SS)
- ultrasonic shear wave (UT)

For each of these methods, the standard Air Force techniques were employed. A set of coupons with different hole diameters, thickness, and fatigue crack locations and sizes

was supplied to TRI/Austin for the study. An initial trial was performed at APES facilities with ET-BH and UT techniques on specimen.

Important conclusions from this effort are summarized here:

- ET methods were insensitive to applied loads on a fatigue crack.
- UT methods were very sensitive to applied external loads on a fatigue crack.
- As described in detail in other sections of the final report, cracks generally form at the mandrel entry surface and grow to a significant length before breaking through to the mandrel exit surface. The mandrel exit surface is the one typically accessible for NDI due to how the CX process is employed.
- Existing fatigue cracks become easier to detect after CX process.
- ET – BH techniques are not significantly affected by the CX process. The capability guidelines for ET - BH listed in the Structures Bulletin EN-SB-012 can still be applied for aluminum structure.
- ET – SS techniques are affected, due to the change in crack shape. ET – SS inspections will normally be conducted from the mandrel exit face of a CX hole. Fatigue cracks growing in a CX hole in thick structure can become very large without breaking through the mandrel exit face.
 - For aluminum structures of 0.100” or thinner, a reliable detectable crack size of 0.250” in length is reasonable.
 - For aluminum structures of greater than 0.100” thickness, ET – SS applied to the mandrel exit face is not reliable at reasonable crack sizes.
- UT techniques are affected by the CX process. There is a difference between the 0.100” thick specimens and the 0.313” and 0.500” thick specimens evaluated in this work.
 - For aluminum structures of 0.100” or thinner, a detectable crack size of 0.250” length is reasonable.
 - For aluminum structures of greater than 0.100” thickness, a detectable crack size of 0.300” length is reasonable.

8 Experimental Validation: Crack Growth Modeling in Residual Stress Fields

Three different demonstration cases were used to exercise the analytical capabilities of the software suite developed under this program. These include:

- Edge Margin Testing and Analysis using a typical aircraft wing tension dominated spectrum
- A typical aircraft fuselage Fatigue Critical Location (FCL)
- A typical aircraft wing FCL

Each of these cases are discussed in detail in the following sections.

8.1 *Edge Margin Testing using Wing Spectrum*

This series of experiments served three purposes. The first was to examine the sensitivity of fatigue response to edge margin, the second was to examine the sensitivity of fatigue response to cold work order (i.e., cracking prior to or after cold working), and third was to provide a modeling condition for our analytical tool kit, which utilized a customer-specific load spectrum.

The spectrum selected for use was for a typical aircraft wing cold worked hole FCL.

Previous work by (Andrew et al., 2013) identified that the presence of a fatigue crack (approximately 0.05 inch in length along the cold-work mandrel entrance face) at the time of cold-work significantly affected fatigue response compared to conditions where the hole was cold-worked first, then cracked. This effect was pronounced at a low edge margin (e/D) of 1.2, but the effect was not as strong at the large edge margin of 4.0 (Warner, 2012). The goal of these experiments is to identify the edge margin at which the pre-crack / cold-work order effect becomes indiscernible.

The following subjects are covered:

- Specimen design
- Test Matrix
- Experimental Results
- Fatigue Life Modeling Results

8.1.1 Specimen Design

For this series of experiments, APES is using a set of left-over coupon blanks that were previously machined for a Cold-Work Phase II SBIR Add-on project. The coupons are made from 2024-T351 aluminum plate, 0.25-inch thick. The longitudinal axis of the coupons is aligned with rolling direction of the plate. The basic specimen design is shown in Figure 107 (without the hole).

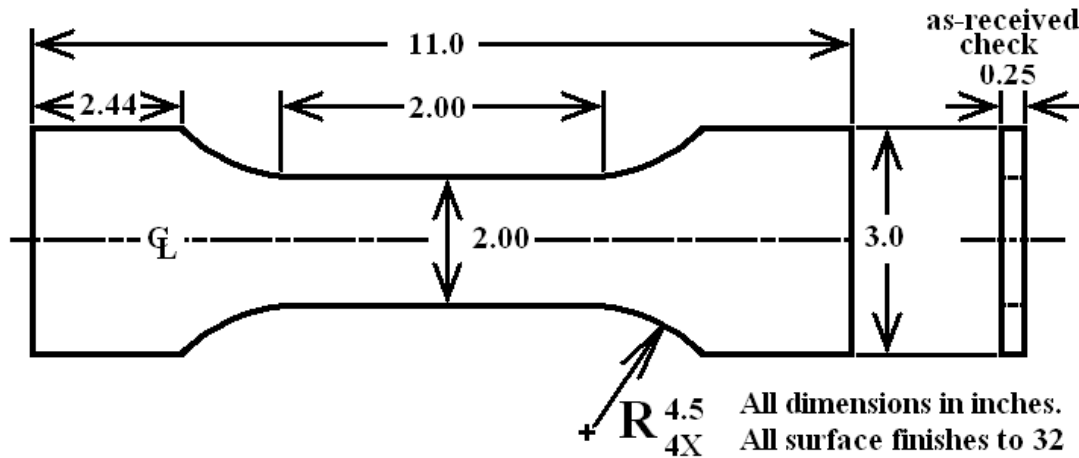


Figure 107. Schematic of cold-work fatigue coupon. Each coupon had one 0.25 inch hole (final ream diameter) at various locations based on target edge margin.

8.1.2 Test Matrix

The test matrix was iterative with the goal of determining the edge margin at which the pre-crack / cold work order effect becomes indiscernible. Key edge margins were selected to be common with statistically-designed residual stress measurement matrices (see Chapter 4) and statistically-designed cold-work fatigue matrices (Chapter 3). The final test plan executed was:

- 2 coupons at $e/D = 1.39$ (hole center to free edge = 0.350 inch), no cold work
- 3 coupons at $e/D = 1.39$, pre-cracked then cold-worked
- 3 coupons at $e/D = 1.39$, cold-worked then pre-cracked
- 2 coupons at $e/D = 1.8$ (hole center to free edge = 0.450 inch), no cold work
- 3 coupons at $e/D = 1.8$, pre-cracked then cold-worked
- 3 coupons at $e/D = 1.8$, cold-worked then pre-cracked
- 2 coupons at $e/D = 2.4$ (hole center to free edge = 0.600), no cold work
- 3 coupons at $e/D = 2.4$, pre-cracked then cold-worked
- 3 coupons at $e/D = 2.4$, cold-worked then pre-cracked

The specimens were all tested using a maximum spectrum stress of 38.5 ksi across the gauge section of the coupon. The spectrum had a marker band inserted at the end (see Figure 108). The X axis in Figure 108 is cycles, and the Y axis is normalized stress. All specimens had starting crack sizes slightly under 0.05 inch (grown by constant amplitude fatigue at 25 ksi, $R = 0.1$ before switching to spectrum loading).

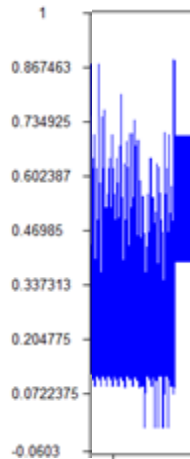


Figure 108. A section of the AFGROW representation of the wing spectrum showing the marker band at the end.

8.1.3 Experimental Results

Fatigue test results are shown in Figure 109, Figure 110, and Figure 111 for edge margins of 1.39, 1.8, and 2.4 respectively. The shortest edge margin represents a condition that is below the manufacturer's recommendation for cold working, but field modifications and repairs have required operating at edge margins this low or even lower. The edge margin of 1.8 coincides with the FTI recommendation of minimum edge margin for CX, and the edge margin of 2.4 produces a situation that is well within acceptable FTI limits.

Each of the three figures have text boxes that show the average life for each condition tested within the edge margin category, namely: no CX, precracking before CX and precracking after CX. The CX order has the biggest impact at the intermediate edge margin of 1.8. It appears that the lowest edge margin, the severe stress state caused by the geometry is washing out much of CX order effects, although it certainly is not negligible. At the high edge margin of 2.4, CX order seems once again be insignificant. The crack growth curves indicate that much of the reduction in life in the group that was precracked prior to CX appears to be associated with an initial burst of growth from the initial crack sizes (approximately 0.05 inch) up to about 0.07 inch. The accelerated growth lasted anywhere from 2 to 10 spectrum passes, depending on edge margin. After that, the specimens tended to behave much like coupons that were cold worked prior to precracking. Thus it appears that cold work order primarily has a detrimental effect on growth local to a pre-existing crack tip. This certainly should be considered in low edge margin conditions however, as performance benefits of CX will be minimized already even without the presence of pre-existing damage.

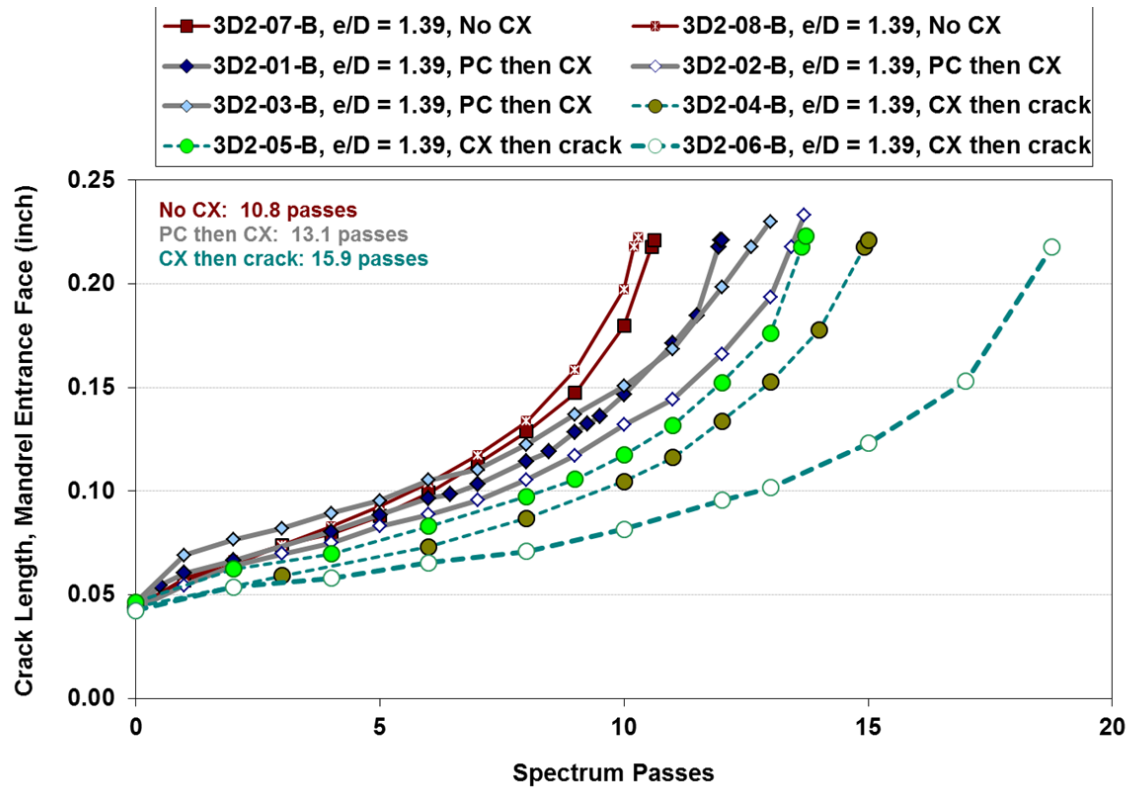


Figure 109. Crack growth curves for wing spectrum tests, $e/D = 1.39$.

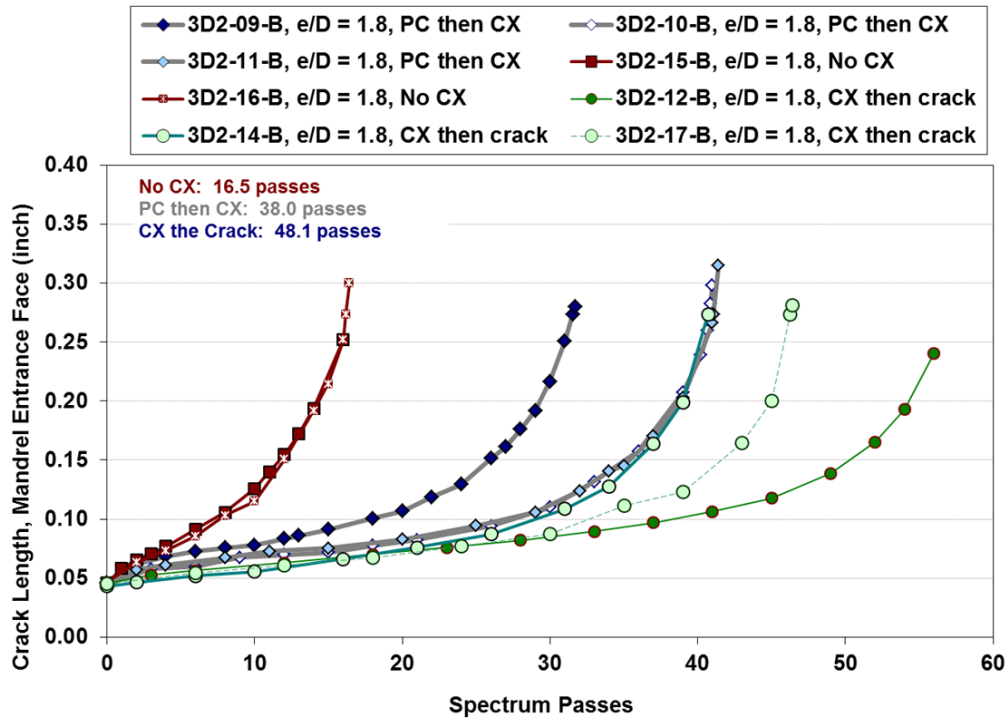


Figure 110. Crack growth curves for wing spectrum tests, $e/D = 1.8$.

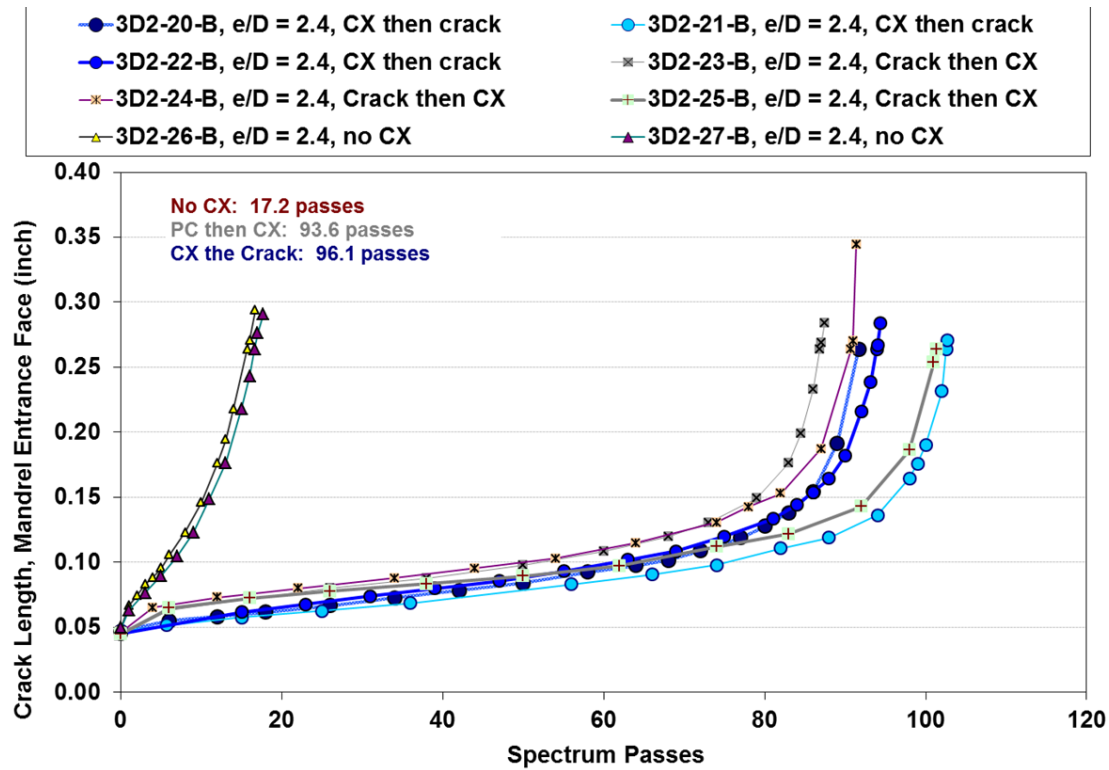


Figure 111. Crack growth curves for wing spectrum tests, $e/D = 2.4$.

Figure 112 compares life improvement factors for the three edge margin groups. The non-CX baseline serves as a normalized life of 1.0 for each of the three groups. This format provides a quick way to assess benefit. For instance, for the edge margin of 1.8, CX of a precracked hole provides a 230% life improvement over baseline. This factor increases to 290% for a hole that develops cracking after CX. **Note** that these factors are completely dependent on material, applied stress level, spectrum type, and interference level of the CX process. These are factors that apply to this specific situation.

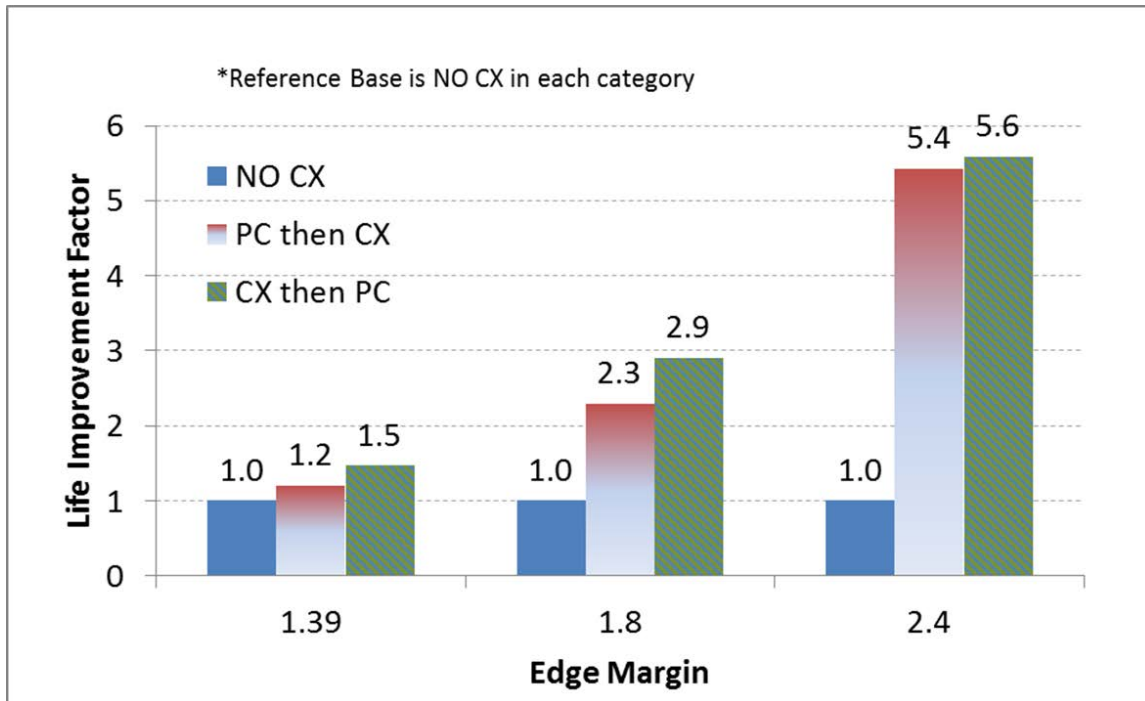


Figure 112. Life improvement factors for various edge margins referenced to “no CX” in each category.

8.1.4 Fatigue Crack Growth Modeling

Both BAMF and CPT were used in conjunction with StressCheck to model fatigue failure. Two individuals blindly predicted the results (they did not know experimental results prior to modeling the crack growth behavior). One analyst worked for the USAF as an onsite support contractor (used BAMF), the other works for APES (used CPT).

Both assessments tended to agree with each other fairly well even though there were some minor differences in solution set-up and execution. The predictions did fall short of the actual lives however, in some cases by quite a bit. Predictions ranged from 30% to 75% of the actual life. However, as can be seen in Figure 113, Figure 114, and Figure 115, the new simulations using RS from a crack size of 0.05 inch bested the Legacy ASIP method by 1.5 to 3 times. **It is important to note, too, that these simulations did not use crack retardation of any sort.** Use of these parameters would likely push simulations to be much closer to the actual, as will be shown in the validation discussions for the CP44 component later.

Crack shapes were also compared for one of the tests run at $e/D = 1.8$ with crack fronts produced by the BAMF simulation. Although we found many simulations had excellent agreement with experimental data, this example did not match up well primarily because the model did not match the overall failure scenario well (see Figure 116 vs. Figure 117). The model had one crack origin at the mandrel entrance corner, whereas the real coupon had multiple origins up the bore, and these bore cracks tended to propagate to become

quite large. Those other active cracks greatly influenced the shape of the primary crack—something that was not captured in the model.

Table 20. Comparison of experimental and predicted lives. Predicted lives underestimate experimental, but no retardation was used in predictions.

Unique Test Information					Predicted SFH to Failure		Predicted / Actual Life Ratio		Corresponding Final Crack Size (Entrance Face)	
Edge Distance (inch)	Edge Margin	Initial Crack Face (inch)	Initial Crack Bore (inch)	Experimental Life (SFH)	BAMF	CPT	BAMF	CPT	BAMF	CPT
0.600	2.4	0.0444	0.0718				0.303	0.320	0.2750	0.2750
0.450	1.8	0.0440	0.0629				0.550	0.471	0.2771	0.2771
0.350	1.4	0.0443	0.077				0.660	0.725	0.1703	0.1703

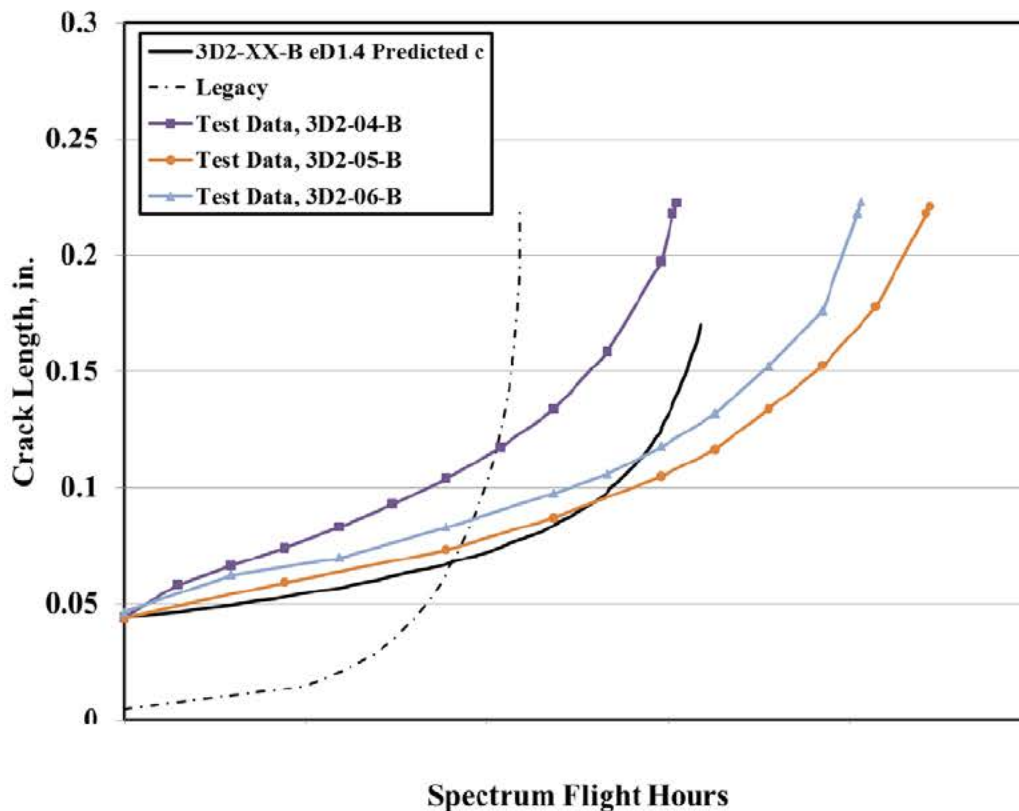


Figure 113. Mandrel entrance face crack growth vs. flight hours. Experimental data are compared with legacy ASIP approach and with CPT prediction, $e/D = 1.4$. Predicted curve is from BAMF.

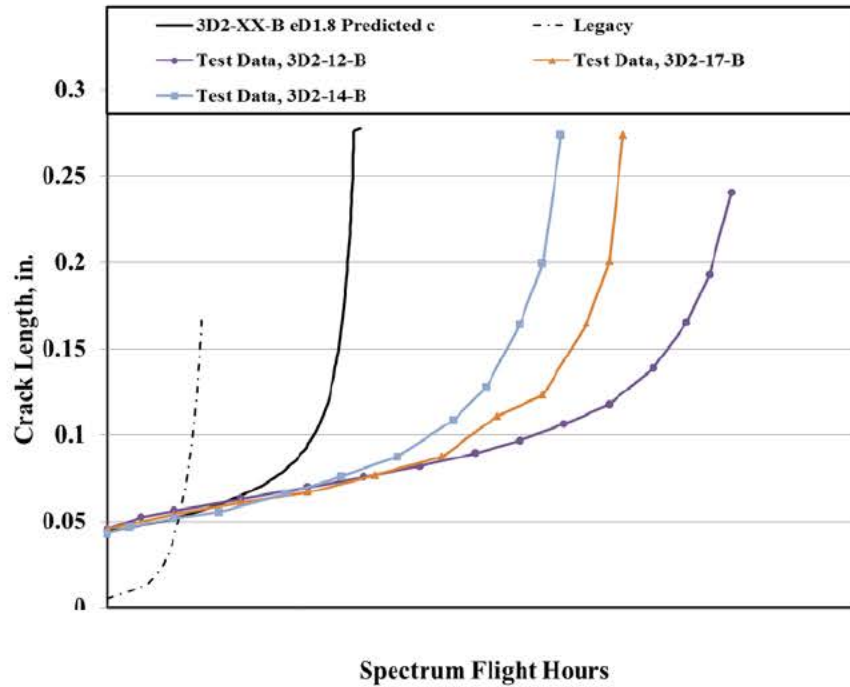


Figure 114. Mandrel entrance face crack growth vs. flight hours. Experimental data are compared with legacy ASIP approach and with CPT prediction, $e/D = 1.8$. Predicted curve is from BAMF.

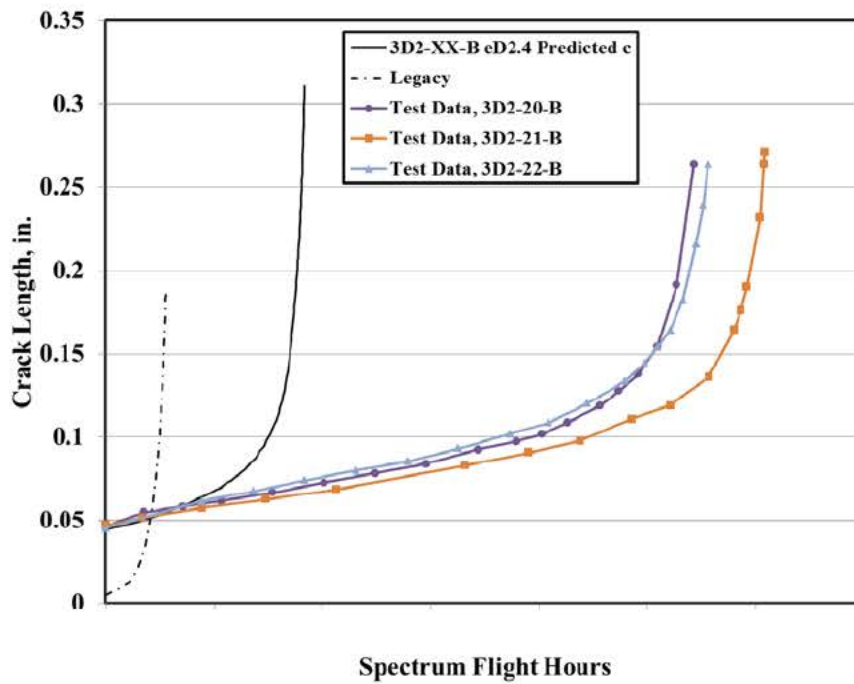


Figure 115. Mandrel entrance face crack growth vs. flight hours. Experimental data are compared with legacy ASIP approach and with CPT prediction, $e/D = 2.4$. Predicted curve is from BAMF.

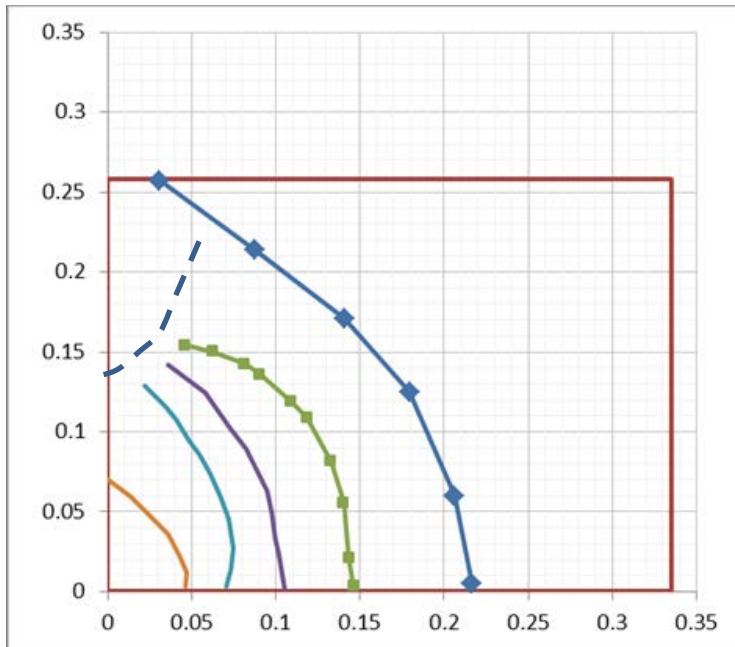


Figure 116. Marker band map from fracture face of $e/D = 1.8$ coupon. Dashed line represents a crack linking line with an active secondary crack.

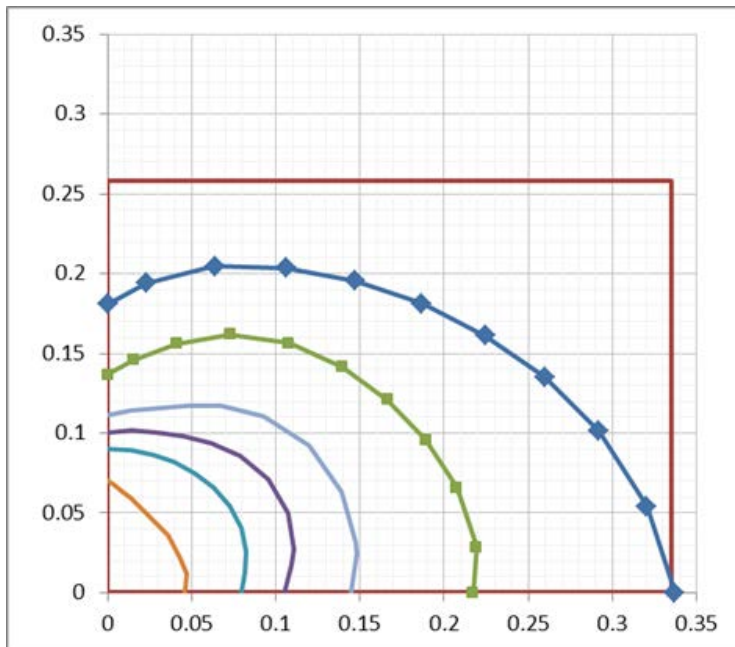


Figure 117. Predicted crack shape from $e/D = 1.8$ coupon.

8.2 Coupon Tests for Fuselage Fatigue Critical Location

This section describes testing and validation that APES, Inc. executed for a series of experiments related to a typical fuselage FCL. In practice, this is not a cold worked location. However, it is possible that in repair situations, the hole may be oversized and then cold worked (CX) at edge margins well below those recommended in normal practice. Thus, we chose to investigate these scenarios by testing non-CX holes in a geometry similar to the actual part, and then by testing oversized holes that have been cold worked to simulate a repair.

The following subjects are covered:

- Specimen design
- Spectrum considerations
- Test Matrix
- Experimental Results
- Fatigue Life Modeling Results

8.2.1 Specimen Design

For this series of experiments, APES designed the coupons after the “AFGROW geometry” shown in the DTA document (referenced above) on page 9-497 with a couple of minor modifications to accommodate our existing cold work tool sets and sheet stock. The material immediately available was 0.19 inch thick 2024-T3 aluminum (compared to 0.183 inch thick in the DTA). The other key difference was hole diameter. The DTA called out a diameter of 0.197 inch. We selected a final ream diameter of 0.250 inch (for the non-CX coupons). Since fatigue performance at a fastener hole is much more sensitive to edge margin than diameter, we proposed to increase the edge distance on our coupon to keep the edge margin the same as that in the real component ($e/D = 2.23$) for the initial non-CX condition. To accommodate this change, we increased the edge distance from 0.44 inch to 0.56 inch. When we produced the repair scenarios with larger diameter holes, the edge distance stayed the same, but the margin reduced.

For the CX coupons, we increased the diameter to 0.375 ($e/D = 1.5$) and then again to 0.4375 ($e/D = 1.28$).

Figure 118 & Figure 119 contrast the DTA AFGROW model for this location with the specimen cross section ultimately produced (non-CX condition). Figure 120 shows the specimen planform.

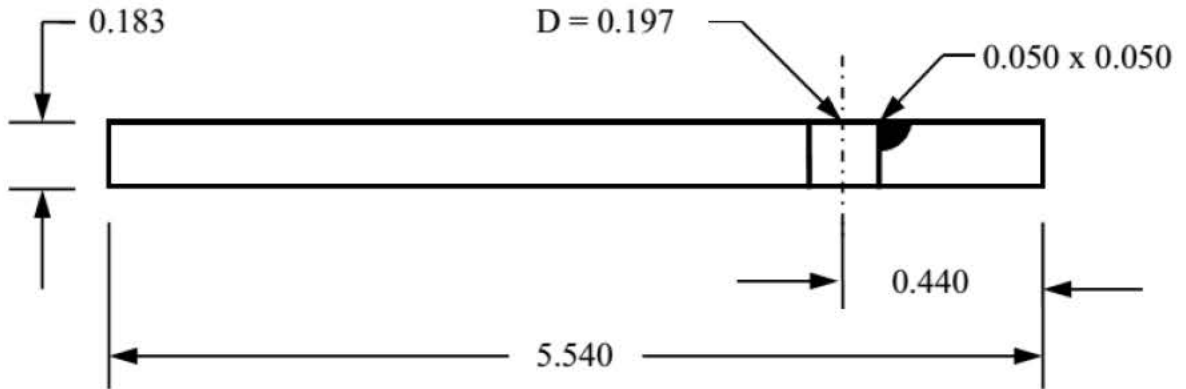


Figure 118. Cross-section of the location as represented in the DTA AFGROW model.

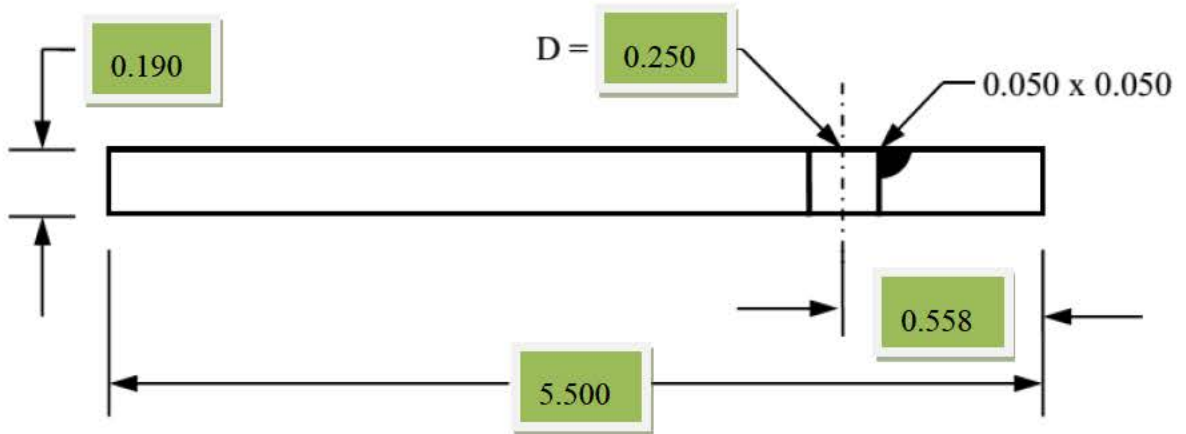


Figure 119. Cross-section of actual coupon in the region of interest (non-CX condition).

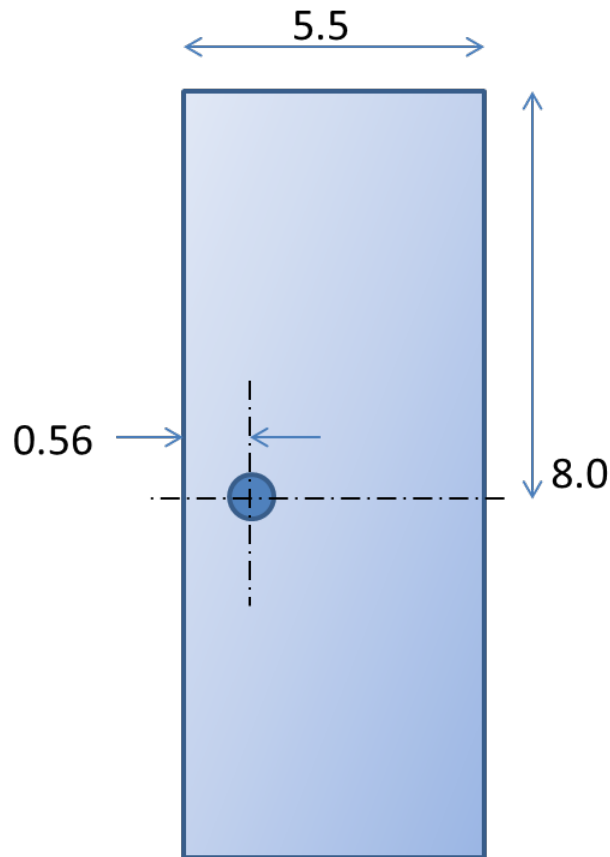


Figure 120. Specimen planform. Hole diameter varies based on condition. Dimensions are in inches.

8.2.2 Spectrum Considerations

The location chosen for demonstration is not an actual cold worked location on the aircraft. The maximum spectrum stress identified is 24.329 ksi. There was some concern that testing at this peak stress in a cold worked condition may not result in fatigue failure from the hole, even with the low edge margin. Instead, we elected to operate at a higher peak stress of 28 ksi.

8.2.3 Test Matrix

The test matrix consisted of eight (8) coupons. All coupons were pre-cracked under constant amplitude load to a mandrel entrance face crack length of 0.05 inch before switching to the spectrum load. Coupons that contained cold worked holes received that treatment first; then they were pre-cracked.

- 2 coupons, 0.25D, no CX
- 2 coupons, 0.375D, CX at 4.0% interference (max spec)

- 2 coupons, 0.375D CX at 3.0% interference (min spec)
- 2 coupons, 0.4375D, CX at 4.0% interference (max spec)

The coupons that contained the cold worked holes 0.375 inch in diameter used one of two tool sets. One pair of coupons used the standard tooling supplied by FTI, 12-0-N, designed to impart maximum degree of cold work (approximately 4%). The other pair of coupons used a custom initial reamer to impart minimum interference within the spec, which was approximately 3% cold work. The 0.4375 inch diameter hole (final ream diameter) was cold worked to maximum interference level using the FTI 14-0-N tool set.

8.2.4 Experimental Results

The experimental results for this demonstration case are shown in Figure 121. All of the test results segregated by condition and followed the expected trends. The average lives per test condition, ordered longest to shortest were:

- MAX CX, $e/D = 1.5$: 58,895 hours
- MIN CX, $e/D = 1.5$: 37,892 hours
- MAX CX, $e/D = 1.3$: 24,995 hours
- NO CX, $e/D = 2.44$: 9,000 hours

Life improvement factors over the non-CX case ranged from 277% to 655%.

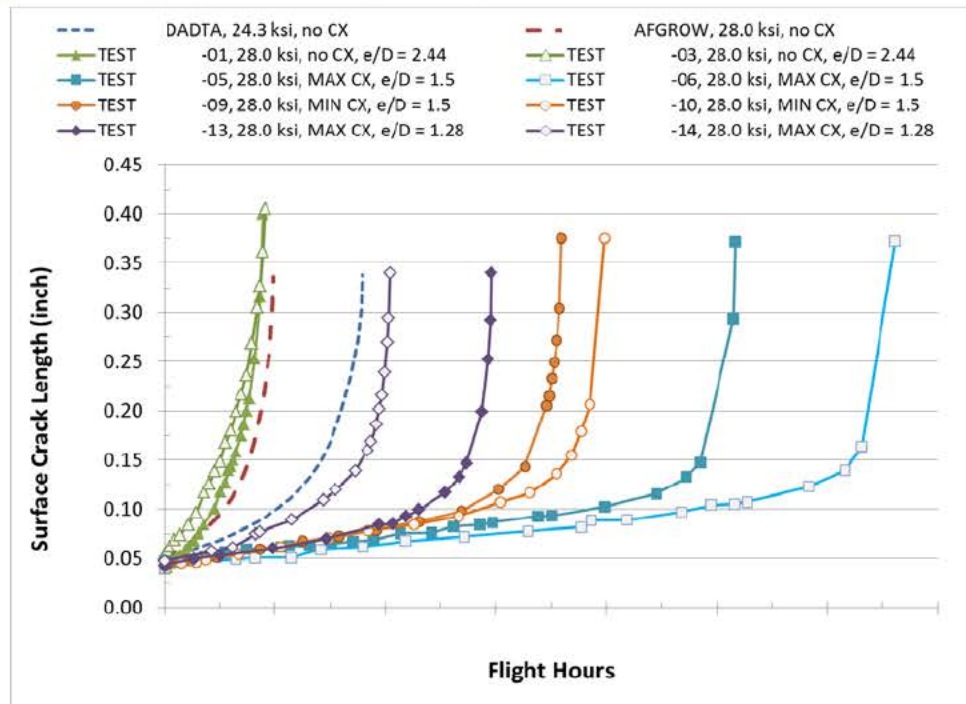


Figure 121. Crack length vs. flight hours for all tests (28 ksi) along with baseline prediction (24.3 ksi) and baseline prediction at the revised, higher stress (28 ksi).

This previous chart also shows a couple of analytical simulations based on non-CX with AFGROW. One shows the original DADTA life prediction for this geometry based on the lower 24.3 ksi; the other shows the DADTA life prediction with the higher stresses actually used for the test conditions—28 ksi.

Figure 122 shows the AFGROW simulation at 28 ksi compared with non-CX tests condition.

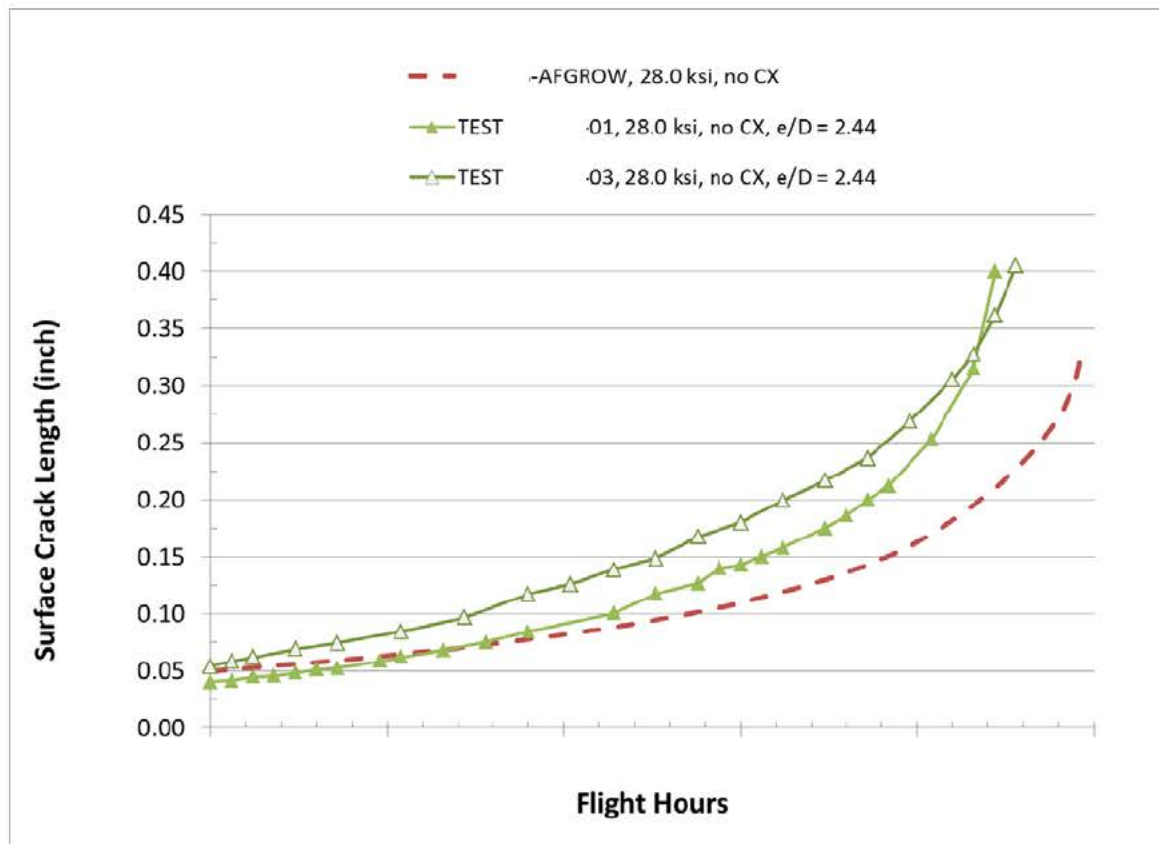


Figure 122. Crack length vs. flight hours for non-CX tests vs. AFGROW simulation of same condition. AFGROW model used Generalized Willenborg model parameters from the DADTA. Results are reasonable.

8.2.5 Modeling Results

The modeling results are summarized in Table 22. As with the edge margin demonstration cases, all analyses using BAMF and CPT were conducted blind. This time, three analysts participated: two used BAMF and one used CPT. A trend similar to the edge margin testing is seen in the results. The analytical runs are much shorter in life than the experiment, averaging around 33%. Agreement between the analysts' results and the different codes is excellent in most cases. To support these runs, two contour method measurements of each CX hole condition were made by Hill Engineering. These data are included in the residual stress database delivered under this contract.

Table 21. Predicted SFH to failure using BAMF and CPT compared with experimental results. Note three different analysts produced similar results with two different codes.

Unique Configuration Information					Predicted SFH to Failure			Predicted / Actual Life Ratio		
Edge Margin	CX Level	RS Distribution	Fatigue Coupon (for Crack Geometry, IFS)	Experimental Life (SFH)	BAMF (analyst 1)	CPT	BAMF (analyst 2)	BAMF (analyst 1)	CPT	BAMF (analyst 2)
1.5	4%	3K1-04-A	.05					0.284	0.298	0.283
1.5	4%	3K1-04-A	.06					0.246	0.262	
1.5	4%	3K1-05-A-rev	.06					0.253	0.262	0.230
1.5	3%	3K1-06-A	.09					0.325	0.292	
1.5	3%	3K1-07-A	.09					0.487	0.435	
1.28	4%	3K1-08-A	.13					0.432	0.459	0.433
1.28	4%	3K1-09-A	.13					0.432	0.306	0.307
Average Life Ratio								0.351	0.331	0.313

Figure 123 shows the experimental results for the 0.375 inch diameter holes cold-worked to the maximum interference. These data are compared with a representative BAMF prediction, the non-CX AFGROW (initial crack size 0.05 inch), and an analysis case representative of the legacy method for accounting for cold-worked holes: a 0.005 inch corner crack for an initial condition but no use of residual stress. The BAMF analysis outperformed the legacy analysis by a factor of 1.5 but did not use crack retardation (more on this shortly).

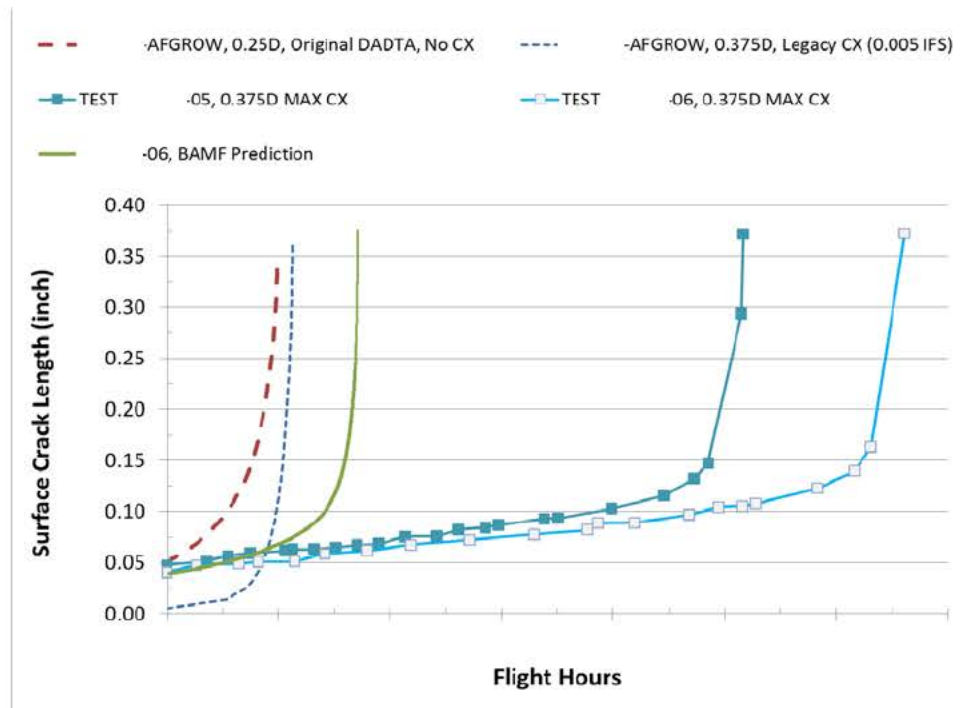


Figure 123. Experimental results compared with non-CX DADTA prediction, Legacy CX assessment (using initial crack size of 0.005 inch and no RS), and a BAMF analysis. BAMF is conservative but does not use retardation.

Figure 124 shows the same type of data for the MIN CX condition for the 0.375 inch diameter hole. However, in this graph we see two different BAMF predictions, which illustrate the variability in computed life resulting from two different residual stress inputs (all other variables remained the same). One of the cases (using RS distribution 07) still outperformed the legacy ASIP method by a factor of 1.5. The other residual stress distribution produced a life prediction nearly identical to the legacy method but did not take advantage of crack retardation effects.

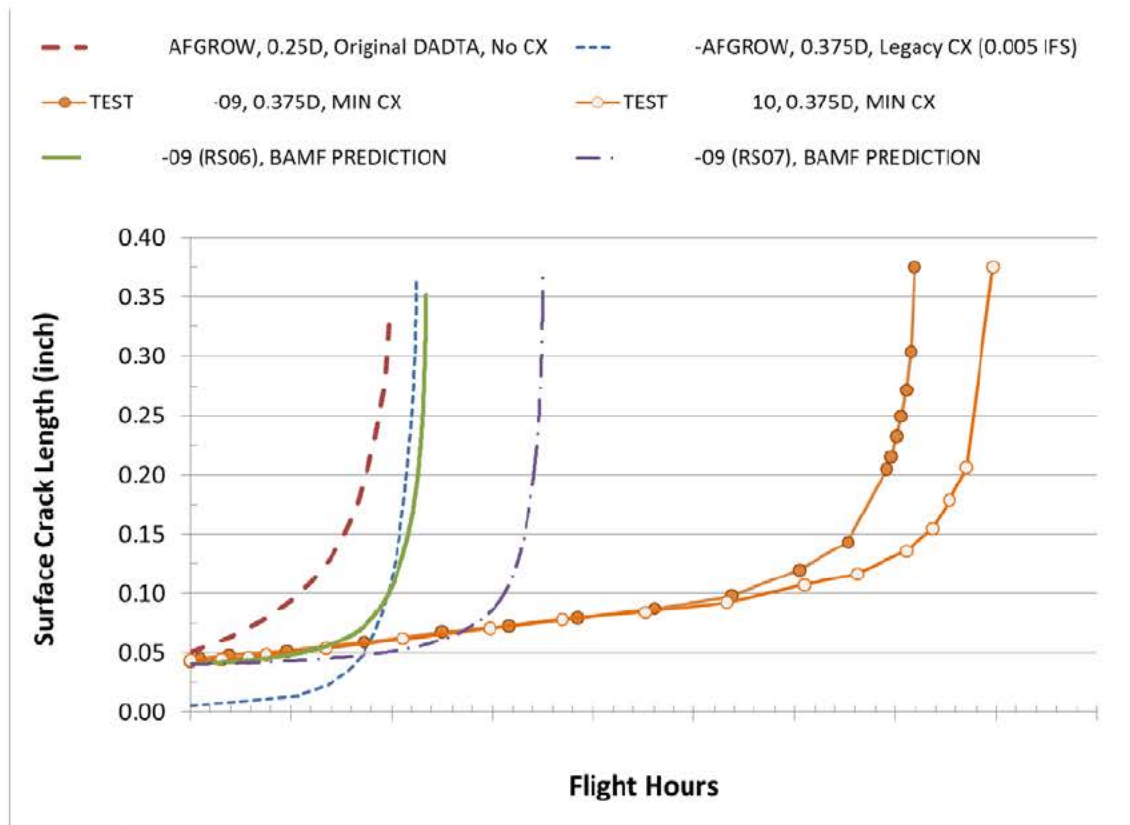


Figure 124. Experimental results compared with non-CX DADTA prediction, Legacy CX assessment (using initial crack size of 0.005 inch and no RS), and a BAMF analysis. BAMF is conservative but does not use retardation.

Figure 125 shows the final group of tests and analyses: 0.4375 inch holes that have been cold worked to the MAX spec. Here the BAMF run falls in between the test data and improves over the legacy ASIP method by about a factor of three. No retardation was used in this analysis.

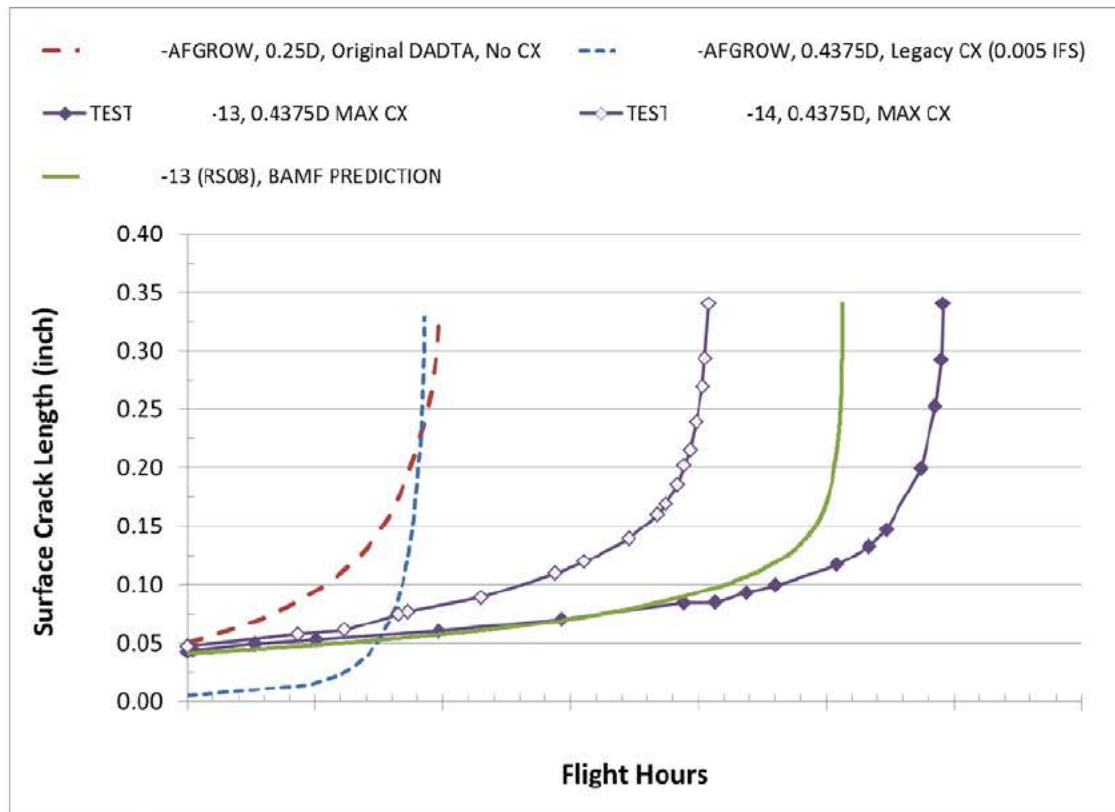


Figure 125. Experimental results compared with non-CX DADTA prediction, Legacy CX assessment (using initial crack size of 0.005 inch and no RS), and a BAMF analysis. BAMF is conservative but does not use retardation.

8.2.6 Effects of Retardation

The repeated conservative results from both the edge margin and fuselage validation cases led us to briefly investigate crack retardation in the fuselage case, even though it was not part of the program originally. For this analysis, ASIP engineering used BAMF to conduct a standard residual stress crack growth analysis without retardation, determined the beta factors for the BAMF run, then loaded those beta factors into AFGROW. Then an AFGROW analysis was run using retardation to see the influence on total life. The full BAMF analysis and the AFGROW analysis using betas derived from BAMF produced similar results, which is an important base comparison to make.

It is important to note that when applying retardation, we used the same Generalized Willenborg SOLR that is found in the DADTA for this location in the non-CX condition. The significance of this fact is that we did generate a new SOLR to further tune the CX crack growth. This is why the retardation demonstration does not exactly match the test. It is unknown at this time whether this relationship is repeatable with other materials, stress levels, geometries, etc., and we recommend it for further study.

Figure 126, Figure 127, and Figure 128 all show applications of retardation to various conditions of hole diameter, cold work level, and edge margin. Predicted over actual fatigue lives for the representative cases vary from 75%, to 90%, to 98%.

Figure 129 shows key takeaway points from a sample crack retardation analysis. In this example, the life improvement over legacy improves from a factor of 1.5x without retardation to a factor of 4.5x with retardation, and the prediction is a much closer match to the experiment.

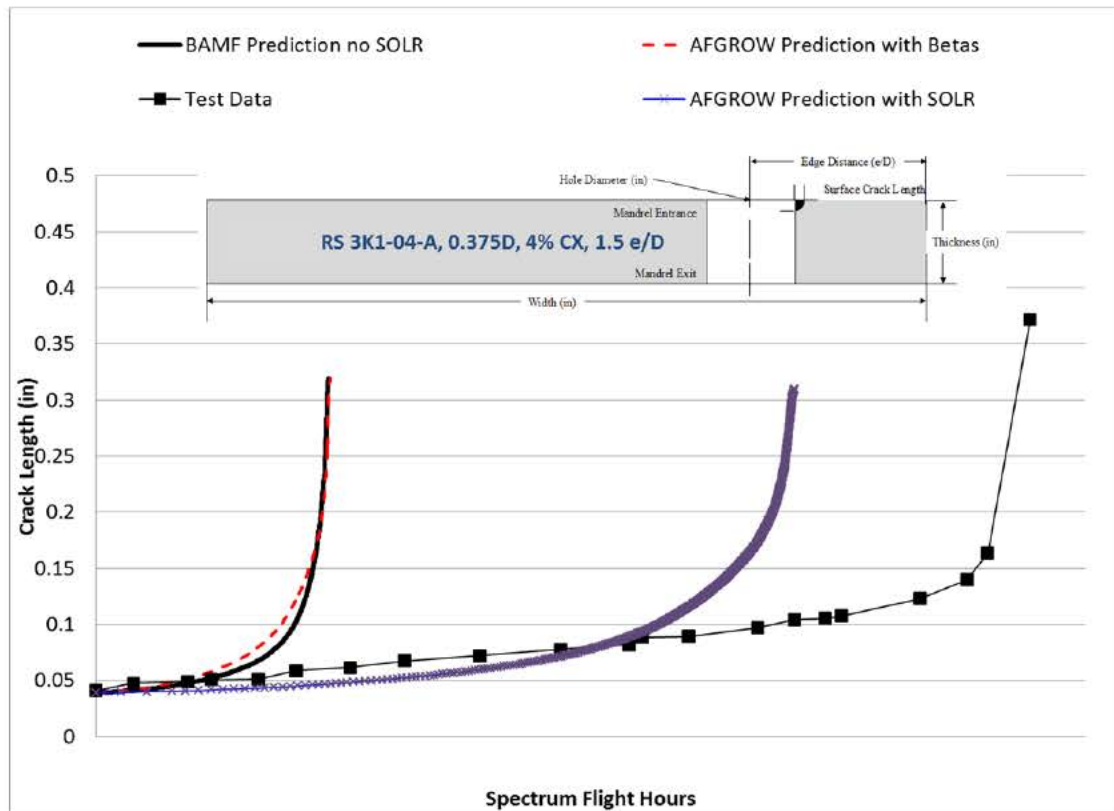


Figure 126. Experimental result for CX coupon compared with analytical results that show the influence of retardation parameters. Retardation parameter for the CX analysis is the same as that used in the in the non-CX DADTA analysis (not returned). Predicted / Actual Life Ratio is now 75%.

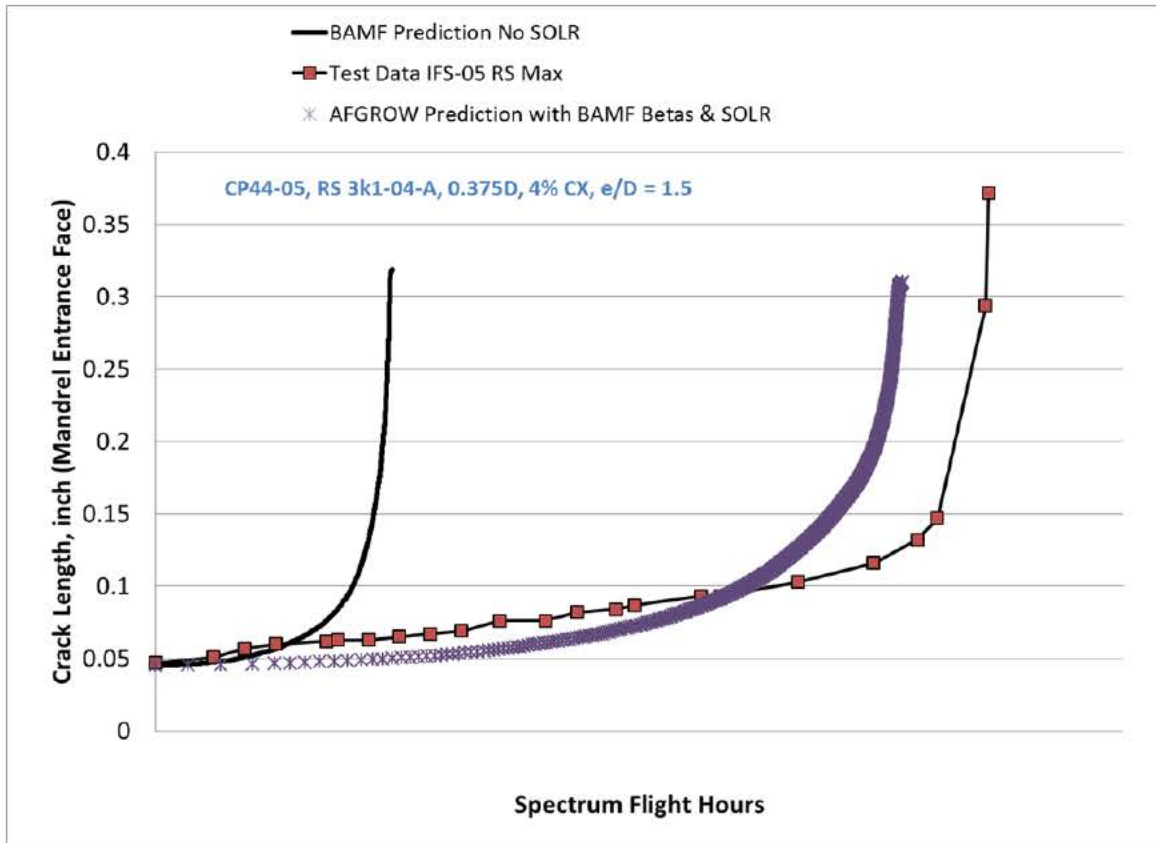


Figure 127. Experimental result for CX coupon compared with analytical results that show the influence of retardation parameters. Retardation parameter for the CX analysis is the same as that used in the non-CX DADTA analysis (not retuned). Predicted / Actual Life Ratio is now 90% for this case.

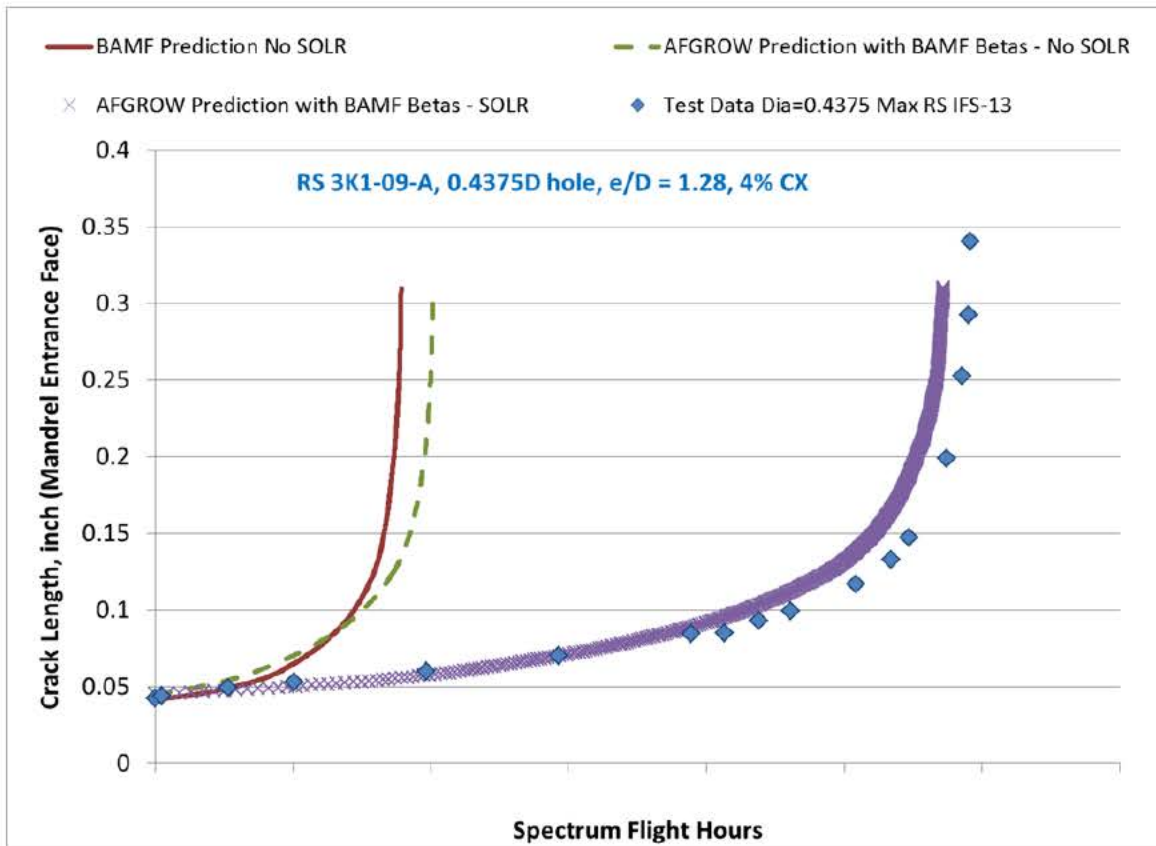


Figure 128. Experimental result for CX coupon compared with analytical results that show the influence of retardation parameters. Retardation parameter for the CX analysis is the same as that used in the in the non-CX DADTA analysis (not retuned). Predicted / Actual Life Ratio is now 98% for this case.

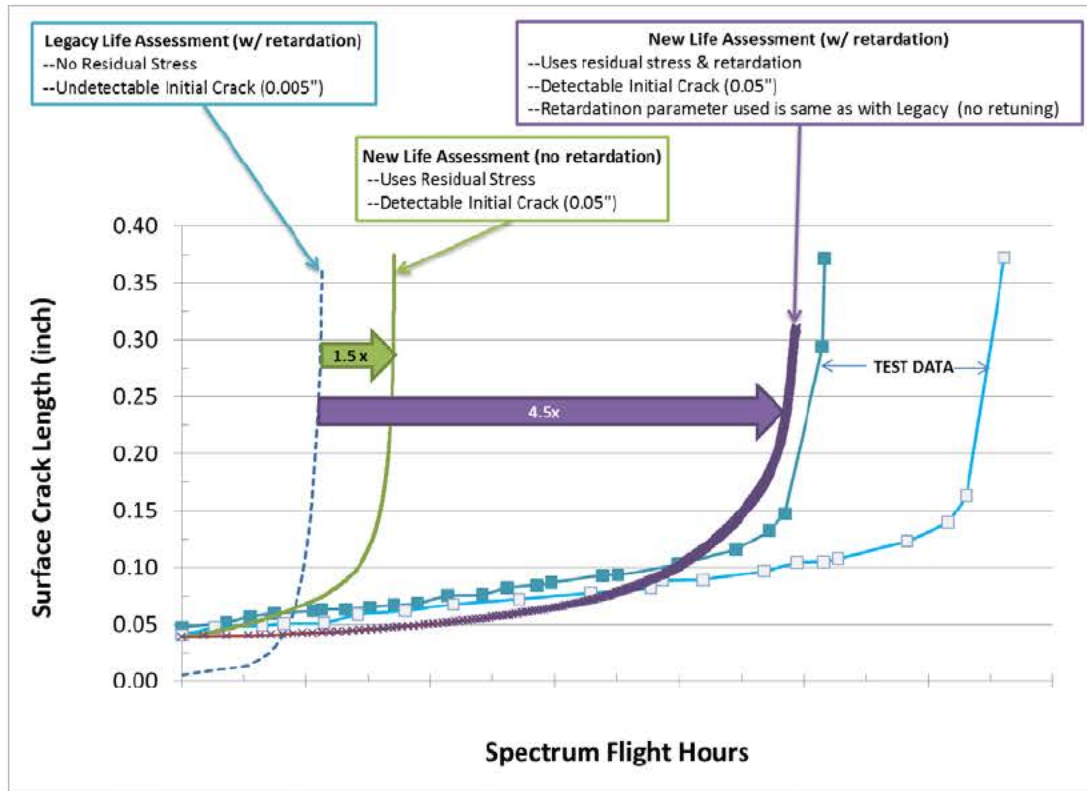


Figure 129. Key take-away points for CX analysis with retardation included.

8.2.7 Crack Shape Comparison: Analytical vs. Experimental

Figure 130 compares crack shapes extracted from prediction (BAMF) with marker band analysis of one of the test coupons. Even with the complexities of multiple site cracking and active secondary cracks during the test, the predicted and actual shapes match very well.

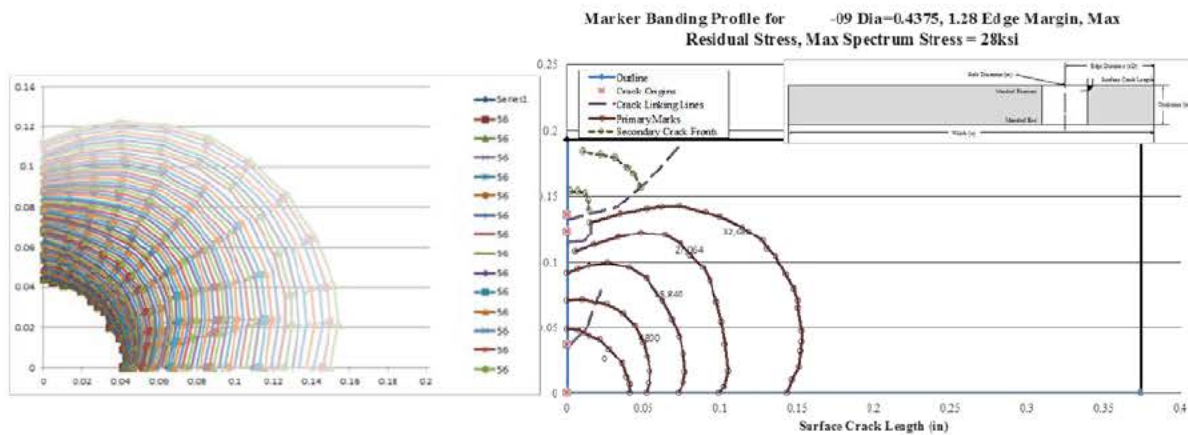


Figure 130. Comparison of crack shapes between BAMF (left) and experiment (right). Despite multiple site cracking that occurs in reality, crack shapes match well.

8.3 Coupon Tests for an Aircraft Wing FCL

This section describes the testing and validation that APES, Inc. executed for a series of experiments related to a typical aircraft wing FCL. The intent of these tests is to demonstrate the ability of experimental and analytical methods developed under this program to accurately predict behavior of cracks growing through a residual stress field under spectrum loading. As with the fuselage demonstration case, these fatigue experiments were paired with residual stress analyses (Contour Method) that used the same conditions of edge margin, hole diameter, CX interference level, thickness, and—of course—alloy.

The following subjects are covered:

- Specimen design
- Spectrum considerations
- Test Matrix
- Experimental Results
- Modeling Results

8.3.1 Specimen Design

The actual AFGROW model for the component is 26.5 inches wide. That was well beyond practical for our load frame capability (55 kip), so the specimen geometry was limited to five inches wide (Figure 131). The critical aspects of the tests, however, are the edge margin ($e/D = 3.77$) and the crack growth within the residual stress affected zone, which is typically less than a hole diameter in size. The material used is 7075-T7351 aluminum, 0.25" thick. Since, the location is cold worked in practice, only cold worked coupons were tested. Note that in reality, the location contains a countersunk hole. For this demonstration, however, the specimens have been prepared with a straight shank hole, which was the scope of the technology development in this program.

8.3.2 Spectrum Considerations

As with all spectrum tests, a constant loading rate was used rather than constant frequency. APES truncated the spectrum and removed 25% of the cycles that were calculated to be “non-damaging.” Using APES in-house spectrum damage calculation routines, we estimate that the damage of one spectrum pass was changed 1% or less. We also used AFGROW to compare the original spectrum with the truncated version using the *.dax file used for the current DADTA, and difference in life to failure was only one spectrum flight hour.

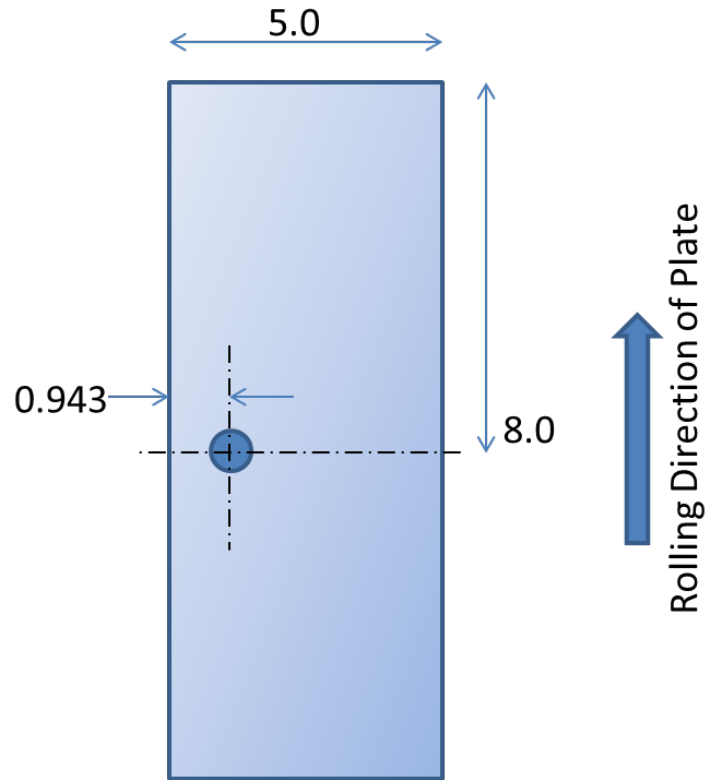


Figure 131. Specimen planform. Thickness is 0.25 inch. Final hole diameter is 0.25"

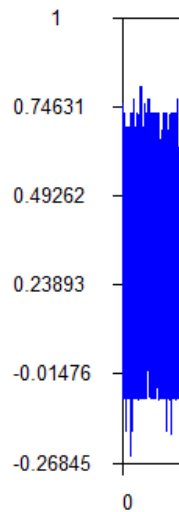


Figure 132. Truncated fatigue spectrum as visualized in AFGROW.

8.4 Test Matrix

The test matrix consists of six coupons. All coupons were pre-cracked under constant amplitude load to a mandrel entrance face crack length around 0.05 inch before switching to the spectrum load. Coupons that are cold worked shall be cold worked first, then pre-cracked.

- 2 coupons, 0.25D, CX at 4.4% interference (max spec)
- 2 coupons, 0.25D, CX at 3.3% interference (mid spec)
- 2 coupons, 0.25D CX at 2.7% interference (min spec)

The cold working of the holes used three different toolsets. The “max spec” group used the standard toolset from FTI, 8-0-N, designed to impart maximum degree of cold work (approximately 4.4%). The other two of coupons used a custom initial reamer to impart minimum interference within the spec, which was approximately 3.3% cold work for the “mid” group and 2.7% cold work for the “min” group.

8.4.1 Experimental Results

The experimental results for this demonstration case are shown in Figure 133. All of the test results segregated by condition and followed the expected trends. The average lives per test condition, ordered longest to shortest were:

- MAX CX: 22,725 hours
- MID CX: 13,004 hours
- MIN CX: 6,689 hours

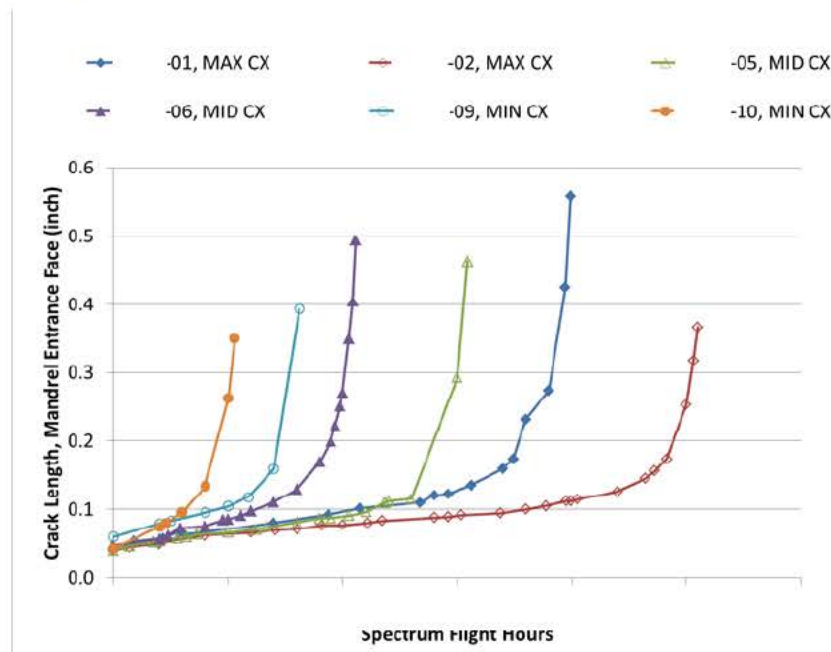


Figure 133. Experimental data from wing tests. Three groups segregate nicely based on interference level, the only variable.

8.4.2 Modeling Results

For this series of correlations, we actually used two different material models, primarily because we were suspect of the material model supplied by the government. It exhibits atypical behavior at low stress intensity, especially at $R = 0.8$. Therefore, we decided to use the Harter-T model for this alloy that is contained in AFGROW. Two plots are shown below, one for $R = -0.3$ (Figure 134) and the other for $R = 0.8$ (Figure 135). We still have some concerns over the extreme threshold behavior in the Harter-T model, but this exercise still provides a good example of the sensitivity to material model seen in CX analyses.

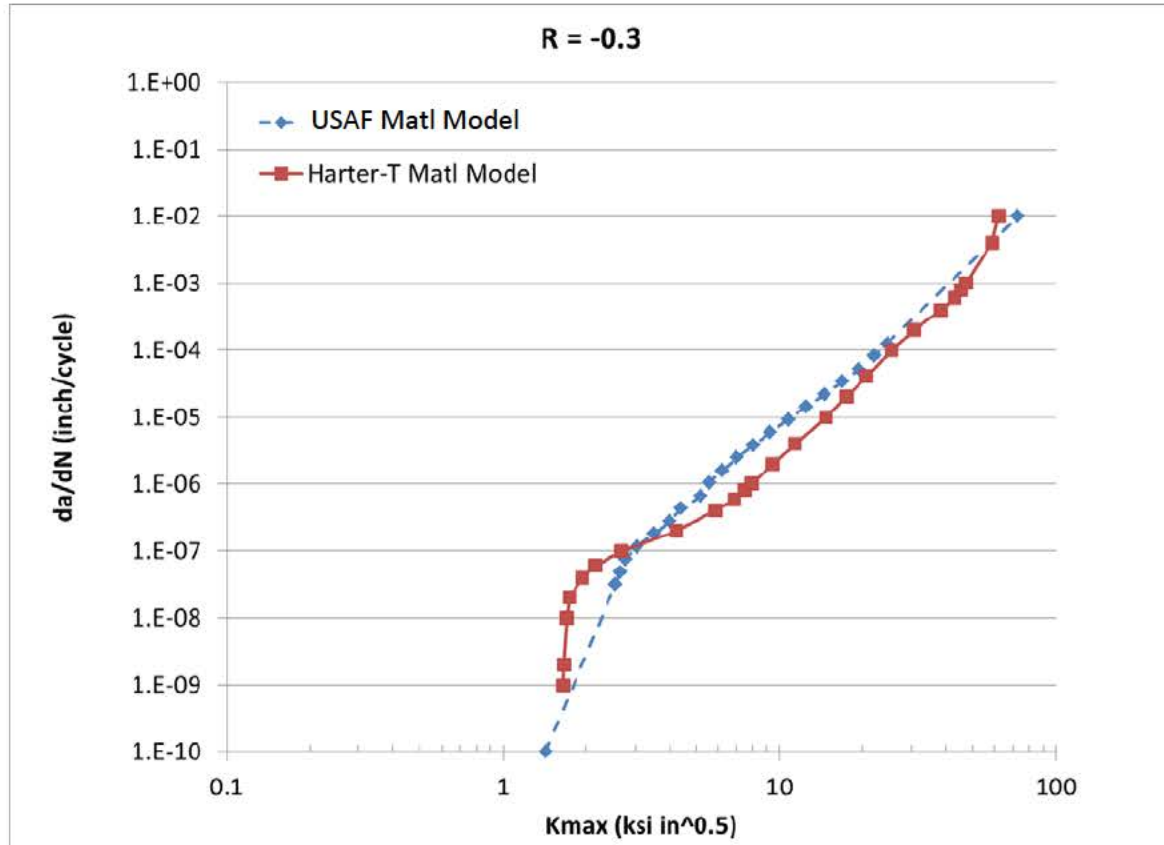


Figure 134. Crack growth behavior for two different material models at $R = -0.3$.

Four of the test cases were analyzed using both material models. Due to time, these were limited to the MIN CX tests (using initial precrack sizes from the two fatigue coupons paired with the two replicates from the residual stress measurements provided by Hill Engineering) and one of the MID CX tests / residual stress pairings. In Table 23, we see that the Harter T material model produces results that are 2.6 times longer life than the USAF supplied material model. In general, the BAMF and CPT lives agree well with each other (as before, the two programs were used by separate analysts) but fall short of the experimental data.

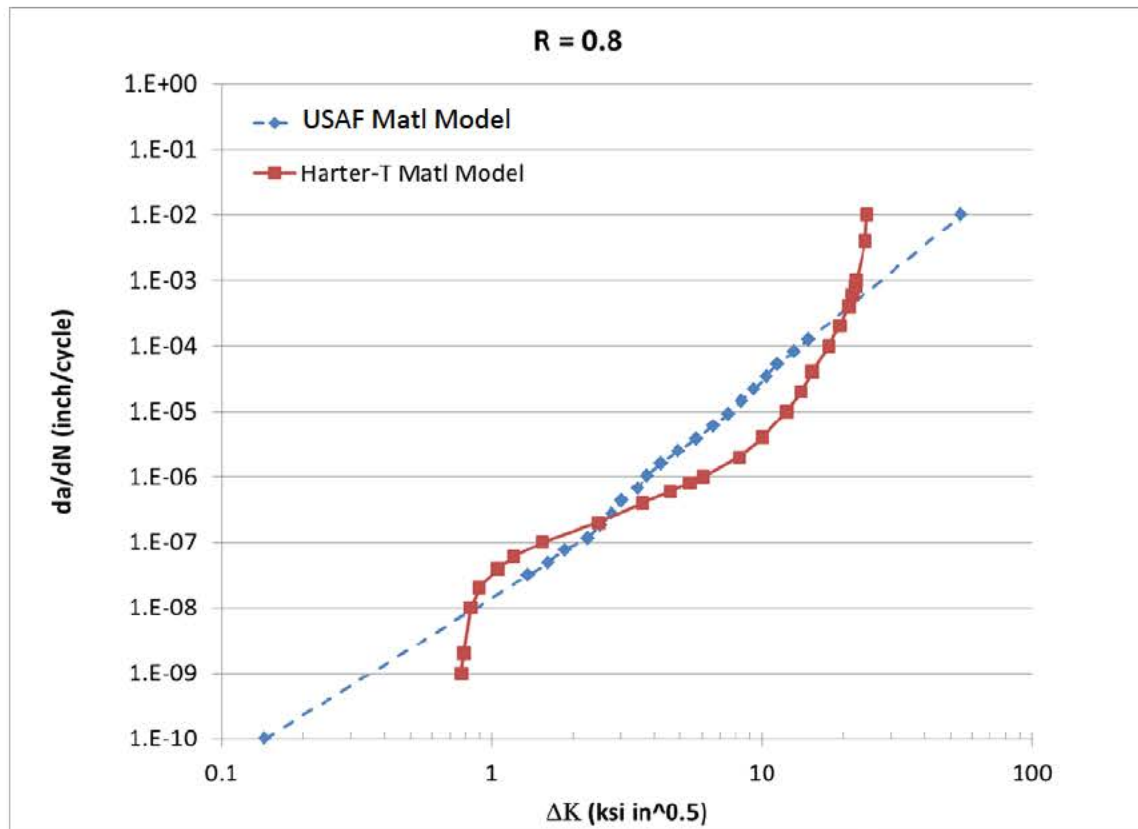


Figure 135. Crack growth behavior for two different material models at $R = -0.8$.

Figure 136 through Figure 143 show test data, CPT predictions, and Legacy ASIP assessments for the first eight conditions in Table 21. In all of these cases, the CPT predictions outperform the legacy method—sometimes by a little and sometimes by a wide margin. In a couple of cases we actually see the CPT prediction outlast the test data, even without retardation. The reasons for this are unknown, but it is safe to say that the material models for this alloy have not been as heavily characterized as models we use for 2024-T351 and 7075-T651. So, this is possible source for problems, as is uncertainty in the residual stress distributions. We see a fair amount of variability in the measured residual stress, even in the replicates.

Table 22. Modeling results compared with experiment for the wing FCL.

[Table removed for public release]

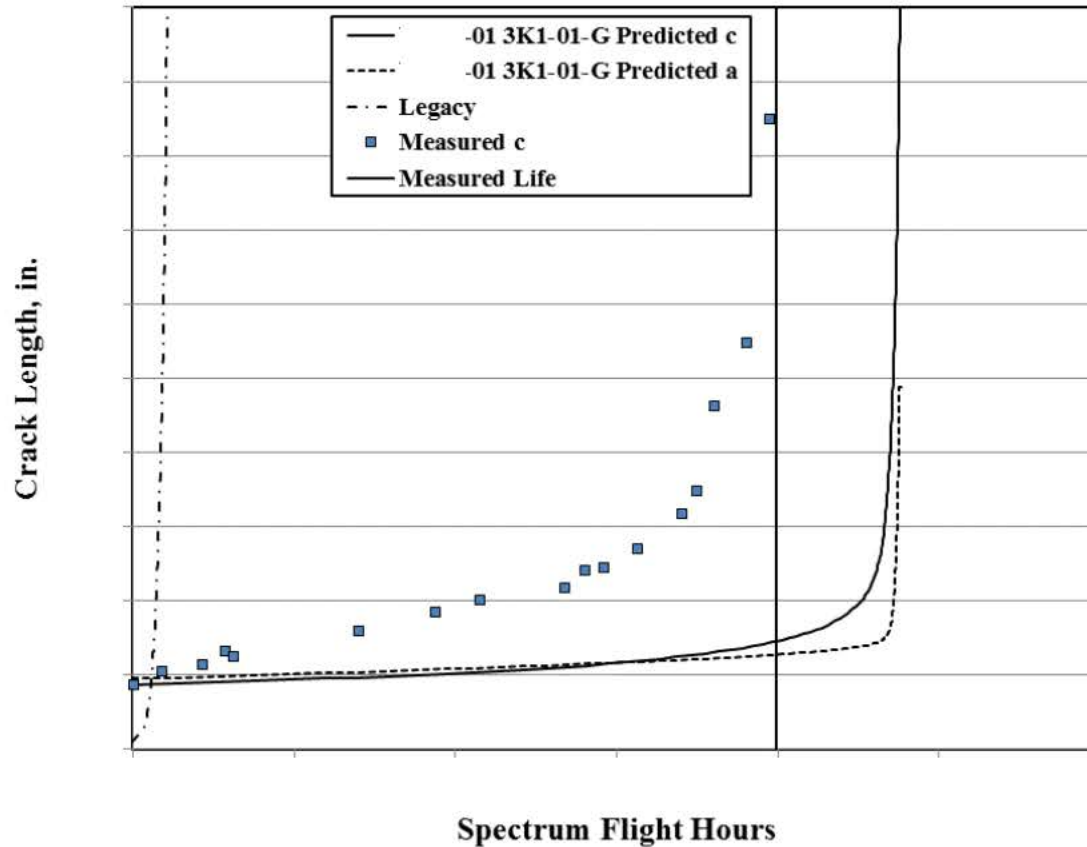


Figure 136. Experimental and analytical crack length vs. spectrum flight hours for MAX CX condition. A Legacy ASIP assessment is also included for reference. The predicted data convention in the legend uses fatigue coupon first (to define initial crack size and shape) and residual stress distribution second.

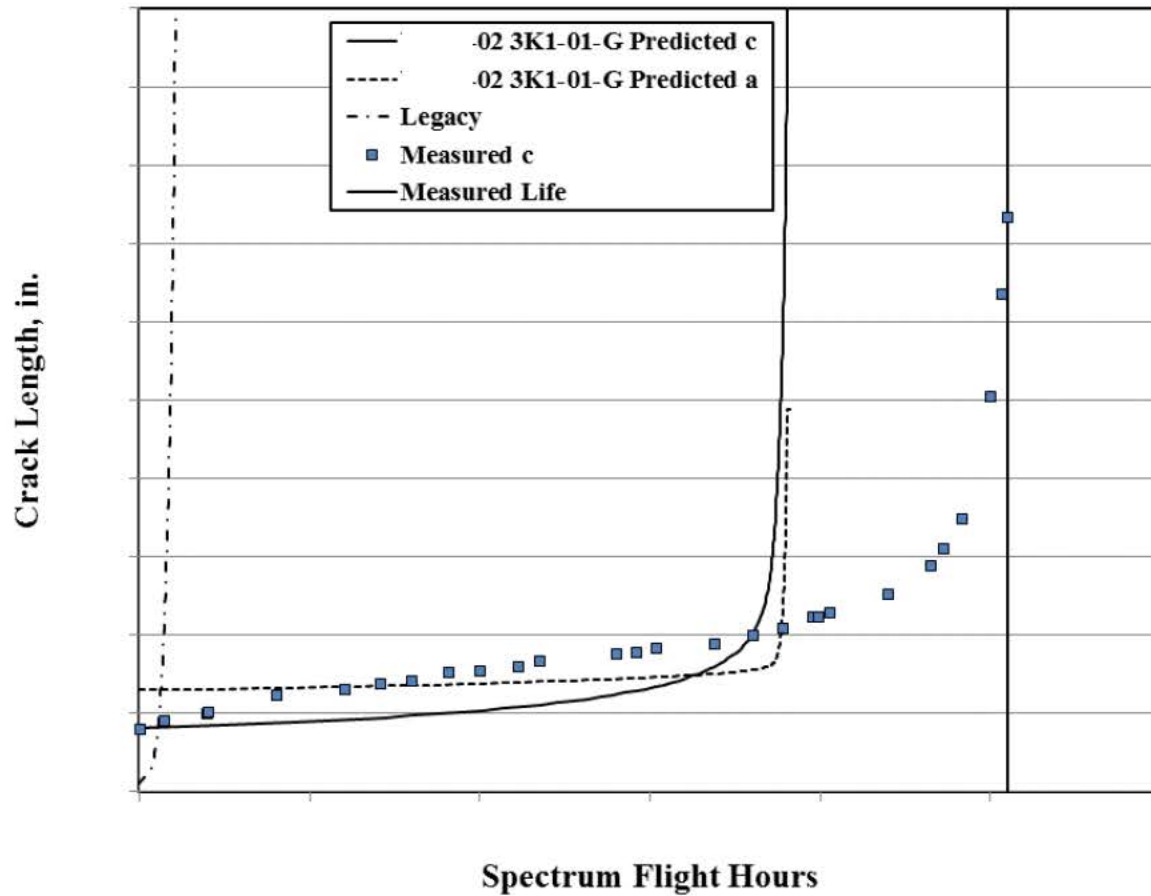


Figure 137. Experimental and analytical crack length vs. spectrum flight hours for MAX CX condition. A Legacy ASIP assessment is also included for reference. The predicted data convention in the legend uses fatigue coupon first (to define initial crack size and shape) and residual stress distribution second.

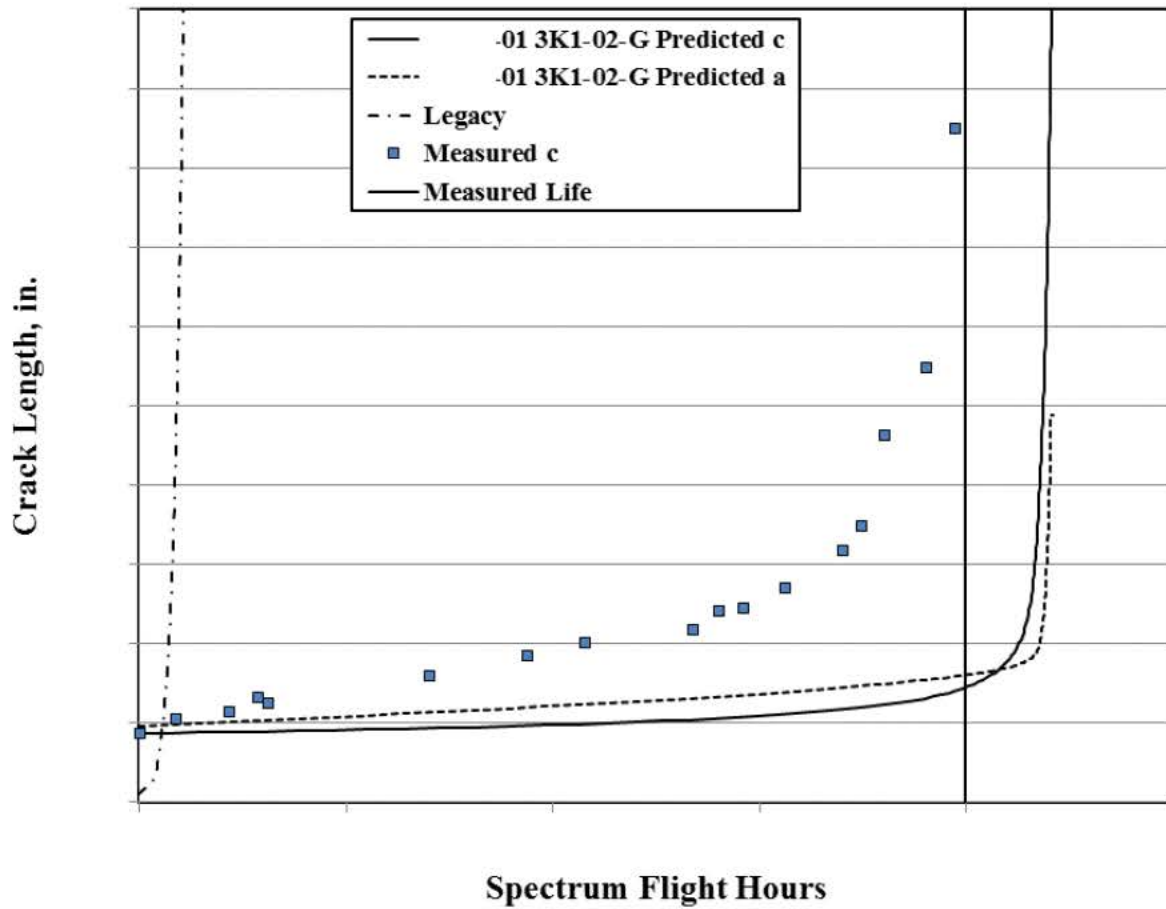


Figure 138. Experimental and analytical crack length vs. spectrum flight hours for MAX CX condition. A Legacy ASIP assessment is also included for reference. The predicted data convention in the legend uses fatigue coupon first (to define initial crack size and shape) and residual stress distribution second.

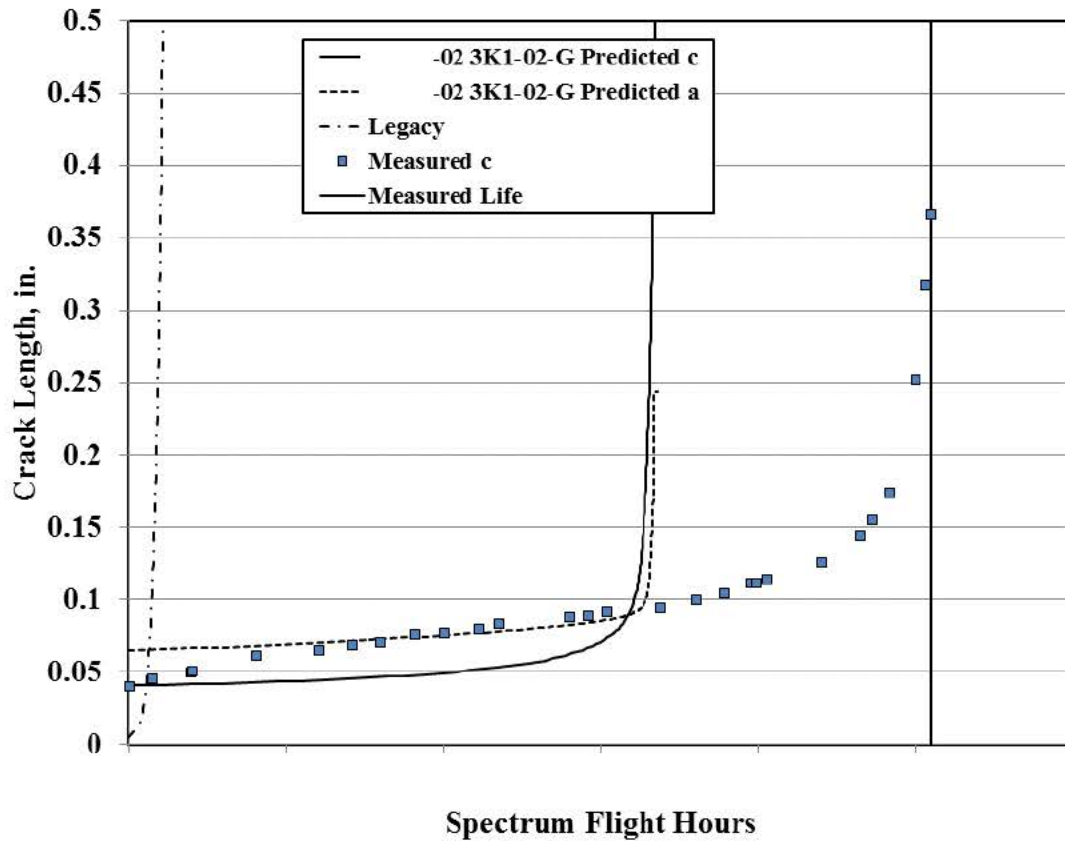


Figure 139. Experimental and analytical crack length vs. spectrum flight hours for MAX CX condition. A Legacy ASIP assessment is also included for reference. The predicted data convention in the legend uses fatigue coupon first (to define initial crack size and shape) and residual stress distribution second.

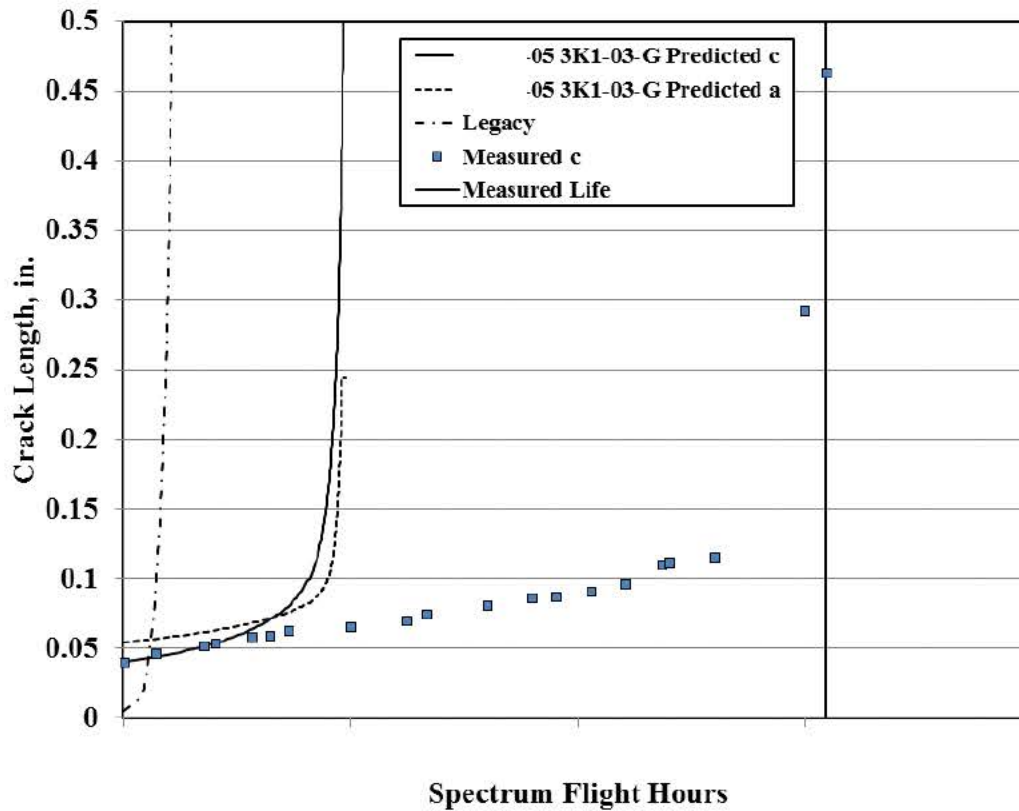


Figure 140. Experimental and analytical crack length vs. spectrum flight hours for MID CX condition. A Legacy ASIP assessment is also included for reference. The predicted data convention in the legend uses fatigue coupon first (to define initial crack size and shape) and residual stress distribution second.

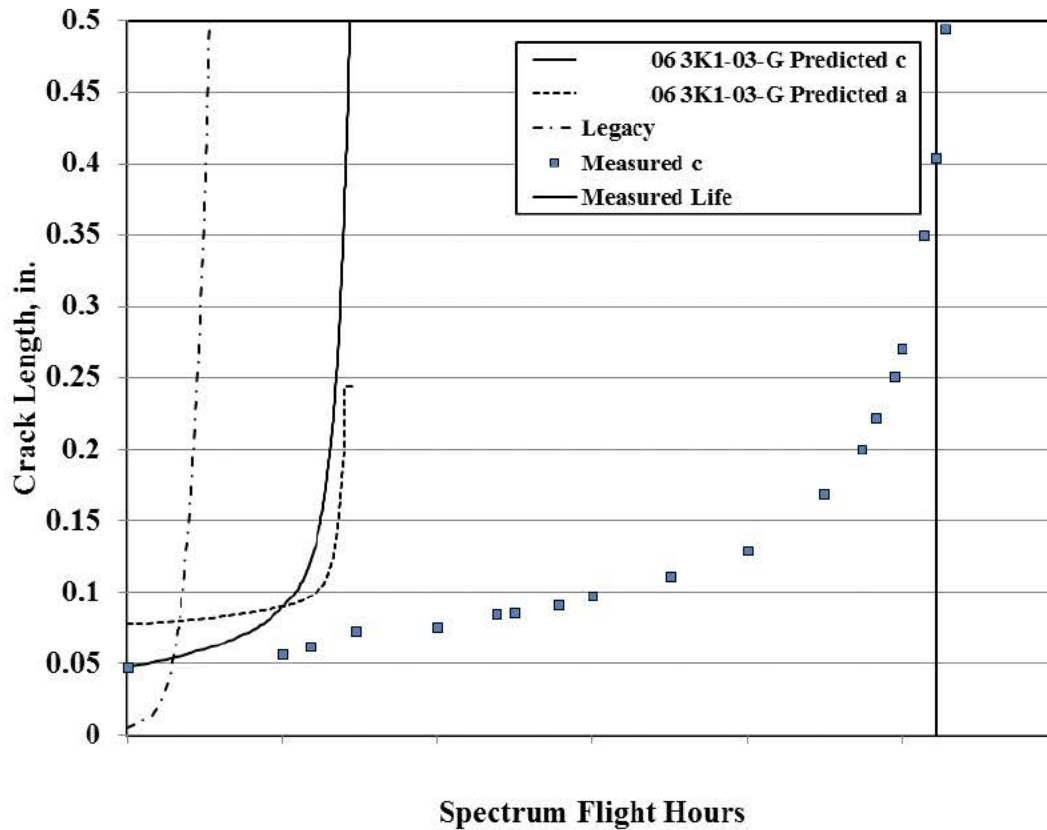


Figure 141. Experimental and analytical crack length vs. spectrum flight hours for MID CX condition. A Legacy ASIP assessment is also included for reference. The predicted data convention in the legend uses fatigue coupon first (to define initial crack size and shape) and residual stress distribution second.

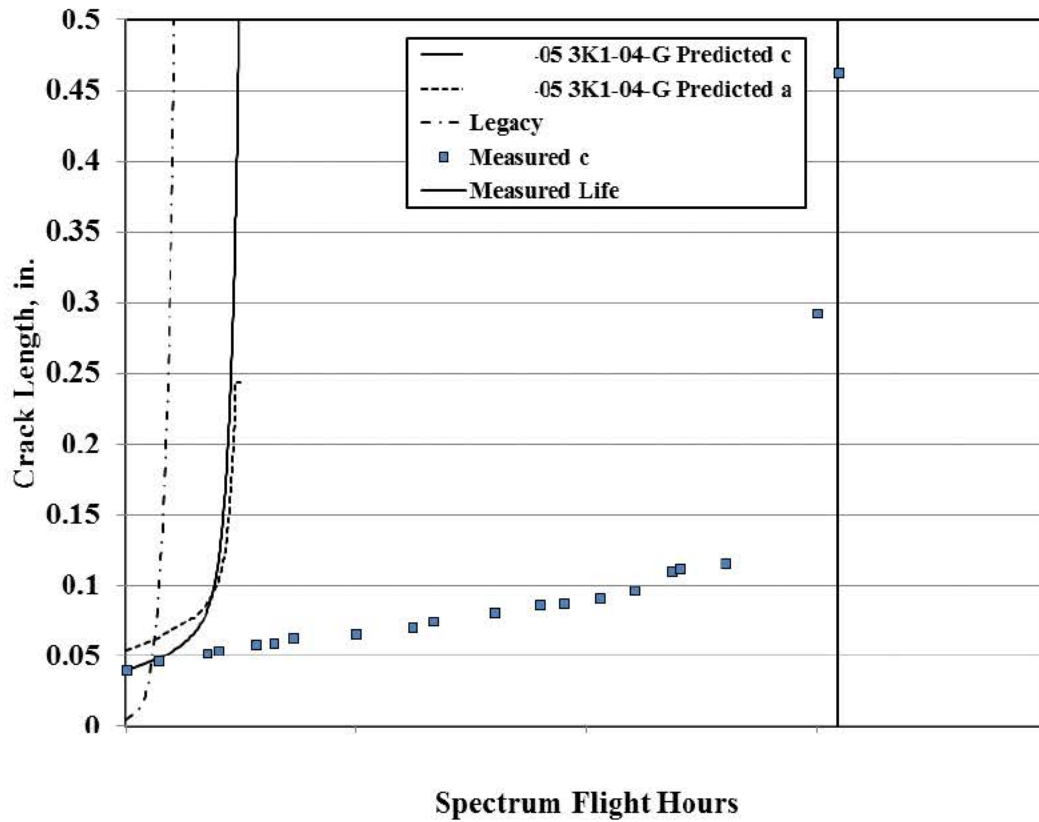


Figure 142. Experimental and analytical crack length vs. spectrum flight hours for MID CX condition. A Legacy ASIP assessment is also included for reference. The predicted data convention in the legend uses fatigue coupon first (to define initial crack size and shape) and residual stress distribution second.

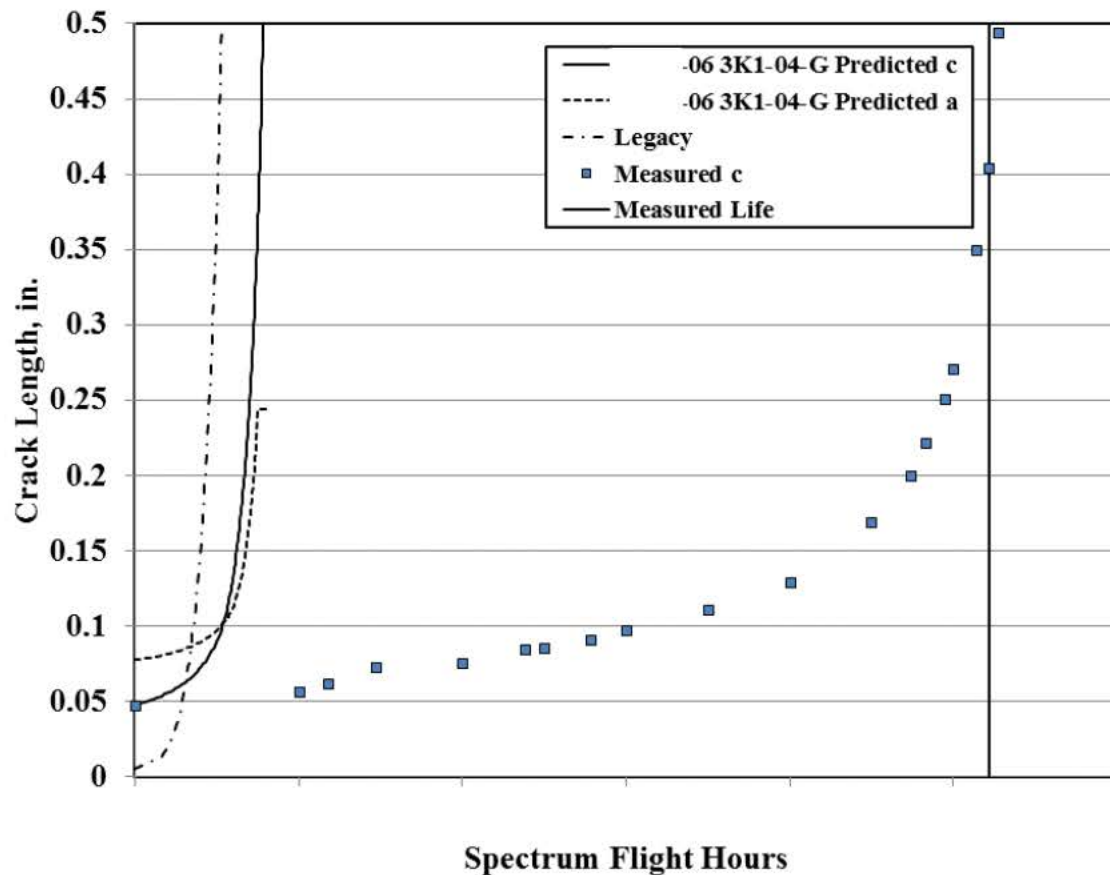


Figure 143. Experimental and analytical crack length vs. spectrum flight hours for MID CX condition. A Legacy ASIP assessment is also included for reference. The predicted data convention in the legend uses fatigue coupon first (to define initial crack size and shape) and residual stress distribution second.

In Figure 144 through Figure 147 we see similar information as to the previous eight figures, but this time the prediction curves use the Harter T material model rather than the ASIP material model. The four cases are the last four lines in Table 21. In one case (Figure 144) the legacy model actually has a longer life than the CPT simulation, although no crack retardation was used in any of the CPT or BAMF simulations for the wing FCL demo articles.

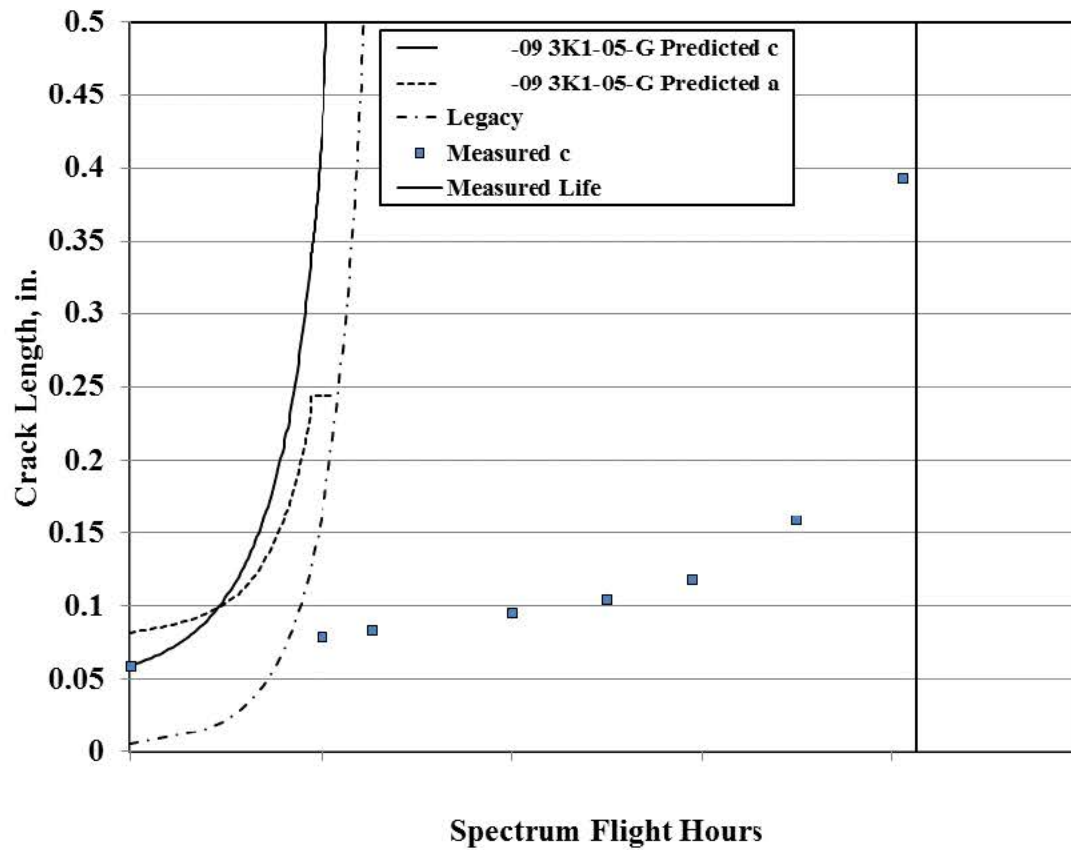


Figure 144. Experimental and analytical crack length vs. spectrum flight hours for MIN CX condition. A Legacy ASIP assessment is also included for reference. The predicted data convention in the legend uses fatigue coupon first (to define initial crack size and shape) and residual stress distribution second.

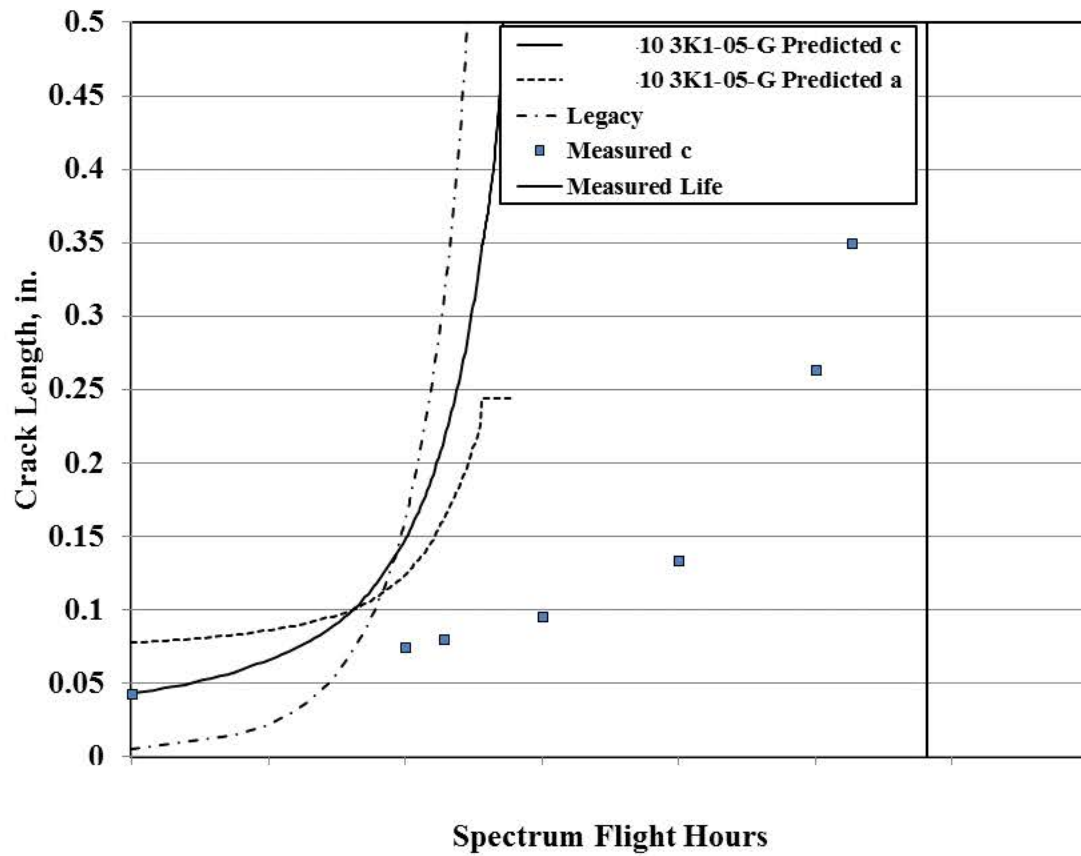


Figure 145. Experimental and analytical crack length vs. spectrum flight hours for MIN CX condition. A Legacy ASIP assessment is also included for reference. The predicted data convention in the legend uses fatigue coupon first (to define initial crack size and shape) and residual stress distribution second.

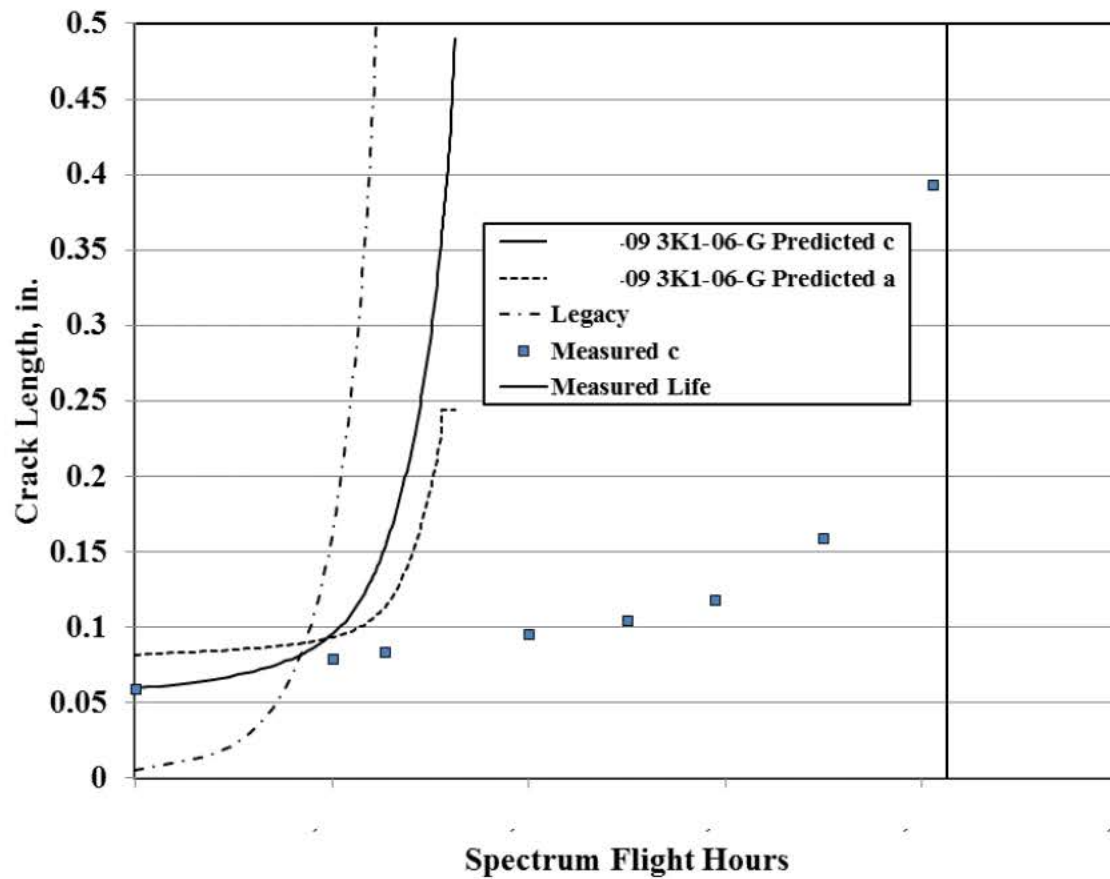


Figure 146. Experimental and analytical crack length vs. spectrum flight hours for MIN CX condition. A Legacy ASIP assessment is also included for reference. The predicted data convention in the legend uses fatigue coupon first (to define initial crack size and shape) and residual stress distribution second.

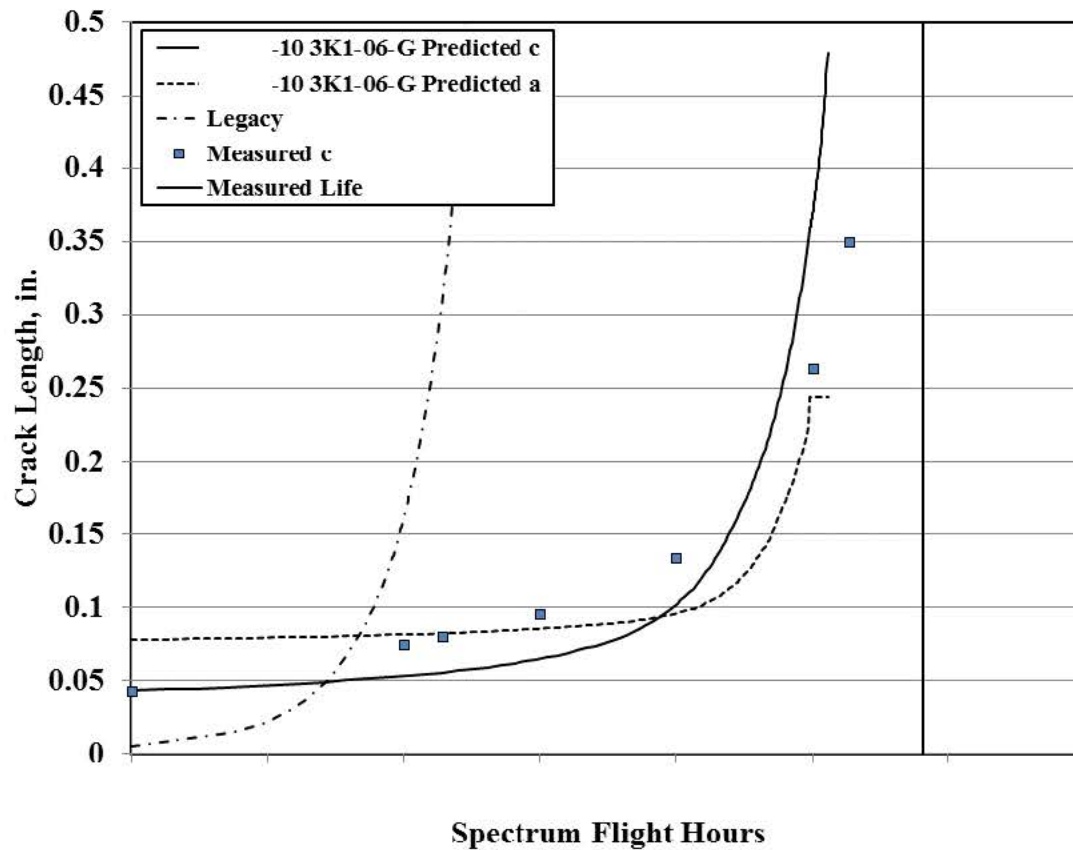


Figure 147. Experimental and analytical crack length vs. spectrum flight hours for MIN CX condition. A Legacy ASIP assessment is also included for reference. The predicted data convention in the legend uses fatigue coupon first (to define initial crack size and shape) and residual stress distribution second.

9 Conclusions and Recommendations

9.1 Conclusions

Quality Assurance for Cold Worked Holes

In the past, these residual stress fields have not been included because of a perceived risk to safety (e.g., the risk that the mechanic did not properly cold work a critical location). Although the manufacturers of the hardware used for cold working have tools used to check the presence of cold work, APES proposed to further this quality control capability through rapid scan, semi-automated, laser inspection of the cold worked holes at a key step in the cold work process. These procedures produce a digital documentation of the hole, based on critical metrology, which can be linked with maintenance records.

The FastnerCam™ prototype developed for this effort currently can measure the amount of cold expansion around fastener holes to within 0.5% for diameters over 0.246 inch and in plate thicknesses 0.19 inch or greater. For this project, the prototype was demonstrated using aluminum alloys 2024-T351 and 7075-T651.

The scaling factor used to determine the amount of cold expansion based on the amount of deformed material around the fastener hole was determined experimentally using only three different plate thicknesses. In order to better understand how the scaling factor depends on the plate thickness, more samples of varying plate thicknesses need to be examined.

Finally, if FastnerCam™ is to be used to measure the amount of cold-work around small (with diameters less than 0.246") fastener holes, its resolution will need to be improved.

In its current form, this tool provides an effective method for establishing pass / fail for a cold worked hole and for recording the data for further use. Utility of the system would be greatly enhanced by increasing resolution and by modifying the function of the system to be non-contact. Both of these possibilities are being examined by the subcontractor, TRI-Austin, for future development.

Non-Destructive Inspection of Cracks at Cold Worked Holes

Another important aspect of the program is inspection for cracks emanating from cold worked fasteners holes. Cracks in these residual stress fields take on unique shapes and behaviors as compared to cracks at non-CX worked holes. The objective of this effort was to look at three common non-destructive inspection methods used around fastener holes and determine what limitations might exist that would require changes in how these methods are used in locations that are cold worked. The three methods were:

1. Bolt-hole eddy current
2. Surface scan eddy Current
3. Ultrasound

Important conclusions from this effort are summarized here:

- ET methods were insensitive to applied loads on a fatigue crack.
- UT methods were very sensitive to applied external loads on a fatigue crack.
- As described in detail in other sections of the final report, cracks generally form at the mandrel entry surface and grow to a significant length before breaking through to the mandrel exit surface. The mandrel exit surface is the one typically accessible for NDI.
- Existing fatigue cracks become easier to detect after CX process.
- ET – BH techniques are not significantly affected by the CX process. The capability guidelines for ET - BH listed in the Structures Bulletin EN-SB-012 can still be applied for aluminum structure.
- ET – SS techniques are affected, due to the change in crack shape. ET – SS inspections will normally be conducted from the mandrel exit face of a CX hole. Fatigue cracks growing in a CX hole in thick structure can become very large without breaking through the mandrel exit face.
 - For aluminum structures of 0.100” or thinner, a reliable detectable crack size of 0.250” in length is reasonable.
 - For aluminum structures of greater than 0.100” thickness, ET – SS applied to the mandrel exit face is not reliable at reasonable crack sizes.
- UT techniques are affected by the CX process. There is a difference between the 0.100” thick specimens and the 0.313” and 0.500” thick specimens evaluated in this work.
 - For aluminum structures of 0.100” or thinner, a detectable crack size of 0.250” length is reasonable.
 - For aluminum structures of greater than 0.100” thickness, a detectable crack size of 0.300” length is reasonable.

Analytical Modeling of Crack Growth through Residual Stress Fields

The technical approach includes enhancements to the StressCheck finite element code for determining stress intensity factors in residual stress fields and the integration of that software package with the commercially-available crack growth code, AFGROW. Provisions were also made to incorporate highly irregular crack shapes associated with cold-worked holes into StressCheck via two separate plug-ins: (1) the Crack Propagation Tool developed by team-member Engineering Software Research & Development, Inc. (ESRD) and (2) the Broad Application for Modeling Failure (BAMF)

In addition to software enhancements, a residual stress database has been developed and populated during this program. The database supports some common aluminum alloys used in aircraft and addresses variations in material thickness, hole diameter, edge margin, and cold work interference level. The database is easily expandable by the customer. The determination of residual stress uses an advanced measurement technique

called the “Contour Method”, a method proven to deliver high-density, two-dimensional representations of residual stress states resulting from the cold work process.

These residual stress inputs have been combined with the analysis suite described above to predict the performance of simulated aircraft components under fatigue load environments, including load spectra specific to wing and fuselage structure on several USAF aircraft.

In most every case, the new methods using BAMF and CPT outperform the legacy ASIP method. However, without crack retardation, the predictions using residual stress tend to fall short of the experimental data by a factor of three.

Important analysis infrastructure has been built and delivered under this program including:

- A residual stress database of common hole diameters, edge margins, and plate thicknesses for 2024-T351 and 7075-T651 aluminum (primarily).
- Two different methods for calculating stress intensity factors for cracks in residual stress fields. Both methods have been incorporated into the fracture mechanics module that is commercially available with StressCheck v10.1
- Two separate codes for doing the multipoint crack progression necessary for allowing cracks form realistic shapes in simulation.

The typically excellent crack shape agreement we see between experiment and analysis have provided a strong validation of the shape of the residual stress being produced by the Contour Method. There still appears to be a fair amount of variability in the RS magnitude even amongst replicates. At this point we do not know how much variability results from uncertainty in measurement and how much of it originates in the cold work process itself.

9.2 Recommendations

This program illustrated the complex nature of modeling fatigue crack growth in residual stress fields. Barring the difficulties, the program has achieved excellent results. That said, we believe there are several areas that require further attention as the USAF and industry seeks to establish the proper guidelines and analysis procedures for this type of work.

9.2.1 Technical Challenge: OVERLOADS & UNDERLOADS in SPECTRA

Preliminary analyses in this program showed that overloads and underloads in typical fighter spectra could cause residual stress redistribution (this is well known for severe overloads). However, analytical results need to be validated with experiment and in a wide range of conditions:

- Straight bore holes
 - Filled (aluminum and steel pins)
 - Unfilled
- Countersunk holes
 - Filled (aluminum and steel pins)
 - Unfilled

As can be seen from the list above, it is likely that hole fill will have an influence on the results, too, so this must be included.

9.2.2 Technical Challenge: LOAD TRANSFER

Models for crack growth in RS have not been validated in load transfer scenarios. The possibility exists that pin loads in a joint could alter the RS distribution during fatigue testing. Validation testing and analysis should be accomplished for the following basic conditions.

- High Load Transfer
 - Straight Bore
 - Countersunk
- Low Load Transfer
 - Straight Bore
 - Countersunk

9.2.3 Technical Challenge: MULTIPLE ACTIVE CRACKS

Additional effort should be channeled to determine the importance of multiple crack origins in modeling fatigue response at CX holes. This would address shifts in failure progression we have observed between constant amplitude and variable amplitude scenarios.

9.2.4 Technical Challenge: CRACK RETARDATION

Future work should examine the influence of crack retardation (load interaction) in fatigue life prediction in residual stress fields. Preliminary analysis under this program shows that retardation has a major influence on computed results. Unfortunately, retardation models have historically been used as “tuning knobs.” Rules for application of retardation in CX solution sets need to be established and validated.

9.2.5 Technical Challenge: MATERIAL MODEL SENSITIVITY

Work under the RIF program showed that life prediction in RS fields is sensitive to the material model used to propagate the crack. Material models with severe thresholds (typical of data developed from long cracks) may cause problems because the RS in a CX hole analysis can “deactivate” many cycles. New standards for material testing need to be established to ensure that behavior at low stress intensities is being properly represented.

9.2.6 Technical Challenge: STRESS RATIO SHIFT

Residual stress fields at CX holes cause many applied load cycles to shift into heavily negative R regimes, where current fatigue crack growth analysis suggests there should be no stress ratio effect, which could in turn degrade prediction accuracy.

9.2.7 Technical Challenge: EFFECT OF CRACKS ON RS REDISTRIBUTION

Residual stress fields at CX holes may relax during crack propagation. This could be modeled via a time- or cycle-dependent stress function if such a phenomenon can be detected and if sensitivity analysis shows that such a response has a significant influence on the life computations.

10 References

Andrew, D. L; Paul N. Clark, David W. Hoepfner (2014), "Investigation of Cold Expansion of Short Edge Margin Holes with Pre-Existing Cracks in 2024-T351 Aluminum Alloy", *Fatigue and Fracture Engineering Materials and Structures*, Vol 37, No. 4, pp 406-416. DOI: 10.1111/ffe.12123.

Damage Tolerance Design Handbook (1983), A Compilation of Fracture and Crack growth Data for High Strength Alloys, Volume 3. Battelle Report MCIC-HB-01R.

Fahr, A, and D. S. Forsyth (1997) Pod Assessment Using Real Aircraft Engine Components, Review of Progress in QNDE, Vol. 17

Forsyth, D. S. (2009), Transferring POD Estimates from Specimens to Reality, American Society for Nondestructive Testing Research Symposium and Spring Conference, 16 – 20 March 2009, St. Louis.

Harding, C. A., Hugo, G. R., & Bowles, S. J. (2006); " Model-Assisted POD for Ultrasonic Detection of Cracks at Fastener Holes," Presented at RPQNDE 2005. In AIP Conference Proceedings (Vol. 820, p. 1862).

Lei, Y., O'Dowd, N.P. and Webster, G.A. (2000); "Fracture Mechanics Analysis of a Crack in a Residual Stress Field", *International Journal of Fracture*, Volume 106, pp 195-216.

Newman, J. C. , Jr., and P.R. Edwards (1989), "Short Crack Growth Behaviour in an Aluminum Alloy—An AGARD Cooperative Test Programme", *AGARD Report No. 732*, Advisory Group for Aerospace Research and Development.

Newman, J.C., Jr. and Raju, I.S. (1986) "Stress-Intensity Factor Equations for Cracks in Three-Dimensional Finite Bodies Subjected to Tension and Bending Loads", Chapter 9 in *Computational Methods in the Mechanics of Fracture*, S.N. Atluri, Editor, pp. 312-334.

Prime, M.B. (2009); "The Contour Method: A New Approach in Experimental Mechanics," Proceedings of the SEM Annual Conference, June 1-4, 2009, Albuquerque, New Mexico, Paper Number 156.

Prime, M.B., Hill, M.R., DeWald, A.T., Sebring, R.J., Dave, V.R. and Cola, M.J. (2003); "Residual Stress Mapping in Welds Using the Contour Method," *Trends in Welding Research*, Proceedings of the 6th International Conference , April 15-19, 2002, Pine Mountain, Georgia, eds: S.A. David et al., ASM International, 2003, pp. 891-896.

Prime, M.B. (2001), "Cross-Sectional Mapping of Residual Stresses by Measuring the Surface Contour After a Cut," *Journal of Engineering Materials and Technology*, vol. 123, pp. 162-168.

Pereira, J.P. and Duarte, C.A. (2006), “The Contour Integral Method for Loaded Cracks”, *Communication in Numerical Methods in Engineering*, Volume 22, pp 421-432. DOI: 10.1002/cnm.824

Pilarczyk, R. (2008), “Experimentally Derived Beta Corrections to Predict Fatigue Crack Growth at Cold Expanded Holes in 7075-T651”, Master Thesis, Department of Mechanical Engineering, University of Utah.

Warner, J. (2012), “Cold Expansion Effects on Cracked Fastener Holes Under constant Amplitude and Spectrum Loading in the 2024-T351 Aluminum Alloy,” Master Thesis, Department of Mechanical Engineering, University of Utah.

11 APPENDIX A: Constant Amplitude CX Fatigue Test Data Tables

This appendix contains all crack growth data recorded for each of the 125 constant amplitude CX fatigue tests (see Section 3 for test program details).

Table 23. Test Data, coupon 3D1-16-A.

Specimen ID	Max Stress (ksi)	"Constant Amplitude" Stress (ksi)	Cycles to Failure	Material	Thickness (inch)	Edge Margin	Nominal Final Ream Diameter (inch)	CX %	CX LEVEL
3D1-16-A	25.3	22.0	100,107	2024-T3	0.1	1.39	0.25	2.78	MIN
Cycles	NE Face, Short (inch)	E Bore, Short (inch)	Aspect Ratio	Spectrum Pass	SFH (where applicable)	NW Face (inch)	SE Face (inch)	SW Face (inch)	W Bore (inch)
65141				14.48			0.0106		
70235				15.61			0.0157		
74102				16.47			0.0206		
81482	0.02076			18.11			0.0326		
88492	0.04660			19.66			0.0468		
95413	0.12020			21.20			0.1045		
96590	0.21700			21.46			0.21700		
100107				22.25					

Table 24. Test Data, coupon 3D1-17-A.

Specimen ID	Max Stress (ksi)	"Constant Amplitude" Stress (ksi)	Cycles to Failure	Material	Thickness (inch)	Edge Margin	Nominal Final Ream Diameter (inch)	CX %	CX LEVEL
3D1-17-A	25.3	22.0	122,409	2024-T3	0.1	1.39	0.25	2.67	MIN
Cycles	NE Face, Short (inch)	E Bore, Short (inch)	Aspect Ratio	Spectrum Pass	SFH (where applicable)	NW Face (inch)	SE Face (inch)	SW Face (inch)	W Bore (inch)
68599				15.24			0.0089		
71310				15.85			0.0103		
76896				17.09			0.0136		
82048				18.23			0.0162		
85981				19.11			0.0197		
91411				20.31			0.0249		
97258	0.01110			21.61			0.03096		
101576	0.02348			22.57			0.03476		
104704	0.03078			23.27			0.03912		
111107	0.04990			24.69			0.04864		
115581	0.07828			25.68			0.05728		
118915	0.10452			26.43			0.07594		
120026	0.12398			26.67			0.08302		
121413	0.18214			26.98			0.15756		
121703	0.22446			27.05			0.22446		
122409				27.20					

Table 25. Test Data, coupon 3D1-18-A.

Specimen ID	Max Stress (ksi)	"Constant Amplitude" Stress (ksi)	Cycles to Failure	Material	Thickness (inch)	Edge Margin	Nominal Final Ream Diameter (inch)	CX %	CX LEVEL
3D1-18-A	25.3	22.0	94,016	2024-T3	0.1	1.39	0.25	2.55	MIN
Cycles	NE Face, Short (inch)	E Bore, Short (inch)	Aspect Ratio	Spectrum Pass	SFH (where applicable)	NW Face (inch)	SE Face (inch)	SW Face (inch)	W Bore (inch)
57354	0.00700			12.75					
65957	0.00964			14.66					
69800	0.01144			15.51					
73370	0.01406			16.30					
75595	0.02056			16.80					
78284	0.03206			17.40					
79969	0.03866			17.77					
82993	0.04966			18.44					
85493	0.06306			19.00					
87670	0.07658			19.48			0.03968		
90227	0.11452			20.05			0.08276		
92095	0.21458			20.47			0.21458		
94016				20.89					

Table 26. Test Data, coupon 3D1-13-A.

Specimen ID	Max Stress (ksi)	"Constant Amplitude" Stress (ksi)	Cycles to Failure	Material	Thickness (inch)	Edge Margin	Nominal Final Ream Diameter (inch)	CX %	CX LEVEL
3D1-13-A	28.75	25.0	81,212	2024-T3	0.1	1.39	0.25	2.77	MIN
Cycles	NE Face, Short (inch)	E Bore, Short (inch)	Aspect Ratio	Spectrum Pass	SFH (where applicable)	NW Face (inch)	SE Face (inch)	SW Face (inch)	W Bore (inch)
50466				11.21					
56693				12.60					
64190				14.26					
70564	0.02906			15.68			0.01234		
79657	0.11876			17.70		0.01124	0.01365		
80045	0.21500			17.79		0.01470	0.21500		
81212				18.05					

Table 27. Test Data, coupon 3D1-14-A.

Specimen ID	Max Stress (ksi)	"Constant Amplitude" Stress (ksi)	Cycles to Failure	Material	Thickness (inch)	Edge Margin	Nominal Final Ream Diameter (inch)	CX %	CX LEVEL
3D1-14-A	28.75	25.0	50,990	2024-T3	0.1	1.39	0.25	2.46	MIN
Cycles	NE Face, Short (inch)	E Bore, Short (inch)	Aspect Ratio	Spectrum Pass	SFH (where applicable)	NW Face (inch)	SE Face (inch)	SW Face (inch)	W Bore (inch)
36074				8.02			0.01440		
39009				8.67			0.02528		
43229	0.00820			9.61			0.04344		
46555	0.01056			10.35			0.06058		
49610	0.08922			11.02		0.02034	0.11280		
50338	0.12062			11.19		0.03146	0.13598		
50743	0.22862			11.28		0.05356	0.22862		
50990				11.33					

Table 28. Test Data, coupon 3D1-15-A.

Specimen ID	Max Stress (ksi)	"Constant Amplitude" Stress (ksi)	Cycles to Failure	Material	Thickness (inch)	Edge Margin	Nominal Final Ream Diameter (inch)	CX %	CX LEVEL
3D1-15-A	28.75	25.0	75,348	2024-T3	0.1	1.39	0.25	2.72	MIN
Cycles	NE Face, Short (inch)	E Bore, Short (inch)	Aspect Ratio	Spectrum Pass	SFH (where applicable)	NW Face (inch)	SE Face (inch)	SW Face (inch)	W Bore (inch)
49641				11 03			0.01020		
59125				13.14			0.01600		
62414	0.00442			13 87			0.01932		
65383	0.01148			14 53			0.02714		
68841	0.02794			15 30			0.03912		
71199	0.06030			15 82			0.06304		
72299	0.08798			16 07			0.08392		
73303	0.10834			16 29			0.0971		
74274	0.21378			16 51			0.21378		
75239				16.72					

Table 29. Test Data, coupon 3D1-02-A.

Specimen ID	Max Stress (ksi)	"Constant Amplitude" Stress (ksi)	Cycles to Failure	Material	Thickness (inch)	Edge Margin	Nominal Final Ream Diameter (inch)	CX %	CX LEVEL
3D1-02-A	25.3	22.0	96,785	2024-T3	0.1	1.39	0.5	3.96	MAX
Cycles	NE Face, Short (inch)	E Bore, Short (inch)	Aspect Ratio	Spectrum Pass	SFH (where applicable)	NW Face (inch)	SE Face (inch)	SW Face (inch)	W Bore (inch)
71716	0.01808			15 94		0.0080			
76204	0.02270			16 93		0.01078			
81947	0.03130			18 21		0.01438			
87219	0.05080			19 38		0.02538			
93276	0.11106			20.73		0.07854			
96785				21 51					

Table 30. Test Data, coupon 3D1-03-A.

Specimen ID	Max Stress (ksi)	"Constant Amplitude" Stress (ksi)	Cycles to Failure	Material	Thickness (inch)	Edge Margin	Nominal Final Ream Diameter (inch)	CX %	CX LEVEL
3D1-03-A	25.3	22.0	86,880	2024-T3	0.1	1.39	0.5	3.93	MAX
Cycles	NE Face, Short (inch)	E Bore, Short (inch)	Aspect Ratio	Spectrum Pass	SFH (where applicable)	NW Face (inch)	SE Face (inch)	SW Face (inch)	W Bore (inch)
62017	0.00584	0.01584		13.78					
69472	0.01450	0.01716		15.44					
73902	0.04354	0.10000		16.42					
77560	0.07606	0.10000		17 24		0.01408			0.02658
81181	0.11248	0.10000		18 04		0.02660			0.04330
85806	0.21482	0.10000		19 07		0.06592			0.06628
86880				19 31					

Table 31. Test Data, coupon 3D1-07-A.

Specimen ID	Max Stress (ksi)	"Constant Amplitude" Stress (ksi)	Cycles to Failure	Material	Thickness (inch)	Edge Margin	Nominal Final Ream Diameter (inch)	CX %	CX LEVEL
3D1-07-A	25.3	22.0	61,187	2024-T3	0.1	1.39	0.5	3.91	MAX
Cycles	NE Face, Short (inch)	E Bore, Short (inch)	Aspect Ratio	Spectrum Pass	SFH (where applicable)	NW Face (inch)	SE Face (inch)	SW Face (inch)	W Bore (inch)
40000	0.01320	0.01520		8.89					
44949	0.01930	0.02374		9.99					
51073	0.04054	0.10000		11.35					
55729	0.09260	0.10000		12.38					
60315	0.18850	0.10000		13.40		0.01160			0.01448
61187	0.44500	0.10000		13.60					

Table 32. Test Data, coupon 3D1-08-A.

Specimen ID	Max Stress (ksi)	"Constant Amplitude" Stress (ksi)	Cycles to Failure	Material	Thickness (inch)	Edge Margin	Nominal Final Ream Diameter (inch)	CX %	CX LEVEL
3D1-08-A	28.75	25.0	36,563	2024-T3	0.1	1.39	0.5	3.93	MAX
Cycles	NE Face, Short (inch)	E Bore, Short (inch)	Aspect Ratio	Spectrum Pass	SFH (where applicable)	NW Face (inch)	SE Face (inch)	SW Face (inch)	W Bore (inch)
25163				5.59		0.0104			0.00916
28324				6.29		0.01782			0.01930
33122				7.36		0.05040			0.08404
36563	0.44500			8.13					

Table 33. Test Data, coupon 3D1-09-A.

Specimen ID	Max Stress (ksi)	"Constant Amplitude" Stress (ksi)	Cycles to Failure	Material	Thickness (inch)	Edge Margin	Nominal Final Ream Diameter (inch)	CX %	CX LEVEL
3D1-09-A	28.75	25.0	30,426	2024-T3	0.1	1.39	0.5	3.91	MAX
Cycles	NE Face, Short (inch)	E Bore, Short (inch)	Aspect Ratio	Spectrum Pass	SFH (where applicable)	NW Face (inch)	SE Face (inch)	SW Face (inch)	W Bore (inch)
23205				5.16		0.0217			0.01824
28074				6.24		0.08556			0.10000
30426	0.44500			6.76					0.10000

Table 34. Test Data, coupon 3D1-01-A.

Specimen ID	Max Stress (ksi)	"Constant Amplitude" Stress (ksi)	Cycles to Failure	Material	Thickness (inch)	Edge Margin	Nominal Final Ream Diameter (inch)	CX %	CX LEVEL
3D1-01-A	30.0	25.0	47,296	2024-T3	0.1	1.39	0.5	3.95	MAX
Cycles	NE Face, Short (inch)	E Bore, Short (inch)	Aspect Ratio	Spectrum Pass	SFH (where applicable)	NW Face (inch)	SE Face (inch)	SW Face (inch)	W Bore (inch)
36807	0.03050			8.18					
42461	0.05298			9.44					
46181	0.10384			10.26		0.06570			
47296				10.51					

Table 35. Test Data, coupon 3D1-19-A.

Specimen ID	Max Stress (ksi)	"Constant Amplitude" Stress (ksi)	Cycles to Failure	Material	Thickness (inch)	Edge Margin	Nominal Final Ream Diameter (inch)	CX %	CX LEVEL
3D1-19-A	25.3	22.0	793,872	2024-T3	0.1	2.4	0.25	4.28	MAX
Cycles	NE Face, Short (inch)	E Bore, Short (inch)	Aspect Ratio	Spectrum Pass	SFH (where applicable)	NW Face (inch)	SE Face (inch)	SW Face (inch)	W Bore (inch)
76503				17 00		0.01190			
81004				18 00		0.01218			
85504				19 00		0.01348			
90005				20 00		0.01408			
94505				21 00		0.01516			
99006				22 00		0.01678			
103506				23 00		0.01684			
108007				24 00		0.01890			
112507				25 00		0.01966			
117008				26 00		0.02100			
121508				27 00		0.02174			
126009				28 00		0.02396			
130509				29 00		0.02396			0.03306
135010				30 00		0.02438			0.03616
139510				31 00		0.02712			0.03828
144011				32 00		0.02732			0.03842
148511				33 00		0.02808			0.03986
153012				34 00		0.02900			0.04454
157512				35 00		0.03090			0.04472
162013				36 00		0.03138			0.04562
166513				37 00		0.03138			0.04602
171014				38 00		0.03138			0.04814
175514				39 00		0.03212			0.04832
184515				41 00		0.03526			0.06494
193515				43 00		0.03540			0.06494
202516				45 00		0.03688			0.08030
211516				47 00		0.03692			0.08030
225017				50 00		0.03846			0.08222
238517				53 00		0.04192			0.10000
252018				56 00		0.04192			0.10000
265518				59 00		0.04278			0.10000
279019	0.01924	0.05938		62 00		0.04424			0.10000
292519	0.02484	0.08480		65 00		0.04522			0.10000
306020	0.02750	0.10000		68 00		0.04672			0.10000
319520	0.03078	0.10000		71 00		0.04986			0.10000
333021	0.03296	0.10000		74 00		0.05166			0.10000
346521	0.03556	0.10000		77 00		0.05166			0.10000
360022	0.03702	0.10000		80 00		0.05166			0.10000
373522	0.03812	0.10000		83 00		0.05402			0.10000
396023	0.04052	0.10000		88 01		0.05678			0.10000
418523	0.04324	0.10000		93 01		0.05678			0.10000
464296	0.04632	0.10000		103.18		0.05818			0.10000
793872	0.47500	0.10000		176.42		0.47500			0.10000

Table 36. Test Data, coupon 3D1-04-A.

Specimen ID	Max Stress (ksi)	"Constant Amplitude" Stress (ksi)	Cycles to Failure	Material	Thickness (inch)	Edge Margin	Nominal Final Ream Diameter (inch)	CX %	CX LEVEL
3D1-04-A	25 3	22.0	764,182	2024-T3	0.1	2.4	0 25	4.21	MAX
Cycles	NE Face, Short (inch)	E Bore, Short (inch)	Aspect Ratio	Spectrum Pass	SFH (where applicable)	NW Face (inch)	SE Face (inch)	SW Face (inch)	W Bore (inch)
141561		0.02374		31.46					
176523		0.02512		39 23					
232897				51.75			0.01420		
236177				52.48			0.01552		
241355	0.00890			53.63			0.01744		
245442	0.01452			54 54			0.01780		
253462	0.02204			56 32			0.01996		
259923	0.02548			57.76			0.02096		
265092	0.02782			58 91			0.02204		
271574	0.02872			60 35			0.02438		
282844	0.03178			62 85			0.02566		
292250	0.03420			64 94			0.02614		
302532	0.03546			67.23			0.02626		
312772	0.03838			69.50			0.02886		
322149	0.03930			71.59			0.02964	0.01054	
332179	0.04070			73.82			0.03138	0.01582	
348127	0.04394			77 36		0.02262	0.03286	0.01848	
356104	0.04550			79.13		0.02804	0.03290	0.01964	
362365	0.04770			80 53		0.02960	0.03290	0.02138	
764182				169.82					

Table 37. Test Data, coupon 3D1-05-A.

Specimen ID	Max Stress (ksi)	"Constant Amplitude" Stress (ksi)	Cycles to Failure	Material	Thickness (inch)	Edge Margin	Nominal Final Ream Diameter (inch)	CX %	CX LEVEL
3D1-05-A	25 3	22.0	262,605	2024-T3	0.1	2.4	0 25	4.18	MAX
Cycles	NE Face, Short (inch)	E Bore, Short (inch)	Aspect Ratio	Spectrum Pass	SFH (where applicable)	NW Face (inch)	SE Face (inch)	SW Face (inch)	W Bore (inch)
63548	0.01474			14.12					
71069	0.02002			15.79					
84548	0.02808			18.79					
95800	0.03312			21 29				0.01094	
104804	0.03554			23 29				0.01914	
118995	0.04014			26.44				0.02726	
132781	0.04230			29 51				0.03486	
146476	0.04602			32 55				0.04266	
154089	0.04830			34 24			0.02578	0.04562	
167477	0.05168			37 22			0.03900	0.05052	
262605				58 36					

Table 38. Test Data, coupon 3D1-06-A.

Specimen ID	Max Stress (ksi)	"Constant Amplitude" Stress (ksi)	Cycles to Failure	Material	Thickness (inch)	Edge Margin	Nominal Final Ream Diameter (inch)	CX %	CX LEVEL
3D1-06-A	25.3	22.0	640,126	2024-T3	0.1	2.4	0.25	4.15	MAX
Cycles	NE Face, Short (inch)	E Bore, Short (inch)	Aspect Ratio	Spectrum Pass	SFH (where applicable)	NW Face (inch)	SE Face (inch)	SW Face (inch)	W Bore (inch)
120558	0.00920			26.79					
131415	0.01308			29.20					
140296	0.01702			31.18					
146767	0.01958			32.61					
155865	0.02308			34.64					
166465	0.02736			36.99			0.01004		
177533	0.03050			39.45		0.01674	0.01046		
187012	0.03312			41.56		0.02304	0.01082		
237094	0.04200			52.69		0.04318	0.01574	0.01464	
251714	0.04548			55.94		0.04658	0.01714	0.01594	
272264	0.04656			60.50		0.04944	0.02104	0.02038	
291622	0.04938			64.80		0.05264	0.02254	0.02458	
319461	0.05246			70.99		0.05590	0.02482	0.02858	
352057	0.05506			78.23		0.06054	0.02722	0.03188	
379437	0.06056			84.32		0.06316	0.02810	0.03530	
410218	0.06238			91.16		0.06528	0.02952	0.03982	
432359	0.06560			96.08		0.06912	0.03150	0.04098	
640126				142.25					

Table 39. Test Data, coupon 3D1-10-A.

Specimen ID	Max Stress (ksi)	"Constant Amplitude" Stress (ksi)	Cycles to Failure	Material	Thickness (inch)	Edge Margin	Nominal Final Ream Diameter (inch)	CX %	CX LEVEL
3D1-10-A	28.75	25.0	139,877	2024-T3	0.1	2.4	0.25	4.3	MAX
Cycles	NE Face, Short (inch)	E Bore, Short (inch)	Aspect Ratio	Spectrum Pass	SFH (where applicable)	NW Face (inch)	SE Face (inch)	SW Face (inch)	W Bore (inch)
84276	0.01246								
89416	0.02326								
94436	0.03254						0.01244		
101358	0.04312						0.01512		
139877									

Table 40. Test Data, coupon 3D1-11-A.

Specimen ID	Max Stress (ksi)	"Constant Amplitude" Stress (ksi)	Cycles to Failure	Material	Thickness (inch)	Edge Margin	Nominal Final Ream Diameter (inch)	CX %	CX LEVEL
3D1-11-A	28.75	25.0	175,844	2024-T3	0.1	2.4	0.25	4.33	MAX
Cycles	NE Face, Short (inch)	E Bore, Short (inch)	Aspect Ratio	Spectrum Pass	SFH (where applicable)	NW Face (inch)	SE Face (inch)	SW Face (inch)	W Bore (inch)
96000				21.33					
131438	0.05160			29.21		0.02970	0.05384	0.03928	
153325	0.07176			34.07		0.05264	0.08634	0.04888	
171790	0.15634			38.18		0.08240	0.16966	0.06998	
175844				39.08					

Table 41. Test Data, coupon 3D1-12-A.

Specimen ID	Max Stress (ksi)	"Constant Amplitude" Stress (ksi)	Cycles to Failure	Material	Thickness (inch)	Edge Margin	Nominal Final Ream Diameter (inch)	CX %	CX LEVEL
3D1-12-A	28.75	25.0	169,598	2024-T3	0.1	2.4	0.25	4.2	MAX
Cycles	NE Face, Short (inch)	E Bore, Short (inch)	Aspect Ratio	Spectrum Pass	SFH (where applicable)	NW Face (inch)	SE Face (inch)	SW Face (inch)	W Bore (inch)
72006				16 00		0.01406	0.00590		
80471				17 88		0.02274	0.01086	0.00436	
85175				18 93		0.02600	0.01574	0.00796	
91693				20 38		0.02994	0.02118	0.00826	
96261				21 39		0.03266	0.02450	0.01076	
101373				22 53		0.03610	0.02854	0.01846	
112737				25 05		0.04362	0.03788	0.03554	
122716	0.00968			27 27		0.04784	0.04592	0.04480	
166474	0.13492			36 99		0.13132	0.14680	0.14288	
169598				37 69					

Table 42. Test Data, coupon 3D3-19-A.

Specimen ID	Max Stress (ksi)	"Constant Amplitude" Stress (ksi)	Cycles to Failure	Material	Thickness (inch)	Edge Margin	Nominal Final Ream Diameter (inch)	CX %	CX LEVEL
3D3-19-A	25.3	22.0	85,260	2024-T3	0.1	2.4	0.5	2.82	MIN
Cycles	NE Face, Short (inch)	E Bore, Short (inch)	Aspect Ratio	Spectrum Pass	SFH (where applicable)	NW Face (inch)	SE Face (inch)	SW Face (inch)	W Bore (inch)
36002				8.00		0.02598			0.06036
45003				10 00		0.04262			0.08816
54003	0.02322			12 00		0.06222			0.10000
63004	0.05494			14 00		0.09030			0.10000
72004	0.09878			16 00		0.13962			0.10000
81005	0.16642			18 00		0.25192			0.10000
85260				18 95					0.10000

Table 43. Test Data, coupon 3D3-20-A.

Specimen ID	Max Stress (ksi)	"Constant Amplitude" Stress (ksi)	Cycles to Failure	Material	Thickness (inch)	Edge Margin	Nominal Final Ream Diameter (inch)	CX %	CX LEVEL
3D3-20-A	25.3	22.0	75,385	2024-T3	0.1	2.4	0.5	2.88	MIN
Cycles	NE Face, Short (inch)	E Bore, Short (inch)	Aspect Ratio	Spectrum Pass	SFH (where applicable)	NW Face (inch)	SE Face (inch)	SW Face (inch)	W Bore (inch)
45003	0.05666					0.03530			
54003	0.09424					0.05068			
58504	0.11126					0.06968			
63004	0.14872					0.09562			
67505	0.19752					0.13032			
75385									

Table 44. Test Data, coupon 3D3-21-A.

Specimen ID	Max Stress (ksi)	"Constant Amplitude" Stress (ksi)	Cycles to Failure	Material	Thickness (inch)	Edge Margin	Nominal Final Ream Diameter (inch)	CX %	CX LEVEL
3D3-21-A	25 3	22.0	78,183	2024-T3	0.1	2.4	0.5	2.6	MIN
Cycles	NE Face, Short (inch)	E Bore, Short (inch)	Aspect Ratio	Spectrum Pass	SFH (where applicable)	NW Face (inch)	SE Face (inch)	SW Face (inch)	W Bore (inch)
45003	0.02600	0.05048		10 00		0.03038			
49503	0.03386	0.07560		11 00		0.04972			
54004	0.04468	0.09712		12 00		0.06652			
58504	0.06164	0.10000		13 00		0.09470			
63005	0.07596	0.10000		14 00		0.12488			
72005	0.13282	0.10000		16 00		0.23582			
78183		0.10000		17 37					

Table 45. Test Data, coupon 3D3-11-A.

Specimen ID	Max Stress (ksi)	"Constant Amplitude" Stress (ksi)	Cycles to Failure	Material	Thickness (inch)	Edge Margin	Nominal Final Ream Diameter (inch)	CX %	CX LEVEL
3D3-11-A	25 3	22.0	94,109	2024-T3	0.1	2.4	0.5	2.84	MIN
Cycles	NE Face, Short (inch)	E Bore, Short (inch)	Aspect Ratio	Spectrum Pass	SFH (where applicable)	NW Face (inch)	SE Face (inch)	SW Face (inch)	W Bore (inch)
45004	0.01076								
49504	0.02272								
54005	0.02590								
58505	0.02974								
63006	0.03628					0.03656			
67506	0.04908					0.04656			
72007	0.05834					0.04998			
76507	0.06930					0.05954			
85508	0.10228					0.15210			
90009	0.17114					0.23312			
94109									

Table 46. Test Data, coupon 3D3-12-A.

Specimen ID	Max Stress (ksi)	"Constant Amplitude" Stress (ksi)	Cycles to Failure	Material	Thickness (inch)	Edge Margin	Nominal Final Ream Diameter (inch)	CX %	CX LEVEL
3D3-12-A	25 3	22.0	89,611	2024-T3	0.1	2.4	0.5	2.84	MIN
Cycles	NE Face, Short (inch)	E Bore, Short (inch)	Aspect Ratio	Spectrum Pass	SFH (where applicable)	NW Face (inch)	SE Face (inch)	SW Face (inch)	W Bore (inch)
49506	0.01276			11 00					
54006	0.02975			12 00					
58507	0.06674			13 00					
63007	0.08492			14 00					
67508	0.10478			15 00		0.01400			
76509	0.15664			17 00		0.06292			
89611				19 91					

Table 47. Test Data, coupon 3D3-13-A.

Specimen ID	Max Stress (ksi)	"Constant Amplitude" Stress (ksi)	Cycles to Failure	Material	Thickness (inch)	Edge Margin	Nominal Final Ream Diameter (inch)	CX %	CX LEVEL
3D3-13-A	28.75	25.0	54,903	2024-T3	0.1	2.4	0.5	2.85	MIN
Cycles	NE Face, Short (inch)	E Bore, Short (inch)	Aspect Ratio	Spectrum Pass	SFH (where applicable)	NW Face (inch)	SE Face (inch)	SW Face (inch)	W Bore (inch)
27001	0.01198			6.00					
40502	0.03950			9.00			0.03274		
54002	0.29654			12 00			0.20458		
54903				12 20					

Table 48. Test Data, coupon 3D3-14-A.

Specimen ID	Max Stress (ksi)	"Constant Amplitude" Stress (ksi)	Cycles to Failure	Material	Thickness (inch)	Edge Margin	Nominal Final Ream Diameter (inch)	CX %	CX LEVEL
3D3-14-A	28.75	25.0	47,529	2024-T3	0.1	2.4	0.5	2.83	MIN
Cycles	NE Face, Short (inch)	E Bore, Short (inch)	Aspect Ratio	Spectrum Pass	SFH (where applicable)	NW Face (inch)	SE Face (inch)	SW Face (inch)	W Bore (inch)
27002	0.02142			6.00					
31503	0.04104			7.00		0.00726			
36003	0.04642			8.00		0.02498			
40504	0.12762			9.00		0.06094			
47529				10 56					

Table 49. Test Data, coupon 3D3-15-A.

Specimen ID	Max Stress (ksi)	"Constant Amplitude" Stress (ksi)	Cycles to Failure	Material	Thickness (inch)	Edge Margin	Nominal Final Ream Diameter (inch)	CX %	CX LEVEL
3D3-15-A	28.75	25.0	41,761	2024-T3	0.1	2.4	0.5	2.67	MIN
Cycles	NE Face, Short (inch)	E Bore, Short (inch)	Aspect Ratio	Spectrum Pass	SFH (where applicable)	NW Face (inch)	SE Face (inch)	SW Face (inch)	W Bore (inch)
18001	0.00586			4.00					
27002	0.01520			6.00					
36002	0.09412			8.00		0.07018			
41760				9.28					

Table 50. Test Data, coupon 3D1-06-B.

Specimen ID	Max Stress (ksi)	"Constant Amplitude" Stress (ksi)	Cycles to Failure	Material	Thickness (inch)	Edge Margin	Nominal Final Ream Diameter (inch)	CX %	CX LEVEL
3D1-06-B	24.15	21.0	672,840	2024-T351	0.314	1.8	0.375	3.42	MID
Cycles	NE Face, Short (inch)	E Bore, Short (inch)	Aspect Ratio	Spectrum Pass	SFH (where applicable)	NW Face (inch)	SE Face (inch)	SW Face (inch)	W Bore (inch)
133912	0.01430	0.01352		29.76					
135002	0.01430	0.01352		30 00					
148503	0.01460	0.06136		33 00					
157504	0.01932	0.06252		35 00					
166504	0.02476	0.07642		37 00					
171005	0.02706			38 00					
175505	0.02746			39 00					
180006	0.02848			40 00					
184506	0.03004			41 00					
189007	0.03136			42 00					
234007	0.04056	0.08464		52 00					
279008	0.04882			62 00					
310004	0.05226			68 89					
331909	0.05568			73.76		0.03562			
672840				149.52					

Table 51. Test Data, coupon 3D1-12-B.

Specimen ID	Max Stress (ksi)	"Constant Amplitude" Stress (ksi)	Cycles to Failure	Material	Thickness (inch)	Edge Margin	Nominal Final Ream Diameter (inch)	CX %	CX LEVEL
3D1-12-B	24.15	21.0	272,797	2024-T351	0.314	1.8	0.375	3.37	MID
Cycles	NE Face, Short (inch)	E Bore, Short (inch)	Aspect Ratio	Spectrum Pass	SFH (where applicable)	NW Face (inch)	SE Face (inch)	SW Face (inch)	W Bore (inch)
139511	0.01148			31 00					
162012	0.06836			36 00					
175512	0.08214	0.16960		39 00					
189013	0.09052	0.19048		42 00					
202513	0.09938	0.20992		45 00					
216014	0.10650	0.23106		48.00					
229514	0.11140	0.24614		51.00		0.04070			0.05032
243015	0.12024	0.26644		54.00		0.05272			0.07446
256615	0.14098	0.28198		57.03		0.06996			0.20770
270016	0.29528	0.31400		60.00		0.08632			0.20770
272750				60.61					
272797				60.62					

Table 52. Test Data, coupon 3D1-01-B.

Specimen ID	Max Stress (ksi)	"Constant Amplitude" Stress (ksi)	Cycles to Failure	Material	Thickness (inch)	Edge Margin	Nominal Final Ream Diameter (inch)	CX %	CX LEVEL
3D1-01-B	25.30	22.0	231,036	2024-T351	0.314	1.8	0.375	3.36	MID
Cycles	NE Face, Short (inch)	E Bore, Short (inch)	Aspect Ratio	Spectrum Pass	SFH (where applicable)	NW Face (inch)	SE Face (inch)	SW Face (inch)	W Bore (inch)
61510	0.01460			13.67					
67474	0.01828			14.99					
75591	0.02036			16.80					
88048	0.03098			19.57					
92661	0.03340			20.59					
97530	0.03932			21.67					
106124	0.04840			23.58					
111359	0.05266			24.75		0.05732			
117734	0.05762			26.16		0.06724			
126404	0.06204			28.09		0.07300			
133373	0.07056			29.64		0.07528			
142815	0.07128			31.74		0.07854			
153098	0.07828			34.02		0.08432			
165666	0.08480			36.81		0.08756			
174309	0.08854			38.74		0.09160			
184597	0.09568			41.02		0.09640			
200021	0.10452			44.45		0.10736			
210402	0.11356			46.76		0.11890			
220668	0.12718			49.04		0.15368			
231036	0.3140			51.34					

Table 53. Test Data, coupon 3D1-02-B.

Specimen ID	Max Stress (ksi)	"Constant Amplitude" Stress (ksi)	Cycles to Failure	Material	Thickness (inch)	Edge Margin	Nominal Final Ream Diameter (inch)	CX %	CX LEVEL
3D1-02-B	25.30	22.0	408,988	2024-T351	0.314	1.8	0.375	3.4	MID
Cycles	NE Face, Short (inch)	E Bore, Short (inch)	Aspect Ratio	Spectrum Pass	SFH (where applicable)	NW Face (inch)	SE Face (inch)	SW Face (inch)	W Bore (inch)
76455	0.00630			16.99					
80993	0.00718			18.00					
85746	0.00754			19.05					
90465	0.00856			20.10					
95224	0.00952			21.16		0.00612			
99282	0.01056			22.06		0.00622			
105037	0.01484			23.34		0.00628			
111442	0.01836			24.76		0.00794			
117286	0.02212			26.06		0.00864			
121823	0.02546			27.07		0.00986			
131137	0.03582			29.14		0.01356			
143209	0.04424			31.82		0.01828			
152223	0.04974			33.83		0.02536			
162190	0.05430			36.04		0.02820			
174824	0.05940			38.85		0.03312			
196681	0.06554			43.71		0.04106	0.04202		
217076	0.07158			48.24		0.04960	0.04688		
236421	0.07592			52.54		0.05618	0.05180		
330485	0.09696			73.44		0.07822			
361098	0.1054			80.24		0.08436			
408988				90.89					

Table 54. Test Data, coupon 3D1-03-B.

Specimen ID	Max Stress (ksi)	"Constant Amplitude" Stress (ksi)	Cycles to Failure	Material	Thickness (inch)	Edge Margin	Nominal Final Ream Diameter (inch)	CX %	CX LEVEL
3D1-03-B	25.30	22.0	266,994	2024-T351	0.314	1.8	0.375	3.36	MID
Cycles	NE Face, Short (inch)	E Bore, Short (inch)	Aspect Ratio	Spectrum Pass	SFH (where applicable)	NW Face (inch)	SE Face (inch)	SW Face (inch)	W Bore (inch)
53934	0.01088			11 99					
63419	0.01696			14 09					
66938	0.01964			14 88					
72470	0.02366			16.10					
80969	0.03022			17 99					
84204	0.03212			18.71					
90900	0.03452			20 20					
96276	0.03924			21 39					
106245	0.04396			23.61			0.01488		
113997	0.04694			25 33			0.02448		
121679	0.05008			27 04			0.03232	0.01508	
133108	0.05366			29 58			0.03972	0.02842	
139800	0.05584			31 07			0.04332	0.03214	
148748	0.05890			33 06		0.01312	0.04772	0.03654	
153909	0.05952			34 20		0.02056	0.04940	0.03722	
203386	0.07972			45 20		0.07208	0.06500	0.04926	
252815	0.11620			56.18		0.09742	0.09780	0.05908	
266369	0.23358			59.19		0.11872	0.27368	0.07024	
266994				59 33					

Table 55. Test Data, coupon 3D1-04-B.

Specimen ID	Max Stress (ksi)	"Constant Amplitude" Stress (ksi)	Cycles to Failure	Material	Thickness (inch)	Edge Margin	Nominal Final Ream Diameter (inch)	CX %	CX LEVEL
3D1-04-B	25.30	22.0	223,229	2024-T351	0.314	1.8	0.375	3.4	MID
Cycles	NE Face, Short (inch)	E Bore, Short (inch)	Aspect Ratio	Spectrum Pass	SFH (where applicable)	NW Face (inch)	SE Face (inch)	SW Face (inch)	W Bore (inch)
73043	0.00464			16 23					
86364	0.00948			19.19					
95359	0.01458			21.19		0.00750			
107397	0.02402			23 87		0.01306			
118250	0.03246			26 28		0.02334			
125077	0.03656			27.79		0.02830			
133411	0.04220			29.65		0.03686	0.00602		
160010	0.05774			35 56		0.06692			
180048	0.06858			40 01		0.08540	0.01430		
201923	0.07840			44 87		0.10746	0.01610		
210553	0.08144			46.79		0.12712	0.01820	0.01572	
215354	0.08572			47 86		0.15870	0.02290	0.03954	
223229				49.61					

Table 56. Test Data, coupon 3D1-05-B.

Specimen ID	Max Stress (ksi)	"Constant Amplitude" Stress (ksi)	Cycles to Failure	Material	Thickness (inch)	Edge Margin	Nominal Final Ream Diameter (inch)	CX %	CX LEVEL
3D1-05-B	25.30	22.0	348,660	2024-T351	0.314	1.8	0.375	3.4	MID
Cycles	NE Face, Short (inch)	E Bore, Short (inch)	Aspect Ratio	Spectrum Pass	SFH (where applicable)	NW Face (inch)	SE Face (inch)	SW Face (inch)	W Bore (inch)
55740	0.00684			12 39					
69237	0.01378			15 39					
76946	0.02046			17 10					
85761	0.02990			19 06					
97615	0.04226			21 69		0.01240			
106763	0.04740			23 73		0.02050	0.00552		
116431	0.05500			25 87		0.02944	0.00626		
126155	0.05960			28 03		0.03606	0.00726		
142993	0.06732			31 78		0.05076	0.01308		
348660				77 48					

Table 57. Test Data, coupon 3D1-07-B.

Specimen ID	Max Stress (ksi)	"Constant Amplitude" Stress (ksi)	Cycles to Failure	Material	Thickness (inch)	Edge Margin	Nominal Final Ream Diameter (inch)	CX %	CX LEVEL
3D1-07-B	28.75	25.0	129,663	2024-T351	0.314	1.8	0.375	3.44	MID
Cycles	NE Face, Short (inch)	E Bore, Short (inch)	Aspect Ratio	Spectrum Pass	SFH (where applicable)	NW Face (inch)	SE Face (inch)	SW Face (inch)	W Bore (inch)
56064	0.00518			12 46					
62168	0.00772			13 82					
71290	0.01226			15 84					
79918	0.01946			17 76		0.00728			
88689	0.03212			19 71		0.05106			
97068	0.05548			21 57		0.06894		0.03894	
103863	0.06550			23 08		0.08138		0.05004	
129663				28 81					

Table 58. Test Data, coupon 3D1-08-B.

Specimen ID	Max Stress (ksi)	"Constant Amplitude" Stress (ksi)	Cycles to Failure	Material	Thickness (inch)	Edge Margin	Nominal Final Ream Diameter (inch)	CX %	CX LEVEL
3D1-08-B	28.75	25.0	96,891	2024-T351	0.314	1.8	0.375	3.41	MID
Cycles	NE Face, Short (inch)	E Bore, Short (inch)	Aspect Ratio	Spectrum Pass	SFH (where applicable)	NW Face (inch)	SE Face (inch)	SW Face (inch)	W Bore (inch)
54117				12 03		0.00738			
58763				13 06		0.01390			
68161	0.03912			15 15		0.02228			
74936	0.06406			16 65		0.03218			
79310	0.07940			17 62		0.04248			
96891				21 53					

Table 59. Test Data, coupon 3D1-09-B.

Specimen ID	Max Stress (ksi)	"Constant Amplitude" Stress (ksi)	Cycles to Failure	Material	Thickness (inch)	Edge Margin	Nominal Final Ream Diameter (inch)	CX %	CX LEVEL
3D1-09-B	28.75	25.0	105,194	2024-T351	0.314	1.8	0.375	3.42	MID
Cycles	NE Face, Short (inch)	E Bore, Short (inch)	Aspect Ratio	Spectrum Pass	SFH (where applicable)	NW Face (inch)	SE Face (inch)	SW Face (inch)	W Bore (inch)
60995	0.00966			13 55					
64809	0.01324			14.40					
69475	0.01764			15.44		0.01280			
73072	0.02388			16 24		0.03838	0.08700		
92307	0.08164			20 51		0.08800			
98273	0.10816			21 84		0.11258			
105194				23 38					

Table 60. Test Data, coupon 3D1-10-B.

Specimen ID	Max Stress (ksi)	"Constant Amplitude" Stress (ksi)	Cycles to Failure	Material	Thickness (inch)	Edge Margin	Nominal Final Ream Diameter (inch)	CX %	CX LEVEL
3D1-10-B	28.75	25.0	97,752	2024-T351	0.314	1.8	0.375	3.42	MID
Cycles	NE Face, Short (inch)	E Bore, Short (inch)	Aspect Ratio	Spectrum Pass	SFH (where applicable)	NW Face (inch)	SE Face (inch)	SW Face (inch)	W Bore (inch)
59727	0.01470			13 27					
75439	0.07572			16.76					
93077	0.16210			20.68		0.05338			
97572				21.68					

Table 61. Test Data, coupon 3D1-11-B.

Specimen ID	Max Stress (ksi)	"Constant Amplitude" Stress (ksi)	Cycles to Failure	Material	Thickness (inch)	Edge Margin	Nominal Final Ream Diameter (inch)	CX %	CX LEVEL
3D1-11-B	28.75	25.0	92,889	2024-T351	0.314	1.8	0.375	3.42	MID
Cycles	NE Face, Short (inch)	E Bore, Short (inch)	Aspect Ratio	Spectrum Pass	SFH (where applicable)	NW Face (inch)	SE Face (inch)	SW Face (inch)	W Bore (inch)
66531	0.04252			14.78		0.05980			
92886				20.64					

Table 62. Test Data, coupon 3D1-35-B.

Specimen ID	Max Stress (ksi)	"Constant Amplitude" Stress (ksi)	Cycles to Failure	Material	Thickness (inch)	Edge Margin	Nominal Final Ream Diameter (inch)	CX %	CX LEVEL
3D1-35-B	25.3	22.0	84,778	2024-T351	0.5	1.39	0.25	4.33	MAX
Cycles	NE Face, Short (inch)	E Bore, Short (inch)	Aspect Ratio	Spectrum Pass	SFH (where applicable)	NW Face (inch)	SE Face (inch)	SW Face (inch)	W Bore (inch)
54002				12.00		0.02402			
58503				13.00		0.03072			0.04280
63003				14.00		0.04238			
67504				15.00		0.05624			
83405				18.53					
84778				18.84					

Table 63. Test Data, coupon 3D1-36-B.

Specimen ID	Max Stress (ksi)	"Constant Amplitude" Stress (ksi)	Cycles to Failure	Material	Thickness (inch)	Edge Margin	Nominal Final Ream Diameter (inch)	CX %	CX LEVEL
3D1-36-B	25.3	22.0	109,346	2024-T351	0.5	1.39	0.25	4.28	MAX
Cycles	NE Face, Short (inch)	E Bore, Short (inch)	Aspect Ratio	Spectrum Pass	SFH (where applicable)	NW Face (inch)	SE Face (inch)	SW Face (inch)	W Bore (inch)
85508	0.02784			19.00					
90008	0.03826			20.00					
94509	0.05294			21.00					
103509	0.11726			23.00					
108700	0.22878			24.16					
109346				24.30					

Table 64. Test Data, coupon 3D1-37-B.

Specimen ID	Max Stress (ksi)	"Constant Amplitude" Stress (ksi)	Cycles to Failure	Material	Thickness (inch)	Edge Margin	Nominal Final Ream Diameter (inch)	CX %	CX LEVEL
3D1-37-B	25.3	22.0	104,392	2024-T351	0.5	1.39	0.25	4.22	MAX
Cycles	NE Face, Short (inch)	E Bore, Short (inch)	Aspect Ratio	Spectrum Pass	SFH (where applicable)	NW Face (inch)	SE Face (inch)	SW Face (inch)	W Bore (inch)
81004	0.02380			18.00					
90004	0.06696			20.00					
99005	0.13432			22.00					
103101	0.22084			22.91					
104392				23.20					

Table 65. Test Data, coupon 3D1-38-B.

Specimen ID	Max Stress (ksi)	"Constant Amplitude" Stress (ksi)	Cycles to Failure	Material	Thickness (inch)	Edge Margin	Nominal Final Ream Diameter (inch)	CX %	CX LEVEL
3D1-38-B	28.75	25.0	54,670	2024-T351	0.5	1.39	0.25	4.2	MAX
Cycles	NE Face, Short (inch)	E Bore, Short (inch)	Aspect Ratio	Spectrum Pass	SFH (where applicable)	NW Face (inch)	SE Face (inch)	SW Face (inch)	W Bore (inch)
45005	0.00938			10.00					
46794	0.02768			10.40					
47711	0.04044			10.60					
49506	0.06812			11.00					
53426	0.19954			11.87					
54006	0.19954			12.00					
54670				12.15					

Table 66. Test Data, coupon 3D1-39-B.

Specimen ID	Max Stress (ksi)	"Constant Amplitude" Stress (ksi)	Cycles to Failure	Material	Thickness (inch)	Edge Margin	Nominal Final Ream Diameter (inch)	CX %	CX LEVEL
3D1-39-B	28.75	25.0	56,784	2024-T351	0.5	1.39	0.25	4.38	MAX
Cycles	NE Face, Short (inch)	E Bore, Short (inch)	Aspect Ratio	Spectrum Pass	SFH (where applicable)	NW Face (inch)	SE Face (inch)	SW Face (inch)	W Bore (inch)
45005	0.00784			10.00					
48234	0.01998			10.72					
49506	0.02136			11.00					
50549	0.04178			11.23					
52243	0.05326			11.61					
54006	0.08770			12.00					
55934	0.16012			12.43					
56145	0.18752			12.48					
56226	0.21020			12.49					
56784				12.62					

Table 67. Test Data, coupon 3D1-40-B.

Specimen ID	Max Stress (ksi)	"Constant Amplitude" Stress (ksi)	Cycles to Failure	Material	Thickness (inch)	Edge Margin	Nominal Final Ream Diameter (inch)	CX %	CX LEVEL
3D1-40-B	28.75	25.0	49,678	2024-T351	0.5	1.39	0.25	4.21	MAX
Cycles	NE Face, Short (inch)	E Bore, Short (inch)	Aspect Ratio	Spectrum Pass	SFH (where applicable)	NW Face (inch)	SE Face (inch)	SW Face (inch)	W Bore (inch)
41788	0.01488			9.29					
42916	0.03400			9.54					
44501	0.06398			9.89					
45005	0.07612			10.00					
46707	0.99100			10.38					
47603	0.13242			10.58					
47983	0.14762			10.66					
48496	0.22258			10.78					
49678				11.04					

Table 68. Test Data, coupon 3D1-44-B.

Specimen ID	Max Stress (ksi)	"Constant Amplitude" Stress (ksi)	Cycles to Failure	Material	Thickness (inch)	Edge Margin	Nominal Final Ream Diameter (inch)	CX %	CX LEVEL
3D1-44-B	25.3	22.0	120,479	2024-T351	0.5	1.39	0.5	2.93	MIN
Cycles	NE Face, Short (inch)	E Bore, Short (inch)	Aspect Ratio	Spectrum Pass	SFH (where applicable)	NW Face (inch)	SE Face (inch)	SW Face (inch)	W Bore (inch)
94504				21 00		0.01064			
99004				22 00		0.04092			
103505				23 00		0.07282			
108005	0.03640			24 00		0.10000			
112506	0.05784			25 00		0.12202			
117006	0.08630			26 00		0.16650			
120479				26.77					

Table 69. Test Data, coupon 3D1-45-B.

Specimen ID	Max Stress (ksi)	"Constant Amplitude" Stress (ksi)	Cycles to Failure	Material	Thickness (inch)	Edge Margin	Nominal Final Ream Diameter (inch)	CX %	CX LEVEL
3D1-45-B	25.3	22.0	89,021	2024-T351	0.5	1.39	0.5	2.99	MIN
Cycles	NE Face, Short (inch)	E Bore, Short (inch)	Aspect Ratio	Spectrum Pass	SFH (where applicable)	NW Face (inch)	SE Face (inch)	SW Face (inch)	W Bore (inch)
45001				10 00					
63002	0.01270			14 00					
81002	0.06678			18 00					
89021				19.78					

Table 70. Test Data, coupon 3D1-46-B.

Specimen ID	Max Stress (ksi)	"Constant Amplitude" Stress (ksi)	Cycles to Failure	Material	Thickness (inch)	Edge Margin	Nominal Final Ream Diameter (inch)	CX %	CX LEVEL
3D1-46-B	25.3	22.0	115,194	2024-T351	0.5	1.39	0.5	2.97	MIN
Cycles	NE Face, Short (inch)	E Bore, Short (inch)	Aspect Ratio	Spectrum Pass	SFH (where applicable)	NW Face (inch)	SE Face (inch)	SW Face (inch)	W Bore (inch)
72003	0.02798			16 00					
76503	0.04346			17 00					
81004	0.06128			18 00					
85504	0.07272			19 00					
90005	0.08860			20 00		0.02828			
94505	0.09814			21 00		0.03988			
99006	0.10706			22 00		0.05240			
108006	0.13556			24 00		0.10276			
115194				25.60					

Table 71. Test Data, coupon 3D1-50-B.

Specimen ID	Max Stress (ksi)	"Constant Amplitude" Stress (ksi)	Cycles to Failure	Material	Thickness (inch)	Edge Margin	Nominal Final Ream Diameter (inch)	CX %	CX LEVEL
3D1-50-B	28.75	25.0	35,251	2024-T351	0.5	1.39	0.5	3.02	MIN
Cycles	NE Face, Short (inch)	E Bore, Short (inch)	Aspect Ratio	Spectrum Pass	SFH (where applicable)	NW Face (inch)	SE Face (inch)	SW Face (inch)	W Bore (inch)
31503	0.04264			7.00					

Table 72. Test Data, coupon 3D1-51-B.

Specimen ID	Max Stress (ksi)	"Constant Amplitude" Stress (ksi)	Cycles to Failure	Material	Thickness (inch)	Edge Margin	Nominal Final Ream Diameter (inch)	CX %	CX LEVEL
3D1-51-B	28.75	25.0	49,106	2024-T351	0.5	1.39	0.5	2.96	MIN
Cycles	NE Face, Short (inch)	E Bore, Short (inch)	Aspect Ratio	Spectrum Pass	SFH (where applicable)	NW Face (inch)	SE Face (inch)	SW Face (inch)	W Bore (inch)
49106				10 91					
no prior crack detected with visual inspections every MB pass									

Table 73. Test Data, coupon 3D1-52-B.

Specimen ID	Max Stress (ksi)	"Constant Amplitude" Stress (ksi)	Cycles to Failure	Material	Thickness (inch)	Edge Margin	Nominal Final Ream Diameter (inch)	CX %	CX LEVEL
3D1-52-B	28.75	25.0	43,309	2024-T351	0.5	1.39	0.5	2.95	MIN
Cycles	NE Face, Short (inch)	E Bore, Short (inch)	Aspect Ratio	Spectrum Pass	SFH (where applicable)	NW Face (inch)	SE Face (inch)	SW Face (inch)	W Bore (inch)
36004	0.01654			8.00					
37997	0.02618			8.44					
40505	0.06370			9.00					
43309				9.62					

Table 74. Test Data, coupon 3D1-59-B.

Specimen ID	Max Stress (ksi)	"Constant Amplitude" Stress (ksi)	Cycles to Failure	Material	Thickness (inch)	Edge Margin	Nominal Final Ream Diameter (inch)	CX %	CX LEVEL
3D1-59-B	24.15	21.0	335,835	2024-T351	0.5	2.4	0.25	2.72	MIN
Cycles	NE Face, Short (inch)	E Bore, Short (inch)	Aspect Ratio	Spectrum Pass	SFH (where applicable)	NW Face (inch)	SE Face (inch)	SW Face (inch)	W Bore (inch)
202504	0.01818	0.02202		45 00					
225004	0.02896	0.05256		50 00					
247505	0.06316	0.07760		55 00					
270005	0.08700	0.10648		60 00					
335835				74.63					

Table 75. Test Data, coupon 3D1-60-B.

Specimen ID	Max Stress (ksi)	"Constant Amplitude" Stress (ksi)	Cycles to Failure	Material	Thickness (inch)	Edge Margin	Nominal Final Ream Diameter (inch)	CX %	CX LEVEL
3D1-60-B	24.15	21.0	274,997	2024-T351	0.5	2.4	0.25	2.7	MIN
Cycles	NE Face, Short (inch)	E Bore, Short (inch)	Aspect Ratio	Spectrum Pass	SFH (where applicable)	NW Face (inch)	SE Face (inch)	SW Face (inch)	W Bore (inch)
157504				35 00		0.01942			0.04432
180004	0.04022	0.05664		40 00		0.03306			0.08160
184505	0.04608	0.05664		41 00		0.04158			0.08235
189005	0.05408	0.05780		42 00		0.04826			0.08235
193506	0.05408	0.07218		43 00		0.05804			0.09508
238507	0.09438			53 00		0.11706			
274997				61.11					

Table 76. Test Data, coupon 3D1-41-B.

Specimen ID	Max Stress (ksi)	"Constant Amplitude" Stress (ksi)	Cycles to Failure	Material	Thickness (inch)	Edge Margin	Nominal Final Ream Diameter (inch)	CX %	CX LEVEL
3D1-41-B	25.30	22.0	428,956	2024-T351	0.5	2.4	0.25	2.74	MIN
Cycles	NE Face, Short (inch)	E Bore, Short (inch)	Aspect Ratio	Spectrum Pass	SFH (where applicable)	NW Face (inch)	SE Face (inch)	SW Face (inch)	W Bore (inch)
378030	0.04606	0.01112		84 01					
382530	0.05492	0.11216		85 01					
391531	0.07510	0.11436		87 01					
428956				95 32					

Table 77. Test Data, coupon 3D1-42-B.

Specimen ID	Max Stress (ksi)	"Constant Amplitude" Stress (ksi)	Cycles to Failure	Material	Thickness (inch)	Edge Margin	Nominal Final Ream Diameter (inch)	CX %	CX LEVEL
3D1-42-B	25.30	22.0	250,432	2024-T351	0.5	2.4	0.25	2.66	MIN
Cycles	NE Face, Short (inch)	E Bore, Short (inch)	Aspect Ratio	Spectrum Pass	SFH (where applicable)	NW Face (inch)	SE Face (inch)	SW Face (inch)	W Bore (inch)
158000				35.11					
199915	0.02316			44.43					
202505	0.03138			45 00					
204054	0.03688			45 35					
207006	0.04804			46 00					
211506	0.06238			47 00					
226351	0.10736			50 30					
250452				55.66					

Table 78. Test Data, coupon 3D1-43-B.

Specimen ID	Max Stress (ksi)	"Constant Amplitude" Stress (ksi)	Cycles to Failure	Material	Thickness (inch)	Edge Margin	Nominal Final Ream Diameter (inch)	CX %	CX LEVEL
3D1-43-B	25.30	22.0	343,509	2024-T351	0.5	2.4	0.25	2.78	MIN
Cycles	NE Face, Short (inch)	E Bore, Short (inch)	Aspect Ratio	Spectrum Pass	SFH (where applicable)	NW Face (inch)	SE Face (inch)	SW Face (inch)	W Bore (inch)
297007				66 00		0.03284			
299433				66 54		0.04756			
313687				69.71		0.09152			
321242				71 39		0.11602			
343309				76 29					

Table 79. Test Data, coupon 3D1-47-B.

Specimen ID	Max Stress (ksi)	"Constant Amplitude" Stress (ksi)	Cycles to Failure	Material	Thickness (inch)	Edge Margin	Nominal Final Ream Diameter (inch)	CX %	CX LEVEL
3D1-47-B	28.75	25.0	113,007	2024-T351	0.5	2.4	0.25	2.8	MIN
Cycles	NE Face, Short (inch)	E Bore, Short (inch)	Aspect Ratio	Spectrum Pass	SFH (where applicable)	NW Face (inch)	SE Face (inch)	SW Face (inch)	W Bore (inch)
67508				15 00		0.02212			
76508				17 00		0.03252			
85509	0.03254			19 00		0.04384			
106314	0.17034			23.63		0.10724			
113007				25.11					

Table 80. Test Data, coupon 3D1-48-B.

Specimen ID	Max Stress (ksi)	"Constant Amplitude" Stress (ksi)	Cycles to Failure	Material	Thickness (inch)	Edge Margin	Nominal Final Ream Diameter (inch)	CX %	CX LEVEL
3D1-48-B	28.75	25.0	99,183	2024-T351	0.5	2.4	0.25	2.58	MIN
Cycles	NE Face, Short (inch)	E Bore, Short (inch)	Aspect Ratio	Spectrum Pass	SFH (where applicable)	NW Face (inch)	SE Face (inch)	SW Face (inch)	W Bore (inch)
54001	0.02044			12 00					
56533	0.02906			12 56					
58502	0.02946			13 00					
63002	0.04062			14 00					
67503	0.05054			15 00					
72003	0.06684			16 00					
81004	0.09632			18 00					
90005	0.15226			20 00					
94506	0.21582			21 00		0.05202			
99006				22 00		0.13194			
99183				22 04					

Table 81. Test Data, coupon 3D1-49-B.

Specimen ID	Max Stress (ksi)	"Constant Amplitude" Stress (ksi)	Cycles to Failure	Material	Thickness (inch)	Edge Margin	Nominal Final Ream Diameter (inch)	CX %	CX LEVEL
3D1-49-B	28.75	25.0	128,659	2024-T351	0.5	2.4	0.25	2.73	MIN
Cycles	NE Face, Short (inch)	E Bore, Short (inch)	Aspect Ratio	Spectrum Pass	SFH (where applicable)	NW Face (inch)	SE Face (inch)	SW Face (inch)	W Bore (inch)
128659									
	fractured without detectable crack								

Table 82. Test Data, coupon 3D1-17-B.

Specimen ID	Max Stress (ksi)	"Constant Amplitude" Stress (ksi)	Cycles to Failure	Material	Thickness (inch)	Edge Margin	Nominal Final Ream Diameter (inch)	CX %	CX LEVEL
3D3-17-B	25.30	22.0	755,006	2024-T351	0.5	2.4	0.5	4	MAX
Cycles	NE Face, Short (inch)	E Bore, Short (inch)	Aspect Ratio	Spectrum Pass	SFH (where applicable)	NW Face (inch)	SE Face (inch)	SW Face (inch)	W Bore (inch)
755,006									
	NO DATA								

Table 83. Test Data, coupon 3D1-18-B.

Specimen ID	Max Stress (ksi)	"Constant Amplitude" Stress (ksi)	Cycles to Failure	Material	Thickness (inch)	Edge Margin	Nominal Final Ream Diameter (inch)	CX %	CX LEVEL
3D3-18-B	25.30	22.0	664,477	2024-T351	0.5	2.4	0.5	3.94	MAX
Cycles	NE Face, Short (inch)	E Bore, Short (inch)	Aspect Ratio	Spectrum Pass	SFH (where applicable)	NW Face (inch)	SE Face (inch)	SW Face (inch)	W Bore (inch)
664,477									
	NO DATA								

Table 84. Test Data, coupon 3D1-30-B.

Specimen ID	Max Stress (ksi)	"Constant Amplitude" Stress (ksi)	Cycles to Failure	Material	Thickness (inch)	Edge Margin	Nominal Final Ream Diameter (inch)	CX %	CX LEVEL
3D3-30-B	25.30	22.0	743,830	2024-T351	0.5	2.4	0.5	3.94	MAX
Cycles	NE Face, Short (inch)	E Bore, Short (inch)	Aspect Ratio	Spectrum Pass	SFH (where applicable)	NW Face (inch)	SE Face (inch)	SW Face (inch)	W Bore (inch)
190,652				42 37			0.01464		
211458				46 99			0.02100		
226839				50.41			0.02714		
239647				53 25			0.03034		
249638				55.48			0.03256	0.02002	
281498				62 56			0.03796	0.03188	
311461				69 21			0.04194	0.04000	
332307				73 85			0.04382	0.04402	
352145	0.06606			78 25			0.04716	0.04820	
364027	0.07588			80 89			0.04740	0.04902	
387767	0.09162			86.17			0.05010	0.05318	
412227	0.10470			91.61		0.01578	0.05040	0.05538	
460143	0.12308			102.25		0.05938	0.05072	0.06046	
743830				165.30					

Table 85. Test Data, coupon 3D1-16-B.

Specimen ID	Max Stress (ksi)	"Constant Amplitude" Stress (ksi)	Cycles to Failure	Material	Thickness (inch)	Edge Margin	Nominal Final Ream Diameter (inch)	CX %	CX LEVEL
3D3-16-B	27.00	23.5	271,111	2024-T351	0.5	2.4	0.5	4.05	MAX
Cycles	NE Face, Short (inch)	E Bore, Short (inch)	Aspect Ratio	Spectrum Pass	SFH (where applicable)	NW Face (inch)	SE Face (inch)	SW Face (inch)	W Bore (inch)
271,111									
	NO DATA								

Table 86. Test Data, coupon 3D1-28-B.

Specimen ID	Max Stress (ksi)	"Constant Amplitude" Stress (ksi)	Cycles to Failure	Material	Thickness (inch)	Edge Margin	Nominal Final Ream Diameter (inch)	CX %	CX LEVEL
3D3-28-B	28.75	25.0	156 057	2024-T351	0.5	2.4	0.5	3.97	MAX
Cycles	NE Face, Short (inch)	E Bore, Short (inch)	Aspect Ratio	Spectrum Pass	SFH (where applicable)	NW Face (inch)	SE Face (inch)	SW Face (inch)	W Bore (inch)
86,507				19 22				0.03258	
100061				22 24			0.06536	0.04238	
128942	0.14228			28.65			0.10870	0.07736	
156057				34.68					

Table 87. Test Data, coupon 3D1-29-B.

Specimen ID	Max Stress (ksi)	"Constant Amplitude" Stress (ksi)	Cycles to Failure	Material	Thickness (inch)	Edge Margin	Nominal Final Ream Diameter (inch)	CX %	CX LEVEL
3D3-29-B	28.75	25.0	189,594	2024-T351	0.5	2.4	0.5	3.95	MAX
Cycles	NE Face, Short (inch)	E Bore, Short (inch)	Aspect Ratio	Spectrum Pass	SFH (where applicable)	NW Face (inch)	SE Face (inch)	SW Face (inch)	W Bore (inch)
32,989				7.33			0.00950		
42776				9.51			0.01256		
52225				11.61			0.02120		
61939				13.76			0.02896		
102615				22.80			0.06290		
116239				25.83		0.04638	0.07342	0.02676	
126676				28.15		0.09082	0.07718	0.03620	
136853				30.41		0.11932	0.08430	0.04286	
156577	0.11062			34.79		0.15854	0.09350	0.04566	
175584	0.16146			39.02		0.22104	0.10172	0.04702	
189594				42.13					

Table 88. Test Data, coupon 3D1-15-B.

Specimen ID	Max Stress (ksi)	"Constant Amplitude" Stress (ksi)	Cycles to Failure	Material	Thickness (inch)	Edge Margin	Nominal Final Ream Diameter (inch)	CX %	CX LEVEL
3D3-15-B	30.00	25.0	218,279	2024-T351	0.5	2.4	0.5	3.98	MAX
Cycles	NE Face, Short (inch)	E Bore, Short (inch)	Aspect Ratio	Spectrum Pass	SFH (where applicable)	NW Face (inch)	SE Face (inch)	SW Face (inch)	W Bore (inch)
218,279									
	NO DATA								

Table 89. Test Data, coupon 3D1-16-C.

Specimen ID	Max Stress (ksi)	"Constant Amplitude" Stress (ksi)	Cycles to Failure	Material	Thickness (inch)	Edge Margin	Nominal Final Ream Diameter (inch)	CX %	CX LEVEL
3D1-16-C	27.6	24.0	61,085	7075-T6	0.1	1.39	0.25	2.76	MIN
Cycles	NE Face, Short (inch)	E Bore, Short (inch)	Aspect Ratio	Spectrum Pass	SFH (where applicable)	NW Face (inch)	SE Face (inch)	SW Face (inch)	W Bore (inch)
45279				10.06			0.0198		
49436				10.99			0.0256		
53097	0.0539			11.80			0.0324		
55072	0.08250			12.24			0.0417		
57212	0.22200			12.71			0.2220		
61085				13.57					

Table 90. Test Data, coupon 3D1-17-C.

Specimen ID	Max Stress (ksi)	"Constant Amplitude" Stress (ksi)	Cycles to Failure	Material	Thickness (inch)	Edge Margin	Nominal Final Ream Diameter (inch)	CX %	CX LEVEL
3D1-17-C	27.6	24.0	46,456	7075-T6	0.1	1.39	0.25	2.83	MIN
Cycles	NE Face, Short (inch)	E Bore, Short (inch)	Aspect Ratio	Spectrum Pass	SFH (where applicable)	NW Face (inch)	SE Face (inch)	SW Face (inch)	W Bore (inch)
45279				10.06			0.0198		
49436				10.99			0.0256		
53097	0.0539			11.80			0.0324		
55072	0.08250			12.24			0.0417		
57212	0.22200			12.71			0.2220		
61085				13.57					

Table 91. Test Data, coupon 3D1-18-C.

Specimen ID	Max Stress (ksi)	"Constant Amplitude" Stress (ksi)	Cycles to Failure	Material	Thickness (inch)	Edge Margin	Nominal Final Ream Diameter (inch)	CX %	CX LEVEL
3D1-18-C	27.6	24.0	39,843	7075-T6	0.1	1.39	0.25	2.57	MIN
Cycles	NE Face, Short (inch)	E Bore, Short (inch)	Aspect Ratio	Spectrum Pass	SFH (where applicable)	NW Face (inch)	SE Face (inch)	SW Face (inch)	W Bore (inch)
24150				5.37			0.0302		
25909				5.76			0.0335		
29186				6.49			0.0401		
32196				7.15			0.0490		
35130				7.81			0.0731		
37028	0.0240			8.23			0.1043		
38022	0.2345			8.45			0.2345		
39305				8.73				0.0349	
39843				8.85					

Table 92. Test Data, coupon 3D1-13-C.

Specimen ID	Max Stress (ksi)	"Constant Amplitude" Stress (ksi)	Cycles to Failure	Material	Thickness (inch)	Edge Margin	Nominal Final Ream Diameter (inch)	CX %	CX LEVEL
3D1-13-C	30.48	26.5	18,318	7075-T6	0.1	1.39	0.25	2.69	MIN
Cycles	NE Face, Short (inch)	E Bore, Short (inch)	Aspect Ratio	Spectrum Pass	SFH (where applicable)	NW Face (inch)	SE Face (inch)	SW Face (inch)	W Bore (inch)
11924	0.02618			2.65					
13016	0.03674			2.89					
13530	0.0388			3.01					
14545	0.04920			3.23					
15535	0.06290			3.45					
16875	0.1015			3.75			0.0638	0.01360	
18021	0.2286			4.00			0.2286	0.0313	
18318				4.07					

Table 93. Test Data, coupon 3D1-14-C.

Specimen ID	Max Stress (ksi)	"Constant Amplitude" Stress (ksi)	Cycles to Failure	Material	Thickness (inch)	Edge Margin	Nominal Final Ream Diameter (inch)	CX %	CX LEVEL
3D1-14-C	30.48	26.5	42,967	7075-T6	0.1	1.39	0.25	2.75	MIN
Cycles	NE Face, Short (inch)	E Bore, Short (inch)	Aspect Ratio	Spectrum Pass	SFH (where applicable)	NW Face (inch)	SE Face (inch)	SW Face (inch)	W Bore (inch)
36628				8.14			0.0214		
38575	0.02482			8.57			0.0388		
40474	0.04966			8.99			0.0558		
41513	0.07338			9.23			0.0761		
42587	0.13040			9.46			0.1332		
42795	0.2230			9.51		0.02862	0.2230		
42967				9.55					

Table 94. Test Data, coupon 3D1-15-C.

Specimen ID	Max Stress (ksi)	"Constant Amplitude" Stress (ksi)	Cycles to Failure	Material	Thickness (inch)	Edge Margin	Nominal Final Ream Diameter (inch)	CX %	CX LEVEL
3D1-15-C	30.48	26.5	37,222	7075-T6	0.1	1.39	0.25	2.79	MIN
Cycles	NE Face, Short (inch)	E Bore, Short (inch)	Aspect Ratio	Spectrum Pass	SFH (where applicable)	NW Face (inch)	SE Face (inch)	SW Face (inch)	W Bore (inch)
31630	0.02536			7.03			0.0182		
35302	0.08238			7.84			0.0408		
36902	0.222			8.20			0.2220	0.01158	
37121	0.22200			8.25		0.06318	0.2220	0.05084	
37190	0.22200			8.26		0.15548	0.2220	0.16418	
37222				8.27					

Table 95. Test Data, coupon 3D1-01-C.

Specimen ID	Max Stress (ksi)	"Constant Amplitude" Stress (ksi)	Cycles to Failure	Material	Thickness (inch)	Edge Margin	Nominal Final Ream Diameter (inch)	CX %	CX LEVEL
3D1-01-C	27.03	23.5	86,110	7075-T6	0.1	1.39	0.5	3.92	MAX
Cycles	NE Face, Short (inch)	E Bore, Short (inch)	Aspect Ratio	Spectrum Pass	SFH (where applicable)	NW Face (inch)	SE Face (inch)	SW Face (inch)	W Bore (inch)
56258				12.50		0.0238			
59983				13.33		0.04312			
61703				13.71		0.04950			
65073				14.46		0.05940			
71953				15.99		0.08144		0.05946	
79995				17.78		0.12272		0.11194	
85248				18.94		0.22536	0.0284	0.2256	
86110				19.14					

Table 96. Test Data, coupon 3D1-02-C.

Specimen ID	Max Stress (ksi)	"Constant Amplitude" Stress (ksi)	Cycles to Failure	Material	Thickness (inch)	Edge Margin	Nominal Final Ream Diameter (inch)	CX %	CX LEVEL
3D1-02-C	27.03	23.5	48,749	7075-T6	0.1	1.39	0.5	3.92	MAX
Cycles	NE Face, Short (inch)	E Bore, Short (inch)	Aspect Ratio	Spectrum Pass	SFH (where applicable)	NW Face (inch)	SE Face (inch)	SW Face (inch)	W Bore (inch)
25915	0.05052	0.06906		5.76					
30002	0.05696	0.06968		6.67					
35096	0.0757	0.10000		7.80			0.0342		
40235	0.10056	0.10000		8.94			0.0685		
46827	0.20578	0.10000		10.41			0.1948		
48749				10.83					

Table 97. Test Data, coupon 3D1-03-C.

Specimen ID	Max Stress (ksi)	"Constant Amplitude" Stress (ksi)	Cycles to Failure	Material	Thickness (inch)	Edge Margin	Nominal Final Ream Diameter (inch)	CX %	CX LEVEL
3D1-03-C	27.03	23.5	50,206	7075-T6	0.1	1.39	0.5	3.86	MAX
Cycles	NE Face, Short (inch)	E Bore, Short (inch)	Aspect Ratio	Spectrum Pass	SFH (where applicable)	NW Face (inch)	SE Face (inch)	SW Face (inch)	W Bore (inch)
25249	0.01790			5.61		0.0349			0.04472
27541	0.02838	0.02906		6.12		0.04946			0.05140
30600	0.03648	0.03534		6.80		0.06138			0.06236
32531	0.03954	0.04990		7.23		0.07058			0.06412
35967	0.04406	0.05036		7.99		0.08602			0.06992
40023	0.0622	0.05748		8.89		0.10842			0.07354
43714	0.0715	0.06588		9.71		0.13362			0.07586
49570	0.08798	0.07866		11.02		0.23654			0.10000
50206				11.16					

Table 98. Test Data, coupon 3D1-07-C.

Specimen ID	Max Stress (ksi)	"Constant Amplitude" Stress (ksi)	Cycles to Failure	Material	Thickness (inch)	Edge Margin	Nominal Final Ream Diameter (inch)	CX %	CX LEVEL
3D1-07-C	30.48	26.5	25,580	7075-T6	0.1	1.39	0.5	3.86	MAX
Cycles	NE Face, Short (inch)	E Bore, Short (inch)	Aspect Ratio	Spectrum Pass	SFH (where applicable)	NW Face (inch)	SE Face (inch)	SW Face (inch)	W Bore (inch)
13643	0.01454	0.01834		3.03					
16471	0.04426	0.04932		3.66		0.01466			0.01918
20140	0.08176	0.10000		4.48		0.03648			0.04362
23175	0.13914	0.10000		5.15		0.04992			0.05938
25580				5.68					

Table 99. Test Data, coupon 3D1-08-C.

Specimen ID	Max Stress (ksi)	"Constant Amplitude" Stress (ksi)	Cycles to Failure	Material	Thickness (inch)	Edge Margin	Nominal Final Ream Diameter (inch)	CX %	CX LEVEL
3D1-08-C	30.48	26.5	33,501	7075-T6	0.1	1.39	0.5	3.88	MAX
Cycles	NE Face, Short (inch)	E Bore, Short (inch)	Aspect Ratio	Spectrum Pass	SFH (where applicable)	NW Face (inch)	SE Face (inch)	SW Face (inch)	W Bore (inch)
17498				3.89		0.0100			0.00724
19807				4.40		0.01870			0.01998
23034				5.12		0.04352			0.04300
25868				5.75		0.07218			0.07562
30830				6.85		0.13092		0.07472	0.10000
33501				7.44		0.19466		0.17076	0.10000

Table 100. Test Data, coupon 3D1-09-C.

Specimen ID	Max Stress (ksi)	"Constant Amplitude" Stress (ksi)	Cycles to Failure	Material	Thickness (inch)	Edge Margin	Nominal Final Ream Diameter (inch)	CX %	CX LEVEL
3D1-09-C	30.48	26.5	23,572	7075-T6	0.1	1.39	0.5	3.93	MAX
Cycles	NE Face, Short (inch)	E Bore, Short (inch)	Aspect Ratio	Spectrum Pass	SFH (where applicable)	NW Face (inch)	SE Face (inch)	SW Face (inch)	W Bore (inch)
11298	0.02906	0.03564							
14304	0.05320	0.06684						0.02024	0.02030
17140	0.0776	0.10000				0.01300	0.0353	0.03320	0.03284
19556	0.09874	0.10000				0.02548	0.0764	0.04672	0.05562
23516									

Table 101. Test Data, coupon 3D1-04-C.

Specimen ID	Max Stress (ksi)	"Constant Amplitude" Stress (ksi)	Cycles to Failure	Material	Thickness (inch)	Edge Margin	Nominal Final Ream Diameter (inch)	CX %	CX LEVEL
3D1-04-C	27.6	24.0	315,715	7075-T6	0.1	2.4	0.25	4.27	MAX
Cycles	NE Face, Short (inch)	E Bore, Short (inch)	Aspect Ratio	Spectrum Pass	SFH (where applicable)	NW Face (inch)	SE Face (inch)	SW Face (inch)	W Bore (inch)
82137				18.25				0.01202	0.01220
92737				20.61				0.01384	0.01876
106037				23.56				0.01650	0.01892
117687				26.15		0.01272		0.02000	0.04808
128164				28.48		0.01390		0.02006	0.04956
143657				31.92		0.01394		0.02302	0.06118
163013				36.23		0.01592		0.0230	0.06220
173549				38.57		0.02856		0.0232	0.06622
181596				40.35		0.03014		0.02338	0.06668
194274				43.17		0.03020		0.02544	0.07404
208257				46.28		0.03026		0.02547	0.07454
253496				56.33		0.03092		0.02550	0.07700
273342				60.74		0.03124		0.02588	0.07710
315715				70.16		0.03178		0.02592	

Table 102. Test Data, coupon 3D1-26-C.

Specimen ID	Max Stress (ksi)	"Constant Amplitude" Stress (ksi)	Cycles to Failure	Material	Thickness (inch)	Edge Margin	Nominal Final Ream Diameter (inch)	CX %	CX LEVEL
3D1-26-C	27.6	24.0	291,083	7075-T6	0.1	2.4	0.25	4.23	MAX
Cycles	NE Face, Short (inch)	E Bore, Short (inch)	Aspect Ratio	Spectrum Pass	SFH (where applicable)	NW Face (inch)	SE Face (inch)	SW Face (inch)	W Bore (inch)
49501	0.01102	0.01748		11.00					
67503	0.01354	0.02118		15.00					
76503	0.01436	0.02854		17.00					
85504	0.01710	0.03632		19.00					
94504	0.01930	0.03814		21.00					
103505	0.0204	0.03814		23.00					
112505	0.0217	0.03814		25.00					
121506	0.02242	0.04266		27.00					
130506	0.02474	0.04460		29.00					
139507	0.02530	0.04576		31.00					
153007	0.02614	0.04898		34.00					
166508	0.02614	0.05236		37.00					
180008	0.02614	0.05726		40.00					
193509	0.02614	0.07050		43.00					
207009	0.02614	0.07050		46.00					
229510	0.02614	0.07050		51.00		0.0145			0.04696
243010	0.02614	0.07230		54.00		0.01888			0.05214
256511	0.02614	0.07388		57.00		0.02102			0.05768
270011	0.02614	0.07388		60.00		0.02238			0.06126
283512	0.0261	0.08028		63.00		0.02238			0.06252
291083				64.69					

Table 103. Test Data, coupon 3D1-05-C.

Specimen ID	Max Stress (ksi)	"Constant Amplitude" Stress (ksi)	Cycles to Failure	Material	Thickness (inch)	Edge Margin	Nominal Final Ream Diameter (inch)	CX %	CX LEVEL
3D1-05-C	27.6	24.0	369,443	7075-T6	0.1	2.4	0.25	4.28	MAX
Cycles	NE Face, Short (inch)	E Bore, Short (inch)	Aspect Ratio	Spectrum Pass	SFH (where applicable)	NW Face (inch)	SE Face (inch)	SW Face (inch)	W Bore (inch)
89935	0.01370			19.99					
97943	0.02014			21.77					
106783	0.02442			23.73					
120756	0.02674			26.83					
130330	0.03044			28.96					
154600	0.0309			34.36					
198399	0.0323			44.09					
226390	0.03652			50.31					
273190	0.03880			60.71		0.02684			
316446	0.04158			70.32					
346082	0.04414			76.91		0.02974			
369443	0.07598			82.10		0.03142	0.03712	0.01340	
374451				83.21					

Table 104. Test Data, coupon 3D1-06-C.

Specimen ID	Max Stress (ksi)	"Constant Amplitude" Stress (ksi)	Cycles to Failure	Material	Thickness (inch)	Edge Margin	Nominal Final Ream Diameter (inch)	CX %	CX LEVEL
3D1-06-C	27.6	24.0	1,452,484	7075-T6	0.1	2.4	0.25	4.22	MAX
Cycles	NE Face, Short (inch)	E Bore, Short (inch)	Aspect Ratio	Spectrum Pass	SFH (where applicable)	NW Face (inch)	SE Face (inch)	SW Face (inch)	W Bore (inch)
21534				4.8					
76638	0.02654			17.0		0.03318	0.0114	0.01203	
87155	0.02814			19.4		0.03380	0.0161	0.01225	
94869	0.02832			21.1		0.03432	0.0170	0.01228	
123142	0.02854			27.4		0.03624	0.0171	0.01686	
145528	0.0286			32.3		0.03690	0.0187	0.01696	
156191	0.0293			34.7		0.03724	0.0201	0.0170	
166554	0.02950			37.0		0.03852	0.0204	0.0170	
181660	0.03074			40.4		0.03862	0.0209	0.01762	
194479	0.03074			43.2		0.03862	0.0209	0.01774	
243885	0.03162			54.2		0.03862	0.0209	0.01778	
279112	0.03246			62.0		0.03876	0.0211	0.02014	
310468	0.03296			69.0		0.03904	0.02131	0.02014	
417721	0.03382			92.8		0.04048	0.02148	0.02186	
861867	0.03412			191.5		0.04454	0.02148	0.02186	
917419	0.03412			203.9		0.04454	0.02196	0.02186	
973715	0.03440			216.4		0.045	0.02196	0.02186	
1067581	0.03440			237.2		0.04608	0.02199	0.02186	
1452484				322.8					

Table 105. Test Data, coupon 3D1-10-C.

Specimen ID	Max Stress (ksi)	"Constant Amplitude" Stress (ksi)	Cycles to Failure	Material	Thickness (inch)	Edge Margin	Nominal Final Ream Diameter (inch)	CX %	CX LEVEL
3D1-10-C	30.48	26.5	109,039	7075-T6	0.1	2.4	0.25	4.32	MAX
Cycles	NE Face, Short (inch)	E Bore, Short (inch)	Aspect Ratio	Spectrum Pass	SFH (where applicable)	NW Face (inch)	SE Face (inch)	SW Face (inch)	W Bore (inch)
30231	0.01098			6.7			0.0233		
35094	0.02668			7.8			0.0253		
40190	0.03206			8.9		0.02416	0.0272		
52152	0.03726			11.6		0.03012	0.0298		
61841	0.04004			13.7		0.03584	0.0307	0.02832	
71948	0.0428			16.0		0.03710	0.0334	0.03064	
83280	0.0446			18.5		0.03924	0.0336	0.0333	
96885	0.04784			21.5		0.04326	0.0343	0.0366	
106822	0.05844			23.7		0.22704	0.04284	0.22868	
109040				24.2					

Table 106. Test Data, coupon 3D1-11-C.

Specimen ID	Max Stress (ksi)	"Constant Amplitude" Stress (ksi)	Cycles to Failure	Material	Thickness (inch)	Edge Margin	Nominal Final Ream Diameter (inch)	CX %	CX LEVEL
3D1-11-C	30.48	26.5	87,962	7075-T6	0.1	2.4	0.25	4.39	MAX
Cycles	NE Face, Short (inch)	E Bore, Short (inch)	Aspect Ratio	Spectrum Pass	SFH (where applicable)	NW Face (inch)	SE Face (inch)	SW Face (inch)	W Bore (inch)
34212				7.6		0.0118			
44174				9.8		0.02714			
51387	0.0121			11.4		0.03150			
64405	0.02204			14.3		0.03776		0.03554	
84347	0.03114			18.7		0.13704	0.0422	0.13458	
87962				19.5					

Table 107. Test Data, coupon 3D1-12-C.

Specimen ID	Max Stress (ksi)	"Constant Amplitude" Stress (ksi)	Cycles to Failure	Material	Thickness (inch)	Edge Margin	Nominal Final Ream Diameter (inch)	CX %	CX LEVEL
3D1-12-C	30.48	26.5	132,279	7075-T6	0.1	2.4	0.25	4.28	MAX
Cycles	NE Face, Short (inch)	E Bore, Short (inch)	Aspect Ratio	Spectrum Pass	SFH (where applicable)	NW Face (inch)	SE Face (inch)	SW Face (inch)	W Bore (inch)
32798				7.3		0.0190			
37207				8.3		0.02636			
44339				9.9		0.03268			
51256				11.4		0.03520			
59259				13.2		0.03740			
69069				15.3		0.04026	0.0116	0.01552	
79613				17.7		0.04208	0.0180	0.0207	
91417				20.3		0.04526	0.0223	0.0240	
104594	0.02344			23.2		0.04744	0.0273	0.02716	
119041	0.02976			26.5		0.05182	0.03074	0.02902	
132279				29.4					

Table 108. Test Data, coupon 3D3-10-C.

Specimen ID	Max Stress (ksi)	"Constant Amplitude" Stress (ksi)	Cycles to Failure	Material	Thickness (inch)	Edge Margin	Nominal Final Ream Diameter (inch)	CX %	CX LEVEL
3D3-10-C	27.6	24.0	42,742	7075-T6	0.1	2.4	0.5	2.89	MIN
Cycles	NE Face, Short (inch)	E Bore, Short (inch)	Aspect Ratio	Spectrum Pass	SFH (where applicable)	NW Face (inch)	SE Face (inch)	SW Face (inch)	W Bore (inch)
9001				2.0		0.0116			
12718				2.8		0.02496	0.0246		
13502				3.0		0.02776			
15678				3.5		0.03712			
18002				4.0		0.05032			
21406				4.8		0.06512			
22503				5.0		0.06606			
27003				6.0		0.08052			
42742				9.5					

Table 109. Test Data, coupon 3D3-11-C.

Specimen ID	Max Stress (ksi)	"Constant Amplitude" Stress (ksi)	Cycles to Failure	Material	Thickness (inch)	Edge Margin	Nominal Final Ream Diameter (inch)	CX %	CX LEVEL
3D3-11-C	27.6	24.0	35,000	7075-T6	0.1	2.4	0.5	2.89	MIN
Cycles	NE Face, Short (inch)	E Bore, Short (inch)	Aspect Ratio	Spectrum Pass	SFH (where applicable)	NW Face (inch)	SE Face (inch)	SW Face (inch)	W Bore (inch)
13502	0.0358	0.0438		3 0					
18002	0.0569	0.1000		4 0					
22503	0.0833			5 0		0.0273			
27003	0.1227			6 0		0.0376			
31504	0.2819			7 0		0.0490			

Table 110. Test Data, coupon 3D3-12-C.

Specimen ID	Max Stress (ksi)	"Constant Amplitude" Stress (ksi)	Cycles to Failure	Material	Thickness (inch)	Edge Margin	Nominal Final Ream Diameter (inch)	CX %	CX LEVEL
3D3-12-C	27.6	24.0	84,025	7075-T6	0.1	2.4	0.5	2.9	MIN
Cycles	NE Face, Short (inch)	E Bore, Short (inch)	Aspect Ratio	Spectrum Pass	SFH (where applicable)	NW Face (inch)	SE Face (inch)	SW Face (inch)	W Bore (inch)
27002	0.0168	0.0621		6 0					
31503	0.0346	0.1000		7 0					
36003	0.0413			8 0					
40504	0.0466			9 0					
45004	0.0507			10.0					
49505	0.0525			11.0					
54005	0.0528			12.0					
58506	0.05526			13.0		0.01652			
63006	0.05586			14.0		0.02892			
67507	0.05526			15.0		0.03470			
72007	0.05582			16.0		0.03708			
76508	0.06874			17.0		0.03978			
81008	0.18524			18.0		0.04058			
84025				18.7					

Table 111. Test Data, coupon 3D3-13-C.

Specimen ID	Max Stress (ksi)	"Constant Amplitude" Stress (ksi)	Cycles to Failure	Material	Thickness (inch)	Edge Margin	Nominal Final Ream Diameter (inch)	CX %	CX LEVEL
3D3-13-C	30.48	26.5	23,744	7075-T6	0.1	2.4	0.5	2.81	MIN
Cycles	NE Face, Short (inch)	E Bore, Short (inch)	Aspect Ratio	Spectrum Pass	SFH (where applicable)	NW Face (inch)	SE Face (inch)	SW Face (inch)	W Bore (inch)
27002	0.0168	0.0621		6 0					
31503	0.0346	0.1000		7 0					
36003	0.0413			8 0					
40504	0.0466			9 0					
45004	0.0507			10.0					
49505	0.0525			11.0					
54005	0.0528			12.0					
58506	0.05526			13.0		0.01652			
63006	0.05586			14.0		0.02892			
67507	0.05526			15.0		0.03470			
72007	0.05582			16.0		0.03708			
76508	0.06874			17.0		0.03978			
81008	0.18524			18.0		0.04058			
84025				18.7					

Table 112. Test Data, coupon 3D3-14-C.

Specimen ID	Max Stress (ksi)	"Constant Amplitude" Stress (ksi)	Cycles to Failure	Material	Thickness (inch)	Edge Margin	Nominal Final Ream Diameter (inch)	CX %	CX LEVEL
3D3-14-C	30.48	26.5	19,771	7075-T6	0.1	2.4	0.5	2.87	MIN
Cycles	NE Face, Short (inch)	E Bore, Short (inch)	Aspect Ratio	Spectrum Pass	SFH (where applicable)	NW Face (inch)	SE Face (inch)	SW Face (inch)	W Bore (inch)
12722	0.0457			2 8		0.0615			
13502	0.0511			3 0		0.07272			
15223	0.0688			3.4		0.0975			
19771				4.4					

Table 113. Test Data, coupon 3D3-15-C.

Specimen ID	Max Stress (ksi)	"Constant Amplitude" Stress (ksi)	Cycles to Failure	Material	Thickness (inch)	Edge Margin	Nominal Final Ream Diameter (inch)	CX %	CX LEVEL
3D3-15-C	30.48	26.5	18,321	7075-T6	0.1	2.4	0.5	2.8	MIN
Cycles	NE Face, Short (inch)	E Bore, Short (inch)	Aspect Ratio	Spectrum Pass	SFH (where applicable)	NW Face (inch)	SE Face (inch)	SW Face (inch)	W Bore (inch)
12875	0.0945			2 9					
13502	0.1022			3 0		0.03060			
16020	0.1700			3.6		0.0643			
18002	0.0400			4 0		0.0113			
18321				4.1					

Table 114. Test Data, coupon 3D1-05-D.

Specimen ID	Max Stress (ksi)	"Constant Amplitude" Stress (ksi)	Cycles to Failure	Material	Thickness (inch)	Edge Margin	Nominal Final Ream Diameter (inch)	CX %	CX LEVEL
3D1-05-D	27.6	24.0	136,907	7075-T651	0.318	1.8	0.375	3.46	MID
Cycles	NE Face, Short (inch)	E Bore, Short (inch)	Aspect Ratio	Spectrum Pass	SFH (where applicable)	NW Face (inch)	SE Face (inch)	SW Face (inch)	W Bore (inch)
24501	0.0362			5.4					
26252	0.0402			5.8					
42256	0.0503			9.4					
52588	0.0555			11.7					
111202	0.0731			24.7					

Table 115. Test Data, coupon 3D1-06-D.

Specimen ID	Max Stress (ksi)	"Constant Amplitude" Stress (ksi)	Cycles to Failure	Material	Thickness (inch)	Edge Margin	Nominal Final Ream Diameter (inch)	CX %	CX LEVEL
3D1-06-D	27.6	24.0	160,794	7075-T651	0.318	1.8	0.375	3.51	MID
Cycles	NE Face, Short (inch)	E Bore, Short (inch)	Aspect Ratio	Spectrum Pass	SFH (where applicable)	NW Face (inch)	SE Face (inch)	SW Face (inch)	W Bore (inch)
27717	0.0428			6.2					
42715	0.0535			9.5		0.0241			
62098	0.0584			13.8		0.0420			
82582	0.0630			18.4		0.0420			
110353	0.0709			24.5		0.0489			
129070	0.0753			28.7		0.0544			
160794				35.7					

Table 116. Test Data, coupon 3D1-07-D.

Specimen ID	Max Stress (ksi)	"Constant Amplitude" Stress (ksi)	Cycles to Failure	Material	Thickness (inch)	Edge Margin	Nominal Final Ream Diameter (inch)	CX %	CX LEVEL
3D1-07-D	27.6	24.0	223,856	7075-T651	0.318	1.8	0.375	3.34	MID
Cycles	NE Face, Short (inch)	E Bore, Short (inch)	Aspect Ratio	Spectrum Pass	SFH (where applicable)	NW Face (inch)	SE Face (inch)	SW Face (inch)	W Bore (inch)
22193				4.9		0.0373			
30252				6.7		0.0423			
41451				9.2		0.0488			
44735				9.9		0.0512			
223856				49.7					

Table 117. Test Data, coupon 3D1-01-D.

Specimen ID	Max Stress (ksi)	"Constant Amplitude" Stress (ksi)	Cycles to Failure	Material	Thickness (inch)	Edge Margin	Nominal Final Ream Diameter (inch)	CX %	CX LEVEL
3D1-01-D	30.48	26.5	42,052	7075-T651	0.318	1.8	0.375	3.43	MID
Cycles	NE Face, Short (inch)	E Bore, Short (inch)	Aspect Ratio	Spectrum Pass	SFH (where applicable)	NW Face (inch)	SE Face (inch)	SW Face (inch)	W Bore (inch)
23104	0.0608			5.1					
42052				9.3					

Table 118. Test Data, coupon 3D1-02-D.

Specimen ID	Max Stress (ksi)	"Constant Amplitude" Stress (ksi)	Cycles to Failure	Material	Thickness (inch)	Edge Margin	Nominal Final Ream Diameter (inch)	CX %	CX LEVEL
3D1-02-D	30.48	26.5	42,239	7075-T651	0.318	1.8	0.375	3.41	MID
Cycles	NE Face, Short (inch)	E Bore, Short (inch)	Aspect Ratio	Spectrum Pass	SFH (where applicable)	NW Face (inch)	SE Face (inch)	SW Face (inch)	W Bore (inch)
23570	0.0616			5.2		0.0703			
42239				9.4					

Table 119. Test Data, coupon 3D1-03-D.

Specimen ID	Max Stress (ksi)	"Constant Amplitude" Stress (ksi)	Cycles to Failure	Material	Thickness (inch)	Edge Margin	Nominal Final Ream Diameter (inch)	CX %	CX LEVEL
3D1-03-D	30.48	26.5	51,485	7075-T651	0.318	1.8	0.375	3.35	MID
Cycles	NE Face, Short (inch)	E Bore, Short (inch)	Aspect Ratio	Spectrum Pass	SFH (where applicable)	NW Face (inch)	SE Face (inch)	SW Face (inch)	W Bore (inch)
6544	0.0180			1.5					
25380	0.0621			5.6		0.0453			
45932	0.1425			10.2		0.0829			
51485				11.4					

Table 120. Test Data, coupon 3D1-11-D.

Specimen ID	Max Stress (ksi)	"Constant Amplitude" Stress (ksi)	Cycles to Failure	Material	Thickness (inch)	Edge Margin	Nominal Final Ream Diameter (inch)	CX %	CX LEVEL
3D1-11-D	27.6	24.0	61,503	7075-T651	0.5	1.39	0.25	4.43	MAX
Cycles	NE Face, Short (inch)	E Bore, Short (inch)	Aspect Ratio	Spectrum Pass	SFH (where applicable)	NW Face (inch)	SE Face (inch)	SW Face (inch)	W Bore (inch)
4500				1.0					
40504	0.0196	0.3970		9.0					
45005	0.0407	0.4344		10.0					
49505	0.0691	0.5000		11.0					
61503				13.7					

Table 121. Test Data, coupon 3D1-12-D.

Specimen ID	Max Stress (ksi)	"Constant Amplitude" Stress (ksi)	Cycles to Failure	Material	Thickness (inch)	Edge Margin	Nominal Final Ream Diameter (inch)	CX %	CX LEVEL
3D1-12-D	27.6	24.0	81,629	7075-T651	0.5	1.39	0.25	4.3	MAX
Cycles	NE Face, Short (inch)	E Bore, Short (inch)	Aspect Ratio	Spectrum Pass	SFH (where applicable)	NW Face (inch)	SE Face (inch)	SW Face (inch)	W Bore (inch)
45003				10.0		0.0194			
49503				11.0		0.0414			
54004				12.0		0.0529			
58504				13.0		0.0636			
63005	0.0076			14.0		0.0725			
67505	0.0461			15.0		0.0911			
72006	0.0750			16.0		0.1024			
81629				18.1					

Table 122. Test Data, coupon 3D1-13-D.

Specimen ID	Max Stress (ksi)	"Constant Amplitude" Stress (ksi)	Cycles to Failure	Material	Thickness (inch)	Edge Margin	Nominal Final Ream Diameter (inch)	CX %	CX LEVEL
3D1-13-D	27.6	24.0	79,703	7075-T651	0.5	1.39	0.25	4.3	MAX
Cycles	NE Face, Short (inch)	E Bore, Short (inch)	Aspect Ratio	Spectrum Pass	SFH (where applicable)	NW Face (inch)	SE Face (inch)	SW Face (inch)	W Bore (inch)
58506	0.0190	thru		13.0					
63007	0.0486			14.0					
67507	0.0737			15.0					
72008	0.1208			16.0					
76508	0.2234			17.0					
79703				17.7					

Table 123. Test Data, coupon 3D1-14-D.

Specimen ID	Max Stress (ksi)	"Constant Amplitude" Stress (ksi)	Cycles to Failure	Material	Thickness (inch)	Edge Margin	Nominal Final Ream Diameter (inch)	CX %	CX LEVEL
3D1-14-D	30.48	26.5	41,313	7075-T651	0.5	1.39	0.25	4.53	MAX
Cycles	NE Face, Short (inch)	E Bore, Short (inch)	Aspect Ratio	Spectrum Pass	SFH (where applicable)	NW Face (inch)	SE Face (inch)	SW Face (inch)	W Bore (inch)
22503	0.0297			5.0					
25549	0.0498	0.0258		5.7					
27003	0.0528	0.0638		6.0					
31504	0.0867	0.0711		7.0					
37108				8.2					
41278				9.2					
41313				9.2					

Table 124. Test Data, coupon 3D1-15-D.

Specimen ID	Max Stress (ksi)	"Constant Amplitude" Stress (ksi)	Cycles to Failure	Material	Thickness (inch)	Edge Margin	Nominal Final Ream Diameter (inch)	CX %	CX LEVEL
3D1-15-D	30.48	26.5	44,605	7075-T651	0.5	1.39	0.25	4.22	MAX
Cycles	NE Face, Short (inch)	E Bore, Short (inch)	Aspect Ratio	Spectrum Pass	SFH (where applicable)	NW Face (inch)	SE Face (inch)	SW Face (inch)	W Bore (inch)
31504	0.0280			7.0					
33450	0.0416			7.4					
36004	0.0646			8.0					
40505	0.1260			9.0		0.0220			
44570				9.9					
44605				9.9					

Table 125. Test Data, coupon 3D1-16-D.

Specimen ID	Max Stress (ksi)	"Constant Amplitude" Stress (ksi)	Cycles to Failure	Material	Thickness (inch)	Edge Margin	Nominal Final Ream Diameter (inch)	CX %	CX LEVEL
3D1-16-D	30.48	26.5	55,555	7075-T651	0.5	1.39	0.25	4.25	MAX
Cycles	NE Face, Short (inch)	E Bore, Short (inch)	Aspect Ratio	Spectrum Pass	SFH (where applicable)	NW Face (inch)	SE Face (inch)	SW Face (inch)	W Bore (inch)
31504				7.0		0.0343			
33968	0.0311			7.5		0.0456			
35004	0.0389			7.8		0.0532			
40505	0.0545			9.0		0.0698			
45005	0.0674			10.0		0.0969			
49506	0.0850			11.0		0.1447			
55475				12.3					
55555				12.3					

Table 126. Test Data, coupon 3D1-20-D.

Specimen ID	Max Stress (ksi)	"Constant Amplitude" Stress (ksi)	Cycles to Failure	Material	Thickness (inch)	Edge Margin	Nominal Final Ream Diameter (inch)	CX %	CX LEVEL
3D1-20-D	27.6	24.0	52,260	7075-T651	0.5	1.39	0.5	3.01	MIN
Cycles	NE Face, Short (inch)	E Bore, Short (inch)	Aspect Ratio	Spectrum Pass	SFH (where applicable)	NW Face (inch)	SE Face (inch)	SW Face (inch)	W Bore (inch)
22500	0.0251			5.0					
27000	0.0383			6.0					
31500	0.0537			7.0					
36000	0.0720			8.0					
40500	0.0890			9.0					
45000	0.1133			10.0					
49500	0.1774			11.0					
52260				11.6					

Table 127. Test Data, coupon 3D1-21-D.

Specimen ID	Max Stress (ksi)	"Constant Amplitude" Stress (ksi)	Cycles to Failure	Material	Thickness (inch)	Edge Margin	Nominal Final Ream Diameter (inch)	CX %	CX LEVEL
3D1-21-D	27.6	24.0	74,315	7075-T651	0.5	1.39	0.5	2.97	MIN
Cycles	NE Face, Short (inch)	E Bore, Short (inch)	Aspect Ratio	Spectrum Pass	SFH (where applicable)	NW Face (inch)	SE Face (inch)	SW Face (inch)	W Bore (inch)
36003	0.0354			8 0					
40503	0.0572			9 0					
45004	0.0710			10.0					
65098	0.1398			14.5		0.0942			
74315				16.5					

Table 128. Test Data, coupon 3D1-22-D.

Specimen ID	Max Stress (ksi)	"Constant Amplitude" Stress (ksi)	Cycles to Failure	Material	Thickness (inch)	Edge Margin	Nominal Final Ream Diameter (inch)	CX %	CX LEVEL
3D1-22-D	27.6	24.0	50,115	7075-T651	0.5	1.39	0.5	2.94	MIN
Cycles	NE Face, Short (inch)	E Bore, Short (inch)	Aspect Ratio	Spectrum Pass	SFH (where applicable)	NW Face (inch)	SE Face (inch)	SW Face (inch)	W Bore (inch)
27001	0.0608			6 0		0.0486			
31502	0.0852			7 0		0.0631			
36002	0.1078			8 0		0.0741			
40503	0.1330			9 0		0.0768			
45003	0.1741			10.0		0.0843			
49504	0.3317			11.0		0.0968			
50115				11.1					

Table 129. Test Data, coupon 3D1-26-D.

Specimen ID	Max Stress (ksi)	"Constant Amplitude" Stress (ksi)	Cycles to Failure	Material	Thickness (inch)	Edge Margin	Nominal Final Ream Diameter (inch)	CX %	CX LEVEL
3D1-26-D	30.48	26.5	29,375	7075-T651	0.5	1.39	0.5	2.89	MIN
Cycles	NE Face, Short (inch)	E Bore, Short (inch)	Aspect Ratio	Spectrum Pass	SFH (where applicable)	NW Face (inch)	SE Face (inch)	SW Face (inch)	W Bore (inch)
18001	0.0905			4 0					
22502	0.1218			5 0		0.0642			
27002	0.1907			6 0		0.1139			
29375				6.5					

Table 130. Test Data, coupon 3D1-27-D.

Specimen ID	Max Stress (ksi)	"Constant Amplitude" Stress (ksi)	Cycles to Failure	Material	Thickness (inch)	Edge Margin	Nominal Final Ream Diameter (inch)	CX %	CX LEVEL
3D1-27-D	30.48	26.5	36,204	7075-T651	0.5	1.39	0.5	2.95	MIN
Cycles	NE Face, Short (inch)	E Bore, Short (inch)	Aspect Ratio	Spectrum Pass	SFH (where applicable)	NW Face (inch)	SE Face (inch)	SW Face (inch)	W Bore (inch)
18002				4 0		0.0334			
22503	0.0266			5 0		0.0657			
27003	0.0712			6 0		0.0884			
31504	0.1126			7 0		0.1144			
36204				8 0					

Table 131. Test Data, coupon 3D1-28-D.

Specimen ID	Max Stress (ksi)	"Constant Amplitude" Stress (ksi)	Cycles to Failure	Material	Thickness (inch)	Edge Margin	Nominal Final Ream Diameter (inch)	CX %	CX LEVEL
3D1-28-D	30.48	26.5	26,603	7075-T651	0.5	1.39	0.5	3	MIN
Cycles	NE Face, Short (inch)	E Bore, Short (inch)	Aspect Ratio	Spectrum Pass	SFH (where applicable)	NW Face (inch)	SE Face (inch)	SW Face (inch)	W Bore (inch)
13502	0.0616	thru		3 0					
18002	0.0919			4 0		0.0450			
22503	0.1269			5 0		0.0838			
26603				5 9					

Table 132. Test Data, coupon 3D1-29-D.

Specimen ID	Max Stress (ksi)	"Constant Amplitude" Stress (ksi)	Cycles to Failure	Material	Thickness (inch)	Edge Margin	Nominal Final Ream Diameter (inch)	CX %	CX LEVEL
3D1-29-D	27.6020702	24.0	106,780	7075-T651	0.5	2.4	0.25	2.21	MIN
Cycles	NE Face, Short (inch)	E Bore, Short (inch)	Aspect Ratio	Spectrum Pass	SFH (where applicable)	NW Face (inch)	SE Face (inch)	SW Face (inch)	W Bore (inch)
72003				16.0		0.0428			0.05776
81003				18.0		0.0676			0.07040
90004				20.0		0.1146			0.09662
99004				22.0		0.2552			0.13382
106710				23.7					
106780				23.7					

Table 133. Test Data, coupon 3D1-30-D.

Specimen ID	Max Stress (ksi)	"Constant Amplitude" Stress (ksi)	Cycles to Failure	Material	Thickness (inch)	Edge Margin	Nominal Final Ream Diameter (inch)	CX %	CX LEVEL
3D1-30-D	27.6	24.0	113,282	7075-T651	0.5	2.4	0.25	2.67	MIN
Cycles	NE Face, Short (inch)	E Bore, Short (inch)	Aspect Ratio	Spectrum Pass	SFH (where applicable)	NW Face (inch)	SE Face (inch)	SW Face (inch)	W Bore (inch)
90002				20.0		0.0809			
112503				25.0		0.6075			
113282				25.2					

Table 134. Test Data, coupon 3D1-17-D.

Specimen ID	Max Stress (ksi)	"Constant Amplitude" Stress (ksi)	Cycles to Failure	Material	Thickness (inch)	Edge Margin	Nominal Final Ream Diameter (inch)	CX %	CX LEVEL
3D1-17-D	27.6	24.0	110,281	7075-T651	0.5	2.4	0.25	2.78	MIN
Cycles	NE Face, Short (inch)	E Bore, Short (inch)	Aspect Ratio	Spectrum Pass	SFH (where applicable)	NW Face (inch)	SE Face (inch)	SW Face (inch)	W Bore (inch)
92461	0.0576			20.5					
98438	0.1011			21.9					
110281				24.5					

Table 135. Test Data, coupon 3D1-18-D.

Specimen ID	Max Stress (ksi)	"Constant Amplitude" Stress (ksi)	Cycles to Failure	Material	Thickness (inch)	Edge Margin	Nominal Final Ream Diameter (inch)	CX %	CX LEVEL
3D1-18-D	27.6	24.0	366,538	7075-T651	0.5	2.4	0.25	2.77	MIN
Cycles	NE Face, Short (inch)	E Bore, Short (inch)	Aspect Ratio	Spectrum Pass	SFH (where applicable)	NW Face (inch)	SE Face (inch)	SW Face (inch)	W Bore (inch)
211522	0.0291			47.0					
216022	0.0295			48.0					
220523	0.0325			49.0					
366538				81.5					

Table 136. Test Data, coupon 3D1-19-D.

Specimen ID	Max Stress (ksi)	"Constant Amplitude" Stress (ksi)	Cycles to Failure	Material	Thickness (inch)	Edge Margin	Nominal Final Ream Diameter (inch)	CX %	CX LEVEL
3D1-19-D	27.6	24.0	63,401	7075-T651	0.5	2.4	0.25	2.75	MIN
Cycles	NE Face, Short (inch)	E Bore, Short (inch)	Aspect Ratio	Spectrum Pass	SFH (where applicable)	NW Face (inch)	SE Face (inch)	SW Face (inch)	W Bore (inch)
NO DATA									

Table 137. Test Data, coupon 3D1-23-D.

Specimen ID	Max Stress (ksi)	"Constant Amplitude" Stress (ksi)	Cycles to Failure	Material	Thickness (inch)	Edge Margin	Nominal Final Ream Diameter (inch)	CX %	CX LEVEL
3D1-23-D	30.5	26.5	39,344	7075-T651	0.5	2.4	0.25	2.58	MIN
Cycles	NE Face, Short (inch)	E Bore, Short (inch)	Aspect Ratio	Spectrum Pass	SFH (where applicable)	NW Face (inch)	SE Face (inch)	SW Face (inch)	W Bore (inch)
22501	0.0271			5.0					
31501	0.1288			7.0					
33722	0.2022			7.5					
36761	0.3023			8.2					
39344				8.7					

Table 138. Test Data, coupon 3D1-24-D.

Specimen ID	Max Stress (ksi)	"Constant Amplitude" Stress (ksi)	Cycles to Failure	Material	Thickness (inch)	Edge Margin	Nominal Final Ream Diameter (inch)	CX %	CX LEVEL
3D1-24-D	30.5	26.5	36,592	7075-T651	0.5	2.4	0.25	2.77	MIN
Cycles	NE Face, Short (inch)	E Bore, Short (inch)	Aspect Ratio	Spectrum Pass	SFH (where applicable)	NW Face (inch)	SE Face (inch)	SW Face (inch)	W Bore (inch)
15095				3.4		0.0513			0.06830
18001				4.0		0.0702			0.09222
22502	0.0604	0.1526		5.0		0.1198			0.32366
27003	0.1358			6.0		0.2373			
31503	0.3605			7.0		0.4739			
36542				8.1					

Table 139. Test Data, coupon 3D1-25-D.

Specimen ID	Max Stress (ksi)	"Constant Amplitude" Stress (ksi)	Cycles to Failure	Material	Thickness (inch)	Edge Margin	Nominal Final Ream Diameter (inch)	CX %	CX LEVEL
3D1-25-D	30.5	26.5	50,449	7075-T651	0.5	2.4	0.25	2.75	MIN
Cycles	NE Face, Short (inch)	E Bore, Short (inch)	Aspect Ratio	Spectrum Pass	SFH (where applicable)	NW Face (inch)	SE Face (inch)	SW Face (inch)	W Bore (inch)
31504				7.0		0.0403			0.03668
36004				8.0		0.0646			0.05988
40505	0.0401			9.0		0.1057			0.07442
46006	0.1018			10.2		0.1977			0.13346
50449	0.2893			11.2		0.3678			

Table 140. Test Data, coupon 3D3-14-D.

Specimen ID	Max Stress (ksi)	"Constant Amplitude" Stress (ksi)	Cycles to Failure	Material	Thickness (inch)	Edge Margin	Nominal Final Ream Diameter (inch)	CX %	CX LEVEL
3D3-14-D	27 0	23.5	999,000	7075-T651	0.5	2.4	0.5	3.88	MAX
Cycles	NE Face, Short (inch)	E Bore, Short (inch)	Aspect Ratio	Spectrum Pass	SFH (where applicable)	NW Face (inch)	SE Face (inch)	SW Face (inch)	W Bore (inch)
50104	0.0198			11.1					
53979	0.0299			12.0					
58167	0.0347			12.9					
62124	0.0403			13.8					
66596	0.0455			14.8		0.0183			
71480	0.0474			15.9		0.0356			
76740	0.0477			17.1		0.0442			
81993	0.0491			18.2		0.0448			
86329	0.0505			19.2		0.0491			
129923	0.0598			28.9		0.0585			
168555	0.0635			37.5		0.0614			
583983	0.0753			129.8		0.0775			
664709	0.0760			147.7		0.0786			
812895	0.0762			180.6		0.0791			
861243	0.0773			191.4		0.0817			
921579	0.0773			204.8		0.0823			
921579	0.0773			204.8		0.0823			
999000	0.0773			222.0		0.0823			

Table 141. Test Data, coupon 3D3-16-D.

Specimen ID	Max Stress (ksi)	"Constant Amplitude" Stress (ksi)	Cycles to Failure	Material	Thickness (inch)	Edge Margin	Nominal Final Ream Diameter (inch)	CX %	CX LEVEL
3D3-16-D	27.6	24.0	4,782,801	7075-T651	0.5	2.4	0.5	3.97	MAX
Cycles	NE Face, Short (inch)	E Bore, Short (inch)	Aspect Ratio	Spectrum Pass	SFH (where applicable)	NW Face (inch)	SE Face (inch)	SW Face (inch)	W Bore (inch)
197361	0.0463			43.9					
210665	0.0533			46.8					
221844	0.0562			49.3					
260039	0.0622			57.8		0.0486			
267297	0.0625			59.4		0.0522			
288323	0.0636			64.1		0.0583			
344033	0.0653			76.5		0.0639			
470677	0.0694			104.6		0.0696			
518415	0.0711			115.2		0.0716			
930302	0.0788			206.7		0.0777			
973789	0.0810			216.4		0.0777			
1084077	0.0821			240.9		0.0789			
1139331	0.0837			253.2		0.0805			
1191813	0.0847			264.8		0.0819			
1559406	0.0864			346.5		0.0819			
1665000	0.0882			370.0		0.0878			
1815111	0.0918			403.4		0.0878			
1999800	0.0941			444.4		0.0888			
2118403	0.09636			470.8		0.08928			
2249834	0.1000			500.0		0.0905			
2416794	0.10412			537.1		0.09262			
4050674	0.12014			900.1		0.10114			
4254180	0.12256			945.4		0.10278			
4668533	0.1312			1037.5		0.1053			
4773930	0.2111			1060.9		0.10634			
4778129	0.33176			1061.8		0.10646			
4782801				1062.8					

Table 142. Test Data, coupon 3D3-28-D.

Specimen ID	Max Stress (ksi)	"Constant Amplitude" Stress (ksi)	Cycles to Failure	Material	Thickness (inch)	Edge Margin	Nominal Final Ream Diameter (inch)	CX %	CX LEVEL
3D3-28-D	27.6	24.0	6,000,000	7075-T651	0.5	2.4	0.5	3.97	MAX
Cycles	NE Face, Short (inch)	E Bore, Short (inch)	Aspect Ratio	Spectrum Pass	SFH (where applicable)	NW Face (inch)	SE Face (inch)	SW Face (inch)	W Bore (inch)
157471				35.0					0.13178
260288	0.0623			57.8		0.0550			
563622	0.0756			125.2		0.0713			
627463	0.0765			139.4		0.0720		0.01750	
649807	0.0771			144.4		0.0720		0.02512	
667762	0.0782			148.4		0.0721		0.02762	
731743	0.0785			162.6		0.0737		0.0303	
876103	0.0797			194.7					
999106	0.0808			222.0		0.0750	0.02698	0.03376	
1363492	0.0853			303.0		0.0777	0.03264	0.03550	
1614596	0.0867			358.8		0.0777	0.03312	0.03780	
2524047	0.0920			560.9		0.0819	0.03299	0.03780	
6000000				1333.3					

Table 143. Test Data, coupon 3D3-13-D.

Specimen ID	Max Stress (ksi)	"Constant Amplitude" Stress (ksi)	Cycles to Failure	Material	Thickness (inch)	Edge Margin	Nominal Final Ream Diameter (inch)	CX %	CX LEVEL
3D3-13-D	28.8	25.0	415,645	7075-T651	0.5	2.4	0.5	3.94	MAX
Cycles	NE Face, Short (inch)	E Bore, Short (inch)	Aspect Ratio	Spectrum Pass	SFH (where applicable)	NW Face (inch)	SE Face (inch)	SW Face (inch)	W Bore (inch)
82225	0.0618			18.3					
86467	0.0702			19.2					
91776	0.0745			20.4					
96427	0.0766			21.4					
104045	0.0813			23.1					
115586	0.0864			25.7					
121170	0.0883			26.9					
415645				92.4					

Table 144. Test Data, coupon 3D3-30-D.

Specimen ID	Max Stress (ksi)	"Constant Amplitude" Stress (ksi)	Cycles to Failure	Material	Thickness (inch)	Edge Margin	Nominal Final Ream Diameter (inch)	CX %	CX LEVEL
3D3-30-D	28.8	25.0	407,535	7075-T651	0.5	2.4	0.5	3.96	MAX
Cycles	NE Face, Short (inch)	E Bore, Short (inch)	Aspect Ratio	Spectrum Pass	SFH (where applicable)	NW Face (inch)	SE Face (inch)	SW Face (inch)	W Bore (inch)
27306	0.0493			6.1		0.0241			
31716	0.0609			7.0		0.0375			
34150	0.0644			7.6		0.0430			
36159	0.0677			8.0		0.0468			
41090	0.0709			9.1		0.0512			
46700	0.0742			10.4		0.0544			
52086	0.0758			11.6		0.0605			
57888	0.0784			12.9		0.0649			
407535				90.6					

Table 145. Test Data, coupon 3D3-17-D.

Specimen ID	Max Stress (ksi)	"Constant Amplitude" Stress (ksi)	Cycles to Failure	Material	Thickness (inch)	Edge Margin	Nominal Final Ream Diameter (inch)	CX %	CX LEVEL
3D3-17-D	30.5	26.5	214,020	7075-T651	0.5	2.4	0.5	4.06	MAX
Cycles	NE Face, Short (inch)	E Bore, Short (inch)	Aspect Ratio	Spectrum Pass	SFH (where applicable)	NW Face (inch)	SE Face (inch)	SW Face (inch)	W Bore (inch)
62202	0.0822			13.8		0.0800			
73663	0.0887			16.4		0.0881			
83402	0.0915			18.5		0.0921			
95593	0.0958			21.2		0.0954			
102018	0.0967			22.7		0.0966			
123416	0.1029			27.4		0.1044			
214020				47.6					

Table 146. Test Data, coupon 3D3-18-D.

Specimen ID	Max Stress (ksi)	"Constant Amplitude" Stress (ksi)	Cycles to Failure	Material	Thickness (inch)	Edge Margin	Nominal Final Ream Diameter (inch)	CX %	CX LEVEL
3D3-18-D	30.5	26.5	214,339	7075-T651	0.5	2.4	0.5	3.97	MAX
Cycles	NE Face, Short (inch)	E Bore, Short (inch)	Aspect Ratio	Spectrum Pass	SFH (where applicable)	NW Face (inch)	SE Face (inch)	SW Face (inch)	W Bore (inch)
30015				6.7		0.0073			
35458	0.0149			7.9		0.0429			
37274	0.0279			8.3		0.0501			
41565	0.0462			9.2		0.0642			
49135	0.0712			10.9		0.0755			
56258	0.0791			12.5		0.0805			
65209	0.0866			14.5		0.0844			
71002	0.0902			15.8		0.0861			
79166	0.0940			17.6		0.0887			
91616	0.0996			20.4		0.0925			
107081	0.1030			23.8		0.0958			
118834	0.1070			26.4		0.0982			
139871	0.1125			31.1		0.1016			
147300	0.1141			32.7		0.1040			
214339				47.6					

Table 147. Test Data, coupon 3D3-29-D.

Specimen ID	Max Stress (ksi)	"Constant Amplitude" Stress (ksi)	Cycles to Failure	Material	Thickness (inch)	Edge Margin	Nominal Final Ream Diameter (inch)	CX %	CX LEVEL
3D3-29-D	30.5	26.5	264,969	7075-T651	0.5	2.4	0.5	4.03	MAX
Cycles	NE Face, Short (inch)	E Bore, Short (inch)	Aspect Ratio	Spectrum Pass	SFH (where applicable)	NW Face (inch)	SE Face (inch)	SW Face (inch)	W Bore (inch)
45000	0.0082			10.0			0.0329		
50429	0.0466			11.2		0.0373	0.0363	0.01574	
51608	0.0504			11.5		0.0448	0.0366	0.01724	
53983	0.0583			12.0		0.0571	0.0370	0.01774	
57947	0.0661			12.9		0.0653	0.0374	0.02180	
64561	0.0729			14.3		0.0730	0.0407	0.02358	
73386	0.0786			16.3		0.0811	0.0427	0.0263	
86261	0.0828			19.2		0.0835	0.0457	0.0286	
124306	0.0941			27.6		0.0942	0.04884	0.03438	
264969				58.9					

12 APPENDIX B: Fatigue Test Data Tables from Demo Tests

This appendix contains all crack growth data recorded for the 38 variable amplitude CX fatigue tests used for validation demonstrations (see Section 8 for test program details).

[Appendix B data removed for public release]

13 APPENDIX C: ASTM E 647 Long Crack Data for 2024-T351 and 7075-T651 Aluminum

This appendix contains all crack growth data recorded for each of the 10 constant amplitude middle-tension panel fatigue tests (see Section 2.3 for test program details). All tests were conducted at $R = +0.1$.

Table 148. Crack growth data from $M(T)$ panels, 2024-T351.

3E2-01-B, 0.319 inch thick		3E2-02-B, 0.319 inch thick		3E2-03-B, 0.319 inch thick		3E2-10-B, 0.5 inch thick		3E2-11-B, 0.5 inch thick	
ΔK_I (ksi in ^{0.5})	da/dN (inch/cycle)	ΔK_I (ksi in ^{0.5})	da/dN (inch/cycle)	ΔK_I (ksi in ^{0.5})	da/dN (inch/cycle)	ΔK_I (ksi in ^{0.5})	da/dN (inch/cycle)	ΔK_I (ksi in ^{0.5})	da/dN (inch/cycle)
5.646	9.682E-07	5.975	6.406E-07	5.865	1.104E-06	6.107	2.982E-07	5.817	2.466E-07
5.827	2.762E-07	6.106	4.048E-07	5.971	4.801E-07	6.160	3.912E-07	5.916	3.026E-07
6.066	7.819E-07	6.236	9.513E-07	6.108	5.580E-07	6.221	4.175E-07	6.035	2.700E-07
6.211	4.416E-07	6.370	1.911E-06	6.236	5.743E-07	6.284	4.039E-07	6.156	2.119E-07
6.343	7.248E-07	6.504	1.014E-06	6.356	5.103E-07	6.344	3.764E-07	6.276	2.221E-07
6.567	1.156E-06	6.629	9.837E-07	6.482	8.709E-07	6.401	3.597E-07	6.402	2.551E-07
6.822	1.323E-06	6.757	1.494E-06	6.613	6.667E-07	6.450	3.717E-07	6.522	3.268E-07
7.021	1.671E-06	6.887	1.269E-06	6.708	6.867E-07	6.495	4.153E-07	6.642	4.905E-07
7.189	2.051E-06	7.020	1.836E-06	6.797	1.156E-06	6.548	4.989E-07	6.770	7.599E-07
7.382	2.004E-06	7.160	1.540E-06	6.891	9.992E-07	6.614	6.310E-07	6.903	1.281E-06
7.585	3.867E-06	7.297	3.850E-06	6.993	1.421E-06	6.698	8.187E-07	7.033	1.487E-06
7.796	2.730E-06	7.433	2.596E-06	7.129	1.507E-06	6.786	1.020E-06	7.161	1.852E-06
8.057	3.124E-06	7.567	3.012E-06	7.265	1.430E-06	6.873	1.214E-06	7.288	2.111E-06
8.345	5.869E-06	7.699	3.264E-06	7.397	1.763E-06	6.977	1.436E-06	7.420	2.304E-06
8.589	2.964E-06	7.841	2.266E-06	7.527	1.553E-06	7.101	1.686E-06	7.554	2.705E-06
8.825	7.748E-06	7.987	5.219E-06	7.662	5.968E-06	7.246	1.962E-06	7.690	3.058E-06
9.027	6.409E-06	8.133	3.922E-06	7.802	3.687E-06	7.417	2.260E-06	7.834	3.322E-06
9.154	5.808E-06	8.279	4.088E-06	7.940	2.111E-06	7.615	2.578E-06	7.982	3.669E-06
9.251	5.851E-06	8.437	4.448E-06	8.086	4.729E-06	7.834	2.896E-06	8.132	3.985E-06
9.348	6.113E-06	8.639	5.093E-06	8.232	2.276E-06	8.123	3.764E-06	8.269	4.313E-06
9.421	5.106E-06	8.842	5.474E-06	8.377	6.607E-06	8.389	3.937E-06	8.413	5.263E-06
9.465	5.027E-06	8.985	3.550E-06	8.524	4.328E-06	8.580	4.487E-06	8.564	4.820E-06
9.556	9.597E-06	9.138	5.853E-06	8.675	2.716E-06	8.802	5.101E-06	8.718	5.240E-06
9.639	9.045E-06	9.267	8.433E-06	8.833	6.969E-06	9.063	5.758E-06	8.915	5.593E-06
9.725	1.019E-05	9.339	8.682E-06	8.981	5.974E-06	9.366	6.434E-06	9.150	5.899E-06
9.813	9.451E-06	9.414	8.309E-06	9.139	2.908E-06	9.718	7.102E-06	9.393	6.904E-06
9.899	8.482E-06	9.481	7.064E-06	9.318	9.021E-06	10.124	7.733E-06	9.547	7.504E-06
9.976	8.699E-06	9.542	7.614E-06	9.479	7.703E-06	10.593	8.300E-06	9.610	7.068E-06
10.055	8.492E-06	9.608	8.218E-06	9.646	6.293E-06	11.130	8.776E-06	9.675	7.273E-06
10.135	8.403E-06	9.677	7.587E-06	9.840	3.702E-06	11.660	2.062E-05	9.743	7.553E-06
10.214	8.103E-06	9.744	7.451E-06	10.019	1.063E-05	12.076	1.372E-05	9.813	7.558E-06
10.290	7.704E-06	9.811	7.330E-06	10.205	9.113E-06	12.418	1.282E-05	9.884	7.657E-06
10.367	8.013E-06	9.873	6.924E-06	10.396	9.214E-06	12.759	1.228E-05	9.959	8.226E-06
10.446	7.847E-06	9.938	7.652E-06	10.594	8.727E-06	13.116	1.265E-05	10.033	7.557E-06
10.529	8.923E-06	10.014	8.924E-06	10.794	8.833E-06	13.526	1.433E-05	10.107	7.307E-06
10.616	8.313E-06	10.090	7.555E-06	10.953	3.933E-06	14.046	1.753E-05	10.187	8.381E-06
10.758	9.599E-06	10.165	8.686E-06	11.135	9.926E-06	14.756	2.213E-05	10.266	8.227E-06
10.860	9.756E-06	10.245	8.276E-06	11.353	1.265E-05	15.765	2.752E-05	10.348	8.261E-06
10.963	9.866E-06	10.327	9.381E-06	11.575	1.319E-05	17.219	3.263E-05	10.439	9.615E-06
11.072	9.939E-06	10.414	8.796E-06	11.724	1.352E-05	19.327	3.607E-05	10.535	9.227E-06
11.186	1.029E-05	10.508	9.956E-06	11.804	8.970E-06	21.399	3.692E-05	10.634	9.879E-06
11.304	1.133E-05	10.606	9.694E-06	11.879	8.820E-06			10.745	1.060E-05
11.437	1.122E-05	10.704	9.860E-06	11.945	1.258E-05			10.854	9.668E-06
11.571	1.145E-05	10.713	-8.749E-06	12.019	1.224E-05			10.959	1.000E-05
11.709	1.184E-05	10.725	1.086E-05	12.093	1.263E-05			11.078	1.038E-05
11.858	1.298E-05	10.836	1.165E-05	12.176	1.257E-05			11.208	1.137E-05

Table 149. Continuation of Table 187. Crack growth data from M(T) panels, 2024-T351.

3E2-01-B, 0.319 inch thick		3E2-02-B, 0.319 inch thick		3E2-03-B, 0.319 inch thick		3E2-10-B, 0.5 inch thick		3E2-11-B, 0.5 inch thick	
ΔK_I (ksi in ^{0.5})	da/dN (inch/cycle)	ΔK_I (ksi in ^{0.5})	da/dN (inch/cycle)	ΔK_I (ksi in ^{0.5})	da/dN (inch/cycle)	ΔK_I (ksi in ^{0.5})	da/dN (inch/cycle)	ΔK_I (ksi in ^{0.5})	da/dN (inch/cycle)
12.017	1.264E-05	10 958	1.170E-05	12.263	1.256E-05			11.335	1.105E-05
12.182	1.258E-05	11 087	1.211E-05	12.345	1.291E-05			11.467	1.131E-05
12.352	1.339E-05	11 219	1.242E-05	12.425	1.308E-05			11.611	1.233E-05
12.532	1.315E-05	11 361	1.330E-05	12.514	1.313E-05			11.764	1.274E-05
12.713	1.287E-05	11 507	1.261E-05	12.605	1.405E-05			11.929	1.292E-05
12.882	1.075E-05	11 660	1.440E-05	12.698	1.430E-05			12.114	1.405E-05
13.052	1.234E-05	11 823	1.374E-05	12.803	1.475E-05			12.300	1.317E-05
13.253	1.445E-05	11 995	1.450E-05	12.905	1.317E-05			12.487	1.384E-05
13.513	1.828E-05	12.174	1.436E-05	13.003	1.489E-05			12.703	1.574E-05
13.812	1.834E-05	12 362	1.508E-05	13.114	1.576E-05			12.942	1.653E-05
13.986	3.292E-05	12 561	1.519E-05	13.235	1.579E-05			13.209	1.786E-05
14.346	1.937E-05	12.773	1.622E-05	13.354	1.670E-05			13.515	1.965E-05
14.420	2.038E-05	13 010	1.758E-05	13.481	1.645E-05			13.843	1.864E-05
14.502	2.224E-05	13 267	1.771E-05	13.615	1.649E-05			14.197	2.051E-05
14.588	2.265E-05	13 536	1.793E-05	13.738	1.161E-05			14.611	2.234E-05
14.669	2.237E-05	13 837	2.052E-05	13.826	7.121E-06			15.097	2.490E-05
14.759	2.436E-05	14.165	1.992E-05	13.902	1.198E-05			15.680	2.779E-05
14.848	2.107E-05	14 579	2.845E-05	14.007	1.508E-05			16.433	3.343E-05
14.932	2.075E-05	14 881	2.360E-05	14.134	1.606E-05			17.498	4.243E-05
15.027	2.125E-05	14 977	2.233E-05	14.273	1.705E-05			19.472	6.929E-05
15.118	2.334E-05	15 064	2.467E-05	14.422	1.759E-05				
15.201	2.354E-05	15.168	2.923E-05	14.579	1.758E-05				
15.287	2.313E-05	15 281	2.815E-05	14.763	2.160E-05				
15.383	2.212E-05	15 398	3.001E-05	14.972	2.128E-05				
15.478	2.437E-05	15 528	3.349E-05	15.199	2.358E-05				
15.581	2.536E-05	15 657	3.042E-05	15.444	2.513E-05				
15.696	2.101E-05	15.787	3.195E-05	15.705	2.546E-05				
15.799	2.524E-05	15 926	3.143E-05	15.994	2.562E-05				
15.914	2.717E-05	16 068	3.463E-05	16.286	2.539E-05				
16.038	2.669E-05	16 220	3.463E-05	16.604	2.762E-05				
16.160	2.687E-05	16 380	3.337E-05	16.862	2.133E-05				
16.286	2.614E-05	16 542	3.592E-05	17.322	3.189E-05				
16.423	3.034E-05	16.729	4.378E-05	17.982	3.795E-05				
16.564	2.844E-05	16 936	4.090E-05	18.590	4.072E-05				
16.711	2.900E-05	17.158	4.715E-05	19.236	3.543E-05				
16.866	3.177E-05	17.424	5.497E-05	19.807	2.775E-05				
17.032	3.144E-05	17.733	5.883E-05	20.557	4.832E-05				
17.200	3.085E-05	18 091	6.687E-05	21.863	6.800E-05				
17.370	3.235E-05	18 526	7.927E-05	25.906	1.757E-04				
17.560	3.621E-05	19 079	9.548E-05						
17.766	3.603E-05	19 899	1.407E-04						
17.989	3.703E-05	22.484	4.218E-04						
18.223	3.780E-05								
18.472	4.165E-05								
18.735	4.047E-05								
19.012	4.399E-05								
19.321	4.347E-05								
19.678	5.383E-05								
20.069	4.973E-05								
20.499	5.564E-05								
20.985	5.987E-05								
21.557	6.355E-05								
22.206	6.673E-05								
22.964	7.713E-05								
24.010	1.011E-04								
25.477	1.168E-04								
28.108	1.904E-04								

Table 150. Crack growth data from M(T) panels, 7075-T651.

3E2-11-D, 0.5 inch thick		3E2-01-D, 0.319 inch thick		3E2-02-D, 0.319 inch thick		3E2-03-D, 0.319 inch thick		3E2-09-D, 0.5 inch thick	
ΔK_I (ksi in ^{0.5})	da/dN (inch/cycle)	ΔK_I (ksi in ^{0.5})	da/dN (inch/cycle)	ΔK_I (ksi in ^{0.5})	da/dN (inch/cycle)	ΔK_I (ksi in ^{0.5})	da/dN (inch/cycle)	ΔK_I (ksi in ^{0.5})	da/dN (inch/cycle)
6.134	1.470E-06	5.876	1.537E-06	5.824	3.527E-06	6.013	3.990E-06	6.351	2.744E-06
6.312	2.217E-06	5.886	1.722E-06	6.042	3.079E-06	6.239	4.572E-06	6.511	3.153E-06
6.472	2.296E-06	5.896	1.566E-06	6.226	2.557E-06	6.484	5.073E-06	6.727	3.200E-06
6.635	2.533E-06	5.906	1.521E-06	6.493	3.364E-06	6.739	6.548E-06	6.925	3.290E-06
6.799	3.040E-06	5.916	1.783E-06	6.762	3.582E-06	6.992	5.798E-06	7.162	4.109E-06
6.960	3.532E-06	5.927	1.901E-06	6.979	3.467E-06	7.238	6.573E-06	7.432	4.760E-06
7.106	3.788E-06	5.939	2.006E-06	7.243	8.464E-06	7.503	7.155E-06	7.652	5.682E-06
7.255	4.210E-06	5.950	1.963E-06	7.510	4.473E-06	7.771	8.718E-06	8.042	6.157E-06
7.416	4.402E-06	5.962	2.312E-06	7.787	9.939E-06	8.026	8.775E-06	8.446	5.931E-06
7.571	4.589E-06	5.975	2.575E-06	8.036	8.787E-06	8.281	8.887E-06	8.720	7.148E-06
7.734	4.738E-06	5.989	2.532E-06	8.258	5.294E-06	8.507	1.023E-05	8.999	8.744E-06
7.901	4.847E-06	6.004	2.301E-06	8.615	1.159E-05	8.728	1.098E-05	9.284	8.769E-06
8.076	4.962E-06	6.018	2.308E-06	8.804	1.200E-05	8.987	1.069E-05	9.587	9.229E-06
8.259	5.061E-06	6.031	2.382E-06	9.079	1.145E-05	9.247	1.250E-05	9.924	9.990E-06
8.434	5.272E-06	6.045	2.327E-06	9.282	1.215E-05	9.508	1.271E-05	10.304	1.073E-05
8.600	5.804E-06	6.059	2.126E-06	9.602	1.210E-05	9.788	1.367E-05	10.764	1.292E-05
8.783	6.112E-06	6.071	1.963E-06	9.741	8.164E-06	10.068	1.628E-05	11.324	1.399E-05
8.962	6.792E-06	6.083	2.143E-06	9.947	1.068E-05	10.301	1.499E-05	11.904	1.580E-05
9.133	7.454E-06	6.096	2.210E-06	10.162	1.085E-05	10.519	1.550E-05	12.812	1.895E-05
9.328	8.166E-06	6.108	1.924E-06	10.252	1.772E-05	10.677	1.636E-05	13.905	2.376E-05
9.509	8.947E-06	6.120	2.069E-06	10.428	1.739E-05	10.763	1.748E-05	14.795	2.727E-05
9.672	9.756E-06	6.131	2.037E-06	10.614	1.871E-05	10.850	1.635E-05	16.062	3.341E-05
10.049	1.129E-05	6.143	1.945E-06	10.804	1.607E-05	10.945	1.837E-05	17.942	4.456E-05
10.269	1.232E-05	6.156	2.080E-06	10.976	1.471E-05	11.045	1.847E-05		
10.450	1.270E-05	6.169	2.072E-06	11.133	1.577E-05	11.140	1.973E-05		
10.580	1.318E-05	6.181	2.183E-06	11.342	2.026E-05	11.241	1.844E-05		
10.717	1.419E-05	6.193	2.156E-06	11.616	2.274E-05	11.347	1.817E-05		
10.862	1.413E-05	6.206	2.132E-06	11.912	2.385E-05	11.448	1.988E-05		
11.016	1.467E-05	6.220	2.127E-06	12.234	2.410E-05	11.559	2.046E-05		
11.178	1.567E-05	6.234	2.286E-06	12.571	2.457E-05	11.676	2.016E-05		
11.318	1.047E-05	6.247	2.214E-06	12.961	2.780E-05	11.802	2.150E-05		
11.460	1.444E-05	6.260	2.200E-06	13.448	3.180E-05	11.918	1.237E-05		
11.634	1.529E-05	6.275	2.251E-06	13.781	4.131E-05	12.021	2.196E-05		
11.819	1.599E-05	6.288	2.442E-06	13.921	3.651E-05	12.165	2.371E-05		
12.016	1.678E-05	6.302	2.370E-06	14.061	3.696E-05	12.335	2.416E-05		
12.229	1.720E-05	6.317	2.569E-06	14.194	3.689E-05	12.505	2.661E-05		
12.459	1.845E-05	6.331	2.402E-06	14.328	3.606E-05	12.685	2.648E-05		
12.708	1.892E-05	6.344	2.361E-06	14.468	3.655E-05	12.876	2.878E-05		
12.979	1.983E-05	6.359	2.529E-06	14.615	3.844E-05	13.075	2.825E-05		
13.272	2.052E-05	6.374	2.557E-06	14.772	3.896E-05	13.288	2.855E-05		
13.592	2.137E-05	6.390	2.671E-06	14.932	3.621E-05	13.517	2.977E-05		
13.973	2.598E-05	6.407	2.696E-06	15.095	3.871E-05	13.766	3.143E-05		
14.321	1.562E-05	6.423	2.699E-06	15.261	3.857E-05	14.039	3.421E-05		
14.775	3.446E-05	6.441	2.957E-06	15.432	4.117E-05	14.343	3.461E-05		
15.451	3.509E-05	6.459	2.906E-06	15.614	3.943E-05	14.674	3.626E-05		
16.139	2.959E-05	6.477	2.931E-06	15.803	4.073E-05	15.041	3.941E-05		
16.830	2.909E-05	6.495	2.874E-06	16.021	4.630E-05	15.630	4.132E-05		
17.730	3.917E-05	6.513	2.918E-06	16.258	4.812E-05	16.297	4.544E-05		
19.302	6.073E-05	6.530	2.956E-06	16.499	4.784E-05	16.882	4.856E-05		
22.377	8.458E-05	6.548	3.124E-06	16.766	5.221E-05	17.576	5.560E-05		
		6.567	3.193E-06	17.053	5.000E-05	18.430	5.912E-05		
		6.586	3.360E-06	17.357	5.476E-05	19.198	3.379E-05		
		6.607	3.394E-06	17.689	5.476E-05	20.096	6.155E-05		
		6.628	3.382E-06	18.061	6.340E-05	21.610	7.880E-05		
		6.648	3.324E-06	18.480	5.931E-05	23.982	9.398E-05		
		6.668	3.143E-06	18.924	6.426E-05	33.326	2.259E-04		
		6.687	2.955E-06	19.402	6.499E-05				
		6.704	2.682E-06	19.975	7.674E-05				
		6.721	2.608E-06	20.697	8.662E-05				
		6.737	2.833E-06	21.689	1.167E-04				
		6.755	3.268E-06	23.862	2.409E-04				

Table 151. Continuation of Table 189. Crack growth data from M(T) panels, 7075-T651

3E2-11-D, 0.5 inch thick		3E2-01-D, 0.319 inch thick		3E2-02-D, 0.319 inch thick		3E2-03-D, 0.319 inch thick		3E2-09-D, 0.5 inch thick	
ΔK_I (ksi in ^{0.5})	da/dN (inch/cycle)	ΔK_I (ksi in ^{0.5})	da/dN (inch/cycle)	ΔK_I (ksi in ^{0.5})	da/dN (inch/cycle)	ΔK_I (ksi in ^{0.5})	da/dN (inch/cycle)	ΔK_I (ksi in ^{0.5})	da/dN (inch/cycle)
		6.776	3.471E-06						
		6.800	3.943E-06						
		6.825	4.140E-06						
		6.853	4.468E-06						
		6.882	4.721E-06						
		6.911	4.722E-06						
		6.939	4.376E-06						
		6.967	4.366E-06						
		6.994	4.245E-06						
		7.022	4.415E-06						
		7.050	4.415E-06						
		7.078	4.610E-06						
		7.107	4.409E-06						
		7.136	4.777E-06						
		7.166	4.835E-06						
		7.198	4.970E-06						
		7.229	4.856E-06						
		7.262	5.091E-06						
		7.295	5.118E-06						
		7.329	5.474E-06						
		7.364	5.463E-06						
		7.400	5.539E-06						
		7.437	5.612E-06						
		7.474	5.783E-06						
		7.513	5.837E-06						
		7.553	5.947E-06						
		7.593	5.789E-06						
		7.634	5.972E-06						
		7.676	6.243E-06						
		7.719	6.299E-06						
		7.763	6.397E-06						
		7.807	6.374E-06						
		7.852	6.393E-06						
		7.897	6.685E-06						
		7.944	6.660E-06						
		7.991	6.729E-06						
		8.040	7.007E-06						
		8.091	7.252E-06						
		8.145	7.581E-06						
		8.201	7.767E-06						
		8.259	7.804E-06						
		8.318	8.024E-06						
		8.378	8.164E-06						
		8.441	8.269E-06						
		8.504	8.329E-06						
		8.569	8.475E-06						
		8.636	8.792E-06						
		8.705	8.893E-06						
		8.775	8.989E-06						
		8.848	9.213E-06						
		8.922	9.373E-06						
		9.001	9.663E-06						
		9.082	9.650E-06						
		9.165	9.707E-06						

Table 152. Continuation of Table 190. Crack growth data from M(T) panels, 7075-T651

3E2-11-D, 0.5 inch thick		3E2-01-D, 0.319 inch thick		3E2-02-D, 0.319 inch thick		3E2-03-D, 0.319 inch thick		3E2-09-D, 0.5 inch thick	
ΔK_I (ksi in ^{0.5})	da/dN (inch/cycle)	ΔK_I (ksi in ^{0.5})	da/dN (inch/cycle)	ΔK_I (ksi in ^{0.5})	da/dN (inch/cycle)	ΔK_I (ksi in ^{0.5})	da/dN (inch/cycle)	ΔK_I (ksi in ^{0.5})	da/dN (inch/cycle)
		9.249	9.994E-06						
		9.337	1.020E-05						
		9.429	1.043E-05						
		9.523	1.064E-05						
		9.619	1.079E-05						
		9.719	1.123E-05						
		9.825	1.149E-05						
		9.936	1.184E-05						
		10.052	1.201E-05						
		10.174	1.266E-05						
		10.306	1.332E-05						
		10.448	1.410E-05						
		10.601	1.482E-05						
		10.766	1.566E-05						
		10.944	1.638E-05						
		11.139	1.743E-05						
		11.349	1.810E-05						
		11.578	1.916E-05						
		11.831	2.036E-05						
		12.111	2.151E-05						
		12.423	2.292E-05						
		12.778	2.490E-05						
		13.143	2.148E-05						
		13.501	2.142E-05						
		15.144	3.689E-05						
		15.272	4.534E-05						
		15.520	4.114E-05						
		15.767	4.227E-05						
		16.038	4.497E-05						
		16.336	4.732E-05						
		16.664	4.963E-05						
		17.025	5.242E-05						
		17.426	5.526E-05						
		17.878	5.866E-05						
		18.393	6.241E-05						
		18.978	6.570E-05						
		19.649	6.987E-05						
		20.444	7.601E-05						
		21.472	9.157E-05						